ᴀUCL

Photocalorimetry for pharmaceutical photostability assessment

Luís Filipe Ramalho de Almeida e Sousa

Thesis submitted in accordance with the requirements of UCL School of Pharmacy for the degree of Doctor of Philosophy

September 2012

UCL SCHOOL OF PHARMACY

29-39 Brunswick Square

London WC1N 1AX

DECLARATION

This thesis describes research conducted in The School of Pharmacy, University of London between September 2008 and September 2012 under the supervision of Dr. Simon Gaisford and Professor Anthony Beezer. I certify that the research described is original and that any parts of the work that have been conducted by collaboration are clearly indicated. I also certify that I have written all the text herein and have clearly indicated by suitable citation any part of this dissertation that has already appeared in publication.

Signature:_____ **Date:**_____

ABSTRACT

There is a requirement to demonstrate photostability of medicines early in development but a lack of clear methodologies for doing so. While the International Conference on Harmonization (ICH) has a guideline on photostability testing (ICH, 1996), it does not specify a universal method for the analysis of samples after irradiation. Moreover, the current methods used in photostability testing separate irradiation of samples from analysis, rendering sample preparation critical in the whole process. In this context, photocalorimetry (the measurement of heat changes when a sample is irradiated) offers an alternative method which addresses most of the issues in current photostability testing. Some of the advantages of this technique include the real-time collection of data, the universal character of heat as a measure of change and the "in situ" analysis of photodegradation processes. Two different photocalorimetric designs were developed in the School of Pharmacy, University of London, to study the photodegradation of pharmaceuticals in any physical form. These instruments used light-emitting diodes (LEDs), as the light source, adapted to an isothermal heat conduction microcalorimeter (TAM 227), in one case, and a Multi-Cell Differential Scanning Calorimeter (MCDSC), in the other. To test the instruments' ability to detect photoreaction heat outputs, known photolabile pharmaceutical formulations were tested in different physical states. Solution phase studies were performed on samples of nifedipine in ethanol and the calorimetric outputs were quantitatively analysed. Solid nifedipine was also tested with the two photocalorimeters, although, data was only analysed qualitatively. Other solid drugs were tested with the photo-MCDSC; some of them are known photolabile compounds (2-nitrobenzaldehyde, benzoquinone, carbamazepine, chloramphenicol, dipyridamole and furosemide) while others are considered stable to light (paracetamol and aspirin). Parallel to the photocalorimetric studies, important progress was made regarding the analysis of calorimetric data for solid state processes and zero-order kinetics in solution.

ACKNOWLEDGMENTS

My long time friends JB, Antonio and Rita. It was an amazing journey. It wouldn't have been the same thing without you. My new London friends Antonia, Bruno, Felipe, Cristina, Andreia, Rita, Xico, Teresa, Luis, Renato, Jeroen, George, Dave, John and Gary. Also to my friends in Portugal.

And, last but not least, the most important people in my life: my parents, my brother, my sisters and all my family. Eu sei que foi difícil para todos mas quero que saibam que vos tive no meu coração todos os dias desta longa caminhada. Fico-vos agradecido para sempre!

TABLE OF CONTENTS

LIST OF FIGURES

LIST OF TABLES

LIST OF ABBREVIATIONS

AA	acetic acid
ASA	acetylsalicylic acid
E_a	activation energy
API	active pharmaceutical ingredient
x	amount of reactant that reacted at a specific time point
A	Arrhenius constant
N_A	Avogadro number
C or [ ]	concentration
$[A]_{tr}$	concentration of A at the transition between kinetics
DSC	Differential Scanning Calorimetry
E	energy
H	enthalpy
S	entropy
^1D	first excited singlet state
α	fraction of reaction
GC	Gas Chromatography
G	Gibbs energy
T_g	glass transition temperature
D_0	ground state
q	heat
C_p	heat capacity
HPLC	High Performance Liquid Chromatography
A_0	initial amount of reactant
IC	internal conversion
U	internal energy

ICH	International Conference on Harmonization
IUPAC	International Union of Pure and Applied Chemistry
ISC	intersystem crossing
IC	Isothermal Calorimetry
ITC	Isothermal Titration Calorimetry
LED	light-emitting diode
L	light power
T_m	melting temperature
^3D	metastable excited triplet state
MCDSC	Multi-Cell Differential Scanning Calorimetry
2-NB	2-nitrobenzaldehyde
NMR	Nuclear Magnetic Resonance
N_p	number of photons
n	order of reaction
h	Planck constant
P	pressure
ϕ	quantum yield
QC	quench-cooling
λ	radiation wavelength
k	rate constant
RRT	relative retention time
RTD	Resistance temperature detectors
RT	retention time
SA	Salicylic acid
m and n	solid-state mechanism descriptors
c	speed of light
T	temperature

TAM	Thermal Activity Monitor
P or Φ or dq/dt	thermal power
TED	Thermo-Electric Devices
TLC	Thin-Layer Chromatography
t	time
Q	total heat output
UV	ultraviolet
R	universal gas constant
VR	vibrational relaxation
V	volume
w	work
XRPD	X-Ray Powder Diffraction
Xe	xenon

1. <u>General introduction</u>

1.1. Overview

One of the most significant aspects of product development in the pharmaceutical industry is the assurance of high quality standards for all medicines. Unlike other products, medicines are therapeutic entities that alter people's health and wellbeing therefore requiring special control throughout all stages of development. As a result, monitoring is critical, not only during the manufacturing stages but also after production. In this context, stability of medicines plays an important role in the sense that any modifications in terms of their physical or chemical properties may result in changes of the quality parameters. These issues are tightly regulated in the pharmaceutical industry by guidelines that cover a wide range of stability factors such as temperature, humidity, oxidation and photolysis (1). Despite all factors being equally important, special attention is given to the latter as a result of the complex nature of the testing procedures involved. As a matter of fact, a guideline on photostability testing of drugs and drug products was specifically elaborated in order to address these demands (2). Although the recommendations included in that document are very useful with respect to the harmonization of the testing procedures, they do not clearly point out a universal analytical approach that may be used with all pharmaceutical products. Furthermore, most of the techniques currently used just analyse the samples after exposure to light thus precluding a real-time analysis of the photodegradation processes. These techniques are, in most cases, chromatographic assays that require some sort of sample preparation prior to the analysis. For example, if a solid drug is tested, dissolution in an appropriate solvent needs to be undertaken before using the chromatographic method. Such procedures may, however, have some issues, not only because the solid state history is lost in the process but also because they may introduce additional chemical changes to the initial sample making the analysis even more complex.

With these considerations in mind, a new methodology has been recently suggested for the real-time photostability testing of pharmaceuticals in any physical state. This technique is called photocalorimetry and consists of the *in situ* and in real-time measurement of the heat involved in any light induced processes. The application of such technique in the area of pharmaceutical sciences was tried before (3-5) but the instruments developed only allowed the detection of small photodegradation signals, with the determination of quantitative reaction parameters proving impossible. The aim

of this project was, therefore, to improve the sensitivity of the latest photocalorimetric design developed by Dhuna (5) and use this instrument to assess the photostability of drugs in a quantitative way. In order to do that several drugs were tested in different physical forms and the outcomes compared with the theoretical background on the photodecomposition of drugs and with the experimental data reported in literature. These studies ultimately allow the evaluation of the potential and limitations of photocalorimetry in photostability testing of pharmaceuticals. Another aspect of photocalorimetry that will be explored in this thesis is the analysis of calorimetric data. Although the detection and measurement of photodegradation signals is very important, the technique is rather useless if data cannot be analysed without recourse to ancillary methods. Therefore, the analysis of calorimetric data for some of the most important photodegradation kinetic schemes will also be addressed here.

To better understand the scope of the project, this chapter will first present some information on the different aspects of drug photodecomposition and photostability testing procedures followed by some basic information on calorimetry and its application to photostability testing of pharmaceuticals. A description of the current approaches used in calorimetric data analysis will also be given.

1.2. Photostability in the pharmaceutical industry

The effect of electromagnetic radiations, such as sunlight, on the properties of materials and products is well documented and is often observed as bleaching or colour change of coloured compounds, like paint and textiles, or as a colouration of colourless products. Other non chromatic changes may occur that can have a great impact on the functionality of the materials. An example of these is the light-induced increase in temperature of a material that, ultimately, may lead to melting and other physical changes. These instability issues have been a major concern in many fields of industry like textile, paint, food, cosmetic and agricultural industries. In the pharmaceutical industry, in addition to these effects, the photostability of medicines and the active pharmaceutical ingredient (API) they contain is also considered an essential quality requirement with the European pharmacopoeia recommending light protection for more than 250 drugs (6). Such stability issues are particularly important in this area because loss of API may lead to loss of efficacy, whilst increase in degradation products may contribute to toxicity with potential consequences for patient treatment.

Two main consequences can result from the interaction of UV and visible light radiation with a drug substance or drug product. Either the absorbed energy is dissipated harmlessly, for example as heat or in luminescent processes, such as phosphorescence or fluorescence; or that energy can lead to bond changes within the molecule leading to photodecomposition or photorearrangement with a subsequent decrease in active drug content. In the case of photodegradation, a loss of potency of the drug is the most obvious result. This decrease in API level can, ultimately, lead to a complete loss of therapeutic effect if the degradation is extensive enough. Moreover, adverse effects may occur as a result of minor photodegradation products being formed. These products can act directly by changing the physiological body functions (7) or they can react with endogenous substrates and indirectly cause undesired effects (8).

In addition to effects on the API itself, the photostability of the formulation and its packaging must also be considered and tested. This can be influenced by the dosage form (tablet, capsules, suspension, solution, cream etc.) whether it is exposed to the light source directly, in the primary packaging or in secondary packaging. Deleterious effects may result if the drug preparation is exposed to indoor or solar light for a significant time. This may be difficult to avoid as is the case for eye drops or

dermatological ointments, as well as infusions, parenteral fluids or solution in disposable plastic syringes (9). A review of the different aspects of formulation and stability testing of photolabile drugs was published by Tønnesen where, amongst other aspects, the effects of excipients and type of dosage form were evaluated (10). The manufacturing process itself must also be considered in the development of stable dosage forms as Thoma and Aman showed in their photostability studies on tablets (11). Investigations of various formulations and manufacturing parameters were undertaken with tablets containing nifedipine and molsidomine with the results showing that the particle size of the drug substance and the type of lubricant had no effect whereas the drug content, compression diluents and geometric alterations significantly affected the photostability. In these studies, manufacturing parameters like compression force and direct compression versus granulation showed less significant effects but it can be envisaged that this would not always be the case.

All these factors render an understanding of the photochemistry of the API and drug product and the potential need for light protection very important across all development stages. Depending on the type of drug, formulation or photodecomposition characteristics, two different strategies are used to protect a drug from light. One of them consists of preventing light from reaching the formulation using an opaque container or, in the case of tablets and capsules, an opaque coating (external protection) (9). The other strategy incorporates additives in the formulation to either absorb light competitively with the drug or quench the photoreaction of the latter (internal protection). With respect to the techniques of external protection, the use of brown glass containers, opaque plastic containers, aluminium foil wraps and tablet coatings with UV absorbers, dyes and opacifiers, such as titanium dioxide, are the most frequent strategies used. In terms of the "internal protection" techniques the incorporation of coloured dyes in a formulation to competitively absorb light of wavelengths that are particularly important for the photochemical reaction (also known as causative wavelengths) is sometimes used to stabilize the drug. Thoma (12), for example used the natural food colourant curcumin to absorb light in the long wavelength region of nifedipine absorption spectrum. The inclusion of excited state quenchers, such as cyclodextrins, has also been used several times to stabilize different drugs (13).

Despite the various undesired effects previously described, light is known to play an important role as a therapeutic agent in some disease states. The use of UV radiation in the treatment of psoriasis is well documented (14). Photodynamic therapy deliberately

utilises the interaction of certain molecules with light to produce a therapeutic effect at the site of irradiation whilst minimising systemic exposure to those molecules. Such photodynamic therapies have been emerging for the treatment of a variety of lesions and diseases such as other skin diseases, age-related macular degeneration, treatment of intra-ocular tumours, various types of cancer, arthritis, bone marrow purging, etc. A potentially very interesting application of such therapies involves the activation of a non-toxic drug by light providing dual sensitivity by restriction of the field of irradiation and preferential localisation of the drug within the target tissue (15). Besides these photodynamic therapies, several new drug delivery systems were reported that use light as a trigger. Examples of these are the use of photoactivated liposomes for tumour treatments (16), drug-releasing model compounds based on photosensitive hydrogels (17) or the development of prodrugs where the conversion from the inactive to the active form is controlled by light (10).

1.3. Theoretical background to photochemistry

1.3.1. Absorption spectra of drugs

Despite hydrolysis and oxidation being the two most common causes of instability of medicines, light is a very important factor that must not be overlooked. The most common light source that medicines are exposed to is the sun. The wavelength spectrum of sunlight reaching the Earth's surface includes the whole region of visible light (400 nm to 800 nm), part of the ultraviolet (UV) region (320 nm to 400 nm) and a broad range of infrared radiation (800 nm to 3200 nm) (18). Other relevant radiation sources used during the manufacturing process, storage and usage of medicines include incandescent, fluorescent and germicidal lamps (the latter also emitting radiation in the very energetic region of the far-UV). Knowledge of the spectral power distribution of all these sources is very important because the wavelength and intensity distribution of the illumination source will determine the amount of energy available for absorption by the molecule.

The property of absorption is the first indication that a drug may be capable of participating in a photochemical process. The first law of photochemistry formulated by Grotthus-Draper states: "Only that light which is absorbed by a system can cause chemical change" (19). If a drug or excipients are coloured, they must absorb radiation in the visible region with the colour exhibited being complementary to the radiation they absorb. This is not the case for the majority of therapeutic substances that are white which means that they do not absorb in the visible. However, they may do so in the UV region depending on their chemical structure.

In order for a drug to absorb radiation it is essential that its spectrum of absorption overlaps with the emission spectrum of the light source. A typical example that illustrates the importance of such property on the extent of degradation is given by the two anti-inflammatory drugs ibuprofen and sulindac. If these drugs are exposed to such conditions that the same amount of radiation is absorbed, ibuprofen is significantly more reactive than sulindac. However, under similar sunlight exposure conditions, sulindac proves to be much more sensitive, therefore, requiring protection from light.

This effect is explained by the fact that ibuprofen has a maximum absorption peak at 265 nm while sulindac has two absorption maximums at 280 nm and 327 nm. Since the latter is the only maximum that overlaps with the emission spectrum of sunlight, absorption of radiation only occurs for sulindac with the subsequent photodecomposition (6).

1.3.2. Light-induced processes

Absorption of radiation by a drug molecule does not always result in degradation or reaction with other molecules. The energy absorbed may, instead, be used in radiative processes like fluorescence or phosphorescence or other non-radiative processes, such as heat and vibrational relaxation (*VR*). In general, upon absorption of photons, a drug molecule in the ground state, D_0, is raised to a higher energy level by transition of electrons to the first excited singlet state, ^1D (the electron spins remain antiparallel). These electrons may also go to higher excited states but ultimately fall back to ^1D, dissipating energy in the process via internal conversion (*IC*) which is a non-radiative transition between states of like multiplicity. This first excited state, in turn, represents a less stable situation than the ground state hence the tendency to return to the initial state. This can be achieved by dissipating energy either via internal conversion or via photon emission (fluorescence). Because the lifetime of that excited singlet state is generally very short, interaction with the neighbouring molecules and subsequent reaction is not probable.

Alternatively, intersystem crossing (*ISC*) may occur from the excited singlet state to a metastable excited triplet state, ^3D (electron spins parallel) which has a much longer lifetime. As a result, the molecules in this triplet state may diffuse longer distances, increasing the possibility of interacting with other molecules and reacting. If no reaction occurs, the molecule goes back to the ground state releasing photons in the process (phosphorescence). All these luminescence events are shown in Figure 1.1.
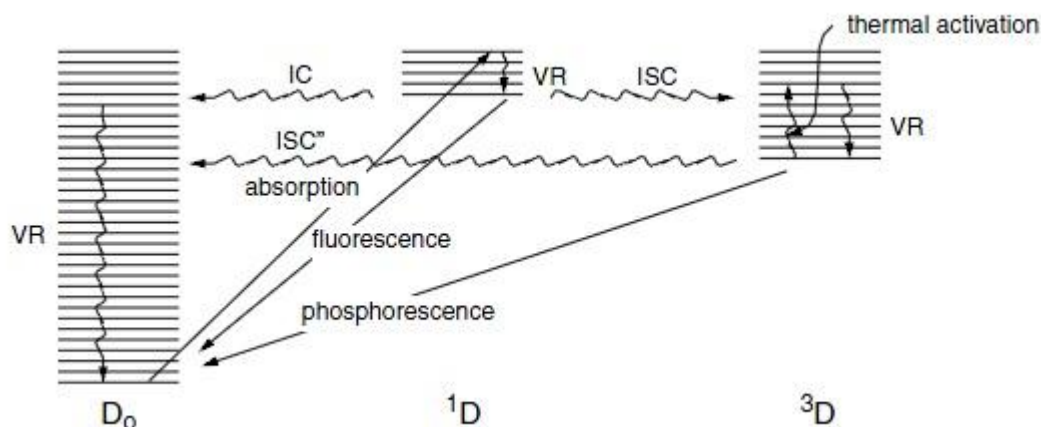
FIGURE 1.1. : Diagram showing the different luminescence processes that may occur following absorption of radiation (figure taken from (6)).

Although this relatively simple situation is the case for API alone, in the presence of excipients, trace impurities etc., singlet oxygen states can be stabilised leading to increased reactivity and the potential for energy to be transferred between different components of the formulation. In some cases this can render API that is photostable when tested alone as photolabile in the formulation.

1.3.3. Dependence on the drug/formulation physical state

Dilute solutions are the best model for studying photochemical reactions. Such conditions allow the degradation kinetics to be studied using the Beer-Lambert equation since absorption takes place across the bulk of the solution. This, however, does not apply to concentrated solutions, where absorption occurs only at the thin layer at the interface, to suspensions, where part of the light is lost by reflection, or solids, where light is completely absorbed by the first thin layers of molecules.

Only two factors determine the rate of photochemical reactions in dilute solutions: the rate of photon absorption (i.e., the number of photons absorbed per second) and the efficiency of the photochemical process (6). The first depends upon the intensity of the photon source and the extinction coefficient of the species in solution for the range of wavelengths emitted. On the other hand, the efficiency of the process is described by the quantum yield of the reaction, ϕ, which is defined as:

$$\phi = \frac{\text{number of molecules reacted/unit volume/unit time}}{\text{number of photons absorbed/unit volume/unit time}} \qquad \text{Equation 1.1.}$$

This number is very useful in comparing experimental data collected in different laboratories because it describes the rate or efficiency of a reaction independently of the experimental conditions (intensity of light). The rate of a photoreaction is, therefore, defined as:

$$\text{rate} = N_p . \phi \qquad \text{Equation 1.2.}$$

For a dilute solution with only one absorbing species, it may be the case that the number of photons absorbed per unit time, N_p, changes with the course of the photoreaction as a result of the decrease in the number of absorbing molecules. This effect leads to a reduction in the rate of photoreaction that is directly proportional to the decrease in concentration of the reacting molecules. The photodegradation process, hence, follows first-order kinetics. On the other hand, if the concentration of drug is very high and all radiation is absorbed, the reaction tends towards pseudo zero-order kinetics. This behaviour is explained by the fact that the intensity of the incident radiation is the rate-limiting factor. In this way, the process will show a constant rate of reaction for as long as the number of absorbing molecules in solution is enough to absorb all incident radiation. This type of kinetics is referred to as saturation kinetics, commonly seen in reactions where one of the important factors is limiting (e.g. enzyme catalyzed reaction). With the course of reaction, the kinetics will eventually switch to first-order with the concentration of molecules being the rate-limiting step. The transition between these two kinetics does not conform to any of these kinetic models, showing instead a non-integral reaction order behaviour (6). If more than one species absorbs radiation, the kinetics become more complex, depending on the participation of those species in other reaction pathways.

Besides these kinetic factors, other variants influence the photodegradation of drugs in solution that do not exist in other physical states. These factors include the viscosity, pH, partial pressure of oxygen or ionic strength of the solution (10).

With respect to photodegradation in the solid state, the change in drug content with time does not necessarily follow any particular order model as a result of the photochemical processes taking place only on the surface of the product. Despite this, first-order decay

has been reported in some studies (20, 21). Although the photodegradation process is greatly dependent on the properties of the solid surface, some important factors may influence the depth of light penetration, hence, affecting the rate of reaction. Such factors include the particle size, crystal modification (polymorphism), colour, thickness of powder bed and coating of the individual particles or the dosage form. The wavelength and hence the energy of the photons is another important factor. All these have an impact either on the absorption of radiation or in terms of the reflective properties of the solid samples.

In addition to those light penetration factors, the photodegradation of drugs in the solid state and solution phase may also differ as a result of different molecular moieties participating in the reaction. In fact, the restrictions imposed by the crystal lattice to molecular motions preclude some otherwise viable paths and vice versa introduce new paths involving interaction between functions that are close one to another in the solid state (9).

1.3.4. Influence of oxygen on photodecomposition

Oxygen has been found to participate in several photochemical processes with different consequences in terms of the extent of photodegradation. For example, oxygen may act as an efficient quencher of excited states leading to decay to the ground state preventing chemical reaction from occurring. Thus, it has a photo-stabilizing effect on reactions involving relatively long-life excited states such as triplets. However, such stabilization effects can generate electrophilic singlet oxygen that may promote some undesired reactions. Other oxygen species that are likely to promote photodegradation processes include the superoxide anion and ground state oxygen itself (9).

1.3.5. Wavelength effect

The broad range of wavelengths that molecules absorb is a clear indication of the variety of excited states that a molecule may have. These multiple excited states are known to decay quickly to the lowest energy excited state through internal conversion thus precluding any reaction in those states. As a consequence, the photochemical reaction is always the same independently of the irradiation wavelength. Therefore, if different lamps are used, the distribution of the reaction products should always be the same whilst the rate of reaction may change depending on the emission spectrum of the source. However, if the products of the photoreaction are themselves photoreactive, exposure to different wavelengths matters and the equilibrium reached will depend on them. A typical example of this effect is the rearrangements of Vitamin D (9).

1.4. Photostability testing methodologies

As was mentioned before, the testing of photostability during development and manufacturing of new drugs and drug products is essential to detect instability issues prior to scale-up investment and to plan adequate strategies of protection from the effects of light. These photostability tests are mandatory for all medicines and authorization into market depends on the observance of certain requirements set by the regulatory authorities. Some of these regulatory issues will be discussed in the next section followed by an overview of the different analytical methods used in photostability testing.

1.4.1. Regulatory background

Unlike other stability plans (e.g. thermal stability), photostability testing of drugs requires control over a great number of conditions which renders the design and planning of experiments complex. Some of the experimental factors that need special attention are the type of light source used, the radiation intensity levels, exposure times, sample presentation and dose monitoring devices. All these influence greatly the outcomes of photostability assays reinforcing the need for standard testing procedures in the pharmaceutical industry. In order to address some of those uniformity issues, the International Conference on Harmonization (ICH) published, in 1996, a guideline named "Photostability Testing of New Drug Substances and Products" (ICH Q1B) that aimed to regulate such procedures. This guideline contains several recommendations on the different aspects of photostability testing including information on the type of light sources used, the exposure conditions, the sampling techniques and analytical protocols.

For example, with respect to the type of light sources used, two options are given to test the effect of different lighting conditions on the stability of the products. One of them indicates the use of light sources with similar output to the lamps D65 and ID65 emission spectra in order to mimic outdoor direct and indoor indirect daylight conditions. The other suggests the use of a cool fluorescent lamp and a near UV fluorescent lamp to mimic indoor lighting conditions. The amount of radiation that

samples should be exposed to is also regulated with an overall illumination of not less than 1.2 million lux hours and an integrated near ultraviolet energy of not less than 200 watt hours/square meter being mandated. In order to ensure that the specified light exposure is obtained, samples may be exposed side-by-side with a validated chemical actinometer.

Besides these and many other recommendations, the guidelines also provide a flow chart to help with the decision on the stability of the products (Figure 1.2.). Each decision step in that diagram only requires the user to decide whether the observed change in the drug or drug product is acceptable.
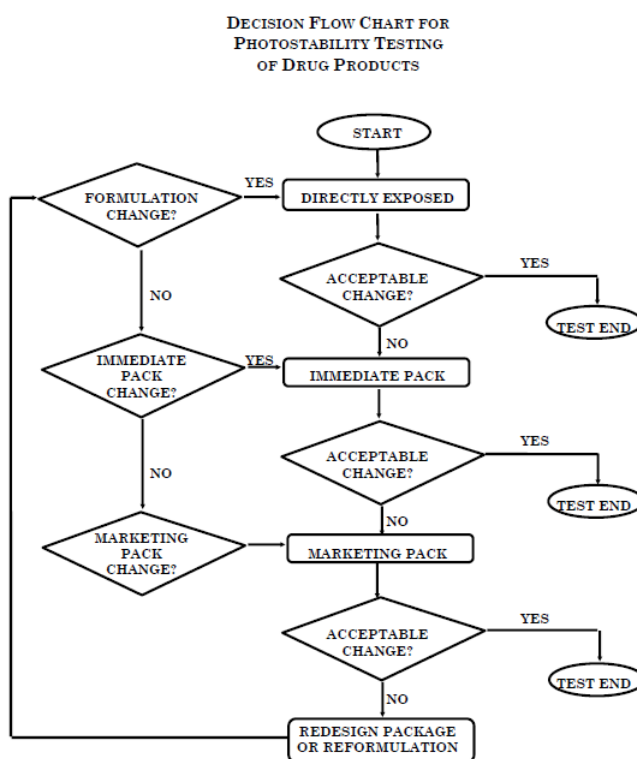
FIGURE 1.2. : Decision flow chart taken from guideline ICH Q1B on "Photostability Testing of New Drug Substances and Products".

In spite of all recommendations, these guidelines lack scientific exactness as well as unequivocal interpretation. An example of this is the missing clarification on the intensity and wavelength distribution of the light sources with the guideline just mentioning that these should be "similar" to the standards suggested. Even the proposed actinometer, quinine, has only been validated for lamps with a spectral power distribution similar to the Sylvania F20T12/BLB UVA fluorescent lamp which may have a very different power output compared to the test lamp.

Another aspect that is relevant, though it is not taken in consideration in this guideline, is the determination of causative wavelengths of degradation. This kind of information is very useful to choose the best strategies to prevent those wavelengths from interacting with the medicines. An example of these protective measures is the inclusion in the package of filters that absorb the causative wavelengths preventing thus access into the formulation.

The analysis of samples after exposure to light is also briefly addressed with no specific methodology being recommended. In fact, the only recommendation given is that samples should be examined for changes in appearance and assayed for loss in concentration and presence of degradants using a "method suitably validated for products likely to arise from photochemical degradation processes". This statement is very ambiguous and does not help much in terms of harmonizing the analytical methods used. Even the decision process that follows sample analysis doesn't include unequivocal guidance. The fact that a decision has to be made on whether an "acceptable change" is observed renders the process itself very subjective. Recently, Baertschi published a review on the several issues of significance that have been identified by both academic and industry researchers and pointed out the need for these guidelines to undergo a revision process (22). Despite all these issues, guideline ICH Q1B constituted a good first attempt at harmonizing the testing procedures in the pharmaceutical industry.

1.4.2. Current analytical methods used in photostability testing

Several analytical techniques have been used in photostability testing of medicines to detect and quantify the active, excipients or degradation products formed during the reaction. The main objectives of those determinations are the detection of degradants that may adversely interfere with biological body functions and the quantification of the drug content over the exposure time. The latter is very important because it allows the extent of drug degradation to be determined as well as the rate of the photoreaction which may be used to establish the shelf-life of medicines. Some of the techniques commonly used in photostability testing include High Performance Liquid Chromatography (HPLC) (23), Thin-Layer Chromatography (TLC) (24), spectrophotometric methods (25) or Nuclear Magnetic Resonance (NMR) (26). Each

technique has its own advantages and their application depends on the physical and chemical properties of the sample as well as on the type of formulation tested.

Despite the multiplicity of techniques currently used in the field, there are some practical issues common to all methodologies. One of the major drawbacks of all these methods is the inability to obtain long-term stability data in real-time. This limitation results from the fact that, in general, the analysis of samples is made separately from the light exposure period rendering the whole process discontinuous. The use of chromatographic techniques, such as HPLC, is a good example of methodologies where sample collection from an irradiated bulk is required before analysis. This discontinuous collection of degradation data may be problematic in cases where the process is so quick that small changes in the kinetics are not detected as a result of low frequency sampling. On the other hand, if the photoreaction is very slow, collection of data may take a long time before any conclusive data are obtained. Other issues may also arise if a change in the physical state of the sample is necessary prior to analysis. This is the case of samples in the solid state that require dissolution in a suitable solvent before analysis. A change in the physical appearance is undesired not only because the solid state history and properties of the sample are lost in the process of dissolution but also because there is a chance that hydrolysis processes and other reactions occur in the new physical state. Adding to all these issues most techniques used in photostability testing are time consuming, labour intensive, invasive or even destructive.

It is, therefore, highly desirable to find an analytical method that can be used to study photoreactions without the limitations described above. Isothermal calorimetry is a technique that is capable of addressing most of those issues and its application to the investigation of other stability issues affecting pharmaceuticals was previously reported (27). The principles of calorimetry and the advantages of using this technique in the field of pharmacy will be described in the next sections followed by an introduction to the use of such methods in photostability testing of pharmaceuticals.

1.5. Calorimetry

1.5.1. Principles and application in the field of pharmacy

Calorimetry [(from *calor* (Latin), heat; *metry* (Greek), measurement] is a technique that uses the measurement of heat to study any kind of processes occurring in a system. This technique is very useful because physical or chemical change occurs invariably with a change in heat content. Calorimetry, therefore, has the potential to analyse any processes irrespective of the specific properties of the system unlike other methods that can only be used if, for example, the study molecule possesses a suitable chromophore (spectroscopic methods). The only requirements for its application to the analysis of samples are that the amount of heat involved in the processes is greater than the detection limit and that the sample fits inside the calorimetric vessel.

The instruments that are used to measure these changes in heat are called calorimeters. Such instruments can be classified into two types depending on the temperature control they maintain over the course of an experiment. Either the sample is subjected to a preprogrammed temperature change over time; the technique is called Differential Scanning Calorimetry (DSC), or the sample is held always at the same temperature as is the case for Isothermal Calorimetry (IC). The first is usually used to study thermodynamically driven processes such as melting or recrystallization whereas the latter is commonly used to study long-term events such as chemical degradation, aging or recrystallization (28). It is, therefore, obvious that Isothermal Calorimetry is the most suitable technique to study the stability of pharmaceuticals over a long period of time. Measuring changes in heat content over time, not only gives information on the thermodynamics of the process, but also, allows calculation of kinetic parameters such as the rate of a reaction.

IC shows several advantages compared with other classical analytical methods. For example, in IC, the sample is analysed in a non-destructive way which means that the technique does not cause any additional degradation to that which would have occurred in storage conditions. This is not the case with analytical methods such as DSC that often destroy the sample or convert it into a different physical form as a result of the

extreme conditions employed. Another advantage of calorimetry is the possibility to test samples in any physical state. The universal character of heat as an indicator of chemical or physical change allows all processes occurring in a sample to be analysed independently of their physical form. This constitutes a major advantage over methods such as HPLC or UV spectroscopy where dissolution of the sample is required before analysis. The issues associated with dissolution of solids before analysis were previously described. Furthermore, in IC the whole of the sample is monitored whereas for spectroscopic methods a small sample is usually taken introducing issues about homogeneity and the representative nature of the sample. On the other hand, the *in situ* monitoring of samples and the continuous collection of thermal data allow processes to be studied in real-time.

However, the universal nature of heat is also the technique's biggest drawback. Considering the calorimetric signal obtained for a study system, it is not possible to determine unequivocally if the value that is measured corresponds to the heat output for a single process or if it results from the contributions of multiple unknown processes occurring simultaneously. That is because calorimeters measure an overall heat change that can be very difficult to deconvolute into the different contributions. For this reason, the occurrence of systematic errors, such as evaporation or erosion of the ampoule, may stay undetected and still influence the overall experimental signal. In addition to these analytical problems, calorimetry is not very useful if information on the mechanism of reaction, intermediates or reaction products is required.

1.5.2. Instrumentation

As mentioned before, heat (q) is the property measured by all calorimeters. This energy is always measured as a function of time irrespective of the type of temperature programme used (DSC or IC) and data is recorded as thermal power, Φ or dq/dt (SI unit is the Watt, W, which corresponds to 1 Joule released per second). In the case of DSC, power is measured for the duration of the temperature step hence data is recorded as power *versus* temperature. With IC, the temperature remains constant throughout the experiment and power is measured across time yielding power *versus* time data. Because IC is the best type of calorimetry for the investigation of long-term

degradation, the following aspects of instrumentation will be described exclusively for this technique.

Depending on the sensitivity of the instrument, isothermal calorimeters may be classified into microcalorimeters if the measurements are made on the micro-Watt scale, or nanocalorimeters if the nano-Watt scale is used. IC may also be classified according to the operating principle as power compensation, adiabatic or heat conduction calorimeters.

Power compensation calorimeters use an electrical element to either add or remove heat from the calorimetric vessel in order to maintain the sample and vessel at the same temperature during the course of reaction. Therefore, the power output from the sample is the inverse of the power supplied by that electrical element. This element is capable of heating and cooling using the Peltier principle.

Adiabatic calorimeters do not allow any exchanges of heat between the calorimetric vessel and its surroundings. Insulation is usually attained by placing an adiabatic shield around the vessel. Therefore, if a reaction occurs in the vessel, temperature will either rise or fall depending on the exothermic or endothermic character of the process. The change in heat content can then be calculated by multiplying that change in temperature with an experimentally determined constant (using electrical calibration). True adiabatic conditions are difficult to achieve because heat inevitably leaks to the surroundings compromising insulation. However, if these heat leaks are balanced by the instrument, semi-adiabatic conditions are achieved and the values obtained require correction.

Heat conduction calorimeters have a heat sink surrounding the measuring unit to maintain the system always at the same temperature. Between these two compartments there is a wall of thermopiles that converts heat signals into electric outputs. If any heat is produced or consumed in the reaction vessel, exchange with the heat sink occurs and the thermopiles generate an electric signal proportional to that heat. Afterwards the signal is amplified and multiplied by the cell constant which is determined with an electrical calibration. Such instruments are preferred to the semi-adiabatic calorimeters in the study of long-term processes because equilibrium is always achieved with the heat sink temperature. Moreover, the sensitivity of the thermopiles is greater than the temperature detectors used in those adiabatic calorimeters which means that smaller samples can be used.

The most suitable calorimeters for the analysis of long-term degradation of pharmaceuticals are the power compensation and heat conduction calorimeters. The first ones have a poorer detection limit despite the capacity to measure higher powers. They are therefore preferred to study very energetic processes where the heat rates are high. On the other hand, heat conduction calorimeters can measure micro- and even nanoWatts, therefore being the best calorimeters for the study of long-tem, low energetic reactions typical of most degradation processes in pharmaceuticals. The adiabatic designs, in turn, are only suitable to study processes that reach completion within one or two hours because of the problems inherent with heat leaks over the long-term.

These different instruments may also be classified into single or twin calorimeters depending on the number of calorimetric vessels they contain. As the name suggests, single calorimeters just have one vessel which means that a blank experiment needs to be done first. The heat output measured for this blank experiment is afterwards subtracted from the power measured for the sample experiment. Twin calorimeters have two similar vessels and measure an overall signal resulting from the difference between the thermal powers measured in each vessel. These twin calorimeters are better in terms of sensitivity because they correct automatically for any environmental factors affecting data and, in case a reference material is available, allow subtraction of the blank signal in the course of the experiment.

In addition to these classifications, the technique, calorimetry, can also be classified according to the type of experiment performed in the calorimeter. The design of each calorimetric unit going into the measuring channels varies with the application:

- Ampoule Calorimetry simply means placing a sample and reference material in sealed ampoules in the calorimeter and measure the difference in heat content of both materials;
- Isothermal Titration Calorimetry measures the heat resulting from the interaction of a solution that is titrated into another solution in the calorimetric ampoule;
- Flow Calorimetry measures the heat of reaction for a solution flowing through the calorimetric cell;
- Solution Calorimetry measures the heat of dissolution of a solid that is released into the calorimetric ampoule filled with the solvent;

- <u>Gas Perfusion Calorimetry</u> uses a system that creates a controlled vapour pressure in the calorimetric ampoule and analyses the processes resulting from the interaction of that vapour with the sample;

- <u>Batch Calorimetry</u> measures the heat of interaction between two samples that are initially in separate compartments and mixed after reaching equilibrium;

- <u>Photocalorimetry</u> studies the light-induced processes occurring in a sample that is placed inside an ampoule being shun with light.

1.5.3. Analysis of calorimetric data

As was mentioned before, isothermal calorimetric data is always recorded as thermal power (dq/dt) versus time. Those data alone prove to be rather useless if no strategies are available to translate them into quantitative parameters of significance. The following section will, therefore, describe the current strategies and equations available in the literature for the analysis of calorimetric data for processes occurring in the solid state and in solution. Before presenting these equations, information on the several aspects involved in a reaction is given to help understanding how those mathematical expressions were obtained.

1.5.3.1. *Requirements for a reaction to occur*

The occurrence of reaction requires three conditions to be fulfilled. Not only must it be well defined in terms of the mechanism of reaction, but also it must meet the requirements for thermodynamic and kinetic feasibility. If any of these requirements is not met, reaction will not occur and the system is considered stable. It is, therefore, necessary to understand the mechanistic, thermodynamic and kinetic aspects of chemical processes.

Mechanistic factors

For a reaction to occur it is necessary that a well defined reaction pathway exists with the reactant species interacting in a certain way to allow formation of products. Those interactions require certain reactive groups to be present within the molecule and the orientation of those molecular domains often proves critical for reaction to occur. The presence of electron withdrawing or donating groups is usually responsible for those interactions with other effects such as conjugation or resonance also playing an important role. The feasibility of reactions also depends on the steric conformation of molecules.

Thermodynamic factors

Thermodynamics corresponds to the study of all energy transformations occurring in the universe. Two compartments are always considered in these studies; the system that corresponds to the part of the universe that is under investigation and the surroundings that consist of all the rest. The system can be classified into open, closed or isolated according to the type of boundary between the system and the surroundings. Open systems allow mass and energy across the boundary whilst in a closed system only energy is transferred through the boundary. On the other hand, isolated systems do not exchange either of these with the surroundings.

The transfer of energy through that boundary can be made in two ways; production of work or transfer of energy as heat. The first corresponds to the "transfer of energy that makes use of organized motion". For instance, work is done when a weight is raised or lowered and its atoms are moved in an organized way. The expansion of a gas that pushes out a piston and raises a weight is an example of work. In contrast, energy may also be transferred as heat which "makes use of chaotic molecular motion" also called "thermal motion". It is said that energy is transferred as heat when the energy of a system changes as a result of a temperature difference between it and its surroundings. Processes that involve transfer of heat can be classified as exothermic, if heat is released from the system, or endothermic, if heat is absorbed by the system.

All processes in the universe involving transfer of energy are governed by the two first "Laws of Thermodynamics" (29). The First Law states that "energy cannot be created or destroyed" and that "the energy of an isolated system remains constant". These remarks are summarized in the following equation where w is the work done on a system, q is

the energy transferred to the system as heat and ΔU is the change in the system's internal energy (U is the total energy of the system):

$$\Delta U = q + w \qquad \text{Equation 1.3.}$$

The internal energy, U, is a state function, which means that, its value only depends on the current state of the system and is independent of how that state was reached. Another example of a state function is the enthalpy of a system, H, which is defined as:

$$H = U + PV \qquad \text{Equation 1.4.}$$

where P is the pressure of the system and V is its volume. Combination of equation 1.3. and 1.4. shows that the change in enthalpy (ΔH) is equal to the heat transferred at constant pressure for a system that does not produce any additional non-expansion work. For an exothermic process this enthalpy change is negative while the opposite is true for an endothermic process. Despite being a measure of the amount of heat transferred in a reaction, the magnitude of ΔH is not an indicator of the ease of reaction or the extent to which it progresses. That is because ΔH is not the only driving force in a chemical process. The change in the degree of disorder, or change in entropy, ΔS, is also important in determining the feasibility of the process and this relationship is governed by the Second Law of Thermodynamics. According to this law, "any spontaneous process that occurs in a system will lead to an increase in the total entropy of the universe":

$$\Delta_{total}S > 0 \qquad \text{Equation 1.5.}$$

with $\Delta_{total}S$ corresponding to the change in total entropy of the universe. The two state functions that determine the spontaneous occurrence of a reaction, ΔH and ΔS, can be correlated using an expression that defines the change in Gibbs energy (ΔG):

$$\Delta G = \Delta H - T.\Delta_{sys}S \qquad \text{Equation 1.6.}$$

with $\Delta_{sys}S$ being the entropy change of the system. A reaction may only take place if ΔG is negative. Even if that is the case, it does not mean it will occur because the reaction may not meet the necessary kinetic requirements. The negative Gibbs energy only suggests that the process is thermodynamically feasible. On the other hand, a positive ΔG means that the process will not occur spontaneously. Furthermore, Equation 1.6. shows that processes that are highly exothermic (negative ΔH) or reactions that result in a marked increase in the system's molecular disorder (positive ΔS) are thermodynamically favourable.

Kinetic factors

In addition to the mechanistic and thermodynamic aspects referred to above, a process must also be kinetically feasible in order for reaction to occur. These kinetic requirements are determined by the rate of reaction, which must be quick enough to allow observation of change with time. For example, if a process has a very large negative ΔG, suggesting that it is thermodynamically very favourable, reaction may not be observable as a result of the extremely slow rate under the experimental conditions. Three main factors influence the rate of reaction; the quantity of reactants available for reaction, the fraction of that quantity that has sufficient energy to overcome the activation energy (E_a) barrier and the order of reaction (n). The relationship between these three factors is expressed in Equation 1.7. :

$$\frac{\mathrm{d}x}{\mathrm{d}t} = k.(\mathrm{A}_0 - x)^n \qquad \text{Equation 1.7.}$$

where $\mathrm{d}x/\mathrm{d}t$ is the rate of reaction, k is the rate constant, A_0 is the initial amount of reactant, x is the amount of reactant that reacted at a specific time and n is the reaction order.

According to the collision theory, reaction occurs when colliding molecules have enough energy, also known as activation energy (E_a), at the moment of impact to break the prexisting bonds and form new bonds. The activation energy can, thus, be viewed as a barrier over which the reactant molecules must pass to form products. Even in the case of exothermic processes, where the energy of the products is lower than the energy of

the reactants, there must be an initial increase in the reactants energy to overcome the activation energy and allow the formation of products (Figure 1.3).
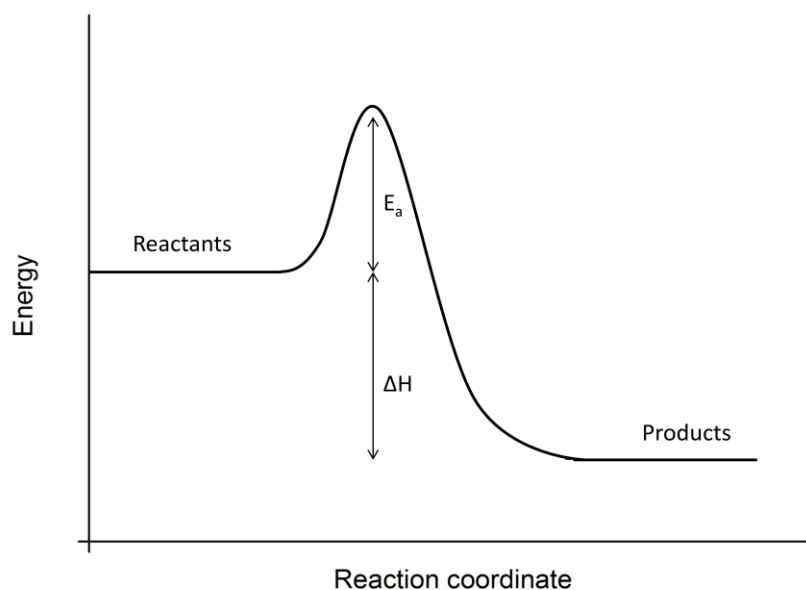
FIGURE 1.3. : Diagrammatic representation of the activation energy for an exothermic process.

The factors influencing the rate of reaction may also be explained with this collision theory. If the concentration of reacting molecules is increased or the temperature of the system is raised, an increase in the rate of reaction is observed as a consequence of more molecules with sufficient energy colliding per unit time. In the case of temperature, the number of collisions is greater because the increase in kinetic energy of the system (increase in temperature) results in more particles overcoming the activation energy barrier. The relationship between the activation energy, temperature and the rate constant is given by the Arrhenius equation (Equation 1.8.).

$$k = A.\,e^{\frac{-E_a}{R.T}}$$
Equation 1.8.

Applying logarithms,

$$\ln k = \ln A - \frac{E_a}{R.T}$$
Equation 1.9.

Where A is the Arrhenius constant, E_a is the activation energy, R is the Universal Gas Constant and T is the absolute temperature (in Kelvin). This equation is only valid when the activation energy is constant over the range of temperature that is being studied. There may be cases where this is not true which means that a change in the mechanism of reaction occurred after a specific temperature was reached.

Experimentally it is often found that the rate of reaction is directly proportional to the concentration of the reactants raised to a power equal to the stoichiometry in the overall reaction. For example, if the following reaction is considered:

$$aA + bB \rightarrow cC + dD$$
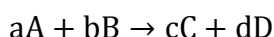
The rate of reaction at a given time is usually described by the following rate law:

$$rate = k.[A]^a.[B]^b \qquad \text{Equation 1.10.}$$

The coefficient k is the previously defined rate constant and the power to which the concentration of a species (A or B) is raised is called the order of reaction with respect to that species. The overall reaction order (n) is therefore a summation of all the individual reaction orders described by the rate equation. In this case, the reaction is ath order with respect to reactant A and bth order with respect to B. The overall reaction order, n, is equal to a+b. For reactions that occur in a single step, the order of reaction is often determined by the stoichiometry of the reactants. However, this simple view is not always experimentally observed. For many complex reaction schemes the observed order can be very different from the stoichiometry. Order is an experimental quantity used to describe the dependence of the reaction rate on the concentration of reactants. It is not the same as the molecularity of a reaction, which provides information about the number of molecules taking part in an individual step within the overall mechanism.

Rate laws such as the one described in Equation 1.10. may be obtained experimentally by calculating the rate of reaction and concentration of reacting species at different time points during the reaction. For any chemical process, the concentration (for a solution phase reaction) or quantity (for reactions in the solid state) of reactants decreases with time, whilst the concentration or quantity of the products increases until the reaction

reaches equilibrium. The average rate of reaction can, therefore, be defined as the change in concentration (or quantity) of a reactant or product, d[ ] (or dx), that occurs within a certain time interval, dt. For example, if that average rate is considered for a reaction in the solution phase, the following equations are obtained:

$$\text{Rate} = -\frac{d[\text{reactant}]}{dt} \quad \text{or} \quad \text{Rate} = \frac{d[\text{product}]}{dt} \qquad \text{Equation 1.11.}$$

Considering a plot of concentration (of reactants and products) versus time for a reaction occurring in the solution phase (Figure 1.4.), the rate of reaction at a specific time point can be calculated by drawing a tangent to the curve at that point and determining its slope. This strategy derives from the determination of the average rate of reaction for a time interval, considering that this interval is infinitesimally small.
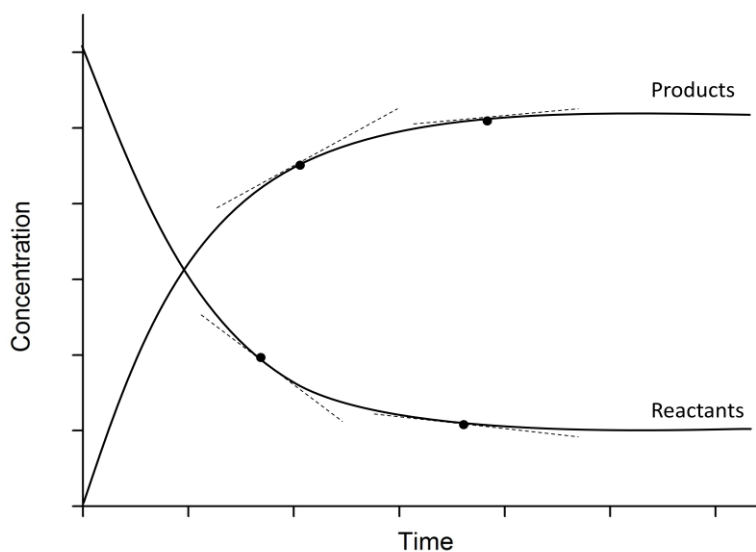
FIGURE 1.4. : Change in concentration of reactant and product with time for a hypothetical solution phase reaction.

Graphical determinations of this type may be exhausting and very laborious in the investigation of the kinetic aspects involved in a process. A more useful way of studying such processes is to use rate equations of the type of Equation 1.10. which relate the rate of reaction at any time t to the concentration of the reactants and products at that time. Equations of that type, that express the rate of reaction as a function of

concentration, are called differential rate equations. Despite describing all kinetic processes in a simple way, differential equations are not ideal in analysing experimental data because they cannot fit data in the form of concentration versus time which is the most observable type. Therefore, it is more convenient to use rate equations that express these changes in concentration as a function of time. These equations are called integrated rate equations. Considering, for example, the differential equation for a first order reaction where the concentration term is raised to the power 1:

$$-\frac{d[A]}{dt} = k.[A]$$

Equation 1.12.

Then, separating the variables and integrating between $t = 0$ and $t = t$ and $[A] = [A]_0$ and $[A] = [A]_t$, for the concentration, yields Equation 1.13.

$$-\int_{[A]_0}^{[A]_t} \frac{d[A]}{[A]} = k.\int_0^t dt$$

Equation 1.13.

After integration, the following equation is obtained:

$$[A]_t = [A]_0.e^{-k.t}$$

Equation 1.14.

The same mathematical treatment can be done for other reaction orders to obtain the respective integrated equations. The following table shows the differential and integrated rate equations for the most common kinetic schemes:

TABLE 1.1.: Differential and integrated rate equations for different solution phase reaction schemes.

Overall reaction order	Differential rate form	Integrated rate form	Linear plot to determine k
Zero	$-\dfrac{d[A]}{dt} = k$	$[A] = [A]_0 - k.t$	$[A]$ *vs t*
First	$-\dfrac{d[A]}{dt} = k.[A]$	$\ln[A] = \ln[A]_0 - k.t$	$\ln[A]$ *vs t*
Second	$-\dfrac{d[A]}{dt} = k.[A]^2$	$\dfrac{1}{[A]} = \dfrac{1}{[A]_0} + k.t$	$1/[A]$ *vs t*
n^{th}	$-\dfrac{d[A]}{dt} = k.[A]^n$	$\dfrac{1}{[A]^{n-1}} = \dfrac{1}{[A]_0^{n-1}} + (n-1).k.t$	$1/[A]^{n-1}$ *vs t*
		(except first order)	

The rate equations presented above describe solution phase processes where the kinetics is largely dependent on the concentration of the species in solution. As a consequence, such expressions cannot be used to describe solid state processes where change is measured in terms of the amount of reactants rather than their concentration. Kinetics in the solid state bear similarities to those in homogenous phase like solution or gas phase and many of the basic mathematical principles are shared among all three phases. However, solid state reactions are very different from those in other physical states because of the unique properties of solid state. For example, many processes occurring in solids depend on the sample's particle size, interface advance and geometrical shape thus rendering analysis much more complex comparing to solution phase reactions (30). These aspects and others related to the heterogeneous morphology of samples are responsible for the reproducibility issues often observed in the analysis of solid state processes.

Despite the complexity of such processes, some kinetic rate equations have been suggested for the analysis of simple solid state processes. Unlike solution phase kinetics, where the property measured is the concentration of species, in solid state kinetics the measure of change is the fraction of material that has reacted (α). This fraction is usually plotted against time and the resulting curve is used in the assignment

of reaction models to the experimental data. Solid state reactions are usually described by a model that can be represented by a mathematical equation. These models are based on certain mechanistic assumptions and the rate equations that describe them are determined with respect to the shape of the α versus time curves. Two types of classification may be used in the assignment of solid state models according to the shape of the isothermal plots (sigmoidal, acceleratory, linear or deceleratory) or the underlying mechanistic assumptions (nucleation, geometrical contraction, diffusion and reaction-order). Table 1.2. shows the differential and integrated equations that describe the different models reported in the literature.

Several attempts have been made to find a general rate equation that is capable of describing all solid state models. Ideally, for each model there would be a unique set of values that, after replacement in that general equation, would give an expression that describes a specific model. In 1971, Sesták and Berggren (31) suggested a general rate equation that can describe all solid state models:

$$\frac{\mathrm{d}\alpha}{\mathrm{d}t} = k.\alpha^m.(1-\alpha)^n.(-\ln(1-\alpha))^p \qquad \text{Equation 1.15.}$$

where dα/dt is the rate of reaction, k is the rate constant, α is the fraction of material that has reacted to time t and m, n and p are the mechanism descriptors. The rate equations for each model would, therefore, be obtained after giving specific sets of values to the model descriptors. A few years later, Ng suggested a similar equation to describe these models (32):

$$\frac{\mathrm{d}\alpha}{\mathrm{d}t} = k.\alpha^{1-p}.(1-\alpha)^{1-q} \qquad \text{Equation 1.16.}$$

where p and q are the mechanism descriptors. This equation was based on a sigmoidal model of decomposition where the rate of reaction increases with time until a maximum rate is obtained. This increase could be explained by three events occurring at that stage; an autocatalytic effect of the solid product phase, partial melting as a result of dissolved product and additional nuclei formed due to strain exerted by the growing nuclei. According to Ng, the reaction rate depends on the number of potential nucleus-forming sites originally present and the fraction of additional nuclei created at fractional

decomposition α. Equation 1.16. clearly shows that the fraction of additional dislocations formed will not only depend on the fraction that has decomposed (α), but also on the fraction of the remaining reactant (1-α). The coefficient of proportionality is called the rate constant, *k*.

A similar equation was recently suggested by Pérez-Maqueda for the analysis and fitting of experimental data to the various solid state models (33). This equation only differs from Ng's equation in the use of *m* and *n* as the mechanism descriptors instead of (1-*p*) and (1-*q*). A slightly different equation was used by Cai and Liu for the analysis of solid state data (Equation 1.17.) for processes that follow the ideal kinetic models in Table 1.2. and others that do not conform to any of the models described (34).

$$\frac{d\alpha}{dt} = \alpha^m.(1 - c.\alpha)^n \qquad \text{Equation 1.17.}$$

where *m*, *n* and *c* are mechanism descriptors for a specific model. Ideal kinetic data was fitted using both Pérez-Maqueda and Cai and Liu equations and it was observed that the residual error is much smaller using the latter. All these equations are, in essence, an attempt to find the best fit for solid state experimental data using the Ng equation as the model equation.

TABLE 1.2. : Solid-state rate expressions for different reaction models - adapted from (30)

Model	Differential form $$f(\alpha) = \frac{1}{k} \cdot \frac{d\alpha}{dt}$$	Integral form $$g(\alpha) = k.t$$
<u>Nucleation models</u>		
Power law (P2)	$2\alpha^{\frac{1}{2}}$	$\alpha^{\frac{1}{2}}$
Power law (P3)	$3\alpha^{\frac{2}{3}}$	$\alpha^{\frac{2}{3}}$
Power law (P4)	$4\alpha^{\frac{3}{4}}$	$\alpha^{\frac{3}{4}}$
Avrami-Erofe'ev (A2)	$2(1-\alpha)[-\ln(1-\alpha)]^{1/2}$	$[-\ln(1-\alpha)]^{1/2}$
Avrami-Erofe'ev (A3)	$3(1-\alpha)[-\ln(1-\alpha)]^{2/3}$	$[-\ln(1-\alpha)]^{2/3}$
Avrami-Erofe'ev (A4)	$4(1-\alpha)[-\ln(1-\alpha)]^{3/4}$	$[-\ln(1-\alpha)]^{3/4}$
Prout-Tompkins (B1)	$\alpha(1-\alpha)$	$\ln[\alpha(1-\alpha)]$
<u>Geometrical Contraction models</u>		
Contracting area (R2)	$2(1-\alpha)^{1/2}$	$[1-(1-\alpha)^{\frac{1}{2}}]$
Contracting volume (R3)	$3(1-\alpha)^{2/3}$	$[1-(1-\alpha)^{\frac{1}{3}}]$
<u>Diffusion models</u>		
1-D diffusion (D1)	$\frac{1}{2}\alpha$	α^2
2-D diffusion (D2)	$[-\ln(1-\alpha)]^{-1}$	$[(1-\alpha)\ln(1-\alpha)]+\alpha$
3-D diffusion-Jander eqn. (D3)	$3(1-\alpha)^{\frac{2}{3}}/2(1-(1-\alpha)^{\frac{1}{3}})$	$[1-(1-\alpha)^{\frac{1}{3}}]^2$
Ginstling-Brounshtein (D4)	$(3/2((1-\alpha)^{-\frac{1}{3}}-1)$	$1-\left(\frac{2\alpha}{3}\right)-(1-\alpha)^{\frac{2}{3}}$
<u>Reaction-order models</u>		
Zero-order (F0/R1)	1	α
First-order (F1)	$(1-\alpha)$	$-\ln(1-\alpha)$
Second-order (F2)	$(1-\alpha)^2$	$(1-\alpha)^{-1}-1$
Third-order (F3)	$(1-\alpha)^3$	$0.5((1-\alpha)^{-2}-1)$

1.5.3.2. *Analysis of solution phase calorimetric data*

The thermal power (Φ or dq/dt) measured in an isothermal calorimetric experiment is always recorded as a function of time and has the units of Joules per second (Watts). Plotting that thermal power against time gives a curve that can be integrated at different time points to yield the time dependent heat-output, q. Upon completion of the reaction, integration of the total area under the thermal power *vs* time curve gives the total heat evolved or absorbed for that process which is denoted as Q. The magnitude of the total heat output is dependent on the energetics of the process and the amount of material available for reaction. Considering a process where a single reactant is completely converted into one or more products, Q can be calculated by multiplying the enthalpy of that process (ΔH) by the number of moles of the starting material (A_0):

$$Q = A_0 . \Delta H \qquad \text{Equation 1.18.}$$

Similarly the heat output, q, until time t (t is any time point before completion) is defined by:

$$q = x . \Delta H \qquad \text{Equation 1.19.}$$

where x is the amount of sample that reacted until time t. If a simple solution phase reaction is considered where reactant A gives product P (A $\rightarrow$ P), a kinetic expression may be written that describes the rate of disappearance of reactant A:

$$\frac{d[x]}{dt} = k . ([A]_0 - [x])^n \qquad \text{Equation 1.20.}$$

where $d[x]/dt$ is the rate of reaction, k is the rate constant, $[A]_0$ is the initial concentration of reactant A and $[x]$ is the concentration of reactant that reacted before time t. Substitution of $[x]$ in Equation 1.20. by $q/(\Delta H . V)$ gives the following equation (35):

$$\Phi = \frac{dq}{dt} = k.\Delta H.V.\left([A]_0 - \frac{q}{\Delta H.V}\right)^n \qquad \text{Equation 1.21.}$$

Equation 1.21. is an example of a differential form of a calorimetric equation. This type of equation can be integrated to give expressions that relate the thermal power measured to time. Isothermal calorimetric data can, therefore, be fitted to such equations to obtain the kinetic and thermodynamic reaction parameters. Taking Equation 1.21. and replacing $[A]_0$ by $Q/(\Delta H.V)$, Equation 1.22. is obtained:

$$\frac{dq}{dt} = k.(V.\Delta H)^{1-n}.(Q-q)^n \qquad \text{Equation 1.22.}$$

Mathematical integration of this equation between time 0 and t and heat output 0 and q gives:

$$(Q-q) = [k.t.(V.\Delta H)^{1-n}.(n-1) + Q^{1-n}]^{\frac{1}{1-n}} \qquad \text{Equation 1.23.}$$

where t is the reaction time. Combining Equations 1.22. and 1.23. yields an expression that allows fitting of isothermal calorimetric data:

$$\frac{dq}{dt} = k.(V.\Delta H)^{1-n}.[k.t.(V.\Delta H)^{1-n}.(n-1) + Q^{1-n}]^{\frac{n}{1-n}} \qquad \text{Equation 1.24.}$$

This calorimetric equation describes single-step solution phase processes for different integral or non-integral reaction orders. However, some cases exist where that equation cannot be used. For example, if first-order reactions are analysed ($n=1$) the exponent in Equation 1.24., $n/(1-n)$, cannot be evaluated because a number divided by zero is always infinite. Moreover, Hills (36) found that, simulation of data for a given exothermic process (negative enthalpy of reaction) resulted in thermal power data with different sign depending on the reaction order considered. A more general equation was, therefore, developed by integrating the basic kinetic equation (Equation 1.20.) rather than the calorimetric form (Equation 1.22.). Equation 1.25. was obtained:

$$\frac{\mathrm{d}q}{\mathrm{d}t} = k.\Delta H.V.\left[\frac{[A]_0^{n-1}}{(n-1).[A]_0^{n-1}.k.t+1}\right]^{\frac{n}{n-1}}$$

<div align="right">Equation 1.25.</div>

This expression does not depend on the sign of the enthalpy term and allows any n^{th}-order process to be studied with the exception of first-order reactions. An alternative approach may, however, be followed to derive an expression that describes first-order reactions calorimetrically. Considering Equation 1.20. and letting n=1, the variables in that equation are separated to give:

$$\frac{\mathrm{d}[x]}{[A]_0 - [x]} = k.\mathrm{d}t$$

<div align="right">Equation 1.26.</div>

Integrating Equation 1.26., solving for [A]=[A]$_0$ when t=0 and making the substitution, [x]=q/($\Delta H.V$) yields a calorimetric equation that describes first-order processes:

$$\Phi = \frac{\mathrm{d}q}{\mathrm{d}t} = k.\Delta H.[A]_0.V.\mathrm{e}^{-k.t}$$

<div align="right">Equation 1.27.</div>

Taking logarithms:

$$\ln(\Phi) = -k.t + \ln(k.\Delta H.[A]_0.V)$$

<div align="right">Equation 1.28.</div>

With this equation, the only kinetic scheme that lacks an expression that relates thermal power to time is zero-order kinetics. In fact, if n is given the value 0 for any of the previous calorimetric equations (Equation 1.21., 1.24. and 1.25.) the resulting equation does not contain time as a variable (Equation 1.29.).

$$\frac{\mathrm{d}q}{\mathrm{d}t} = k.\Delta H.V$$

<div align="right">Equation 1.29.</div>

As a consequence, isothermal calorimetric data in the form of thermal power versus time cannot be fitted to Equation 1.29. To analyse those data, the rate constant or enthalpy of reaction must be determined first with ancillary methods, followed by replacement of all known variables in Equation 1.29.

Other, more complex, reaction schemes were also investigated and several equations were developed based on the expressions described above (36-38). Some of these schemes include parallel first and second order reactions with the same reactant or with different reactants, consecutive reactions, parallel and consecutive and concurrent processes.

Two different approaches may be used to determine the thermodynamic and kinetic parameters described in the calorimetric equations; either iterative methods are used to fit the data to a calorimetric equation or direct calculation methods are applied to retrieve the quantitative reaction parameters. The first method makes use of specialized software to fit the experimental data to a specific equation and return the reaction parameters using least-square minimization. This analysis, however, requires a large portion of data to be recorded in order for the software to pick up a tendency in the signal change. Moreover, iterative methods require that the mechanism of reaction is known prior to analysis in order for the correct equation to be selected for the empirical fitting technique. Another important aspect of such methods is the fact that an estimate of the reaction parameters must be given before iteration. The closer these estimated values are to the real value the more accurate the fitting process is. Most of the times, these values are not available or prove difficult to determine thus increasing the uncertainty of the returned parameters. In Chapter 2 an estimation method for enthalpies of reaction is described which is very useful to reduce the burden of iterative method in calorimetric data analysis.

An alternative to iterative methods, and one that sidesteps many of the issues referred above, is the use of direct calculation methods. Such methods take the calorimetric equations described earlier and transform them to allow calculation of each of the desired parameters using only a few data points (28, 39-41). The only drawback of these methods is that at least one of the reaction parameters (n, k or Q) must be known prior to analysis. An example of the type of equations used in these direct calculation methods is given below (Equation 1.30.) for the determination of the reaction order, n, for a process that progresses to completion (known Q). If two values of thermal power, Φ_1 and Φ_2, are selected at two different time points, t_1 and t_2, and the respective heat

outputs, q_1 and q_2, are calculated, the reaction order can be determined after replacing the total heat output, Q, in Equation 1.30 (41).

$$\frac{\Phi_1}{\Phi_2} = \left(\frac{Q - q_1}{Q - q_2}\right)^n$$

Equation 1.30.

After calculation of n, the other reaction parameters are easily determined using the equations described in the literature (28, 39-41).

1.5.3.3. Analysis of solid state calorimetric data

Kinetic processes in the solid state are considerably different from solution phase processes because of the specific morphological and physical properties of solid samples. Therefore, it is not appropriate to apply the calorimetric equations derived above to study solid state systems.

Several methods can be found in the literature for the investigation of the kinetics involved in solid state processes using thermal methods, but the vast majority require knowledge of the fraction of material reacting at different time points (α). Most of these methods are summarized in a review published by Khawam (30) where different model-fitting and model-free methods are described for the analysis of isothermal and non-isothermal data. Those methods focused on the analysis of reactions involving weight loss (i.e., Thermogravimetric Analysis) although analysis with other thermal methods, such as DSC, can also be done. The only requirement for application is that the data collected are converted to the degree of reaction (α) versus time or temperature. Isothermal calorimetric data, however, is usually recorded as Φ versus time which means that it cannot be directly used with those methods. Nevertheless, the fraction of reaction, α, can be calculated at different time points if the process is allowed to progress to completion and the total heat output (Q) is calculated:

$$\alpha = \frac{q}{Q}$$

Equation 1.31.

where q is the heat output at time t.

The first attempt at deriving a solid state calorimetric equation that allows thermal power (Φ) data to be used was done by Willson (35, 42). In a similar manner to that described for the solution phase models, Willson used the Ng equation (Equation 1.32.) and converted it to a form that describes calorimetric data obtained from a solid state reaction.

$$\frac{\mathrm{d}\alpha}{\mathrm{d}t} = k.\,\alpha^m.\,(1-\alpha)^n \qquad \text{Equation 1.32.}$$

Replacing α by q/Q in that expression the following calorimetric equation results:

$$\Phi = \frac{\mathrm{d}q}{\mathrm{d}t} = k.\,Q.\left(\frac{q}{Q}\right)^m.\left[1-\left(\frac{q}{Q}\right)\right]^n \qquad \text{Equation 1.33.}$$

Despite this equation describing solid state processes calorimetrically, its integrated form was never derived, which constitutes a problem if thermal power versus time data is used in the analysis. Alternatively, the time dependent heat output (q) can be calculated by integration of the area under the Φ–time curve at different time points allowing Φ-q data to be plotted. For most solid state models (if m and n have the same sign and $\neq 0$) the resulting curve shows a peak that corresponds to the maximum rate of reaction. An example of such curves is given in Figure 1.5.
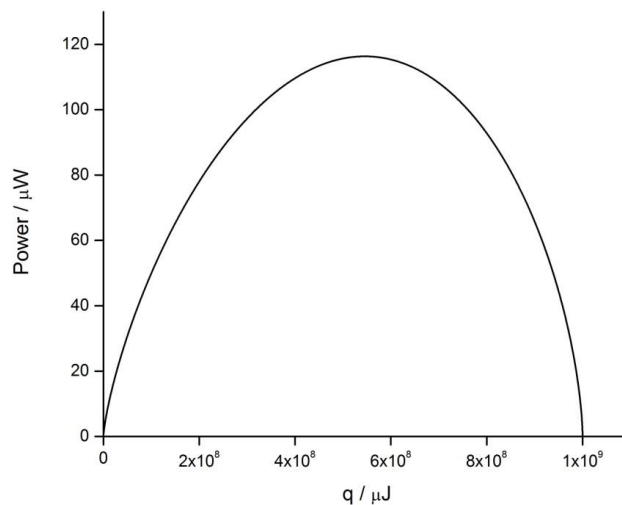
FIGURE 1.5. : Simulated Φ-q data for a solid state process with the following reaction parameters: $Q = 1\text{x}10^9$ µJ, $k = 3\text{x}10^{-7}$ s^{-1}, $m = 0.75$ and $n = 0.625$.

Those *Φ-q* data can, afterwards, be used to determine the solid state reaction parameters in Equation 1.33 by an iterative process. This method, however, is more complex than the empirical fitting used in solution phase analysis as a result of the mechanism descriptors, *m* and *n*, having non-integral values. Furthermore, the number of unknown parameters in Equation 1.33. is greater than that for solution phase calorimetric equations, therefore, increasing the burden on the iterative process.

It is, therefore, preferable to use direct calculation methods similar to the ones used in solution phase analysis. The parameters *m*, *n*, *Q* and *k* can be calculated for the solid state using the methods reported by O'Neill (43). The first step usually consists of determining the mechanism descriptors *m* and *n*. Some of the values that these parameters can take and the mechanisms they describe can be found in the literature (35). According to O'Neill, *m* and *n* can be calculated using a technique of data pairing that was initially described for the determination of the reaction order in solution phase (41). This method relies on the knowledge of *Φ* and *q*, for paired time points and application of an algorithm across the whole range of data. The mathematical expression adapted from that solution phase algorithm is:

$$\frac{\Phi_1}{\Phi_2} = \frac{(q_1)^m \cdot (Q - q_1)^n}{(q_2)^m \cdot (Q - q_2)^n}$$

Equation 1.34.

Two problems arise from the adaptation of such method to the analysis of solid state calorimetric data. Firstly, the method requires that the total heat of reaction, *Q*, is known prior to analysis which means that the reaction must progress to completion. The second issue concerns the range of data that the method can be applied to. In the specific case of solid state processes, the calorimetric data usually progresses through a maximum decreasing thereafter until the end of the process. If the initial part of data is analysed, determination of *m* is favoured as a result of changes in $(Q-q)^n$ in Equation 1.34. not being very significant. On the other hand, if data pairs from the descending part of the *Φ-q* curve are used, a more accurate determination of *n* is likely to occur. This dependence on the range of data constitutes a big limitation of this adapted method.

If the values of *m* and *n* are known prior to analysis, a value for the total reaction heat output (*Q*) must be determined. This parameter is usually very difficult to calculate experimentally because, most of the times, solid state processes are too slow to be

analysed within an acceptable period of time. Instead, the total heat output may be determined through analysis of paired data points. If Equation 1.33. is written for two data points and a ratio between them is formed then the following equation is obtained:

$$\frac{\Phi_1}{\Phi_2} = \frac{\left(\frac{q_1}{Q}\right)^m \cdot \left(1 - \frac{q_1}{Q}\right)^n}{\left(\frac{q_2}{Q}\right)^m \cdot \left(1 - \frac{q_2}{Q}\right)^n} \qquad \text{Equation 1.35.}$$

If the values of q_1 and q_2 are selected such that q_2 is a factor of q_1 ($q_2 = c.q_1$ or $c = q_2/q_1$), and setting R as:

$$R = \left(\frac{\Phi_1}{\Phi_2} \cdot (c)^m\right)^{\frac{1}{n}} = \frac{\left(1 - \frac{q_1}{Q}\right)}{\left(1 - \frac{c.q_1}{Q}\right)} \qquad \text{Equation 1.36.}$$

Equation 1.36. can be solved to find Q:

$$Q = \frac{q_1 \cdot (c.R - 1)}{(R - 1)} \qquad \text{Equation 1.37.}$$

The rate constant, k, can then be calculated after rearranging Equation 1.33. and replacing all known values in that expression:

$$k = \frac{\Phi}{Q \cdot \left(\frac{q}{Q}\right)^m \cdot \left[1 - \left(\frac{q}{Q}\right)\right]^n} \qquad \text{Equation 1.38.}$$

Although all these analytical methods are very useful in determining the solid state reaction parameters, they are not free from assumptions and there is a clear dependence on the range of data used in the analysis (even iteration is dependent on the range of data used). Moreover, these methods depend on previous knowledge of, either, the

mechanism of reaction, or, the total heat of reaction, and these are not usually available for samples that are analysed for the first time. Hence, it is very important to find new strategies for the calorimetric analysis of solid state processes without any previous assumptions.

1.6. Photocalorimetry

1.6.1. Overview of the method

Isothermal calorimetry's great potential in the analysis of small changes and its numerous advantages compared to traditional analytical methods (non-invasive, non-destructive, analysis *in situ*, etc.) are responsible for the growing interest it has received from different areas such as microbiology, chemistry or material sciences. As a result of this widespread interest, the number of adaptations and applications of isothermal calorimetry has increased greatly, in recent years, with new instruments being developed at a fast speed.

An example of such new applications is photocalorimetry. As the name suggests, photocalorimetry is an extension of classical calorimetry for the study of light induced processes. Photochemical processes, like any other type of chemical or physical events, are always accompanied by heat changes. These energy transfers can be measured by calorimetric designs specially adapted to the analysis of light-dependent processes which are called photocalorimeters. Many different photocalorimetric designs have been built and used (44); however, a basic structure is common to all of them:

- A "standard" calorimeter;
- An optical irradiation system;
- A connection between these two parts, sometimes incorporated in the calorimetric unit.

Photocalorimetry may be used to study reactions that are too slow for observation under thermal activation conditions, but that are activated after irradiation. It can also be applied to study the thermodynamics of complex photoreactions for which literature data is not available. In addition to the energetics of the photo-processes, the measurement of heat transfers across time allows determination of some kinetic information, as well as, quantum yields of reaction. Common applications of photocalorimetry include the investigation of photosynthesis, processes associated with the chemistry of vision, photopolymerisation and photodegradation.

A typical photocalorimetric experiment always involves a control or blank experiment and the main photochemical experiment. In the control experiment, a reference photoinert material is always placed inside the ampoule. In studies in solution, for example, this photoinert substance is usually the solvent or an absorbent substance that is not affected by light. Depending on the instrument, this control can be performed at the same time as the main experiment (in a twin calorimeter) or at different times (in the case of calorimeters that just have one measuring channel). In both cases, light guides are usually used to direct radiation from a light source into the calorimetric ampoules that are placed inside the measuring chamber.

In the blank experiment, the total energy supplied by the light source (E_p) is quantitatively converted into heat, Q', that is measured by the calorimeter (Equation 1.39.). This is only valid for the simplest cases where no heat losses are observed.

$$E_p = Q'$$ Equation 1.39.

Ideally, for the main experiment, the same amount of energy (E_p) is supplied to the photolyte under study providing the testing conditions are similar to the blank experiment. In this case, however, a light induced chemical process occurs. The scheme below shows the chain of events that a photolyte A usually follows after exposure to radiation.

$$A \xrightarrow{h\nu} A^* \longrightarrow B$$
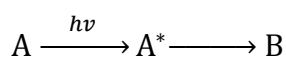
Initially, the light sensitive compound A is activated by the radiation, going from the ground state to an excited state, A^* which undergoes reaction. Because of this additional process, the heat measured for the main experiment, Q, is different from that for the blank experiment. The energy balance is represented in Equation 1.40., where $\Delta_p H_n$ is the change in enthalpy of the net photoreaction (44).

$$E_p = Q + \Delta_p H_n$$ Equation 1.40.

The molar enthalpy of reaction, $\Delta_p H_m$, may then be calculated using Equation 1.41.

$$\Delta_p H_m = \frac{\Delta_p H_n}{x} = \frac{Q' - Q}{x}$$

Equation 1.41.

where x is the amount of A converted to product B. Unless the reaction goes to completion and the initial amount of A is known, x may only be determined by an ancillary method. These calculations are only possible if both experiments are performed under the same conditions. This means that, not only the energy supplied to the system, E_p, should be the same, but also the way that radiation interacts with the photocalorimetric system should be similar for both experiments. An example of such interactions is the reflection, E_r, of incident radiation by several components of the vessel, such as stirrers, light guides, etc. which leads to a decrease in the amount of energy available for reaction. If the calorimetric vessel is transparent, a certain amount of radiation can also be transmitted to the surroundings, E_t, particularly if the absorbance of the contents is small or significantly decreases in the course of reaction. The occurrence of luminescence processes, E_l, also influences the measurements and these should be taken into account. Equations 1.42. and 1.43. describe the factors influencing the net amount of energy, E_{pcorr}, reaching the system in the blank and main experiment, respectively.

$$E_{pcorr} = E_p - E_r' - E_t' - E_l' = Q'$$

Equation 1.42.

$$E_{pcorr} = E_p - E_r - E_t - E_l = Q + \Delta_p H_n$$

Equation 1.43.

Often, the energy losses are either negligible or are cancelled in the calculation of $\Delta_p H_m$ using Equation 1.41. if similar conditions are used in the two experiments. However, if x is not available, calculation of $\Delta_p H_m$ proves impossible with that equation. A different equation may be derived for the determination of that parameter using the quantum yield of reaction, ϕ_λ; if monochromatic radiation of wavelength λ is employed, the energy per quantum supplied to the system is known and Equation 1.46. is obtained:

$$\phi_\lambda = \frac{\text{rate of reaction}}{\text{photon flux}} = x/N_p \qquad \text{Equation 1.44.}$$

where N_p is the number of moles of photons that are used in the conversion of x moles of photolyte.

$$N_p = \frac{Q'}{N_A \cdot \left(\frac{h.c}{\lambda}\right)} \qquad \text{Equation 1.45.}$$

where N_A is the Avogadro number, h is the Planck constant and c is the speed of light.

$$\Delta_p H_m = \left(1 - \frac{Q}{Q'}\right) \cdot ((N_A \cdot h.c)/\lambda) \cdot \left(\frac{1}{\phi_\lambda}\right) \qquad \text{Equation 1.46.}$$

Accurate knowledge of ϕ_λ is, however, critical for the successful application of Equation 1.46.

1.6.2. Brief history of the development of photocalorimetry

The first photocalorimeter described in the literature dates back to 1939 when Magee and co-workers developed an instrument to determine thermally the quantum efficiency of photosynthesis by *Chlorella* (45). The calorimeter (Figure 1.6.) consisted of a thin-walled quartz cell mounted in a cylindrical aluminium container with a multijunction thermocouple measuring the difference in temperature between the cell and the container. A double thermostat maintained the container at constant temperature. A thermopile was placed behind the cell to measure the amount of radiation transmitted. The determination of thermal efficiency of the photosynthesising algae was conducted using a 500 W projector lamp which introduced light through the front wall of the quartz cylinder. That thermal efficiency was calculated based on the differential signal obtained between the process of respiration and photosynthesis. The same instrument was later used to study the quantum yields and the influence of oxygen in the kinetics of hydrocarbons' photobromination (46).

69
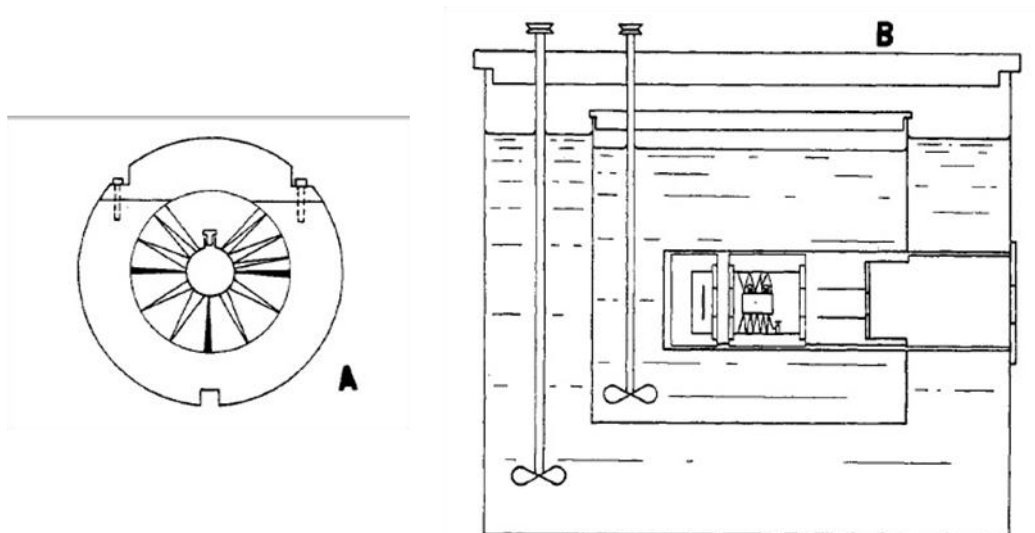
FIGURE 1.6. : Magee's photocalorimeter for the investigation of quantum yields of photosynthesis processes. A - end view; B – side view of the thermostat.

After thirty years, apparently without any significant contributions in the area, photocalorimetry slowly started to develop with several instrument designs being reported for application in different areas. Some of these applications included the determination of ϕ_λ of fluorescence of organic dyes (47-49), calculation of enthalpies of photolysis of organic compounds (50, 51), coordination chemistry (52-56) and studies on the chemistry of vision (57-60).

Also, in that period, two techniques related to photocalorimetry were described for the investigation of processes that are not induced by light: calorimetry-spectrophotometry and calorimetry-photometry. The first one uses spectrophotometric inserts adapted to a calorimetric vessel to simultaneously measure the production of heat and the changes in optical density (61, 62) or colour of test solutions or suspensions (63). The other technique (calorimetry-photometry) measures photon production inside the calorimetric vessel by adapting it with a fibre optic light guide to conduct photons into an external photometer. This technique can be used to study the metabolism of luminescent bacteria (64, 65).

During the eighties, there was a fast development of photocalorimetry in the field of material sciences with most of the studies focusing on the investigation of photopolymerisation, photodegradation of UV curable solid materials, characterisation of thin films, etc (66-68). The majority of photocalorimetric designs were built from differential scanning calorimeters (DSC) adapted with quartz windows or light guides to direct light into the sample. Also, during this decade, new "non-classical"

70

photocalorimetric methods emerged for the study of short-lived species. Pyroelectric photocalorimetry (69), photoacoustic spectroscopy (70) or laser calorimetry (71) are some examples of those techniques.

From the early nineties until present, the number of new applications of photocalorimetry did not increase much and most of the progress came from the development of more robust and sensitive instruments. Thermopile heat conduction microcalorimeters, such as the TAM (ThermoMetric AB, Jarfalla, Sweden) (72), started to be used in photocalorimetric studies instead of the DSC-type photocalorimeters. The TAM is a much more sensitive and versatile instrument compared to normal DSCs and the fact that it can incorporate different types of vessels, such as steel ampoules, perfusion-titration vessels, etc, makes it an extremely suitable measuring unit for photocalorimetric studies. Examples of photocalorimeters developed from TAM units are Wadso's photocalorimeter to study photosynthesis in plant tissue (73) and Mukhanov's LED-photocalorimeter used in the investigation of photosynthesis and respiration in *Dunaliella maritime* motile cells (74).

One of the most recent applications of photocalorimetry, and one that is extremely important in the context of this thesis, is the investigation of photostability issues in pharmaceuticals. The various aspects of its specific application in the field of pharmacy and the different instruments developed are described in the following section.

1.6.3. Application of photocalorimetry in the analysis of pharmaceuticals

As was mentioned before, photostability testing of medicines is an important requirement before authorization into market. Although the testing procedures are regulated by an ICH guideline, the current analytical methods used in photostability testing have several issues (previously described in section 1.3.2.) that preclude the unequivocal analysis of photodegradation processes. An alternative method with great potential for the investigation of photoreactions is calorimetry. This technique has several advantages compared to the traditional analytical methods and its specific application to the study of light induces process is called photocalorimetry.

The use of photocalorimetry in the analysis of photodegradation of drugs was first reported by Lehto et al in 1999 (3, 75). These authors developed an irradiation cell that can be used as an accessory for an isothermal microcalorimeter and tested its suitability

71

to detect photoreactivity in pharmaceutical solutions and solids. The cell was engineered to fit into the commercial 4 mL ampoule calorimetric unit of the isothermal heat conduction microcalorimeter TAM 2277 (former Thermometric AB, Sweden, now TA Instruments) which was first described by Wadso (72). Light was emitted by a 75 W Xe-arc lamp and introduced through a grating monochromator via focusing mirrors and a shutter. The beam was then split into two parts before entering two identical optical cables that were connected to the irradiation cell and, ultimately, to the hermetically sealed reaction vessel. During the actual measurement, two separate and technically identical irradiation cells were positioned in the sample sides of two twin calorimetric units. One of the irradiation cells was used with the photocalorimetric reaction vessel that gives the response to both the thermally active reactions and the absorption of light. The other one operated as a reference cell giving a response only to the radiant power. This arrangement allowed detection of fluctuations in the light intensity and the measurement of the amount of radiant energy reaching the sample vessel. The apparatus was used to study the photodegradation of nifedipine and L-ascorbic acid at different wavelengths and in different physical states. The method consisted of a quick and versatile way of investigating the photosensitivity of materials in any physical state and under different simulated conditions to mimic real storage conditions. Although detection of photodegradation signals was possible with that photocalorimeter, the determination of relevant quantitative data was still not possible. Apparently, the light intensity reaching the calorimetric vessels was not enough to allow complete analysis of the degradation processes within an acceptable time frame. According to the data presented in those papers (3, 75) the light power measured in the reference vessel was only of a few hundreds of µW. Moreover, most of the studies were performed using a wavelength scan program, therefore, precluding analysis of the long-term effect of single wavelengths on the degradation signal.

More recently, Morris built an instrument, based on Lehto's photocalorimetric design, for the qualitative and quantitative analysis of photodegradation processes occurring in pharmaceuticals (4). In this instrument, light was emitted by a high-intensity 300 W xenon arc lamp, passing through a monochromator before reaching the light guides. This allowed the investigation of the effect of selected wavelengths in the photodegradation of drugs. Light was then transmitted through a trifurcated bundle of optical fibres; two of those cables were inserted into the sample and the reference cells of a commercial twin isothermal heat conduction microcalorimeter, TAM, while the

third cable was connected to a spectroradiometer. This third cable allowed direct measurement of the radiant power reaching the ampoules in "real time", assuming that light was equally split between the three branches. All the light guides were contained within a stainless steel structure to ensure the optical cables were fixed in position relative to each other. This would avoid any changes in the orientation, shape and position of the cables minimizing, thus, the variations in light transmittance. Furthermore, well defined light guides were used to ensure that the optic cables were at a fixed distance apart to allow an easy and consistent entry into the calorimetric units. Figure 1.7. shows a picture of such photocalorimetric design.

FIGURE 1.7. : Morris' photocalorimeter (taken from (4)). A: lamp housing fitted with a 300 W Xe arc lamp; B: filter/lens assembly; C: plastic shrouding surrounding light guide; D: hand-wound lab jacks; E: optical cables lowered into TAM calorimetric unit. Note: monochromator not shown.

The photocalorimeter was designed to study pharmaceuticals' photoreactions in solution or in the solid state and determine the kinetic and thermodynamic parameters associated with those processes. The suitability of 2-nitrobenzaldehyde's photodegradation and potassium ferrioxalate photoreduction (a IUPAC recommended chemical calibrant) were investigated for validating the method for solution phase photodegradation. The photodegradation of nifedipine was also suggested as a calibrant in the solid-state.

The photocalorimeter developed by Morris, whilst useful to provide proof-of-concept data, was not ideal because it proved impossible to attain a zero signal for the baseline with and without irradiation of the ampoules. In fact, the combination of a highly

sensitive instrument like the TAM with a large mass of stainless steel containing the lighting system was rather challenging and initial tests showed baseline outputs to be arbitrary, therefore, making it difficult to determine any quantitative data.

Following Morris' work, Dhuna decided to implement some major modifications to the photocalorimetric design described above in order to obtain a more reliable and stable instrument (5). The first modifications aimed at improving the reproducibility of the baseline signal without light in the system and involved breaking the fixed geometry of the sample and reference ampoules. This would allow each one of them to be independently inserted into the TAM ensuring that the fit was adequately air tight. Modifications were also made to the various supporting lids surrounding the metal column which contained the fibre-optic cable. Having successfully dealt with the issue of the baseline stability with the light off, the next step was to obtain a zero baseline with the light on. Several reasons were thought for the differences in heat flow measured between the two channels during the irradiation period. The fibre-optic cable could be incorrectly positioned in the exit slit or it could be changing position during measurement. Differences in the beam's radiant power distribution after being split into the trifurcate fibre bundle could also explain the differences in the heat flux measured.

Two major changes were made in order to solve such problems; the trifurcated fibre bundle was replaced by a polka-dot optical beam splitter and the fibre-optic cables were replaced with liquid-filled light guides. The great advantage of using a beam splitter is the possibility to control the light intensity going to both vessels by intercalating a system of shutters and mirrors after the beam is split. A picture and a scheme of the photocalorimeter after these changes are shown in Figures 1.8.:
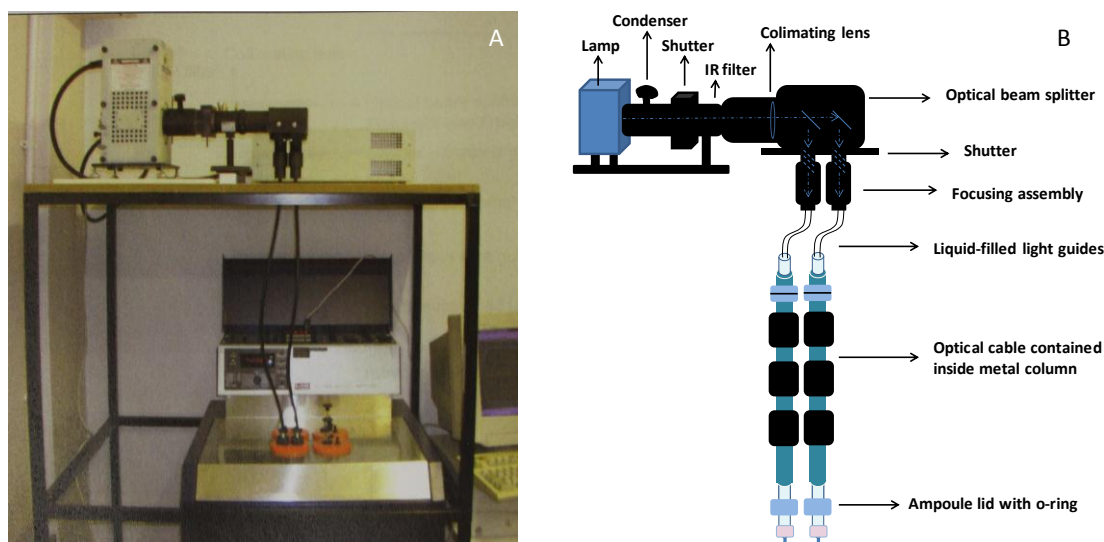
FIGURE 1.8. : Dhuna's photocalorimetric design after the initial modifications. A: Picture of the instrument; B: Scheme of the instrument (redrawn from (5)).

These changes resulted in a system that was stable enough to measure baseline signals near zero. Although these changes improved the instrument's performance greatly, a decline in the calorimetric signal was still observed over a short period of time as a result of the lamp's performance decaying with time. An alternative light source was thus considered to replace the powerful Xe-arc lamp. Light-emitting diodes (LEDs) were chosen to replace the widely used Xe lamps because of the advantages they offer over the latter. LEDs are a more suitable light source because they:

- have an extremely long life span;
- emit light in a narrow wavelength spectrum;
- are low-self heating;
- can be switched on and off very quickly and hence light up very quickly;
- do not suffer with problems associated with arc imaging/alignment and collimation of the light each time prior to the light being switched on;
- can achieve full brightness in a few microseconds whereas Xe lamps require a warm up period of at least one hour prior to sample exposure;
- are widely available in different intensities, shapes and sizes;
- are inexpensive compared to the cost of a Xe arc lamp.

Hence, the final design developed by Dhuna had an array of LEDs coupled to each liquid light guide going into the sample and reference ampoules, respectively (Figure 1.9.).
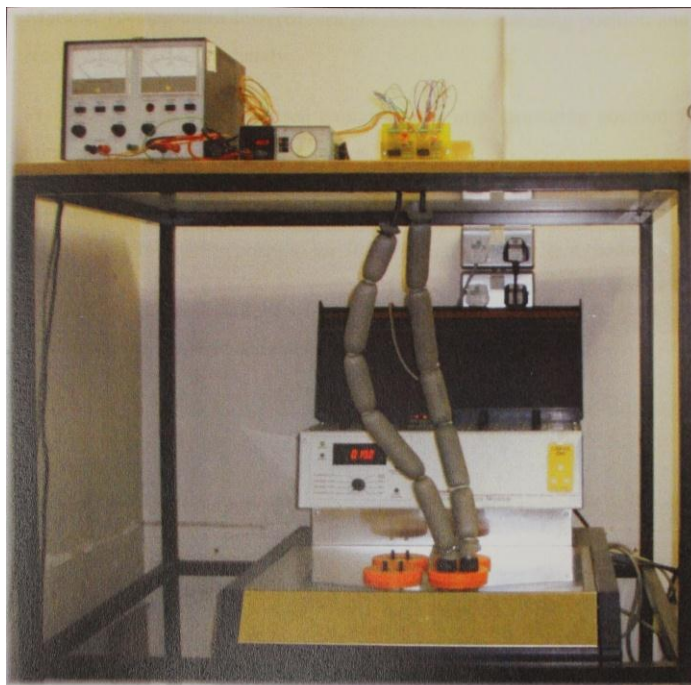
FIGURE 1.9. : Dhuna's final photocalorimetric design using LEDs as the light source.

Two separate arrays of LEDs were adapted to the light guides going into each ampoule and the intensity of light emitted by the bulbs was controlled electronically. It was therefore possible to adjust the light power going into each channel and zero the calorimetric signal before testing any photosensitive samples. Furthermore, the incorporation of an external circuit board with individual switches for each LED allowed different combinations of wavelengths to be tested as well as the investigation of causative wavelengths of degradation. An autobalance power supply was also being developed at that time, for the automatic zeroing of the calorimetric signal by increasing gradually the voltage applied to the reference side and maintaining the voltage applied to the sample side until reaching a zero baseline. Using this photocalorimeter, Dhuna performed actinometric studies with 2-nitrobenzaldehyde and studied the photodegradation of nifedipine in solution using different wavelengths (76). Despite these experiments proving that the instrument was suitable for the detection of photodegradation signals, the determination of quantitative parameters, such as the enthalpy of reaction or the rate constant, was still not possible. Most of the signals

recorded in those experiments were very small and constant with time which means that either the photodegradation of nifedipine was not very energetic or the rate of reaction was very slow. An increase in the light power reaching the sample would be beneficial, in this case, because it would lead to an increase in the rate of photoreaction and, thus, the heat measured per unit time.

Hence, the main objective of the work presented in this thesis was to re-design Dhuna's photocalorimeter and build an instrument that is capable of measuring large photoreaction signals that can be analysed quantitatively. Such instrument development works are described in Chapter 3 for two different photocalorimetric designs that use LEDs as the light source. One of the photocalorimeters was developed from an isothermal heat-conduction microcalorimeter (TAM 2277) while the other one used a Multi-Cell Differential Scanning Calorimeter (MCDSC) as the calorimetric unit. In turn, Chapters 4 and 5 describe the photodegradation studies performed with those two photocalorimeters using pharmaceutical preparations in solution and in the solid state, respectively. Before those photocalorimetric studies, Chapter 2 will address some of the underlying issues with calorimetric data analysis and present new methods that can be applied to the analysis of isothermal calorimetric data for zero-order kinetic processes in solution and solid state processes.

1.7. Summary

This thesis is primarily concerned with the development and application of photocalorimetry to study photochemical processes in pharmaceuticals. The current methods used in photostability testing of pharmaceuticals are not ideal because they separate irradiation of samples from analysis of the degradants which is problematic when the samples are affected by the preparation techniques used prior to analysis. Furthermore, the classical analytical techniques used in photostability testing (e.g. HPLC) can be time consuming and require extensive sample preparation. An alternative technique that offers many advantages over the classical analytical methods is calorimetry, the measurement of heat transfers occurring in a system. This technique does not depend on the specific properties of samples (e.g. the presence of a chromophore for detection with UV spectophotometric techniques), is invariant to physical form and allows continuous collection of degradation data "in situ". All these features render the use of thermal methods to monitor photochemical processes (photocalorimetry) particularly interesting in a pharmaceutical context. An example of pharmaceutical studies where the technique shows great potential is the investigation of causative wavelengths of degradation. The use of classical methods to study these wavelengths requires a series of experiments at each wavelength, which is extremely time consuming and hence will not be undertaken unless absolutely necessary. With photocalorimetry, these experiments can be undertaken in a fraction of the time which is a great advantage over the classical methods.

Despite the great potential of calorimetric techniques to investigate physicochemical processes, the issues related with analysis of calorimetric data are still one of the major drawbacks of the technique. Such analytical issues are even more relevant when it comes to the investigation of photochemical processes because these are usually very complex and dependent on a wide range of factors. For example, the kinetics of photodegradation of solid drugs depend on several physical properties that affect the absorption of light, such as the particle size, crystal modification (polymorphism), colour, thickness of powder bed and coating of the individual particles or the dosage form. Although such complex systems are still very difficult to study quantitatively, this project also aimed at developing new strategies of analysis of calorimetric data for simpler processes. Chapter 2 describes some of these strategies for the analysis of solid state processes and zero-order kinetics in solution.

The subsequent chapters will show the development works done on two different photocalorimetric designs (Chapter 3) and their application to the analysis of solution phase (Chapter 4) and solid state (Chapter 5) pharmaceutical preparations.

2. Analysis of isothermal calorimetric data

2.1. Introduction

The development and establishment of photocalorimetry in the various areas of analytical sciences has been accompanied throughout the years by an increase in the number of photocalorimetric designs and instrument adaptations built in response to the increasing demand for sensitivity and accuracy of the measurements performed. Although the design of an instrument or experimental plan is a crucial step in the development of a new analytical methodology, one should not underestimate the importance of data analysis in the successful development and establishment of such methods. The strategies used to analyse the experimental outcomes are, indeed, essential for the translation of those data into meaningful quantitative parameters and the success of the methodology is totally dependent on them.

In the specific case of photocalorimetry, the data analysis strategies required for the interpretation of data are similar to the ones used in any other isothermal calorimetric method. In Chapter 1 several equations were described for the analysis of such data for a wide range of kinetic processes that vary from simple first-order kinetic events to more complex simultaneous or consecutive processes occurring in the solution phase. Some equations were also presented for the calorimetric analysis of solid state processes but this area still needs further investigation. Despite the comprehensive set of equations available in the literature for the analysis of isothermal calorimetric data, there are still two cases of processes where the analytical strategies at our disposal are insufficient and need further development. These are the analysis of processes in samples in the solid state and the investigation of zero-order kinetics in solution. The lack of strategies to analyse these two processes constitutes an important gap in the existing set of calorimetric tools and, thus, urgently needs to be addressed. This issue is particularly important in the context of photostability testing of pharmaceuticals because most of the pharmaceutical formulations in the market are in the solid state (tablets, powders, etc.) and even if they are prepared in solution there is a chance that photodegradation follows zero-order kinetics if the appropriate light exposure conditions are met (77).

This chapter will, therefore, focus on the development of strategies that can be used to analyse quantitatively solid sate processes and zero-order reactions in solution using isothermal calorimetric data. The work presented here was published in two papers in the Journal of Physical Chemistry B (78, 79).

2.2. Analysis of solid state calorimetric data

Isothermal microcalorimetry is a particularly useful technique for studying solid-state processes, because almost invariably such complex events will progress with changes in enthalpy. In addition, the physical form of the sample has no bearing on the operation of the instrument, and the environmental factors, such as temperature and relative humidity, are easy to control. Data analysis can present a challenge, however, especially if the reaction has not progressed to completion or multiple processes are occurring.

The kinetics of solid-state processes are usually described by expressions cast in terms of fraction of reaction (α). Hence, if data are plotted against α, analysis is straightforward using any of the multitude of models available in the literature (30, 33). From the perspective of calorimetric data, conversion of data to α is easy if the total enthalpy of the process (Q) is known:

$$\alpha = \frac{q}{Q}$$

Equation 2.1.

where q is the heat output to time t. The analysis of this kind of data and the determination of reaction parameters was previously discussed for solid state data where Q is available (43, 80) and for several kinetic processes occurring in solution (39, 81, 82). However, while calorimetry is extremely well suited to the study of solid-state processes, it is highly likely that only partial data will be available. If the process is reasonably fast, the initial data will be missing (a consequence of the time required to prepare and load the sample in the ampoule, external to the calorimeter), and if the process is very slow, data may not have returned to baseline within an acceptable period of time. In either case it is not possible to determine the value of Q by simple integration of the data, and hence conversion to α is impossible.

An alternative approach is to fit the data to a suitable model, using least-squares minimization, to determine the values of all reaction parameters, including Q. This approach was used in previous works (39, 43, 80-82), but it is only applicable in cases where the fitting model can be integrated with respect to time. Several solid-state models, however, cannot be integrated with respect to time (e.g. most crystallization processes) and hence cannot be cast in a form that describes power-time data. Consideration of these issues, thus, led to the development of a series of mathematical

strategies that allow a more comprehensive analysis of this kind of process. These will be discussed in detail in this part of the chapter.

The equation that will be used as the basis for all mathematical treatments is that suggested by Pérez-Maqueda et al. (33), which is an adaptation of the Ng equation (32):

$$\frac{\mathrm{d}\alpha}{\mathrm{d}t} = k.\,\alpha^m.\,(1-\alpha)^n \qquad \text{Equation 2.2.}$$

where $\mathrm{d}\alpha/\mathrm{d}t$ is the rate of reaction, k is the rate constant and m and n are the mechanism descriptors. Data that conform to this equation will progress through a maximum (assuming that the values of m and n are greater than 0) and the position of that maximum with respect to the α-axis is dependent upon the values of m and n. The determination of α where the rate of reaction is maximum (α_{peak}) can, thus, be very useful in the assignment of a solid-state model.

Substitution of Equation 2.1. into Equation 2.2. and rearrangement gives a calorimetric form of the kinetic expression:

$$\frac{\mathrm{d}q}{\mathrm{d}t} = \Phi = k.\,Q.\,\alpha^m.\,(1-\alpha)^n \qquad \text{Equation 2.3.}$$

Although this equation cannot be used to analyse isothermal calorimetric data (in the form of thermal power *vs* time) it constitutes the basic calorimetric equation for all the mathematical treatments described throughout this section.

Firstly, two strategies will be presented for the simulation of power-time data for processes in the solid state using Equation 2.3. After that, some equations will be described for the determination of α_{peak} and for the calculation of the total heat output (Q) using only 3 data points. Finally 3 methods will be presented for the determination of all solid-state parameters (k, Q, m and n) using only partial calorimetric data. The validity of these 3 approaches will then be demonstrated using simulated data. Application to real data is also demonstrated, using the crystallization of indomethacin from an amorphous glass as a model solid-state process.

2.2.1. Simulation of solid state calorimetric data

The use of simulated data to test the validity of analytical methods is of great importance because these are free from random noise and other errors and the values of the variables describing the process are known absolutely. However, generation of simulated power-time data from the Pérez-Maqueda equation and similar models has proved impossible to date because the function cannot be directly integrated. Previous work by O'Neill (43) used simulated power-heat data (Φ vs q) to evaluate the theoretical solid state models developed at the time. Simulation of this kind of data is straightforward if Equation 2.3. is used, after replacing α by q/Q.:

$$\frac{\mathrm{d}q}{\mathrm{d}t} = \Phi = k.Q.\left(\frac{q}{Q}\right)^m.\left(1 - \frac{q}{Q}\right)^n \qquad \text{Equation 2.4.}$$

If the variables in that equation are given selected values, it is easy to simulate Φ-q data using computer dedicated software like Mathcad. Figure 2.1. shows an example of simulated Φ-q calorimetric data using the following parameters: $Q = 1\times10^9$ µJ, $k = 3\times10^{-7}$ s^{-1}, $m = 0.75$, $n = 0.625$.
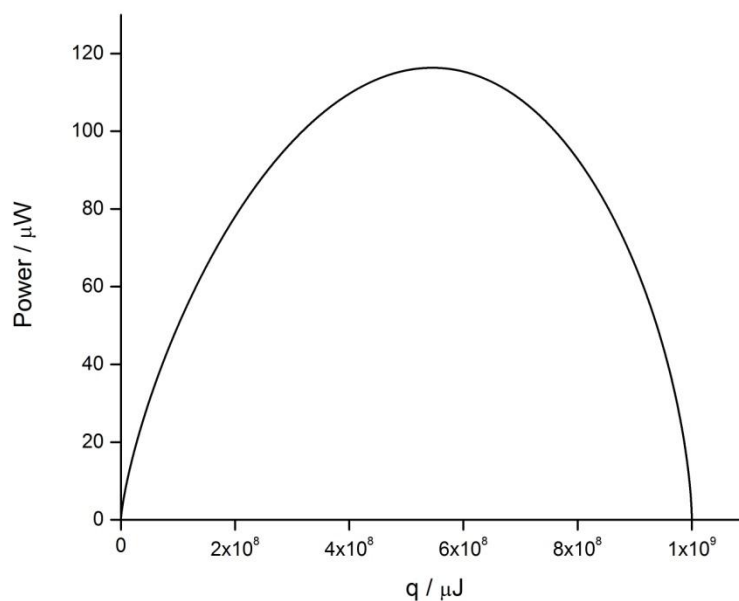
FIGURE 2.1. : Simulated Φ-q data using the parameters $Q=1\times10^9$ µJ, $k=3\times10^{-7}$ s^{-1}, $m=0.75$, $n=0.625$.

Although the simulation of power-heat data can be useful in some cases it is not ideal in isothermal calorimetric studies since heat-conduction and power-compensation calorimeters record data in the form of thermal power versus time. For this reason, two methods are suggested here for the simulation of power-time data for solid state processes studied calorimetrically.

Method A

This first method is based on the mathematical "Method of the Rectangles" for the approximate determination of an area under a curve. If the space below the curve is divided into several rectangles with known heights (given by the values of the function) and known widths (dividing the time axis by a number N of rectangles), it is then possible to calculate the area for each rectangle and, subsequently, the approximate area under the curve after summing up the areas calculated for all rectangles.

Simulation of thermal power versus time data, however, requires a slightly different approach since the aim is to determine the time-axis after assigning a defined value for the total area under the curve (Q). The strategy followed in this method considers, instead, that the space below the curve is occupied by several rectangles with the same area (q), obtained after dividing Q by N (number of rectangles within this space), but different heights (given by the values of the Φ function) and widths (different time intervals) as Figure 2.2. shows:
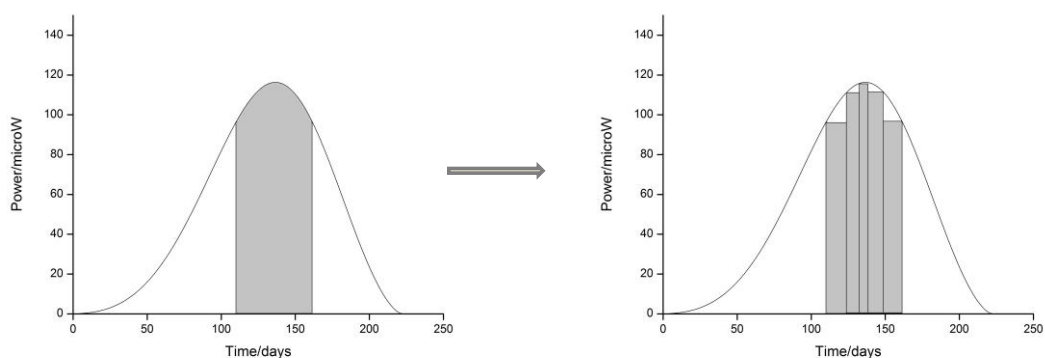
FIGURE 2.2. : Adaptation of the "Rectangle Method" for the determination of the time-axis.

The first step in this methodology corresponds to the establishment of a fixed value for the rectangles' areas (q). After that, some values are assigned to all parameters in Equation 2.3., and the height of each rectangle (Φ) is determined by varying α (from 0

to 1) in that same equation. The increments in α that are used in this simulation are also fixed and equal to q/Q. The time intervals associated with each rectangle are then calculated using Equation 2.5. and the time-axis is built after cumulative sum of all these parcels.

$$\mathrm{d}t = \frac{\mathrm{d}q}{\Phi} \qquad\qquad \text{Equation 2.5.}$$

Method B

This second method uses mathematical rearrangements of Equation 2.4. to determine the time-axis in a thermal power versus time plot. That equation is, first, rearranged to its inverse as shown below:

$$\frac{\mathrm{d}t}{\mathrm{d}q} = \frac{1}{k.Q.\left(\frac{q}{Q}\right)^m.\left(1 - \frac{q}{Q}\right)^n} \qquad\qquad \text{Equation 2.6.}$$

If the integral of this equation is taken with respect to q, Equation 2.7. is obtained. This new expression allows the determination of the time-axis in a power-time graph:

$$\int \frac{\mathrm{d}t}{\mathrm{d}q}\,\mathrm{d}q = t = \int \frac{1}{k.Q.\left(\frac{q}{Q}\right)^m.\left(1 - \frac{q}{Q}\right)^n}\,\mathrm{d}q \qquad\qquad \text{Equation 2.7.}$$

This integral is, however, not possible to be cast in the form of a simple mathematical equation and, hence, no solid-state calorimetric equation was ever described as a function of time. In spite of this, the graphical determination of the time axis can still be done by, first, simulating data in *Mathcad* for $1/\Phi$ (increasing q gradually in Equation 2.6. up to Q), followed by graphical integration of a plot of $(1/\Phi)$ *vs* q using the integration function in the *Origin* software (Figure 2.3.). The partial integration results will, thus, form the time-axis of the graph and allow power-time data to be plotted after pairing with the corresponding power values.

	A(X)	B(Y)	C(Y)	D(Y)	E(Y)
Long Name	q	1/P	Integrated Y1	Time	Power
Units	J	W^{-1}	s	days	microW
Comments			Mathematical Integral Area of B"1/P"		
1	10000	18.74483	0	0	0.05335
2	20000	11.14581	149453.2	1.72978	0.08972
3	30000	8.2233	246298.73	2.85068	0.12161
4	40000	6.62742	320552.32	3.7101	0.15089
5	50000	5.60615	381720.185	4.41806	0.17838
6	60000	4.88969	434199.405	5.02546	0.20451
7	70000	4.35586	480427.185	5.5605	0.22958
8	80000	3.94079	521910.435	6.04063	0.25376
9	90000	3.60762	559652.49	6.47746	0.27719
10	100000	3.33354	594358.32	6.87915	0.29998
11	110000	3.10359	626543.97	7.25167	0.32221
12	120000	2.90754	656599.6	7.59953	0.34393
13	130000	2.73815	684828.015	7.92625	0.36521
14	140000	2.59013	711469.365	8.2346	0.38608
15	150000	2.45952	736717.61	8.52682	0.40658
16	160000	2.34332	760731.845	8.80477	0.42674
17	170000	2.23919	783644.24	9.06996	0.44659

◄ ► Sheet1 /

FIGURE 2.3. : Simulated data for a solid-state process with the following parameters using Method B: $Q=1\times10^9$ µJ, $k=3\times10^{-7}$ s^{-1}, $m=0.75$, $n=0.625$ (picture taken from Origin Software).

The two methods described above were used to simulate power-time data for a solid-state process with the following parameters: $Q=1\times10^9$ µJ, $k=3\times10^{-7}$ s^{-1}, $m=0.75$, $n=0.625$. Plotting of both sets of data on the same graph (Figure 2.4.) clearly shows an overlap of both calorimetric signals which proves that the two methods produce similar outcomes.
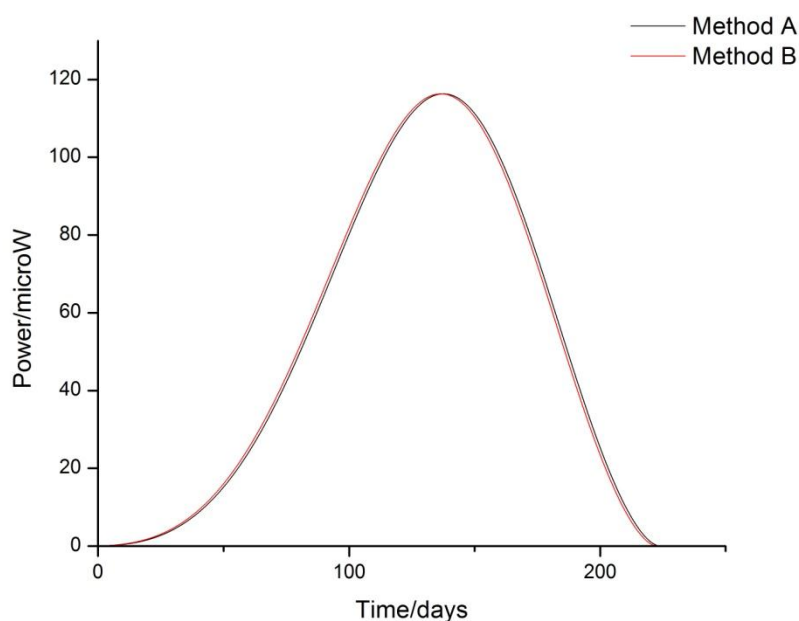
FIGURE 2.4. : Graph showing simulated power-time data using Methods A and B.

2.2.2. Determination of α_{peak} in solid state processes

The fraction of solid that reacted at the time where the process reaches its maximum rate of convertion (α_{peak}) is an important parameter in the analysis of solid state reactions that show an accelerating period followed by a decelerating phase (when both m and n in Equation 2.4. are different from 0). Not only is α_{peak} indicative of the predominance and extent of each period in the overall process (e.g. if α_{peak} is high, the accelerating period is predominant), but also, it constitutes a very good solid-state model descriptor since its value only depends on the mechanism of reaction observed. This dependence was demonstrated by Ng (32) with an equation (Equation 2.8.) for the determination of α_{peak} using only the reaction mechanism descriptors.

$$\alpha_{peak} = (1-p)/(2-p-q) \qquad \text{Equation 2.8.}$$

where p and q are the mechanism descriptors in Ng's solid state equation. Although this equation was described for that specific model, it can also be applied to that used in our calorimetric studies (Equation 2.3.) as will be demonstrated below.

It was previously mentioned that α_{peak} corresponds to the fraction of solid that reacted when the reaction reaches its maximum rate for a solid state process that has both accelerating and decelerating phases. This means that, if the rate of reaction ($d\alpha/dt$) is plotted against α for such processes, it is possible to determine α_{peak} by determining the point in the graph where the slope of the tangent to the curve at that point is equal to zero (i.e. the point where the derivative is zero). The same strategy can be used if thermal power (dq/dt) is plotted against α, both sets of data going through a maximum at the same α_{peak} value.

The first challenge was, therefore, to find a mathematical expression for the derivative of Equation 2.3. with respect to α so that the maximum could be determined. To date, and to our knowledge, no one ever found the derivative for this calorimetric equation, despite its determination being easy if the adequate derivatisation rules are applied. If Equation 2.3. is rearrange in such way that it is presented as the product of two functions (v and u) the following derivatisation rule can be used:

$$\frac{dq}{dt} = [k.Q.\alpha^m].[(1-\alpha)^n]$$

Equation 2.9.

$$\underbrace{}_{u}\underbrace{}_{v}$$

Derivatisation rule:

$$\boxed{\frac{d(u.v)}{d\alpha} = v.\frac{du}{d\alpha} + \frac{dv}{d\alpha}.u}$$

Equation 2.10.

Derivatisation of equation 2.3. with respect to α, hence, results in the following equations:

Equation 2.11.

$$\frac{d^2q}{dt.d\alpha} = (k.Q.\alpha^m).[-n.(1-\alpha)^{n-1}] + (1-\alpha)^n.(k.Q.m.\alpha^{m-1})$$

$$\frac{d^2q}{dt.d\alpha} = (k.Q.\alpha^m).\left[-n.\frac{(1-\alpha)^n}{(1-\alpha)}\right] + (1-\alpha)^n.k.Q.m.\frac{\alpha^m}{\alpha}$$

Equation 2.12.

$$\frac{d^2q}{dt.d\alpha} = k.Q.(1-\alpha)^n.\alpha^m.\left[\frac{-n}{(1-\alpha)} + \frac{m}{\alpha}\right]$$

Equation 2.13.

Equation 2.13. can ultimately be rearranged to an expression that includes d*q*/d*t* by replacing Equation 2.3. in that equation:

$$\frac{d^2q}{dt.d\alpha} = \frac{dq}{dt}.\left[\frac{-n}{(1-\alpha)} + \frac{m}{\alpha}\right]$$

Equation 2.14.

The same strategy can be used to determine the derivative of d*α*/d*t* with respect to *α*:

$$\frac{d^2\alpha}{dt.d\alpha} = \frac{d\alpha}{dt}.\left[\frac{-n}{(1-\alpha)} + \frac{m}{\alpha}\right]$$

Equation 2.15.

Although either of these two equations (2.14. and 2.15.) can be used to calculate α_{peak}, only Equation 2.14 will be used in these mathematical treatments. The derivative of thermal power (dq/dt) with respect to α can, thus, be made equal to zero to determine the fraction of solid that reacted until maximum thermal power is reached:

$$\frac{\mathrm{d}^2\alpha_{peak}}{\mathrm{d}t.\,\mathrm{d}\alpha} = \left(k.\,\alpha_{peak}{}^m\right).\left[-n.\frac{\left(1-\alpha_{peak}\right)^n}{\left(1-\alpha_{peak}\right)}\right]$$
$$+ \left(1-\alpha_{peak}\right)^n.\,k.\,m.\frac{\alpha_{peak}{}^m}{\alpha_{peak}} = 0$$

<div align="right">Equation 2.16.</div>

$$\left(k.\,\alpha_{peak}{}^m\right).\left[-n.\frac{\left(1-\alpha_{peak}\right)^n}{\left(1-\alpha_{peak}\right)}\right] = -\left(1-\alpha_{peak}\right)^n.\,k.\,m.\frac{\alpha_{peak}{}^m}{\alpha_{peak}}$$

<div align="right">Equation 2.17.</div>

$$\frac{n}{\left(1-\alpha_{peak}\right)} = \frac{m}{\alpha_{peak}}$$

<div align="right">Equation 2.18.</div>

$$\alpha_{peak} = \frac{m}{n+m}$$

<div align="right">Equation 2.19.</div>

As Equation 2.19. shows, the determination of α_{peak} only requires that the mechanism descriptors m and n are known. This equation is similar to the one reported by Ng (Equation 2.8.) for the determination of α_{peak}, the difference being that, 1-p and 1-q are used instead of m and n. The fact that only the mechanism descriptors are used in its determination makes α_{peak} a very useful parameter in the characterization of solid state models, helping in the assignment of reaction models to solid state processes. Table 2.1. shows a list of solid state parameters, including α_{peak}, for a series of models studied by Ng.

TABLE 2.1. : Solid state parameters for the different models studied by Ng.

Solid state model	M	n	α_{peak}
Modified Prout-Tompkins	1-1/k	1+1/k	0.5-0.5k
Roginskii-Shultz	0.670	0.670	0.500
Erofeev (N=2)	0.500	0.770	0.394
Erofeev (N=3)	0.670	0.700	0.489
Erofeev (N=4)	0.750	0.660	0.532
Erofeev (N=5)	0.800	0.640	0.556
Avrami ($k_1t{\geq}1$)	0.670	0.670	0.500
Avrami ($k_1t{\leq}1$)	0.750	0.625	0.545
Avrami ($k_1t{\approx}1$)	0.730	0.680	0.518

2.2.3. Determination of Q using q_{peak}

The determination of the total heat output (Q) for a solid state process, studied calorimetrically, may not always be possible for the reasons mentioned earlier. If the process is too quick, data may be missing as a consequence of the time required to prepare the sample and load it into the calorimetric system, as well as, the time taken for the sample to equilibrate to the instrument's temperature. In the opposite extreme, if the process is too slow, the time frame for data collection may not be acceptable and only partial data is recorded. The following mathematical treatments, therefore, aim to develop a strategy to determine Q using only partial data. This strategy, however, only applies to data where the final portion is missing, meaning that, it is essential that data is recorded from the processes' early stages.

The first step in this analysis involves determining the ratio between the two solid state mechanism descriptors, m and n. This ratio can be determined by selecting two data points with the same thermal power in a plot of Φ versus time (considering that data progresses through a maximum):

For $t=t_1$

$$\Phi_1 = k.Q.\left(\frac{q_1}{Q}\right)^m \cdot \left(1 - \frac{q_1}{Q}\right)^n$$

<div align="right">Equation 2.20.</div>

For $t=t_2$

$$\Phi_2 = k.Q.\left(\frac{q_2}{Q}\right)^m \cdot \left(1 - \frac{q_2}{Q}\right)^n$$

<div align="right">Equation 2.21.</div>

where $\Phi_1 = \Phi_2$ and q_1 and q_2 are the heat outputs at times t_1 and t_2, respectively. Equations 2.20. and 2.21. can, thus, be equated to give:

$$\left(\frac{q_1}{Q}\right)^m \cdot \left(1 - \frac{q_1}{Q}\right)^n = \left(\frac{q_2}{Q}\right)^m \cdot \left(1 - \frac{q_2}{Q}\right)^n$$

<div align="right">Equation 2.22.</div>

$$\left(\frac{Q - q_1}{Q - q_2}\right)^n = \left(\frac{q_2}{q_1}\right)^m$$

<div align="right">Equation 2.23.</div>

After taking the logarithms in Equation 2.23., the following expression is obtained:

$$\frac{n}{m} = \frac{\ln\left(\frac{q_2}{q_1}\right)}{\ln\left(\frac{Q - q_1}{Q - q_2}\right)}$$

<div align="right">Equation 2.24.</div>

Equation 2.19., itself, can also be rearranged to show the ratio between the descriptors m and n. First, that equation needs to be cast in a form that allows calorimetric data to be used, replacing α_{peak} by (q_{peak}/Q) in that expression:

$$\frac{q_{peak}}{Q} = \frac{m}{n + m}$$

<div align="right">Equation 2.25.</div>

Rearrangement of this equation gives:

$$\frac{n}{m} = \frac{Q - q_{peak}}{q_{peak}}$$

<div align="right">Equation 2.26.</div>

If Equations 2.24. and 2.26. are combined, a new expression is derived with Q as the only unknown:

$$Q = \frac{q_{peak} \cdot \ln\left(\frac{q_2}{q_1}\right)}{\ln\left(\frac{Q - q_1}{Q - q_2}\right)} - q_{peak}$$

Equation 2.27.

Despite displaying Q as the only unknown, Equation 2.27. cannot be solved easily since it is not possible to separate this variable from the rest of the equation. An alternative strategy for its determination consists of subtracting the two sides of Equation 2.27. and varying Q within an acceptable range of values, until that difference becomes zero. This approximate determination can be done using Mathcad, after simulation of a series of values for Q and determination of the value that makes the residual, R, in Equation 2.28., equal to zero.

$$Q - \left(\frac{q_{peak} \cdot \ln\left(\frac{q_2}{q_1}\right)}{\ln\left(\frac{Q - q_1}{Q - q_2}\right)} - q_{peak}\right) = R$$

Equation 2.28.

The validity of this approach was demonstrated with reference to simulated data, using the same set of data produced in section 2.2.1. ($Q=1 \times 10^9$ μJ, $k=3 \times 10^{-7}$ s^{-1}, $m=0.75$, $n=0.625$). A value of 9.9996×10^8 μJ was calculated for Q using the parameters listed below:

$q_{peak} = 5.4545 \times 10^8$ μJ $\qquad$ $q_1 = 2.0858 \times 10^8$ μJ $\qquad$ $q_2 = 8.5422 \times 10^8$ μJ

$\phi_{peak} = 116.3$ μW $\qquad$ $\phi_1 = 80.0$ μW $\qquad$ $\phi_2 = 80.0$ μW

Comparision with the value used in the simulation process, 1×10^9 μJ, demonstrates the validity of this method for the determination of Q for processes where the final portion of data is missing.

2.2.4. Development of three methods for the direct determination of all solid state reaction parameters using only partial calorimetric data

Knowledge of the total heat output (Q) for a solid state process is essential in the analysis of isothermal calorimetric data because it allows conversion of the time axis of data to α hence enabling the remaining reaction parameters in Equation 2.3. to be determined. Two different methods can be used for the determination of such parameters. One of them consists of using least-squares minimization techniques to fit the data to a solid state model, while the other is the method described by Willson and Beezer (41) for the determination of m and n using a technique of data pairing. Although both methods are valid for the calculation of such parameters, they are indirect analytical techniques that return an approximate solution for the unknowns in a system. Furthermore, the data pairing method is not free from assumptions.

In this context, 3 new methods are presented for the direct determination of Q and the two reaction mechanism descriptors, m and n, using only partial data. These methods were developed for the general case of processes that show an accelerating phase followed by a decelerating phase, i.e., processes that go through a maximum rate of reaction. After calculating those parameters, determination of the rate constant, k, is straightforward using Equation 2.3. Compared with the model fitting approach, the strategies shown here are in principle much easier to use, requiring the analyst only to select a few data points and introduce them into the equations presented. The 3 methodologies developed are appropriate for the analysis of data where one of the following situations occurs:

- The initial data are missing, but the process has progressed to completion (*Method 1*).
- The initial data are captured, but the process has not progressed to completion (*Method 2*).
- Neither the initial nor final data are captured, but the data progressed through a maximum (*Method 3*).

The validity of these approaches will be demonstrated with reference to simulated data and an example of their application to the analysis of real data will also be given, using the crystallization of indomethacin from a glass as a model solid-state process.

2.2.4.1. Method 1

This strategy was developed for the analysis of calorimetric data for processes where the initial part of data is missing but, still, it progressed to completion. It is thus evident that the time at which the power signal returns to zero denotes the end of reaction (the point at which α=1). Selection of any earlier time (t_1) and corresponding power (Φ_1) allows a partial area (q_1) to be determined.
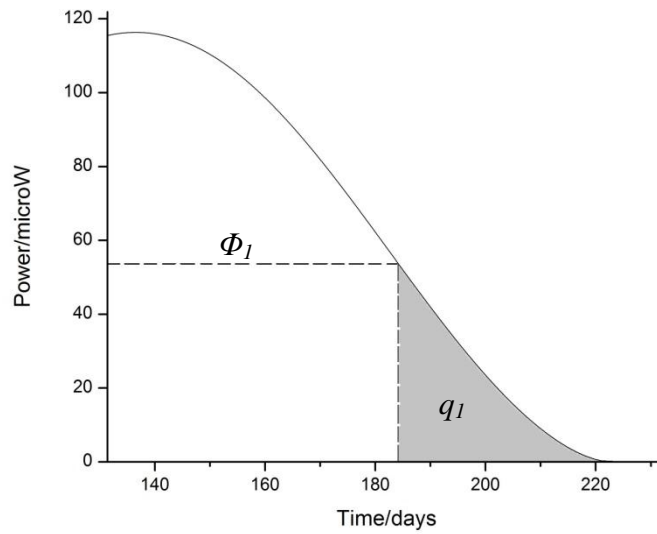
FIGURE 2.5. : Graph showing q_1 considering the last portion of data.

Substitution of those values into Equation 2.4. yields:

$$\Phi_1 = k.Q.\left(\frac{Q-q_1}{Q}\right)^m . \left(1 - \frac{Q-q_1}{Q}\right)^n \qquad \text{Equation 2.29.}$$

Similar equations can be constructed for three other randomly selected time points:

$$\Phi_2 = k.Q.\left(\frac{Q-q_2}{Q}\right)^m . \left(1 - \frac{Q-q_2}{Q}\right)^n \qquad \text{Equation 2.30.}$$

$$\Phi_3 = k.Q.\left(\frac{Q-q_3}{Q}\right)^m.\left(1-\frac{Q-q_3}{Q}\right)^n \qquad \text{Equation 2.31.}$$

$$\Phi_4 = k.Q.\left(\frac{Q-q_4}{Q}\right)^m.\left(1-\frac{Q-q_4}{Q}\right)^n \qquad \text{Equation 2.32.}$$

If the following are defined for clarity:

$$\log\left(\frac{\Phi_1}{\Phi_2}\right) = \log(R_1) \qquad \text{Equation 2.33.}$$

$$\log\left(\frac{\Phi_1}{\Phi_3}\right) = \log(R_2) \qquad \text{Equation 2.34.}$$

$$\log\left(\frac{\Phi_1}{\Phi_4}\right) = \log(R_3) \qquad \text{Equation 2.35.}$$

Then, there are three equations and three unknown variables. By substitution and rearrangement of Equations 2.33., 2.34. and 2.35. the following expressions are obtained for the calculation of Q, m and n:

$$\frac{\log R_2 . \log\left(\frac{q_1}{q_2}\right) - \log R_1 . \log\left(\frac{q_1}{q_3}\right)}{\log\left(\frac{q_1}{q_2}\right) . \log\left(\frac{Q-q_1}{Q-q_3}\right) - \log\left(\frac{q_1}{q_3}\right) . \log\left(\frac{Q-q_1}{Q-q_2}\right)}$$
$$- \frac{\log R_3 . \log\left(\frac{q_1}{q_2}\right) - \log R_1 . \log\left(\frac{q_1}{q_4}\right)}{\log\left(\frac{q_1}{q_2}\right) . \log\left(\frac{Q-q_1}{Q-q_4}\right) - \log\left(\frac{q_1}{q_4}\right) . \log\left(\frac{Q-q_1}{Q-q_2}\right)} = 0 \qquad \text{Equation 2.36.}$$

$$m = \frac{\log R_3 \cdot \log\left(\frac{q_1}{q_2}\right) - \log R_1 \cdot \log\left(\frac{q_1}{q_4}\right)}{\log\left(\frac{q_1}{q_2}\right) \cdot \log\left(\frac{Q - q_1}{Q - q_4}\right) - \log\left(\frac{q_1}{q_4}\right) \cdot \log\left(\frac{Q - q_1}{Q - q_2}\right)}$$

<div align="right">Equation 2.37.</div>

$$n = \frac{\log R_2 - m \cdot \log\left(\frac{Q - q_1}{Q - q_3}\right)}{\log\left(\frac{q_1}{q_3}\right)}$$

<div align="right">Equation 2.38.</div>

The determination of m and n using Equations 2.37. and 2.38., is only possible if Q is first calculated. Although Q is the only unknown in equation 2.36., its determination is not straightforward because it cannot be isolated from that expression. A similar approach to the one used for its determination in section 2.2.3. can, thus, be followed, by varying Q in the left side of Equation 2.36. until it equals the right side. The parameters m and n can then be easily determined in succession leaving k as the only unknown in Equation 2.4. which can then be easily solved.

2.2.4.2. Method 2

The following strategy was developed to deal with solid state calorimetric data where the final part of data is missing. Progression through a maximum is, nevertheless, required in order for the correct values to be returned. This maximum corresponds to the time point where the slope of the tangent to the curve is equal to zero ($d^2q/(dt)^2=0$). This approach starts with the rearrangement of Equation 2.14.:

$$\frac{d^2q}{dt \cdot d\alpha} = \frac{dq}{dt} \cdot \left[\frac{-n}{(1 - \alpha)} + \frac{m}{\alpha}\right]$$

<div align="right">Equation 2.14.</div>

To give:

$$\frac{d^2q}{dt} = \frac{dq \cdot \frac{dq}{Q}}{dt} \cdot \left[\frac{-n}{(1 - \alpha)} + \frac{m}{\alpha}\right]$$

<div align="right">Equation 2.39.</div>

$$\frac{d^2q}{dt \cdot dt} = \frac{dq \cdot dq}{dt \cdot dt} \cdot \frac{\left[\frac{-n}{(1-\alpha)} + \frac{m}{\alpha}\right]}{Q}$$

Equation 2.40.

$$\frac{d^2q}{(dt)^2} = \left(\frac{dq}{dt}\right)^2 \cdot \frac{\left[\frac{-n}{(1-\alpha)} + \frac{m}{\alpha}\right]}{Q}$$

Equation 2.41.

$$\frac{d^2q}{(dt)^2} = \left(\frac{dq}{dt}\right)^2 \cdot \frac{\left[\frac{-n \cdot Q}{(Q-q)} + \frac{m \cdot Q}{q}\right]}{Q}$$

Equation 2.42.

$$\frac{d^2q}{(dt)^2} = \left(\frac{dq}{dt}\right)^2 \cdot \left[\frac{-n}{(Q-q)} + \frac{m}{q}\right]$$

Equation 2.43.

If three power-time points (dq/dt) are selected with three corresponding tangents ($d^2q/(dt)^2$), then:

$$\frac{d^2q_1}{(dt_1)^2} = \left(\frac{dq_1}{dt_1}\right)^2 \cdot \left[\frac{-n}{(Q-q_1)} + \frac{m}{q_1}\right]$$

Equation 2.44.

$$\frac{d^2q_2}{(dt_2)^2} = \left(\frac{dq_2}{dt_2}\right)^2 \cdot \left[\frac{-n}{(Q-q_2)} + \frac{m}{q_2}\right]$$

Equation 2.45.

$$\frac{d^2q_3}{(dt_3)^2} = \left(\frac{dq_3}{dt_3}\right)^2 \cdot \left[\frac{-n}{(Q-q_3)} + \frac{m}{q_3}\right]$$

Equation 2.46.

Letting:

$$A = \frac{d^2q_1}{(dt_1)^2}$$

Equation 2.47.

$$B = \left(\frac{dq_1}{dt_1}\right)^2$$

$$C = \frac{d^2 q_2}{(dt_2)^2}$$

$$D = \left(\frac{dq_2}{dt_2}\right)^2$$

$$E = \frac{d^2 q_3}{(dt_3)^2}$$

$$F = \left(\frac{dq_3}{dt_3}\right)^2$$

By substitution and rearrangement of Equations 2.44., 2.45. and 2.46., it is possible to solve for Q directly:

$$Q = \frac{\frac{A.F}{B}.(q_1{}^2.q_2 - q_1{}^2.q_3) + \frac{C.F}{D}.(q_2{}^2.q_3 - q_2{}^2.q_1) + E.(q_3{}^2.q_1 - q_3{}^2.q_2)}{\frac{A.F}{B}.(q_1.q_2 - q_1.q_3) + \frac{C.F}{D}.(q_2.q_3 - q_2.q_1) + E.(q_3.q_1 - q_3.q_2)}$$

Once the value of Q is known, the values of m and n may be calculated:

$$m = \frac{\frac{A}{B}.q_1.q_2 - \frac{A}{B.Q}.q_1{}^2.q_2 + \frac{C}{D.Q}.q_2{}^2.q_1 - \frac{C}{D}.q_2.q_1}{q_2 - q_1}$$

$$n = \frac{\frac{A}{B}.(q_1.Q - q_1{}^2 - q_1.q_2) - [\frac{C}{D}.(q_2.Q - q_2{}^2 - q_1.q_2)] + \frac{A}{B.Q}.q_1{}^2.q_2 - \frac{C}{D.Q}.q_2{}^2.q_1}{q_2 - q_1}$$

<div align="right">Equation 2.55.</div>

After calculation of all these parameters, the rate constant, k, can be easily determined using Equation 2.4. for a single data point.

2.2.4.3. *Method 3*

This strategy assumes that neither the initial nor final data have been captured, but that the reaction has progressed through a maximum ($d^2q/(dt)^2=0$). This condition makes it impossible to calculate Q using *Method 2* because determination of q at different time points requires data to be collected from the beginning. Although the absolute values of q_1, q_2 and q_3 cannot be known, it is possible to define the additional area between q_1 and the larger q values:

$$q_2 = q_1 + a \hspace{3cm} \text{Equation 2.56.}$$

$$q_3 = q_1 + b \hspace{3cm} \text{Equation 2.57.}$$

Replacing these equations in Equation 2.53. gives:

$$Q = \frac{\frac{A.F}{B}.q_1{}^2.(a - b) + \frac{C.F}{D}.(q_1 + a)^2.b + E.(q_1 + b)^2.(-a)}{\frac{A.F}{B}.q_1.(a - b) + \frac{C.F}{D}.(q_1 + a).b + E.(q_1 + b).(-a)}$$

<div align="right">Equation 2.58.</div>

Although the number of unknown variables in the system went down to two (Q and q_1), this equation cannot yet be solved to find Q. A similar procedure to the one used in *Method 2* can thus be followed to find another equation for Q using a fourth data point. First, an additional power value and corresponding tangent are taken:

$$\frac{\mathrm{d}^2 q_4}{(\mathrm{d}t_4)^2} = \left(\frac{\mathrm{d}q_4}{\mathrm{d}t_4}\right)^2 . \left[\frac{-n}{(Q - q_4)} + \frac{m}{q_4}\right]$$

<div align="right">Equation 2.59.</div>

As before, letting:

$$G = \frac{\mathrm{d}^2 q_4}{(\mathrm{d}t_4)^2}$$

<div align="right">Equation 2.60.</div>

$$I = \left(\frac{\mathrm{d}q_4}{\mathrm{d}t_4}\right)^2$$

<div align="right">Equation 2.61.</div>

Then by substitution of Equations 2.44., 2.45. and 2.59. another equation for Q is found:

$$Q = \frac{\frac{A.I}{B}.(q_1{}^2.q_2 - q_1{}^2.q_4) + \frac{C.I}{D}.(q_2{}^2.q_4 - q_2{}^2.q_1) + G.(q_4{}^2.q_1 - q_4{}^2.q_2)}{\frac{A.I}{B}.(q_1.q_2 - q_1.q_4) + \frac{C.I}{D}.(q_2.q_4 - q_2.q_1) + G.(q_4.q_1 - q_4.q_2)}$$

<div align="right">Equation 2.62.</div>

Considering now:

$$q_4 = q_1 + c$$

<div align="right">Equation 2.63.</div>

And replacing Equations 2.56. and 2.63. in Equation 2.62. gives:

$$Q = \frac{\frac{A.I}{B}.q_1{}^2.(a - c) + \frac{C.I}{D}.(q_1 + a)^2.c + G.(q_1 + c)^2.(-a)}{\frac{A.I}{B}.q_1.(a - c) + \frac{C.I}{D}.(q_1 + a).c + G.(q_1 + c).(-a)}$$

<div align="right">Equation 2.64.</div>

The two expressions for Q, Equations 2.58. and 2.64., can, afterwards, be set equal and rearranged:

$$\frac{\frac{A.F}{B} \cdot q_1{}^2 \cdot (a - b) + \frac{C.F}{D} \cdot (q_1 + a)^2 \cdot b + E \cdot (q_1 + b)^2 \cdot (-a)}{\frac{A.F}{B} \cdot q_1 \cdot (a - b) + \frac{C.F}{D} \cdot (q_1 + a) \cdot b + E \cdot (q_1 + b) \cdot (-a)}$$

$$- \frac{\frac{A.I}{B} \cdot q_1{}^2 \cdot (a - c) + \frac{C.I}{D} \cdot (q_1 + a)^2 \cdot c + G \cdot (q_1 + c)^2 \cdot (-a)}{\frac{A.I}{B} \cdot q_1 \cdot (a - c) + \frac{C.I}{D} \cdot (q_1 + a) \cdot c + G \cdot (q_1 + c) \cdot (-a)} = 0$$

Equation 2.65.

Despite q_1 being the only unknown in this equation, its calculation is not straightforward because it cannot be isolated from the rest of the variables. Instead, it may be determined in the same way that Q was determined in *Method 1* using Mathcad. After q_1 is calculated, Q can be found by replacing all known values in Equation 2.58. All other solid state parameters can be determined using the equations described in *Method 2*.

2.2.4.4. Testing with simulated data

The three methodologies described above allow, in theory, the analysis of a broad range of solid state systems with different kinetics. The validity of these theoretical models, however, needs to be proved and the best way to do this is to test them with simulated data because they are free from random noise and other errors and the values of the variables describing the process are known absolutely. Using the methods described previously in section 2.2.1., data was simulated for a solid state process with the following parameters: $Q=1 \times 10^9$ µJ, $k=3 \times 10^{-7}$ s^{-1}, $m=0.75$, $n=0.625$. The three methods were then applied to these data.

Method 1 deals with the final portion of data and only requires 4 data points to be used with the array of equations described. Data points were selected at random covering various percentages of the data set (20, 40 and 60%), and the values of Q, m and n were calculated (Table 2.2.). It is apparent that the method consistently returned the correct values, irrespective of the percentage of data used.

TABLE 2.2. : Calculated values for the reaction variables using *Method 1*.

% Data used	Q / μJ	m	n
20%	1×10^9	0.75	0.625
40%	1×10^9	0.75	0.625
60%	1×10^9	0.75	0.625

Method 2 requires only 3 data points to be chosen and the respective derivatives and heat outputs determined graphically. Various sets of 3 points were selected throughout the whole data set and the values for Q, m and n calculated. As Table 2.3. shows, not all sets of data return the correct values for the reaction variables. Although the determination of Q and m is possible, independently of the 3 points selected, it is clear that in order for n to be returned correctly it is imperative that the point where the derivative is zero is included.

TABLE 2.3. : Calculated values for the reaction variables using *Method 2*.

Data points selected	Q / μJ	m	n
Maximum derivative; minimum derivative; zero derivative	1.0×10^9	0.75	0.625
Maximum derivative; minimum derivative; random point between them	1.0×10^9	0.75	1.306
1 point before maximum power; 1 after the maximum power; 1 near maximum power	1.0×10^9	0.75	1.071
3 points before maximum power	9.8×10^8	0.75	5.419
3 points after maximum power	1.0×10^9	0.75	-12.849
1 random point before and after the maximum; zero derivative	1.0×10^9	0.75	0.625

Method 3 requires calculation of q_1 before determination of Q. Four points were selected at random and used to determine the value of q_1. Points were selected either all before or before and after the maximum (Table 2.4.). In either case, excellent agreement with the correct q_1 value was observed. Calculation of the remaining parameters can, afterwards, be done using the equations presented in *Method 2* by selecting the appropriate data points.

TABLE 2.4. : Calculated q_1 values compared with actual q_1 values using *Method 3*.

Data points selected	q_1 (calculated) (J)	q_1 (actual) (J)
4 points before maximum	0.133	0.133
2 points before and 2 points after the maximum	0.884	0.880

2.2.4.5. *Testing with real data*

One obvious drawback of the methods outlined here is that, in selecting only a few data points from a large data set, much of the information in the recorded data is not used. Mathematically this does not matter if, as in the case of simulated data, there is no noise. In the case of real data, the presence of noise in the selection of a few data points could be problematic, especially with *Method 2*, since it utilizes a derivative signal. Hence, the methods were applied to real (i.e. noisy) data to determine their utility. The solid state process that was chosen for these studies was the crystallization of indomethacin from a glass.

Experimental methods:

Talc (extra pure) was purchased from VWR International. Crystalline indomethacin (>99%) was purchased from Molekula, Ltd. Amorphous indomethacin glass was prepared by melt-cooling. Crystalline indomethacin was first melted in aluminium foil on a hot plate ($\approx$ 175 ºC) and quench-cooled in liquid nitrogen before being stored in a desiccator over P_2O_5 for 1h. The dried sample was then ground gently using a mortar

and pestle and then passed through a 90 μm sieve. The sieved sample was further dried over P_2O_5 and then stored at -80 ºC until further use.

Calorimetric measurements were conducted with a 2277 Thermal Activity Monitor (TAM, TA Instruments Ltd.) at 35 ºC. The sample side ampoules were loaded with approximately 300 mg of amorphous indomethacin while the ampoules in the reference channel were filled with 300 mg of talc. These were left in the equilibrium position for 30 minutes before being lowered to the measuring position. Data capture was subsequently initiated with the dedicated software package Digitam 4.1. The time axis was corrected before analysis to account for the 30 minutes delay in data capture. The instrument was calibrated prior to use with the electrical substitution method and operated on an amplifier range of 100 μW.

After the calorimetric measurements, the samples were characterised with X-ray powder diffraction (XRPD). The X-ray diffractometer (Philip PW 3710, Holland) used CuKα radiation with 45 kV voltage and 30 mA current. Samples were scanned from 5º to 35º at a scanning speed of 0.25 º/min.

Results and discussion:

An indomethacin glass was allowed to crystallize with time in the TAM at 35 ºC and this physical change was observed as an exothermic peak (Figure 2.6.). XRPD data confirmed that the final material was crystalline.
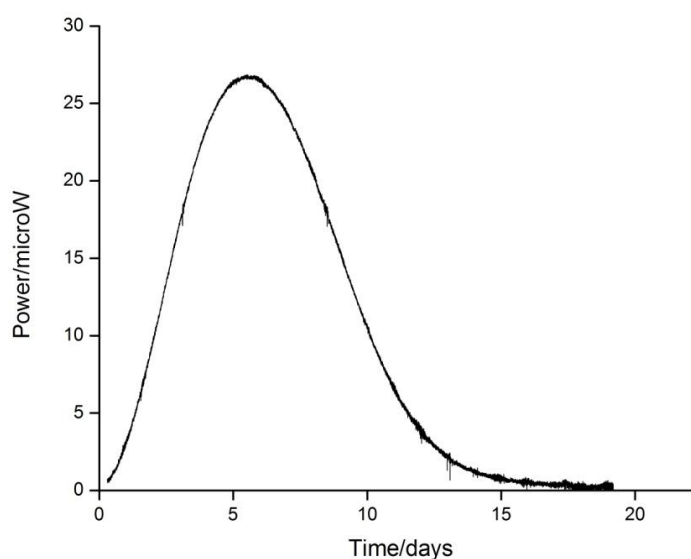
FIGURE 2.6. : Calorimetric data for the crystallization of amorphous indomethacin from a glass at 35 ºC.

105

Because the process progressed to completion, it was possible to integrate the data to obtain Q directly (16.62 J). This provided a reference value to check the validity of the analysis methods. Data were analysed with methods 1, 2 and 3 as described above and the calculated values are shown in Tables 2.5., 2.6. and 2.7.

TABLE 2.5. : Calculated values for the reaction variables for indomethacin crystallization from a glass at 35 ºC using *Method 1*.

% Data used	Q (J)	m	n
20%	Couldn't calculate	Couldn't calculate	Couldn't calculate
40%	128.8	12.005	1.013
60%	33.2	2.299	0.940
80%	19.7	1.016	0.905
90%	14.8	0.186	0.390
100%	16.5	0.527	0.745
2 close points before maximum Φ and 2 close points after maximum Φ	16.8	0.580	0.766

TABLE 2.6. : Calculated values for the reaction variables for indomethacin crystallization from a glass at 35 ºC using *Method 2*.

Data points selected	Q (J)	m	n
1 random point before and after the maximum; zero derivative	16.351	0.589	0.767

TABLE 2.7. : Calculated values for the reaction variables for indomethacin crystallization from a glass at 35 ºC using *Method 3*.

Data points selected	Q (J)	m	n
2 random points before and 1 after the maximum; maximum	16.215	0.556	0.736

Considering *Method 1* first, it is evident that the robustness of the technique is not so good with real data compared with simulated data. This could be a function of noise or the fact that the data points were taken primarily from the region in which the crystallization process is finishing. It is well known that Avrami models begin to fail at high (>0.8) α values because they do not account for impingement of individually growing crystals (83). This may explain the unrealistic values obtained if only the very last portion of data is used. If the total data set (which rather negates the point of the exercise), or power-time points selected in close pairs before and after the maximum, are used, the method returns excellent values (indicated by the values of Q close to 16.62 J). Equations of the form of Ng and Pérez-Maqueda contain two terms representing growth and decay. Selecting data pairs on either side of the maximum ensures that in one region growth predominates and in the other decay predominates. This probably provides sufficient information in the data for correct analysis. Using the values determined by selecting data pairs, the rate constant was determined to be 3.98 x 10^{-6} s^{-1}.

The issue of noise is very important in these analyses because all methods require selection of just a few data points from a large set of data and, obviously, random fluctuations in the signal may adversely affect the calculated parameters. This is particularly important with respect to *Method 2* because the whole analysis is based on the use of differential data which is greatly influenced by the level of noise in the data. Here the data were smoothed using the appropriate function in Origin, prior to analysis. Application of *Method 2* to the analysis of indomethacin data returned the solid state parameters shown in Table 2.6. These values were then replaced in Equation 2.4. and a value for the reaction rate constant, k, was determined (4.13 x 10^{-6} s^{-1}). Comparision with the results obtained with *Method 1* shows that these are in excellent agreement.

Using *Method 3* also gave excellent results, listed in Table 2.7. The total area was calculated to equal 16.215 J and m and n were 0.556 and 0.736, respectively. These values gave a rate constant of 3.98 x 10^{-6} s^{-1}.

The values obtained with these 3 methods can be further confirmed by selecting different sets of points across the whole range of data and calculating the reaction parameters. In doing so, two different outcomes are possible; either the parameters are the same throughout the whole process, confirming that the mechanism of reaction does not change with time; or, different values are obtained, hence indicating a change in the

mechanism. Such analysis, therefore, provides an excellent way of assessing mechanistic changes during a solid state process.

The reaction parameters calculated above for all three methods were then used to generate simulated data and the fit lines were plotted (Figure 2.7.). The overlap of all four sets of data (real data and data simulated with the 3 methods) demonstrates the validity of the three methods of analysis to study solid state processes using only partial calorimetric data.
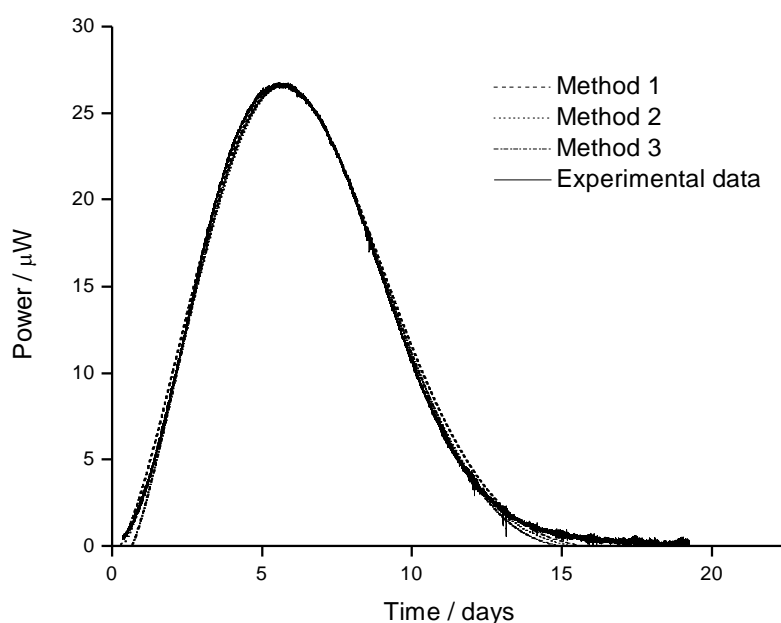
FIGURE 2.7. : Calorimetric data for the crystallization of amorphous indomethacin from a glass at 35 ºC (solid line) and the fit line obtained using analysis methods 1,2 and 3. Residual values (areas under experimental curve – area under each fit curve; *Method 1*, -0.217 J (1.31%); *Method 2*, 0.267 J (1.61%); *Method 3*, 0.402 J (2.42%)).

In addition to the determination of the solid state parameters k, Q, m and n, these methods also allow the calculation of α at maximum power (α_{peak}) after determination of Q. This parameter is very useful in the study of processes in the solid state because it allows the assignment of theoretical models to the experimental data. Once Q is known, α_{peak} is calculated by taking the value of the heat released up to maximum power and dividing it by Q. Because the process studied here progressed to completion it was possible to determine Q using the experimental data and hence determination of α_{peak} was straightforward (0.4225) (Figure 2.8.). This parameter was also calculated using the three methods described after determination of Q. *Method 1* gave an expected ratio of 0.431, *Method 2* a ratio of 0.429, and *Method 3* a ratio of 0.430. Comparison of these

values with the data in Table 2.1. suggests that there is a heterogeneous nucleation and growth mechanism involved in the crystallization of indomethacin from a glass at 35 °C because the values of α_{peak} calculated above lay between those listed for Erofeev's models where N=2 (α_{peak}=0.394) and N=3 (α_{peak}=0.489).
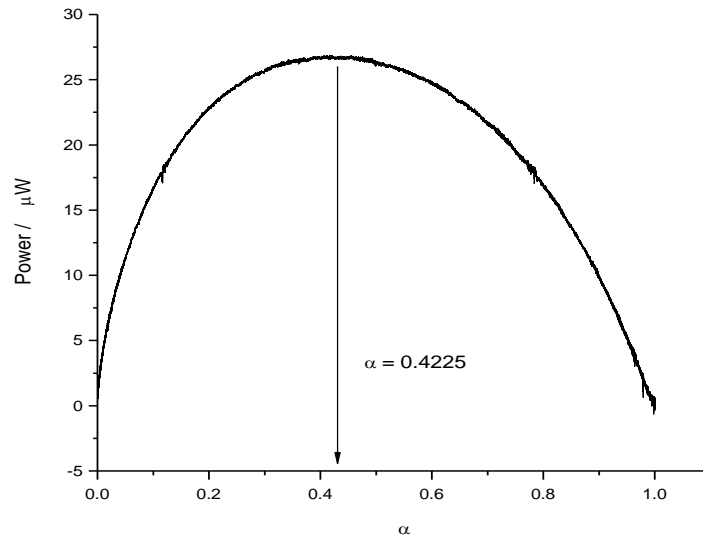
FIGURE 2.8. : Crystallization of indomethacin from a glass at 35 ºC showing power versus α and the value for α at the maximum.

2.3. Analysis of zero-order kinetics in solution

Isothermal microcalorimetry has been known for a long time to be a great technique in the investigation of the thermodynamic and kinetics aspects of physical and chemical processes. However, its huge potential has always been limited by the lack of methods available for the quantitative analysis of such processes. In recent years, significant progress has been made in this area and a number of approaches have been developed for the analysis of calorimetric data for processes undergoing different kinetic schemes. Some of these strategies were presented in Chapter 1 and they include methods for the investigation of first-, second- or n^{th}-order kinetics in solution, consecutive or parallel reactions, as well as, processes in the solid state (as shown in the previous section). Although the determination of quantitative parameters is possible for most of these situations, there is one case where this has proved difficult: the study of zero-order kinetics in solution. Until now, analysis of such processes has only been possible with the help of ancillary methods with the current calorimetric strategies proving insufficient to analyse real data. In Chapter 1, the derivation of a calorimetric equation that describes zero-order processes in solution was demonstrated by, first, taking the general calorimetric expression for n^{th}-order processes (Equation 2.66.):

$$\Phi = k.V.\Delta H^{1-n}.[k.\Delta H^{1-n}.(n-1).t + Q^{1-n}]^{\frac{n}{1-n}} \qquad \text{Equation 2.66.}$$

And making *n*=0:

$$\Phi = k.\Delta H.V \qquad \text{Equation 2.67.}$$

This equation shows that the thermal power measured for a zero-order process is only dependent on parameters that, in general, remain constant throughout the whole experiment: k is the rate constant; ΔH is the enthalpy of reaction (constant if the mechanism of reaction does not change during the process) and V is the volume of the sample. As a consequence, the thermal power measured for a zero-order process does not change with time and a straight line, parallel to the time axis, is observed if thermal power is plotted against time (Figure 2.9.). This outcome is consistent with the kinetics

involved in these processes since the rate of reaction, and thus the rate of heat exchange, for a zero-order process is always the same independently of the concentration of the chemical species in solution.
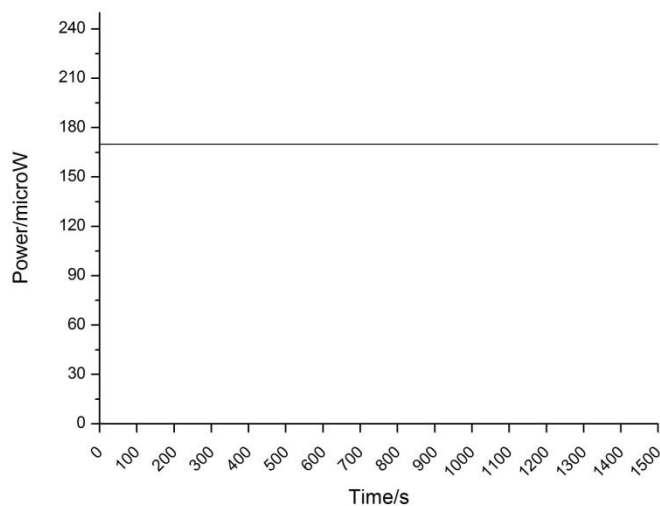
FIGURE 2.9. : Simulated data for a zero-order process studied with isothermal microcalorimetry (ΔH=20.22 kJ/mol, k=2.8 x 10^{-6} mol/dm^3.s, V=3 mL).

Although the equation shown above is cast in a form that allows thermal power to be described as a function of the thermodynamic and kinetic reaction parameters, this expression is not appropriate to use with isothermal calorimetric data, in the form of Φ versus time, because it does not include time as a factor. In addition, the fact that all parameters on the right-hand side of Equation 2.67. are constant throughout the process, renders analysis unfeasible if no values, other than the volume, are known prior to the experiment. A common alternative approach is to make use of ancillary methods to determine one of the parameters (usually the rate constant, k) and calculate the other parameter left by replacing all values in Equation 2.67. For example, Dhuna used a pH titration method to determine the rate constant associated with the photodegradation of 2-nitrobenzaldehyde in solution and calculated the reaction enthalpy using photocalorimetric data (76). This alternative, however, is not interesting in a calorimetric perspective because it negates the use of isothermal calorimetry as an analytical tool for the combined determination of the kinetic and thermodynamic reaction parameters.

Several examples can be found in literature for zero-order processes that were studied calorimetrically and for which no extensive quantitative analysis was made because of those analytical constraints. Some of these examples include studies on the autocatalytic

oxidation of drugs (84), polymer curing (85), oxidation of lipids (86) or enzymatic reactions (87). Another case of zero-order reactions that is very interesting, in the scope of this thesis, is the photodegradation of pharmaceuticals in solution. The kinetics involved in these reactions depend on several factors (intensity of light, wavelength, initial concentration of drug, etc.) but pseudo zero-order behaviour is commonly observed when the absorbance of the solution is so large that essentially all photons are absorbed and hence the rate is determined by the intensity of the radiation (77, 88). These zero-order photoreactions were studied before using calorimetric techniques (3, 76) but the quantitative analysis of data proved impossible because of the analytical issues referred to above.

In this context, three strategies are proposed here for the analysis of zero-order processes using only calorimetric data. The first strategy is used to analyse processes that progress to completion and consists of a relatively straightforward analysis method. The second strategy only applies to reactions that involve proton exchange with a buffer and is based on the use of different buffer systems with different enthalpies of ionization to modulate the thermal power measured. This method does not require the process to reach an end point allowing only partial data to be collected. The final method is a predictive method that uses tabulated data on enthalpies of formation to estimate enthalpies of reaction that can be used to determine the rate constant after substitution in Equation 2.67.

2.3.1. Analysis of zero-order processes that progress to completion

This first strategy can only be applied to the analysis of isothermal calorimetric data for zero-order processes that progress to completion. In these cases, because the entire energetic profile and the duration of the process are known, the determination of the thermodynamic and kinetic reaction parameters is straightforward using Equation 2.67.

It is well known that processes that follow zero-order kinetics eventually go through a final period where a change in the kinetics occurs just before reaching completion (35). This alteration in the kinetics is observed, in a power-time graph, as a change in the steady zero-order signal and decay to a zero baseline (Figure 2.10.).
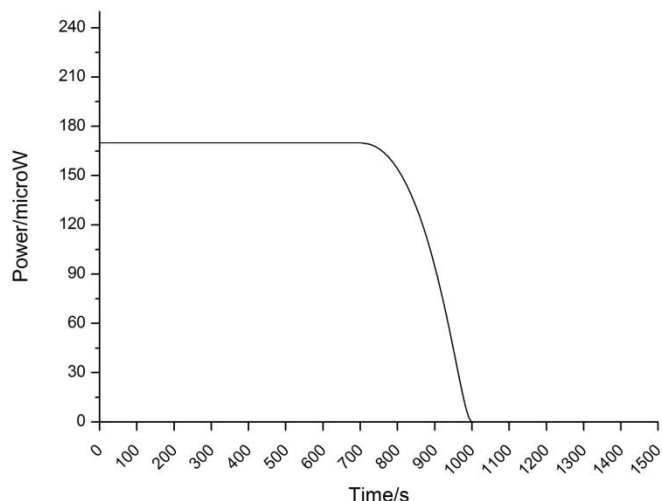
FIGURE 2.10. : Isothermal calorimetric data for a zero-order process that progresses to completion

Once the signal reaches that final baseline, the total heat of reaction (Q) may be determined by integrating the area under the curve. Assuming that the mechanism of reaction does not change throughout the whole process, and so, the enthalpy of the overall process (ΔH) remains constant during that period, the latter can be determined by dividing the total heat output by the initial amount of reacting species. Determination of ΔH leaves the reaction rate constant (k) as the only unknown parameter in Equation 2.67. which may be easily solved after replacing all known values in that expression. It is thus possible to calculate both the thermodynamic and kinetics parameters associated with these zero-order processes without the need for any ancillary methods. Despite the convenience of such a method, the fact that data collection is required until the end of the process limits its application to processes that are quick enough to allow data recording within an acceptable period of time.

The same sort of analysis can, in principle, be done if, instead of the enthalpy of reaction, the rate constant/rate of reaction is determined in the first place. In order to do that, the fraction of reaction, α, at the time that the process deviates from zero-order behaviour, needs to be determined first. That can be done by dividing the area under the curve up to that time (q) by the total area under the curve (Q). If that fraction is multiplied by the initial concentration of reactant, the concentration at the time point where the zero-order process terminates can be calculated. The rate of reaction is, afterwards, determined by dividing that concentration by the duration of the zero-order

113

period. That value can be replaced in Equation 2.67. to calculate the enthalpy of the process.

A different strategy may be used to determine ΔH based on the total heat released in a process; if Q is measured for two processes occurring in samples with the same volume but different initial concentrations of reacting species, the enthalpy of the process can be calculated with Equation 2.68.

$$\Delta H = \frac{Q_2 - Q_1}{(C_2 - C_1).V}$$
<div align="right">Equation 2.68.</div>

with Q_2 and Q_1 being the total heat released in experiments 2 and 1 respectively, C_2 and C_1 the initial concentration of the solutions used in both experiments and V the volume used. This approach is, in essence, very similar to the one previously described. However, it has the big advantage of being applicable to the analysis of processes where the initial part of data is missing because it only requires knowledge of the difference in Q measured for two experiments. Hence, as long as it is possible to calculate this difference, it is not mandatory that the whole data set is recorded.

Methods such as the ones described above were used in the photodegradation studies presented in the chapter dedicated to the photocalorimetric experiments in the solution phase.

2.3.2. Analysis of zero-order reactions occurring in different buffer systems

2.3.2.1. Theoretical approach

This method uses the differences in thermal power measured for a zero-order process occurring in different buffers to assess the influence of the reaction parameters on the calorimetric signal. The concept behind this method is very similar to the one used in the thermodynamic analysis of the binding properties of proteins and their substrates in a buffered system (89, 90). These studies use isothermal titration calorimetry (ITC) to determine the overall enthalpy ($\Delta_{obs}H$) for the buffered system which contains

contributions from both the intrinsic enthalpy of the protein-ligand binding interactions ($\Delta_{binding}H$) and the ionization enthalpy of the buffer species ($\Delta_{ion}H$). If the binding processes change the protonation states of free or complexed macromolecule and/or ligand, proton transfer between the binding complex and the buffer solvent occurs. As a consequence, $\Delta_{obs}H$ can be represented by the following equation:

$$\Delta_{obs}H = \Delta_{binding}H + \Delta n. \Delta_{ion}H$$

Equation 2.69.

where Δn is the number of protons exchanged with the buffer medium upon binding. In order to perform adequately this analysis, it is necessary that the system is tested in a minimum of two different buffer systems. Once these are tested with ITC, the $\Delta_{obs}H$ for the different buffered systems may be determined with the instrument's software and plotted against the respective $\Delta_{ion}H$ of each buffer. The values of $\Delta_{binding}H$ and Δn may, afterwards, be calculated from the values of the intercept on the abscissa and the slope of the line, respectively. This method thus allows the enthalpy of a process to be determined by coupling it with other processes of known enthalpy and assess the effect of the different contributions on the overall outcome.

A similar strategy, based on this multiple buffer method, is suggested here for the determination of the thermodynamic and kinetic parameters associated with zero-order processes using calorimetric data. Although this method will only be demonstrated for reactions that generate or consume protons, the general idea of coupling a process with others of known enthalpy may be used in the analysis of a broad range of reactions (e.g. oxidation reactions, etc.). Considering that a zero-order process occurs with formation of protons and that these are exchanged with the components of a buffer solution, the overall enthalpy of the system can be considered as a sum of the contributions of the zero-order process and the ionization enthalpy of the buffer species. If such reactions are set up in two different buffers, the overall enthalpy of those systems will be different and so will the thermal power measured for each experiment. These differences allow the enthalpy of the main process to be determined using the approach described below.

Considering the following reactions occurring in parallel:

$$DH_n \rightarrow D^{n-} + nH^+ \qquad \Delta_r H \text{ (reaction enthalpy)} \qquad \text{Equation 2.70.}$$

$$nH^+ + nB^- \rightarrow nBH \qquad -n.\Delta_i H \text{ (ionization enthalpy)} \qquad \text{Equation 2.71.}$$
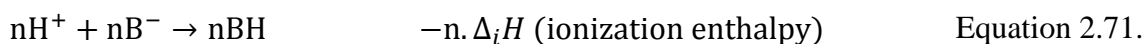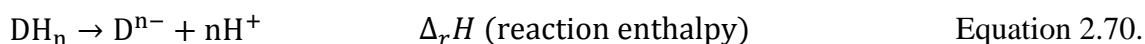
where DH_n corresponds to the drug molecule, B^- and BH are the buffer components and n is the number of protons released per drug molecule. The overall enthalpy of this buffered system may thus be represented by:

$$\Delta H_T(\text{overall}) = \Delta_r H - n.\Delta_i H \qquad \text{Equation 2.72.}$$

If two different buffers are used with that zero-order process, the difference between the two overall enthalpies becomes:

$$\Delta H_{T1} - \Delta H_{T2} = -n.(\Delta_i H_1 - \Delta_i H_2) \qquad \text{Equation 2.73.}$$

where ΔH_{T1} and ΔH_{T2} are the overall enthalpies for the systems with buffers 1 and 2, respectively, and $\Delta_i H_1$ and $\Delta_i H_2$ are the ionization enthalpies for buffers 1 and 2, respectively. The overall enthalpies for those systems may be replaced with Equation 2.67. for zero-order processes giving:

$$\frac{\Phi_1}{k_1.V} - \frac{\Phi_2}{k_2.V} = -n.(\Delta_i H_1 - \Delta_i H_2) \qquad \text{Equation 2.74.}$$

where Φ_1, Φ_2, k_1 and k_2 are the values for the thermal power measured and the rate constants for the overall reactions in buffer 1 and 2, respectively.

The following rearrangement of Equation 2.74. requires the rate of reaction/rate constant (k) to be similar for the two buffered systems. Since the kinetics of such

processes is totally dependent on the pH of the medium, it is possible to make k similar for the two systems by adjusting their pH to the same value. Therefore, $k_1=k_2=k$. This overall rate constant, k, is, in fact, the rate of reaction for the process described in Equation 2.70., the rate limiting step, since buffer ionization reaction are, in general, much quicker. With all this in mind, Equation 2.74. may be rearranged to give:

$$\frac{\Phi_1 - \Phi_2}{k.V} = -\text{n}.(\Delta_i H_1 - \Delta_i H_2)$$
<div align="right">Equation 2.75.</div>

If the number of protons involved in the process, n, is known, it is possible to determine the rate constant, k, by replacing all known values in Equation 2.76.:

$$k = -\frac{\Phi_1 - \Phi_2}{\text{n}.(\Delta_i H_1 - \Delta_i H_2).V}$$
<div align="right">Equation 2.76.</div>

The overall enthalpy of reaction for one of the buffered systems may, afterwards, be determined by replacing the rate constant, k, the volume, V, and thermal power measured in Equation 2.67. Since this parameter combines contributions from the enthalpy of ionization of the selected buffer and the enthalpy of the main zero-order process, the latter may be calculated using Equation 2.69.

2.3.2.2. *Application to real data*

In order to test the method with real calorimetric data, it is very important to choose a model reaction that meets all the requirements for its correct application. Not only that process needs to follow zero-order kinetics but also it must involve generation or consumption of protons so that it can be coupled with buffer ionization reactions. With these considerations in mind, the enzymatic hydrolysis of urea was chosen as the model process to be used in these studies. This reaction, like most enzymatic processes, exhibits pseudo zero-order behaviour in saturation conditions as a result of all enzyme binding sites being occupied by substrate molecules. In this situation, the rate of reaction reaches a maximum, remaining constant as long as an excess of urea is

maintained. Its concentration, however, must not be too high otherwise inhibition of the enzyme by the substrate molecules occurs (91, 92). This effect leads to a decrease in enzyme activity hence a decrease in the rate constant which precludes the desired zero-order behaviour. However, if that concentration is kept slightly above saturation levels, pseudo zero-order kinetics may be attained. In addition to these kinetic features, the hydrolysis of urea also meets the requirement for proton exchange with the components of the buffer system.

Two criteria were used in the selection of such buffers. First of all, they need to possess a pK_a in the region of the experimental pH so that a maximum buffer capacity is achieved. This pH was set to 6.6 which is near the optimal pH for urease activity (around pH 7 depending on the type of buffer used) (92). The other criterion of selection involves the energetics of the ionization reactions. Since this method is based on the differences in thermal power measured for two systems, the use of buffers with very different enthalpies of ionization is preferred to better discriminate between the two signals. With all this in mind, the two buffers chosen were imidazole (pK_a=6.993, $\Delta_i H$=36.64 kJ/mol) and phosphate (pK_a=7.198, $\Delta_i H$=3.6 kJ/mol) buffers (93).

Materials and methods:

Urease from jack beans 0.98 U/mg, imidazole, ACS reagent ≥99% and sodium phosphate dibasic *puriss*., anhydrous (Na_2HPO_4) were purchased from Sigma-Aldrich. Potassium dihydrogen orthophosphate (KH_2PO_4) was purchased from Fisher Scientific. Urea *purum* was purchased from Fluka. Potassium chloride (KCl) was purchased from VWR International Ltd. Hydrochloric acid (HCl) 5 M was purchased from Fisher Scientific.

The two buffer solutions were prepared with a concentration of 0.75 M and a pH of 6.6. KCl was used to adjust the ionic strength of the imidazole buffer. Phosphate buffer solutions were prepared by adding 2.662 g of Na_2HPO_4 and 2.552 g of KH_2PO_4 to a 50 mL volumetric flask before making up that volume with distilled water. The imidazole buffer solutions were prepared by adding 2.553 g imidazole, 2.252 g KCl and 5.7 mL HCl 5 M to a 50 mL flask and making up to volume with distilled water. Solutions of 0.4 M urea and 0.5 U/mL urease in 0.4 M urea were prepared, afterwards, using these two buffers, to provide the reference and testing solutions.

All calorimetric measurements were performed in an isothermal heat conduction microcalorimeter (TAM 2277, TA Instruments) at 25 ºC. Reference and sample ampoules were, first, filled with 3 mL of the respective solutions. Then, they were inserted into the calorimeter and left in the equilibrium position for 20 minutes. Afterwards, they were lowered into the measuring position and data started to be recorded. This procedure was performed in triplicate for each buffer used.

Results and discussion:

Figure 2.11. shows the calorimetric signal measured for the enzymatic hydrolysis of urea in the two buffers used:
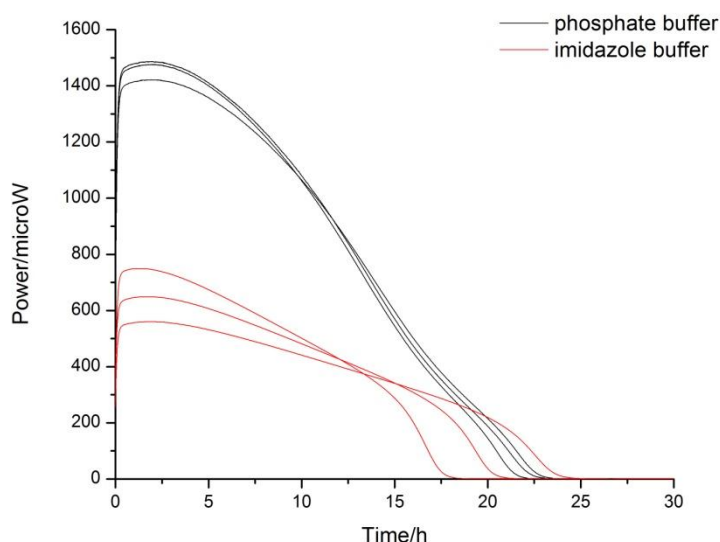
FIGURE 2.11. : Calorimetric data for the urea-urease experiments in phosphate and imidazole buffers.

Analysis of that graph indicates a very different signal from the constant heat output that was initially expected. In fact, a zero-order behaviour is only observed in the first 3 to 5 hours, with the signal decreasing in a two-step way after that initial stage. Comparison of these two decay periods clearly shows that the rate at which the signal decreases in the first stage is much slower than the rate in the final part of the process.

The initial decline was thought to be the result of a failure in the buffering capacity of the system as a result of the extreme basic character of the hydrolysis process. In these circumstances, the pH of the system would increase suddenly, affecting the rate of reaction and the thermal power measured during that period. In order to prove this, the

119

pH of the testing solution was measured in the beginning and end of the process and the following values were obtained: 6.6 at time zero and approximately 8 in the final stages of the process. This difference is quite significant explaining thus the changes in the rate of reaction during the initial period of decline in the signal. A higher buffer capacity could have been used to minimize this effect but the increase in ionic strength also interferes with the enzyme's activity.

In the final stages of the process a steeper decrease in the signal is observed which is thought to be the result of a change in the saturation state of the enzyme. This modification leads to a decrease in the number of binding complexes with time which, in combination with the pH effect previously described, explains the steeper decay in the thermal power measured.

Despite the complexity of the calorimetric signal, analysis of the initial pseudo zero-order phase is still possible after taking the average heat output for the two experimental conditions. That constant thermal power was found to be 1460.98 ± 28.32 µW for the experiments performed in phosphate buffer and 652.93 ± 77.29 µW for those run in the imidazole buffer. These differences are consistent with the ionization enthalpies of the two buffers (3.6 kJ/mol for the phosphate buffer and 36.64 kJ/mol for the imidazole buffer (93)) with the greatest heat output corresponding to the least endothermic ionization process. Despite the endothermic contributions of the ionization reactions, a positive thermal power is measured which demonstrates the exothermic character of the uncoupled hydrolysis process.

The average values for the zero-order heat output were, afterwards, used to calculate the kinetic and thermodynamic parameters associated with the hydrolysis of urea, using the set of equations previously described (Equations 2.76. and 2.69.). These equations may only be used with real data if the same rate of reaction is considered for the two experimental conditions. This was confirmed by measuring the duration of the whole process and comparing it between the two buffers. A value of approximately 22 hours was determined for both phosphate and imidazole buffers, thus, demonstrating the similarity of those rates. Afterwards, the reaction rate constant was calculated with Equation 2.76. This equation requires the number of protons exchanged with the buffer components, n, to be known. Based on the research done by Huttl et al. (94) on the reaction pathways of urea hydrolysis, this parameter was given the number 1 and replaced in that equation along with all other available values. A value of 8.15×10^{-6} mol/dm^{-3}.s was obtained for k using the average zero-order power deflection values. If

the hydrolysis process is considered in only one of the buffers, it is possible to calculate the overall enthalpy of that system by replacing all known values in Equation 2.67. For example, if the zero-order thermal power for the hydrolysis of urea in phosphate buffer (1460.98 µW) is replaced in that equation along with the volume (3 mL) and the rate constant (8.15 x 10^{-6} mol/dm^{-3}.s), a value of -59.75 kJ/mol is obtained for the overall enthalpy of the system. The same parameter was determined for the reaction in the imidazole buffer: -26.71 kJ/mol. After calculating these values, the enthalpy of the uncoupled hydrolysis process was determined by replacing the overall enthalpies and the respective enthalpies of ionization in Equation 2.69. A value of -63.35 kJ/mol was calculated for $\Delta_r H$.

Despite demonstration of its application to the analysis of real data, the strategy needs to be validated using a different non-calorimetric approach. Assessment of the rate of reaction using a method of quantification of urea in solution could have been used; however, the short duration of the zero-order period precludes the use of such methods. A different approach was, thus, chosen to assess the enthalpy of the hydrolysis process(es) by comparing the experimental value with the literature data. Huttl et al. (94) studied the energetics involved in the hydrolysis of urea and compiled a list of eight different partial reactions that may occur in such conditions. Different combinations of these reactions may occur, depending on the system's pH. However, three of those are always present independently of that value. The schematic of these partial reactions and the respective enthalpies are shown below:

$$CO(NH_2)_2 + H_2O \xrightarrow{urease} NH_2COO^- + NH_4^+ \qquad \Delta H = -24.27 \text{ kJ/mol}$$

$$NH_2COO^- + H_2O \rightarrow NH_3(aq) + HCO_3^- \qquad \Delta H = 12.584 \text{ kJ/mol}$$

$$NH_3(aq) + H^+ \rightarrow NH_4^+ \qquad \Delta H = -52.216 \text{ kJ/mol}$$
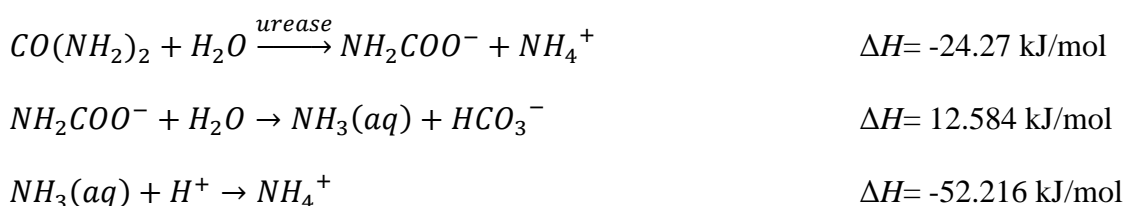
If the sum of all three enthalpy contributions is calculated, a value of -63.902 kJ/mol is obtained which is very similar to the enthalpy of the uncoupled process calculated with the method described here (-63.35 kJ/mol). If these partial reactions are considered, the increase in pH is easily explained by the consumption of protons in the last reaction step.

This exercise shows that, at pH 6.6, probably only those three partial reactions are involved in the enzymatic hydrolysis of urea. O'Neill (87) and Beezer (95) studied the same reaction in phosphate buffer at pH 7 using isothermal flow calorimetry and found an overall enthalpy of -10.6 kJ/mol and -33 kJ/mol, respectively (the difference between these two values was explained by a difference in the thermal volume assumed for the two experiments). Although those values included the ionization enthalpy of the phosphate buffer ($\Delta_i H$=3.6 kJ/mol), the big differences observed between them and the enthalpy determined with the double buffer method (-63.35 kJ/mol) cannot be explained exclusively with that contribution. Those differences may, instead, be explained by the fact that O'Neill and Beezer analysed the decay period assuming that it followed first-order kinetics, while Figure 2.11. shows that two different kinetic events occurred during the decay phase. Hence, a zero-order calorimetric method such as the one presented here is preferred for this kind of studies.

Compared to the method described in section 2.3.1., this strategy has the advantage of using only a few data points and it does not require the process to progress to completion. Furthermore, this method allows the zero-order rate constant, k_0, to be determined without previous knowledge of the enthalpy of the process. The only information it requires is the difference between the ionization enthalpies of the two buffers. Despite these advantages, the method is an indirect approach to the determination of zero-order parameters because it is based on the combination of two distinct processes. Another disadvantage of this method is the limited range of reactions that it can be applied to, which precludes its establishment as a universal method.

2.3.3. Predictive method for the determination of $\Delta_r H$

The analysis of calorimetric data for zero-order processes has always been dependent on ancillary methods to provide information on one of the reaction parameters expressed in Equation 2.67., k or ΔH. After one of these is determined, calculation of the other parameter is straightforward after replacing all known values in that equation. The most common strategy used in such analyses consists of determining, first, the rate constant using a method of quantification of the reaction species across time, followed by calculation of the enthalpy of the process using the calorimetric equation that describes

zero-order processes. This strategy, however, is not ideal because it proves even more complex in terms of the analytical procedures.

An alternative approach is, thus, presented here for the analysis of calorimetric data for zero-order processes using a predictive method that allows determination of the enthalpies of reaction. The standard enthalpy of reacton ($\Delta_r H°$) can be defined in terms of the standard enthalpies of formation of the reactants ($\Delta_f H°_{react}$) and products of reaction ($\Delta_f H°_{prod}$) by the following equation (96):

$$\Delta_r H° = \sum v.\Delta_f H°_{prod} - \sum v.\Delta_f H°_{react} \qquad \text{Equation 2.77.}$$

v is the stoichiometric coefficient. Determination of $\Delta_r H°$ is, therefore, straightforward if the standard enthalpies of formation for all species involved are known. This, however, is very unlikely as a result of the limited number of molecules with such information. In this context, the use of predictive methods for the estimation of standard enthalpies of formation seems like a good alternative approach.

Most methods reported in literature for the estimation of standard enthalpies of formation consider this parameter to be the sum of different energetic contributions from substructural components within the molecule. Benson and co-workers (97) were one of the first groups to use such a method based on group additivity schemes with most of their work focussing on the estimation of standard enthalpies of formation for molecules in the gaseous phase. Three levels of contributions were considered in that method: contributions from the atoms in a molecule, from the bonds between those atoms and from the steric effects of the different chemical groups (cyclic, aromatic, functional groups, next-nearest neighbour interactions, etc.). An example of the application of such method follows for the estimation of $\Delta_f H°$ for triethylamine (Figure 2.12.) in the gas phase:
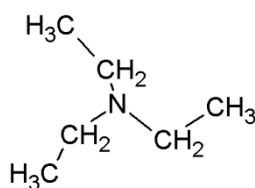
FIGURE 2.12. : Molecular structure of triethylamine.

The contributing groups are symbolically represented by a central atom linked to a varying number of different atoms, all represented by a letter. For example, if a group composed of a central carbon atom linked to another carbon atom and three hydrogen atoms is considered, the following scheme is used: C-(C)(H)$_3$. Using this symbology, the molecule of triethylamine can be divided into the following groups:

3 x C-(C)(H)$_3$ + 3 x C-(N)(C)(H)$_3$ + N-(C)$_3$

The energy values associated with each group can be found in several tables published in the literature and are usually listed for standard state conditions (25 ℃ and 1 atmosphere) (97). These values were determined by comparison of the experimentally derived standard enthalpies of formation for molecules differing only in one specific group. Using those tabulated values, the standard enthalpy of formation of triethylamine was determined:

$\Delta_f H° = $ 3 x (-42.18 kJ/mol) + 3 x (-27.62 kJ/mol) + 102.09 kJ/mol

+ 3 x gauche interactions (3.35 kJ/mol each)

$\Delta_f H° = $ -97.26 kJ/mol

The experimental value obtained for that $\Delta_f H°$ was -100 kJ/mol (97) which is similar to the estimated value. Other researchers followed Benson's work and developed similar methods with more extensive lists of group values. Pedley (98), for example, described an additivity method that includes a larger number of steric interactions between non-bonded atoms and conjugative effects. On the other hand, Cohen (99) extended Benson's method to the estimation of parameters for molecules in physical states other than the gaseous (liquid and solid). An updated list of values was presented for groups containing atoms of oxygen, carbon and hydrogen. Nitrogen-containing molecules, however, were still not possible to use with these estimation methods.

In 1993, Domalski and Hearing demonstrated the possibility of extending Benson's group additivity approach to the condensed phase for molecules containing C, H, N, O, S and halogen atoms. Although the list of group values was extensive for the gas phase, several group contributions were still missing for the condensed phase. Knowledge of these values is, however, very important in the analysis of zero-order processes in solution since the thermodynamic properties of this phase are very different from the gas phase.

In recent years, a new additivity method was suggested by Salmon and Dalmazzone (100, 101) for the prediction of standard enthalpies of formation for molecules in the solid state (at 298.15 K) containing atoms of carbon, oxygen, hydrogen and nitrogen. Although the analytical procedures were very similar to all previously described methods, a much broader range of group values was available for molecules in the solid state. This was a result of the large database of thermochemical properties used in the determination of the solid state group values.

This last method is believed to be the best one in terms of determining standard enthalpies of formation for molecules in the solid state. Although, these parameters cannot be exactly correlated with those for a reaction occurring in the solution phase, it may still be used in these predictive studies. Salmon and Dalmazzone's method was, therefore, chosen for the estimation of enthalpies of reaction for zero-order process occurring in solution. Once the enthalpy is calculated, the rate constant for these processes can be easily determined using Equation 2.67.

In order to demonstrate the validity of this approach, the hydrolysis of acetylsalycilic acid in solution was chosen as the model solution phase reaction. This reaction was previously studied by Skaria using isothermal microcalorimetry and a value of -23.6 ± 2.4 kJ/mol was determined for the enthalpy of aspririn hydrolysis in 0.1 M HCL at 25 ℃ (102). Considering the hydrolysis process described in Figure 2.13., the following method may be applied to determine $\Delta_r H°$:
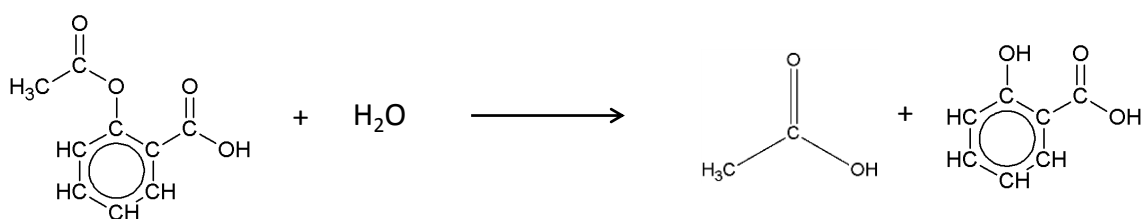
FIGURE 2.13. : Hydrolysis of acetylsalycilic acid.

Standard enthalpy of formation of acetylsalycilic acid (ASA) (s):

4 x C_b-(H) = 4 x 3.1 kJ/mol

C_b-(O) = -67.9 kJ/mol

C_b-(CO) = -110.5 kJ/mol

CO-(C_b)(O) = -86.7 kJ/mol

O-(CO)(H) = -212.4 kJ/mol

O-(CO)(C_b) = -31.7 kJ/mol

CO-(O)(C) = -183.1 kJ/mol

C-(H)$_3$(CO) = -85.8 kJ/mol

Ortho polar-polar correction = -1.2 kJ/mol

Intramolecular H bond = 19.8 kJ/mol

$\Delta_f H° = -747.1$ kJ/mol

Standard enthalpy of formation of H$_2$O (l) = -285.83 kJ/mol

Standard enthalpy of formation of salycilic acid (SA) (s):

4 x C_b-(H) = 4 x 3.1 kJ/mol

C_b-(O) = -67.9 kJ/mol

C_b-(CO) = -110.5 kJ/mol

CO-(C_b)(O) = -86.7 kJ/mol

O-(CO)(H) = -212.4 kJ/mol

O-(C_b) (H) = -125.9 kJ/mol

Ortho polar-polar correction = -1.2 kJ/mol

Intramolecular H bond = 19.8 kJ/mol

$\Delta_f H° = -572.4$ kJ/mol

Standard enthalpy of formation of acetic acid (AA) (s):

C-(H)$_3$(CO) = -85.8 kJ/mol

CO-(O)(C) = -183.1 kJ/mol $\qquad$ $\Delta_f H° = $ -481.3 kJ/mol

O-(CO)(H) = -212.4 kJ/mol

$$\Delta_r H° = \left(\Delta_f H° \, (SA) + \Delta_f H° \, (AA)\right) - \left(\Delta_f H° \, (ASA) + \Delta_f H° \, (H_2O)\right)$$

Equation 2.78.

$$\Delta_r H° = -20.7 \text{ kJ/mol}$$

This estimated value is similar to the one obtained experimentally (-23.6 ± 2.4 kJ/mol) which demonstrates the validity of the method. Despite the similar values obtained in this example, there were other cases where the prediction method failed to return good estimations. For example, the enthalpy of reaction estimated for the imidazole catalysed hydrolysis of triacetin was -24.3 kJ/mol whereas the experimental results obtained from inter-laboratory trials (36) showed an average enthalpy of reaction of -91.71 kJ/mol.

Compared to the two strategies previously described, this one loses in terms of accuracy as a consequence of its predictive nature. Its accuracy is also dependent on the temperature at which the process occurs as a result of all group values being listed for a temperature of 298.15 K. Furthermore, the method requires that the reaction products and, hence, the mechanism of reaction are known which may not happen in many cases. Finally, the fact that this method does not take into consideration the enthalpies of solvation of all species involved in the reaction renders the analysis outcomes even more uncertain. Despite all disadvantages, such approach constitutes a very useful tool if only an estimation of the reaction parameters is required. The use of iterative methods in the analysis of calorimetric data is a good example of techniques that require an estimation of the unknown parameters before proceeding with the actual analytical process. A predictive method such as the one presented here constitutes, thus, a very useful ancillary method.

2.4. Summary

Despite the significant progress made in the area of calorimetric data analysis, the strategies and equations available in the literature are still insufficient to analyse calorimetric data for some of the simplest and fundamental kinetic processes. Chapter 2 tried to explore some of these issues with special focus on the analysis of solid state reactions and zero-order processes in solution. Several mathematical methods were presented for the determination of the thermodynamic and kinetic reaction parameters and the validity of those methods was demonstrated with recourse to real and simulated data.

The issue with quantitative analysis of solid state processes has always been the requirement for processes to progress to completion. That is because the calorimetric equation that describes solid state processes is cast in the form of thermal power versus α (fraction reaction) which can only be determined if Q is known. However, calculation of Q may be difficult in cases where the process is too fast (initial data missing) or slow (final data missing). To address this issue, several mathematical methods were developed for the direct calculation of Q by selection of just a few data points when only partial data is available. All equations were derived from the calorimetric form of Ng's solid state model previously reported by Willson (42). In addition to the determination of Q, those methodologies allow direct calculation of the mechanism descriptors m and n and the reaction rate constant, k, once all other parameters are found. Two graphical methods for the generation of power-time data for solid state processes were also described. The validity of the direct calculation methods was, afterwards, demonstrated using simulated calorimetric data obtained with those methods. Application of those methodologies to the analysis of real calorimetric data was also demonstrated using isothermal calorimetric data for the crystallization of indomethacin from a glass.

Regarding the analysis of zero-order kinetics in solution, the main obstacle to quantitative determination of the reaction parameters is the fact that the equation that describes these processes cannot fit data in the form of power versus time (Equation 2.67.). To address this issue, three methods were suggested for the analysis of calorimetric data for zero-order processes. The first strategy requires that the processes progress to completion in order to determine Q and ΔH before calculation of k. The

second strategy only applies to reactions that involve proton exchange with a buffer and is based on the use of different buffer systems with different enthalpies of ionization to modulate the thermal power measured. This method does not require the process to reach an end point allowing only partial data to be collected. The final method is a predictive method that uses tabulated data on enthalpies of formation to estimate enthalpies of reaction that can be used to determine the rate constant after substitution in Equation 2.67.

3. Photocalorimetry: development of new instrument designs

3.1. Introduction

This chapter aims to provide a detailed description of the various stages involved in the development of two new photocalorimeters for the photostability assessment of pharmaceuticals. The two instruments use light-emitting diodes (LEDs) as the light source, incorporated into different calorimetric units with specific operation characteristics and performance. One of the instruments was built after re-designing Dhuna's photocalorimeter (described in section 1.6.3.) and consists of a heat-conduction microcalorimeter (TAM 2277) adapted with two arrays of LEDs to irradiate the sample and reference channels of the TAM. The other design also uses LEDs as the light source, although, in this case, a Multi-Cell Differential Scanning Calorimeter (MCDSC) is used as the calorimetric unit. Details of the instruments' design, components and operation procedures are given here along with a description of the modifications made to the systems as the project progressed. Baseline reproducibility tests were also performed using the two instruments to assess their performance with and without light irradiating the system.

3.2. The Photo-TAM

3.2.1. Re-design considerations of Dhuna's LED-array photocalorimeter

The photocalorimetric design developed by Dhuna was briefly outlined in Chapter 1. The instrument consisted of a heat-conduction microcalorimeter (TAM 2277) coupled with two identical arrays of LEDs that irradiated the two sides of a calorimetric unit. Those LEDs were mounted on a metal holder outside the calorimeter and light was conducted into the calorimetric unit by liquid light guides that fitted the sample and reference ampoules. Despite the same voltage being applied to both arrays of LEDs, an imbalance in the light power going into the ampoules was usually observed as a result of small differences in the performance of the LEDs. Those differences in light power were detected by the calorimeter and a non-zero signal was measured. In order to zero that signal, the voltage applied to the sample LEDs was fixed while the voltage on the reference side was adjusted until a zero net signal was obtained. Testing of photosensitive samples would then be possible after these adjustments.

Two photoreactions were analysed in that photocalorimeter using an array of 5 different LEDs to irradiate the samples (4 LEDs emitted at peak wavelengths of 360 nm, 370 nm, 380 nm and 395 nm while the other one emitted in the range of 400-700 nm). One of those photoreactions was the photodegradation of a proposed actinometric compound, 2-nitrobenzaldehyde (2-NB) in solution, which was used to quantify the photon flux of the LED-array. The thermal power measured in the 2-NB photocalorimetric experiments showed a constant deflection from zero which is consistent with the zero-order behaviour reported in the literature (76, 103). Despite the experiments demonstrating that the photocalorimeter was able to detect photodegradation signals, quantitative analysis was only possible, at that time, using ancillary methods. The other reaction that was tested with that system was the photodegradation of nifedipine in solution. Similarly to the 2-nitrobenzaldehyde experiments, the photoreaction signals measured were constant with time demonstrating that zero-order kinetics were followed. Studies on the causative wavelengths of degradation were also performed using the individual LEDs and it was found that the 360 nm radiation had the largest effect on the magnitude of the photoreaction signal (76).

Although the experiments done with 2-nitrobenzaldehyde and nifedipine were very important as a proof of concept, the lack of strategies for the analysis of the zero-order signals recorded during those experiments was an important drawback. Figure 3.1. gives an example of the zero-order signals recorded during the studies performed with nifedipine.
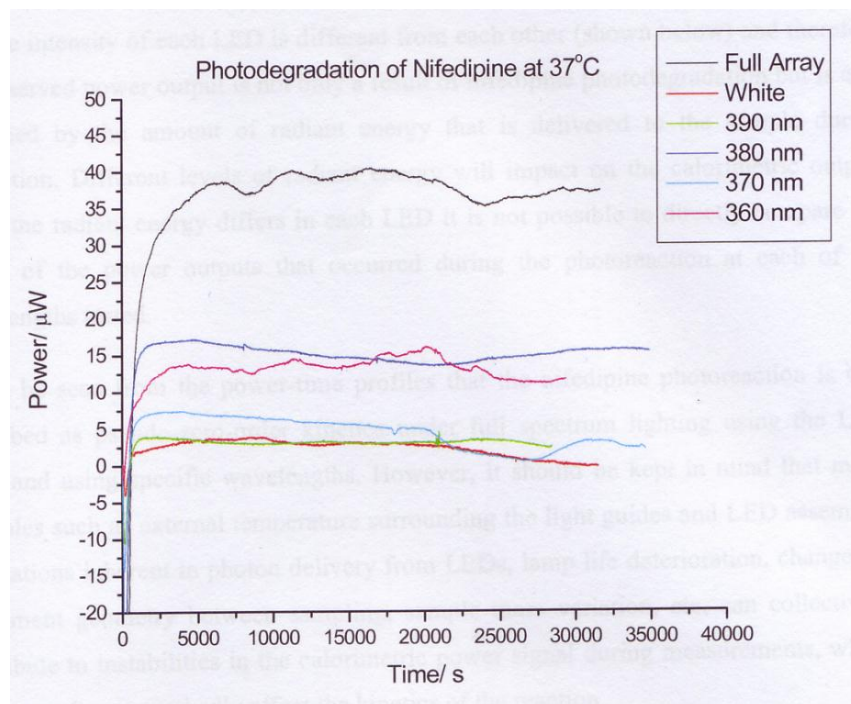
FIGURE 3.1. : Calorimetric signals recorded for the photodegradation of nifedipine using Dhuna's photocalorimeter (Figure taken from (5)).

Some comments have to be made regarding the data plotted in Figure 3.1. To begin with, the approximate 10 hours of irradiation (≈36000 s) were clearly insufficient for the process to progress to completion. Had that happened, a change in the kinetics and decline to zero baseline would be observed towards the end. That would be very useful because it would allow quantitative analysis of the process using the method described in section 2.3.1.

Furthermore, Figure 3.1. shows that the magnitude of the signals was quite small which means that either the process is not very energetic or the rate of reaction was very slow. In any case, the results obtained were not very encouraging considering that nifedipine is one of the most light-sensitive drugs on the market. Application of that instrument to the analysis of other less sensitive drugs could, therefore, be questioned. Adding to

133

those issues, most signals recorded showed significant variations with time which indicate influence of other factors on those measurements.

In this context, and considering all the issues raised above, a re-design of Dhuna's LED-array photocalorimeter was decided upon. The main idea was to bring the light source closer to the ampoules, therefore, providing direct irradiation of the samples and eliminating the interference of light-guiding components on the thermal measurements. In order to achieve this, two changes were considered; either the LEDs would be embedded in the ampoule lid or suspended just above it using a windowed lid to allow passage of light. The two options were tested and a detailed discussion of the results is given later in this chapter. In any case, a lighting column with the LED-array had to be designed to lower the LEDs into the calorimetric chambers.

Direct irradiation of samples is very advantageous because it minimises the energy losses inherent in the transmission of light through light guides and increases the light power reaching the samples as a result of the shorter distance between the light source and the ampoule. This larger light power is expected to increase the rates of photodegradation, therefore, increasing the rate of heat production or thermal power measured. Such increase in the magnitude of the signals is very important because it allows less energetic photoprocesses to be investigated. On the other hand, an increase in the rate of photodegradation with light power results in shorter times to completion which is an advantage, for example, in the study of long zero-order processes. The insertion of the light source inside the calorimeter is also thought to improve the signal-to-noise ratio because it prevents fluctuations in the outside temperature from interfering with the thermal measurements. However, such modifications may also result in baseline issues and difficulties in zeroing the signal as a consequence of the light power (and associated heat) that reaches the measuring sites increasing considerably.

In addition to these changes in the lighting system, an automated electronic-balancing power supply was developed to autobalance the light power going into the sample and reference ampoules and zero the thermal power measured in a blank experiment. The different components of the re-designed photocalorimeter will be described in the following sections.

3.2.2. The new photocalorimetric design

A picture of the final photocalorimetric design is shown in Figure 3.2. The different parts of the photocalorimeter include the isothermal microcalorimeter (TAM 2277), the autobalance power supply, an electronic circuit board with individual switches for each LED, two lighting columns, that incorporate the LEDs, placed inside the calorimetric chambers and the photocalorimetric ampoules.
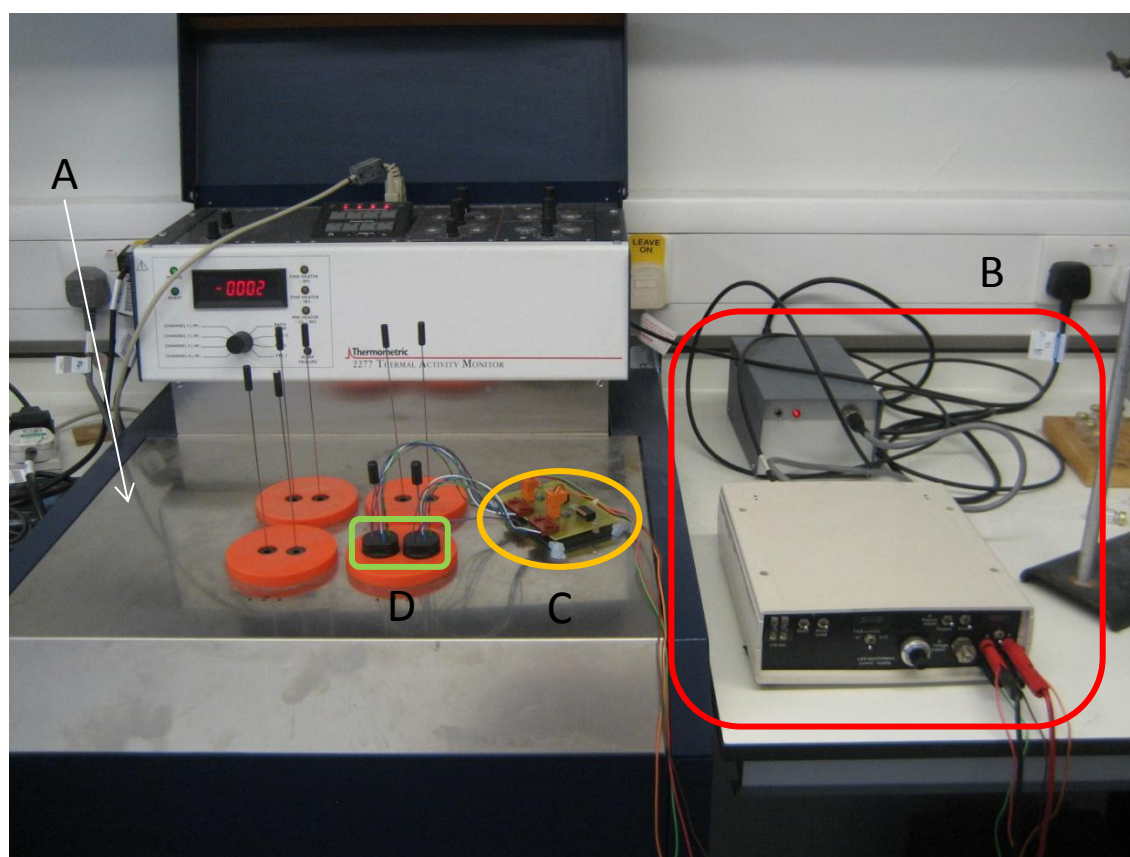
FIGURE 3.2. : The new LED-array photo-TAM. A- TAM 2277; B- autobalance power supply; C-circuit board with switches; D- lighting columns inserted in the calorimetric channels.

3.2.2.1. The isothermal calorimeter

The calorimeter that forms the basis of this photocalorimetric design is the heat conduction microcalorimeter, TAM (Thermal Activity Monitor) 2277. These calorimeters measure the heat produced or absorbed by the samples using thermopiles that are heat flow sensors situated between the calorimetric vessels and the surrounding

heat sink. This heat sink acts to maintain the system at a constant temperature by exchanging heat with the calorimetric vessel. Such heat transfers are measured quantitatively and the potential generated by the thermopiles is amplified and recorded as thermal power (Watts) versus time.

The TAM 2277 is a multichannel microcalorimeter that has four separate channels, allowing four different experiments to be conducted simultaneously (Figure 3.3.).
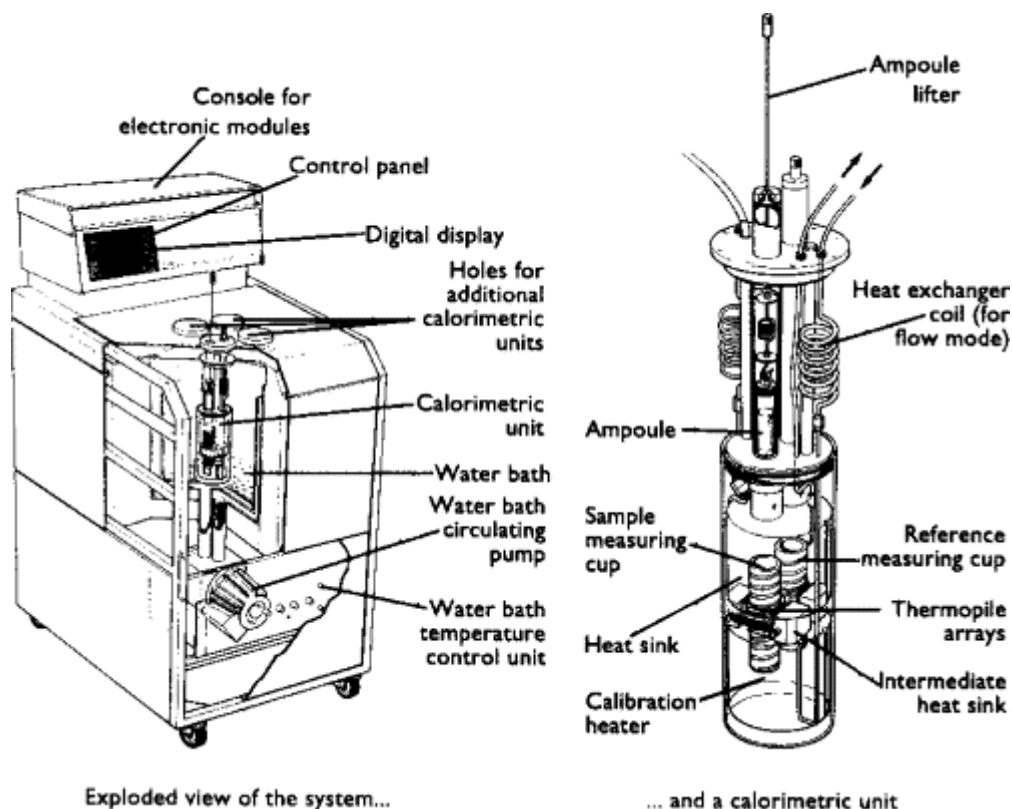
FIGURE 3.3. : A scheme of the TAM 2277 is shown on the left. A single calorimetric unit is shown on the right. This figure was taken from the Thermometric AB (now TA Instruments) manual.

Each channel has two identical chambers adjacent to each other where the reference (right-hand side) and test (left-hand side) samples are placed. Generally, an inert material, of similar heat capacity and quantity to the sample, is placed on the reference side and the heat flow difference between the two sides is measured. This differential mode allows any thermal powers measured to be attributed to the reaction taking place in the sample side. If that reaction is exothermic (negative enthalpy), the signal recorded by the calorimeter will have a positive sign while an endothermic reaction (positive enthalpy) results in a negative thermal power. That is because the calorimeter reports a

136

heat gain (positive) or heat loss (negative) signal from the perspective of the surroundings and not that of the system.

The instrument has two types of channels that can be used with different sized ampoules. The two most common ampoules have 3 and 20 mL volume. There are different performance specifications for these two types of channels. The limit of detectability and baseline stability over 8 hours are 0.15 µW and ± 0.2 µW for the channels that use 3 mL ampoules while the values for those using the 20 mL ampoules are 1 µW and ± 2 µW, respectively. All channels are immersed in a closed thermostated water bath (ca. 25 L) maintained to ± 2 x 10^{-4} ℃ within the working range of 5 to 80 ℃.

Each channel can be set to one of seven sensitivity ranges: 3, 10, 30, 100, 300, 1000 or 3000 µW (104). The TAM's high sensitivity comes from having an accurate and precise control of temperature. It has been claimed that the TAM is sufficiently sensitive to monitor slow reactions with lifetimes lasting up to 10000 years. Moreover, it has been reported that the instrument can discriminate between a reaction that has a first-order rate constant of 1 x 10^{-11} s^{-1} and 2 x 10^{-11} s^{-1} after collection of 50 hours of data (35).

This calorimeter is connected to a computer via a 25 pin RS232 serial port. Data capture and control of many of the calorimeter's functions are achieved by use of Thermometric's dedicated software, Digitam^{TM}.

3.2.2.2.   The light source: light-emitting diodes (LEDs)

Similarly to Dhuna's photocalorimeter, the instrument described here uses Light-Emitting Diodes (LEDs) to irradiate the chambers of the isothermal microcalorimeter TAM 2277. Light-emitting diodes are made of semi-conductive crystals that are doped with impurities to create a p-n junction where the p-side consists of a positively charged electrode (anode) while the n-side is a negatively charged electrode (cathode). Current is able to flow from the p-side of the diode to the n-side but it cannot flow in reverse direction. Electrons, however, only flow from the n-side to the p-side. The junction boundary is called the depletion zone. As the electrons cross the depletion zone and fill a hole, they drop into a state of lower energy and the excess energy is released in the form of a photon. The structure of a LED is shown in Figure 3.4.
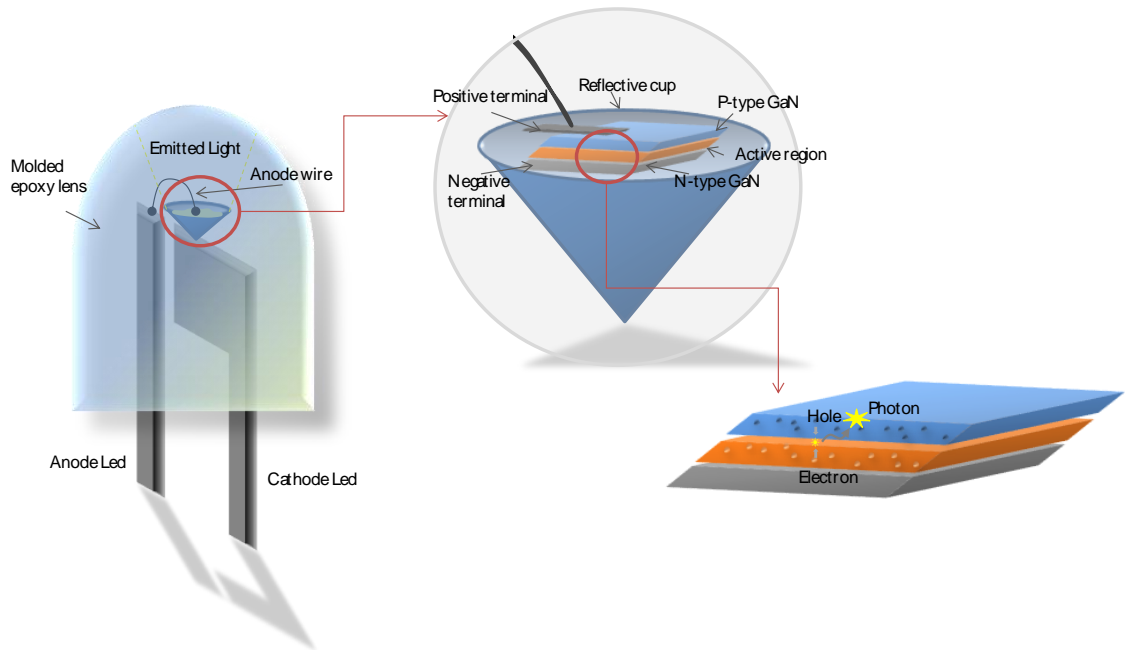
FIGURE 3.4. : Scheme of the light-emitting diode structure (LED) (adapted from http://www.omslighting.com/ledacademy/282/).

The selection of semiconductor and doping materials determines the exact wavelengths emitted by the diode when a photon is released. For example, Gallium Arsenide (GaAs) is used to produce infrared radiation while Aluminium gallium nitrate (AlGaN) is used to produce near to far ultraviolet and violet. Moreover, the intensity of light emitted by the LEDs is proportional to the current that passes through them which allows a fine control of the irradiation conditions.

The use of LEDs as a light source is greatly advantageous compared to other traditional light sources such as the Xe arc lamp. Some of these advantages are:

- their extremely long life span. Typical lifetimes between 50000 and 100000 hours have been reported when operated at their rated power and 5000 hours for shorter wavelength LEDs below 380 nm (100 times greater than for a 300 W Xe lamp).

- a narrow spectrum of emission of approximately 10 nm bandwidth providing almost monochromatic lighting conditions (Figure 3.5.). The combination of different wavelength LEDs allows the creation of a customised spectrum of irradiation.

- a reduced production of heat upon emission of light and low power consumption.

- the ability to be switched on and off very quickly and hence light up very quickly.

- the wide variety of different intensities, shapes and sizes. The relative small size of most commercially available LEDs is very useful to create an array of LEDs that could be placed inside a calorimetric chamber.

- the low cost of each LED compared to the very expensive Xe arc lamps.

- the ability to precisely modulate the irradiance from the LED by controlling the electrical supply with no damage to the LED and no significant change in spectral power distribution.

Such features make LEDs a great choice as a light source for application in photocalorimetry.

Similarly to Dhuna's photocalorimeter, the instrument described here uses an array of 5 LEDs to irradiate the sample and reference chambers of an isothermal heat conduction microcalorimeter, TAM 2277. However, in this case, the LEDs are inserted in a special holder that is lowered inside the calorimetric chambers. More details regarding the arrangement of the LEDs and the design of the LED-holder will be given later in this chapter. Two different arrays of LEDs were used in the photocalorimeter; one of them comprised five similar 5 mm high brightness ultraviolet LEDs with a wavelength of emission of 410 nm. These were purchased from RadioShack (Fort Worth, TX, USA). Figure 3.5. shows the range of wavelengths emitted by the 410 nm LEDs.
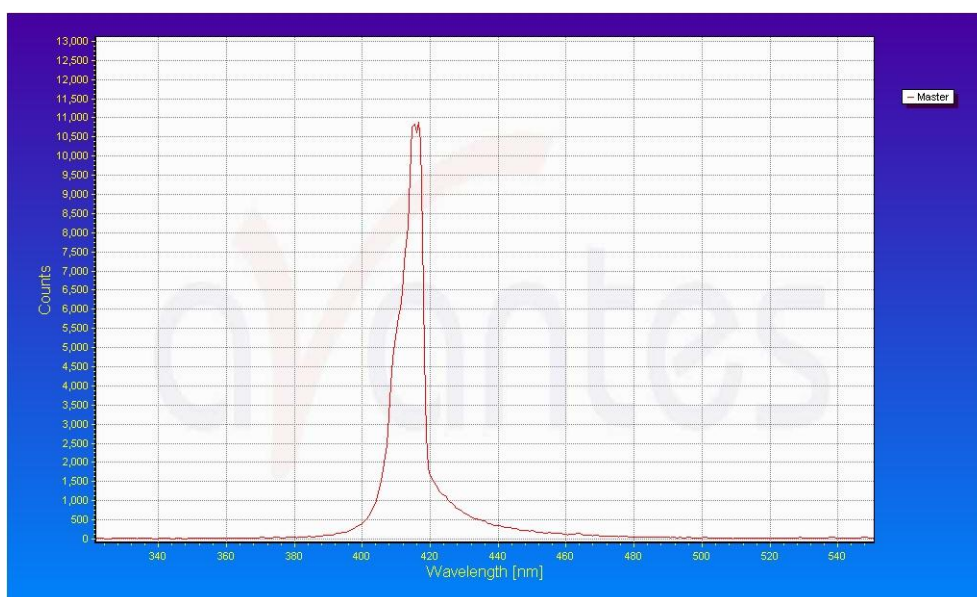
FIGURE 3.5. : Wavelength spectrum emitted by the 410 nm LEDs. Picture of the *Avasoft* application window showing the signal measured with the spectroradiometer, AvaSpec-2048 (Avantes, Apeldoorn, The Netherlands).

The other LED-array included five different LEDs purchased from Roithner LaserTechnik GmbH (Vienna, Austria) with the following wavelengths of emission: 395 nm (RLS-UV395), 380 nm (RLS-UV380), 370 nm (XSL-370-5E), 360 nm (RLT360-1.0-15) and white light (5W4HCA-P).

All LEDs had a diameter of 5 mm which allowed perfect fitting to the grooves in the LED-holder. However, the use of such small size light bulbs constitutes a limitation in terms of the type of LEDs that can be used in the photocalorimeter. For example, the short wavelength LEDs made by Roithner LaserTechnik GmbH (ranging from 245 nm to 360 nm peak wavelengths) could not be used here because they were too large to fit the LED-holder (more than 9 mm diameter in some cases). Furthermore, these short wavelength LEDs were very expensive and had a small optical power output (typically 300 µW). That is why the LEDs used in this photocalorimeter did not cover a wider range of UV wavelengths. Of course, in order to cover the full solar spectrum, LEDs with outputs down to 310 nm (and preferably 290 nm) would be required. Research continues in the field of UV LEDs which aims to produce powerful and relatively inexpensive mid UV LEDs. Once these become commercially available, it will be a relative trivial matter to include extra UV LEDs (or a broad spectrum UV LED) into the light array.

3.2.2.3. *The electronic circuit board*

An electronic circuit board, with individual switches for all LEDs, was intercalated between the LEDs and the power supply. Each LED can be switched on or off, individually, allowing monochromatic lighting conditions to be tested even if the LED-array contains different wavelength LEDs. Figure 3.6. shows a picture of the circuit board.
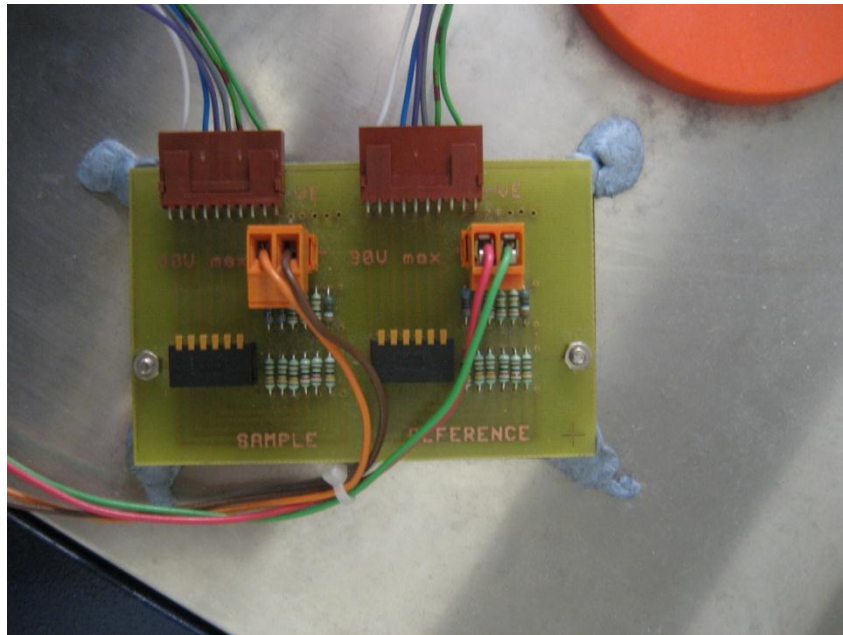
FIGURE 3.6. : Circuit board with individual switches for all LEDs.

The sample and reference side LEDs are wired to this circuit board using the two brown connectors shown in Figure 3.6. Each LED is wired with an in-line resistor built into the circuit board to limit the current in the LED to a safe value. Different types of resistors were inserted in the circuit according to the individual rated operating power of the different wavelength LEDs used. Figure 3.7. shows a basic diagram of the circuit.


```
WHT 1340 ohms white
350nm 1285 ohms Green/Red
360nm 1285 ohms Blue
370nm 1320 ohms Violet
380nm 1330 ohms Grey
395nm 1330 ohms White/Red
```
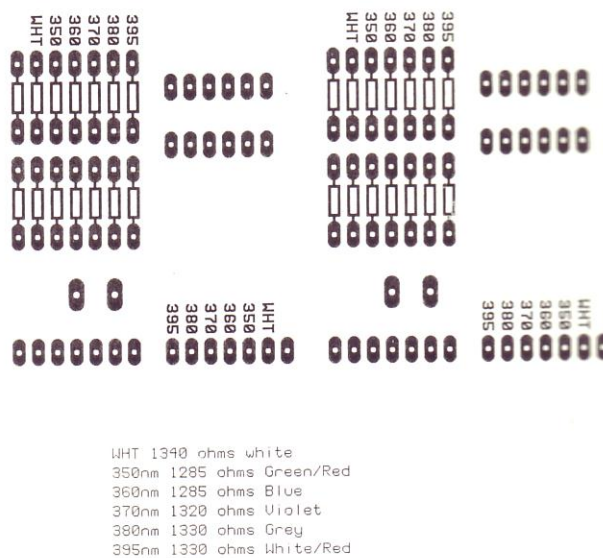
FIGURE 3.7. : Basic diagram showing information etched onto the LED circuit board. The different types of resistors are shown below the diagram.

Despite the fact that the circuit was designed with resistors for 6 different types of LEDs (white, 350 nm, 360 nm, 370 nm, 380 nm and 395 nm), other LEDs may be used with this system, as long as the current that passes through them does not damage the light bulbs.

Other components of the circuit board include the two blocks of individual switches (yellow) and the orange connectors where the sample and reference wires are plugged into. These wires connect the circuit board to the power supply. Contrary to the legends in the circuit board (Figure 3.6.), the right side of the device controls the sample side LEDs while the left side controls the reference LEDs.

3.2.2.4. *The automated electronic-balancing power supply*

The previous photocalorimetric design, developed by Dhuna, used a power supply with two output controls to generate a constant current to the reference and sample side LEDs. The voltage applied on each side could be controlled independently to adjust the intensity of light going into the two calorimetric channels and zero the calorimetric signal with the light on. In order to do that, the voltage on the sample side was set to a desired value and the voltage on the reference side was manually adjusted until the signal reached zero.

This zeroing process was very time consuming and required the operator to be constantly monitoring signal changes. Furthermore, the number of adjustments was greatly dependent on the operator because the control knob was quite sensitive. Therefore, an automated electronic-balancing device was designed, in the UCL School of Pharmacy, to automatically balance the light power going into the sample and reference channels.

This piece of equipment allows the calorimetric signal to be zeroed by gradually changing the voltage applied on the reference side until the signal reaches zero. This process is fully automated and only requires the operator to initiate it using a "start" switch. The time interval between each voltage step is set in the autobalance device and, ideally, should be enough for the signal to stabilise before an additional voltage adjustment is made. This interval is, typically, 900 seconds. When the signal reaches zero, the system automatically stops adding voltage steps and the voltage difference between the two sides is fixed.

Despite the great advantages of using such automated electronic-balancing device, the current system is not perfect because it only allows stepwise increases in the voltage applied to the reference LEDs. This constitutes a problem when the calorimetric signal is negative as the zeroing process requires a reduction in the voltage applied to the reference side (for constant sample irradiation conditions). In these cases, it is necessary, first, to decrease manually the voltage applied on the reference side until the thermal power measured becomes positive. Only then, it is possible to zero the calorimetric signal using the automated stepwise adjustments. Figure 3.8. shows a picture of that automated electronic-balancing power supply.
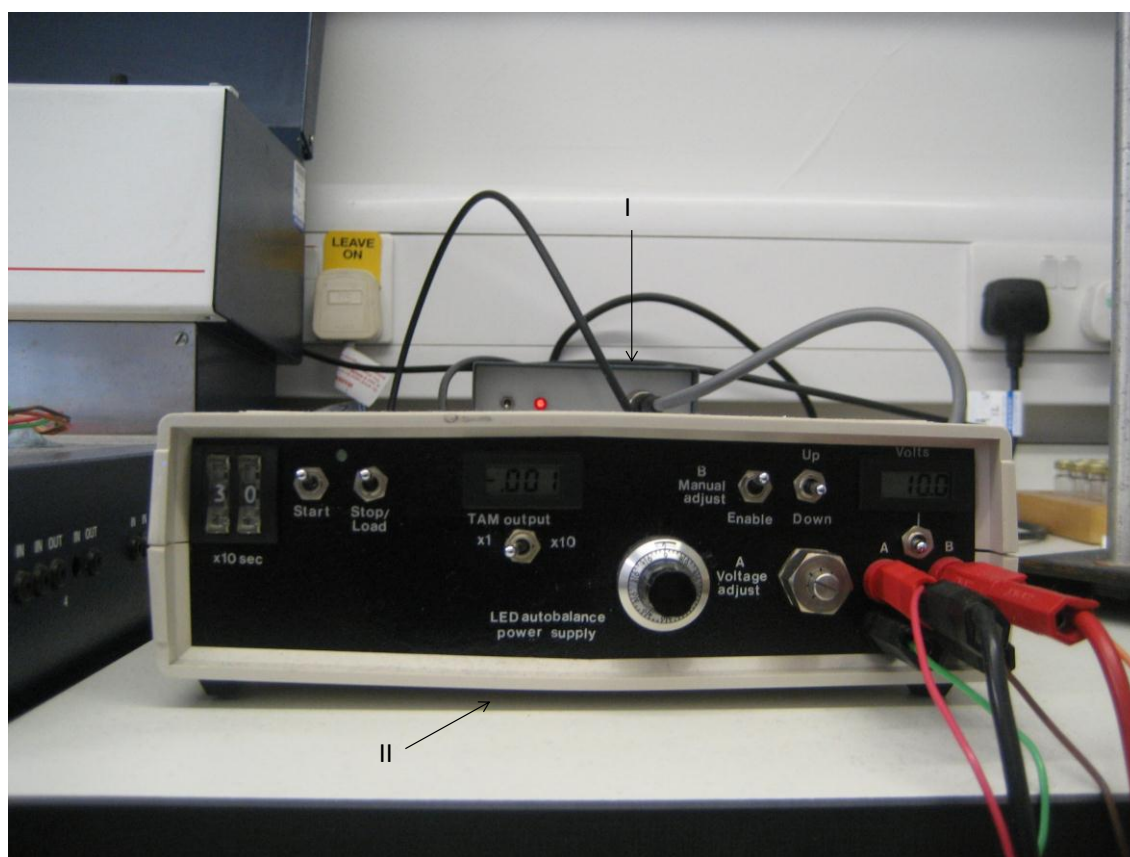
FIGURE 3.8. : Automated electronic-balancing power supply. I- Power supply, II- autobalance device.

This instrument comprises a power supply (I in Figure 3.8.) connected to an autobalance device (II in Figure 3.8.) that performs the automated voltage adjustments. The front panel of the autobalance device shows several knobs, switches and digital displays that are very important in the zeroing process. On the right hand side of that panel there are four ports that connect the sample and reference sides of the circuit board to the autobalance device. The red and black ports on the left (A) are connected to the sample

side wires whereas the two ports on the right (B) are connected to the reference side wires. Above those ports, there is a digital display that shows, alternately, the voltage applied to the sample and reference sides using the switch below it to select which voltage to display. Left of the red and black ports, there is a silver knob that regulates the voltage applied to both sets of LEDs, while maintaining the voltage difference between the two sides. For example, if, initially, the voltages applied to the sample and reference sides are 4 V and 5 V, respectively, an increase in the sample side voltage to 5 V results in an equal increase in the reference side voltage to 6 V. The maximum voltage that can be applied to each side is 30 V.

Above the silver knob there are two switches that regulate the voltage applied to the reference side without changing the sample side voltage. Such manual adjustments are only allowed within a range of ± 2.5 V with respect to the voltage applied to the sample side. In order to make those adjustments, the left switch needs to be pressed down towards the "enable" position while the right switch is pressed up, to increase the voltage, or down, to decrease it. During the process, the left switch is maintained in the "enable" position.

Also, in the front panel of the autobalance device, there is a central digital display that shows a signal which is proportional to the thermal power measured in the TAM. This signal is very important for the automated zeroing process because the size of the voltage steps depends on the magnitude of the TAM output (i.e. large signals result in big voltage steps). Furthermore, it is when that signal reaches zero that the autobalance process automatically stops. Communication between the TAM and the autobalance device is made via a cable that connects the output panel in the back of the TAM to the back of that device.

Below that digital display, there is another switch that allows the TAM output to be multiplied by a factor of 10. This feature is very helpful in those cases where the thermal power is so large that the zeroing process is too lengthy. Instead, multiplication of the output value allows big voltage steps to be applied from the beginning of the autobalance process, hence reducing its length.

On the left hand side of the panel, it is possible to see a "start" switch, that allows the autobalance process to start, and a "stop/load" switch that manually terminates it. Next to those switches, there are two more buttons with numbers that are used to set the duration of the voltage steps. Figure 3.8. shows that an interval of 300 s (30 x 10 s) between each adjustment was set for that specific experiment. Finally, there is an extra

144

black knob in the middle of the panel that functions as the sample side manual regulator. However, this feature is now redundant.

Despite the apparent complexity of the front panel, the procedures used to initiate the automated balancing process are fairly simple and easy to follow. First, the voltage applied to the sample side is set to the desired value using the silver knob. Then, the reference side voltage is adjusted to the same value using the two switches "enable" and "up/down". After switching on all LEDs in the circuit board, light goes into the calorimetric channels and the calorimetric signal shows in the TAM display. If the resulting thermal power, measured in the TAM, is positive, the duration of each voltage step is set and the "start" switch is pressed to start the autobalance process. In case the thermal power is negative, the voltage applied to the reference side must be decreased, first, using the "enable" and "down" switches until the thermal power becomes positive. Only then, the step duration is set and the "start" switch is pressed down to begin the automated zeroing of the signal. An example of the calorimetric signal obtained during zeroing of the calorimetric signal with the lights on is given in Figure 3.9.
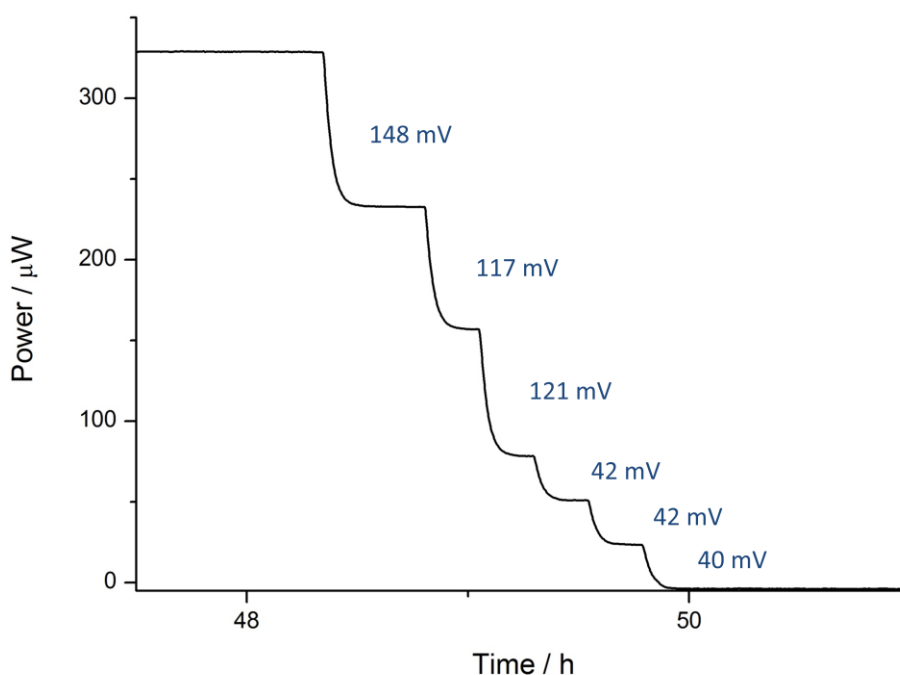
FIGURE 3.9. : Calorimetric signal measured during the zeroing process with the automated electronic-balancing power supply. Two separate arrays of five 410 nm LEDs were used to irradiate light into each calorimetric chamber. Similar voltage was applied initially to the sample and reference sides (7.5 V). The difference in voltage between each step is shown in blue.

That figure clearly shows that, initially, the voltage steps were much bigger compared to those observed in the final part of the automated zeroing process. This is consistent with the previous description of the operation principles behind the process. The calorimetric signal in Figure 3.9. also shows that an error occurred during the first voltage step change. The duration of each step was set to 900 seconds prior to the experiment. However, the first step took twice that time which means that accidentally the instrument missed a step change.

3.2.2.5. *The lighting system*

As mentioned before, the most important design modification made to Dhuna's photocalorimeter was the position of the light source relative to the sample. Previously, the two arrays of LEDs were placed outside the calorimeter and light was conducted to the ampoules, inside the chambers, by liquid light guides. With the new design, the two arrays of LEDs are positioned inside the calorimetric chambers providing a larger amount of light power to the samples and, in addition, reducing the effect of external factors on the signal stability. Two design changes were considered for this purpose: either the LEDs were embedded in the ampoule lid or placed just above it. The latter required a modified ampoule with a windowed lid to allow passage of light. Regardless of the design implemented in the new photocalorimeter, it was obvious that some sort of lighting column was necessary to position the LEDs in the bottom of the chamber.

The first design modifications made to Dhuna's photocalorimeter consisted of inserting 5 LEDs in a standard TAM ampoule lid (Figure 3.10.). In order to do that, the lids were drilled with 5 holes around the central eyebolt and the LEDs were inserted using an epoxy resin to hold them in place. The lid was hooked on a modified calorimetric lifter that had a metal heat shunt, intercalated in the centre shaft, and several discs to prevent air convection phenomena. All discs were drilled with 6 holes to allow passage of the wires connecting the LEDs to the external circuit board. Five of these holes allowed insertion of the wires connected to the LED anodes while the extra hole allowed passage of the common wire that linked all cathodes. The heat shunt only had 5 holes, forcing the common wire to go through a hole occupied by an anode wire. Figure 3.10. shows a picture of the modified lifter hooked on the ampoule lid with the LEDs embedded.
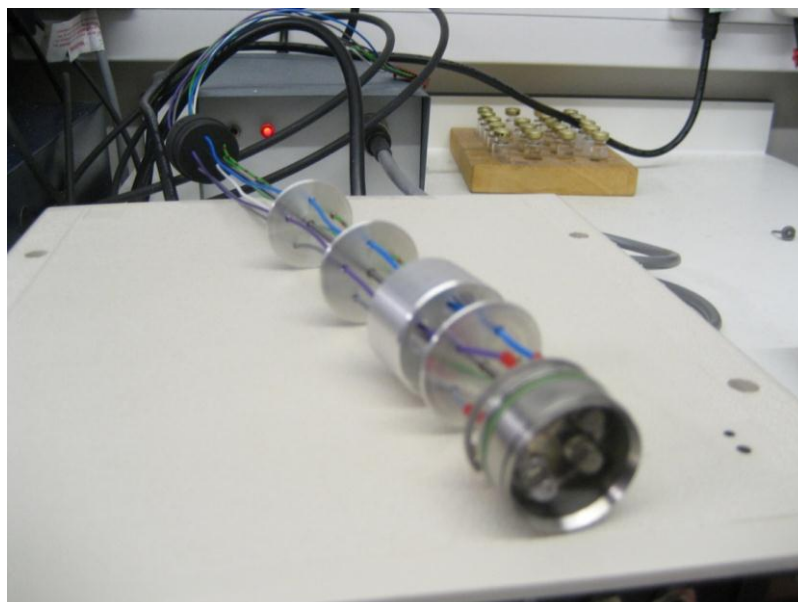
FIGURE 3.10. : Modified lifter hooked on the new lid that contains an array of 5 LEDs.

Afterwards, the new lids were fitted to the sample and reference ampoules to form the lighting columns. Note that all three parts (lifter, lid and ampoule) are connected in series. Once all modifications were made, the signal stability and baseline reproducibility, with the lights on, were assessed. These studies used five different LEDs (360 nm, 370 nm, 380 nm, 395 nm and white light LEDs) to irradiate the two empty calorimetric ampoules. In order to test the signal properties the following method was used:

1- The two lighting columns were lowered in the sample and reference chambers and the system was left to equilibrate at 25 ℃ in the TAM. The amplifier was set to 3000 μW.

2- The resulting thermal power was adjusted to zero and the instrument was electrically calibrated using the TAM software.

3- After calibration, the voltage applied to the reference and sample LEDs was set to 10 V and the LEDs were switched on using the electronic circuit board.

4- Once the signal stabilised with the lights on, the autobalance power supply was used to bring it to zero.

5- Then, the LEDs were switched off and the lighting column was taken out of the chambers. The ampoules were opened to simulate the loading of sample, re-closed and lowered into the chambers. The system was left to equilibrate.

6- Finally, the LEDs were switched on a second time, maintaining the voltage difference between the two sides, and the baseline reproducibility was assessed.

Figure 3.11. shows the typical calorimetric signal recorded during the baseline reproducibility studies.
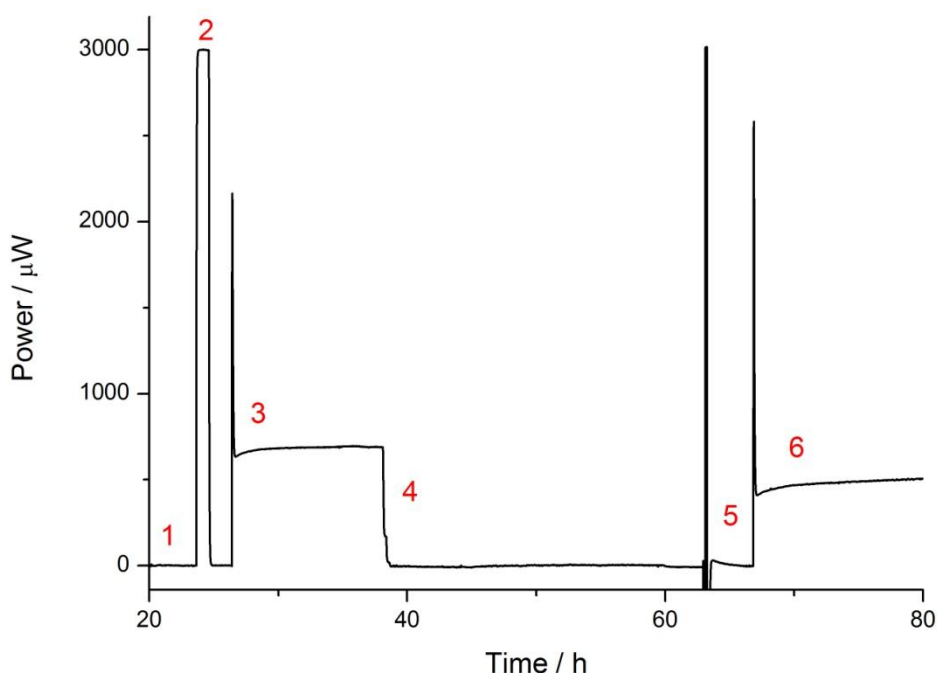
FIGURE 3.11. : Typical calorimetric signal recorded in the baseline reproducibility studies performed with the photocalorimetric design that had the LEDs embedded in the lid. The numbers in red correspond to the different steps of the method used in these studies.

The various tests performed with this photocalorimetric design showed that the signal always returned to zero when the LEDs were switched off. However, considering the repeatability of the signal, with the lights on, the results were not satisfactory. Figure 3.11. shows an example of the different signals measured before and after simulation of the ampoule loading process. In this case, the signal measured after the LEDs were switched on a second time (6 in Figure 3.11.) was significantly different from that measured after the zeroing process (4 in Figure 3.11.). Almost 500 µW separated the two signals measured with the lights on. Other tests showed differences ranging from tens to hundreds of microwatts. The possibility that the light power was changing every time the LEDs were switched on was ruled out after several experiments were performed switching the LEDs on and off repeatedly without taking the lighting columns out of the calorimeter. Figure 3.12. shows an example of these light on/off experiments. The signal was not zeroed, on purpose, to show a clear difference between the thermal power measured with and without light.
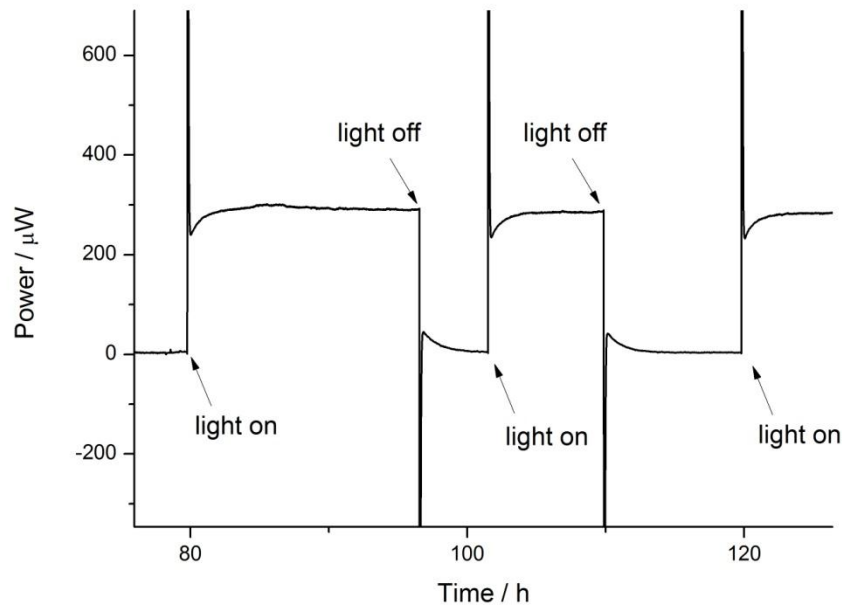
FIGURE 3.12. : Light on/off experiments using the photocalorimetric design where the LEDs are placed in the ampoule lid.

Figure 3.12. shows that no significant differences were observed in the calorimetric signal, every time the LEDs were switched on, which meant that the light power did not change in those experiments. Something else in the process of taking the lighting columns out of the calorimeter, opening/closing the ampoules and lowering the lighting columns back in the chambers was affecting the signal.

One of the major concerns regarding this new design was that the wires connecting the LEDs could get damaged during the opening of the ampoules. The reason for that is that the eyebolt that was used to pull the lid out of the ampoule was positioned right in the middle of the wiring system. No matter how careful one would be, it was almost inevitable that those wires were touched or even bent while trying to pull the lid out. As a result, changes in the circuitry were likely to occur, affecting the performance of the LEDs. This might explain the differences between the signal before and after the ampoules were opened. Another possible explanation is the different positioning of the LEDs relative to the base of the ampoule every time it was closed. Such changes could lead to different illumination patterns.

To address this issue, the standard TAM ampoules were replaced by customised screw-top ampoules that were much easier to open. Figure 3.13. shows the two types of ampoules and the respective lids, side by side.

149
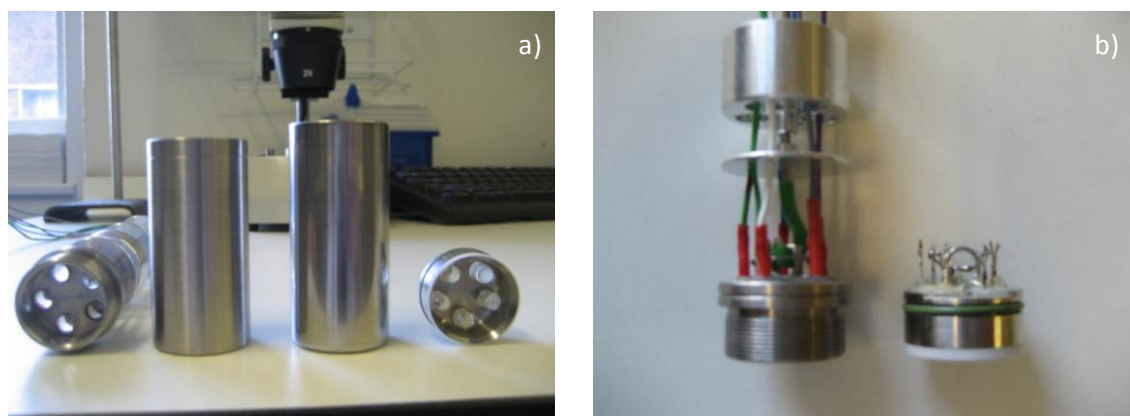
FIGURE 3.13. The two types of ampoules and lids developed for the new photocalorimeter. a) the screw top ampoule (on the left) and the adapted standard TAM ampoule (on the right); b) the two types of lids: lid with thread (left) and adapted standard TAM ampoule lid (right).

Some baseline stability tests were also performed with the new screw-top ampoules but the signal with the lights on was still different before and after opening the ampoules. However, the magnitude of those differences was much smaller compared to the signals measured with the standard TAM ampoules.

After another unsuccessful attempt at re-designing Dhuna's photocalorimeter, the idea of having the LEDs in the ampoule lid was abandoned for two main reasons:

- The presence of 5 highly energetic LEDs in each lid, near the measuring thermopiles, may affect the temperature of the thermostated bath, leading to erratic measurements every time that equilibrium is broken.
- The ampoules in the calorimetric chambers are in thermal contact with the outside because of the wires that connect the LEDs in the lid to the external circuit board. As a consequence, the time required for the whole system to reach equilibrium varies greatly with the outside temperature. In extreme circumstances there is even the chance that equilibrium is never reached. These external factors can affect significantly the thermal power measured by the calorimeter.

With these considerations in mind, it was decided that the photo-TAM had to be modified, once again. The idea behind the new design was to suspend the LEDs above the calorimetric ampoules, creating a thermal break between the ampoule and the lighting column. This change would, in theory, prevent conduction of heat along the lighting column, therefore, minimizing the influence of external factors on the signal and reducing the equilibration time of the system. In order to implement the design

changes, a new lighting column and a modified ampoule lid were developed in the School of Pharmacy's workshop.

The new lighting column is very similar to the one used in the previous design, the only difference being the arrangement of the LEDs in the lower end. That column comprises a centre shaft with several metal discs, a metal block that acts as a heat shunt and a structure that contains the array of LEDs (Figure 3.14. and 3.15.). Furthermore, it has six wires, which connect the LEDs to the circuit board, passing through the several discs and blocks. Five of them are connected to the anodes while the sixth corresponds to a common wire that links all cathodes.
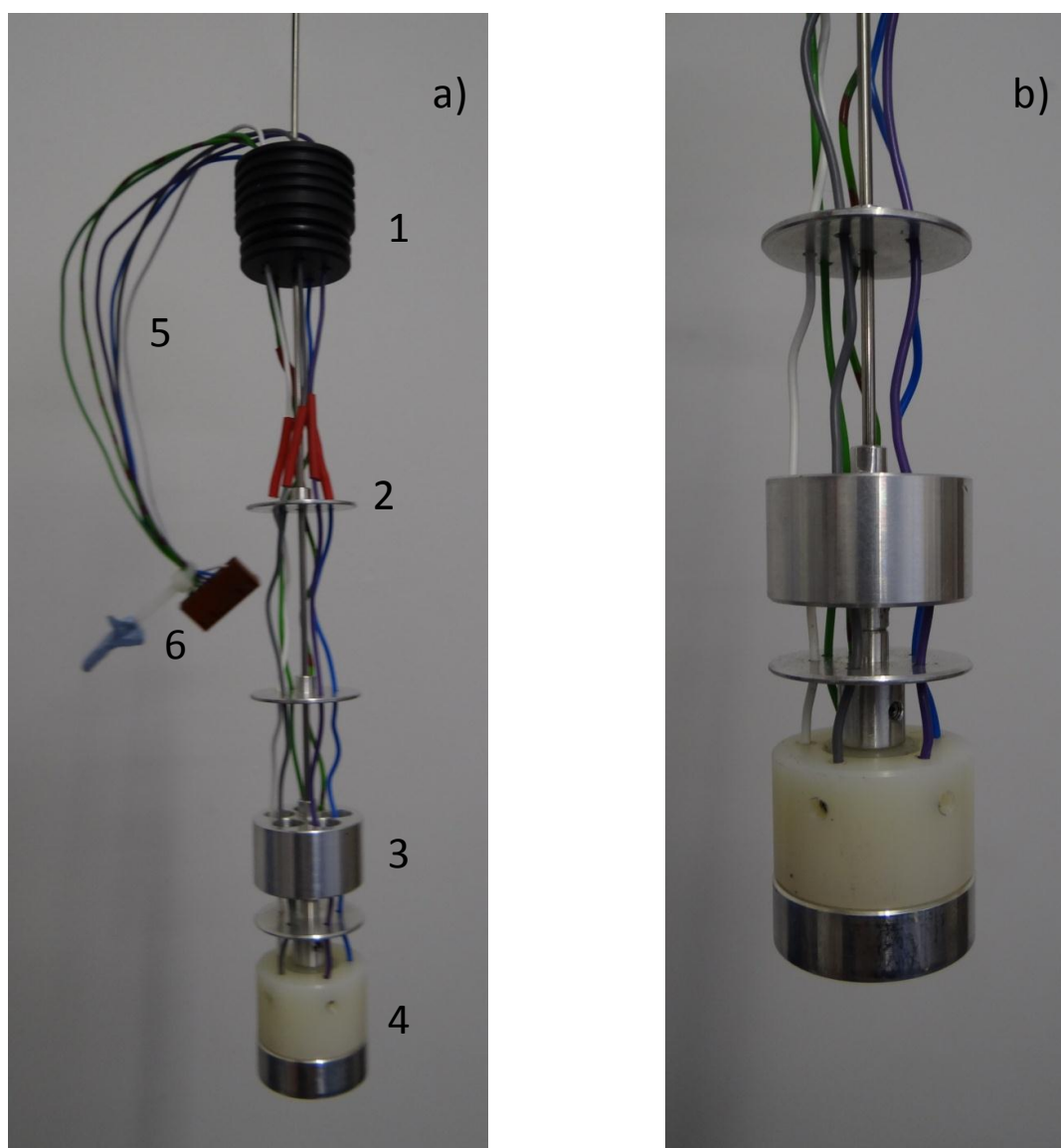
FIGURE 3.14. : The lighting column a) picture of the whole column b) picture of the end that contains the LEDs 1. Supporting lid at the top of the column 2. Metal disc 3. Heat shunt 4. Holder containing the LED-array 5. Wires that connect the LEDs to the circuit board 6. Brown connectors that link the lighting column to the circuit board.

151
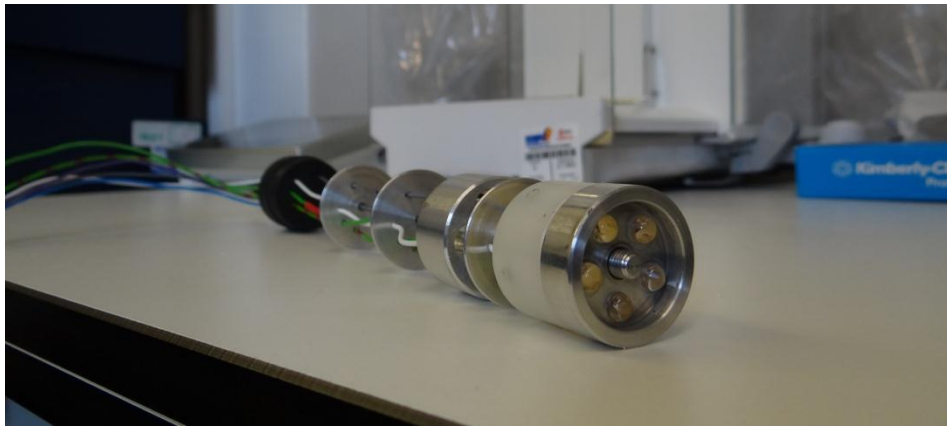
FIGURE 3.15. : Another view of the lighting column used in the new photo-TAM design.

The structure of the holder that contains the LEDs was designed with two purposes: to fit as many light bulbs as possible in that end of the column and to develop a mechanism that allows easy insertion and removal of the LEDs. As Figure 3.15. shows, the maximum number of LEDs that can be housed in that structure is 5. Only bulbs that have a diameter of 5 mm can be used in the array which excludes the shorter wavelength LEDs (255 nm to 350 nm) that have a very large window. Contrary to the previous designs, where the LEDs were soldered to the wires that connect them to the circuit board, the LEDs housed in this structure are clamped to the wires using a screw that forces contact between them. Figure 3.16. shows a scheme of that structure, highlighting the parts involved in the connection of the LEDs to the wires.
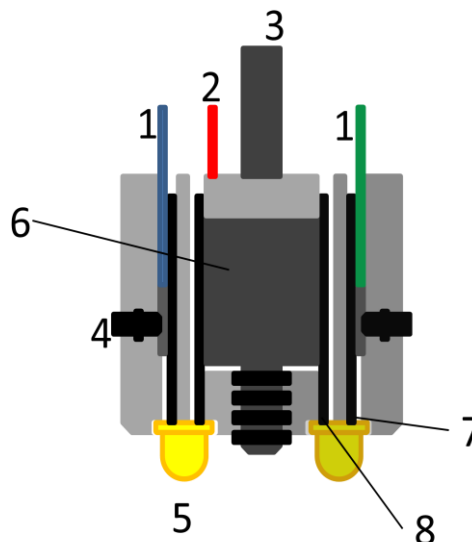
FIGURE 3.16. : Scheme of the structure that contains the LEDs 1. Wires that connect the LED anodes 2. Common wire 3. Centre shaft 4. Screw 5. LED 6. Metal block that connects all LED cathodes 7. LED anode 8. LED cathode.

This design allows all parts of the circuit to be connected without having to solder the LED cathodes and anodes to the wires. The anodes are in close contact with the wires that connect them to the circuit board and a small screw (4 in Figure 3.16.) is used to hold them together. On the other hand, all five cathodes are positioned against a central block of metal that conducts the electrical current back to the circuit board via a common wire (2 in Figure 3.16.). This assembly not only facilitates the replacement of damaged light bulbs without having to physically break connections, but also, eliminates the possibility of damage to the LEDs during soldering.

The position of the holders inside the chambers is set using a screw in the supporting lids (1 in Figure 3.14a.), to adjust the length of the lighting columns. This feature is extremely important for the success of the design because it allows the LEDs to be positioned in a thermostated area above the thermopiles that shunts the heat produced by the bulbs to the chamber sidewalls. As a consequence, the signals measured by the photocalorimeter are not affected by the heat dissipated by the LEDs. Another advantage of this positioning of the LEDs inside the chamber is the uniform illumination of the ampoule contents due to the cone shape of the output.

The other modification that was made had to do with the design of the 20 mL ampoules. Because the LEDs are placed outside the calorimetric ampoules, their lids must be re-designed to allow passage of light through them. That was achieved by inserting a quartz window in each screw top lid (Figure 3.17.). Quartz was used instead of normal glass because it has better ultraviolet transmission properties. Both ampoules and lids were made of stainless steel.
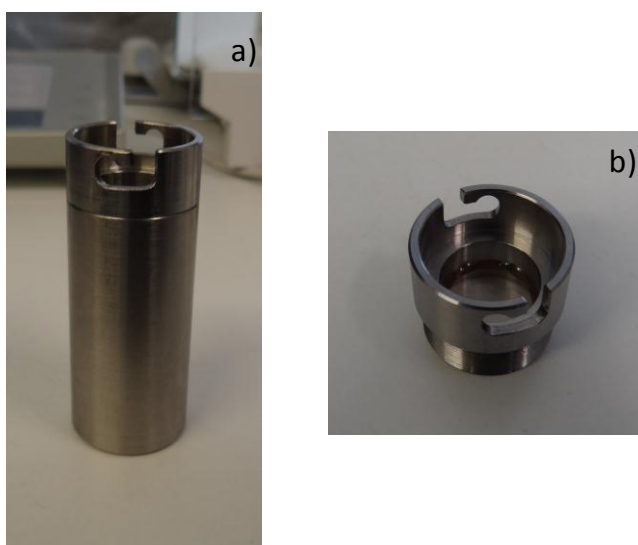
FIGURE 3.17. : a) Screw top ampoule with the new quartz-windowed lid. b) New lid.

Because the modified lids have a quartz window in the centre, the new ampoules could not be taken out of the calorimeter or lowered into it using the centre hook present in the standard TAM lids. To address this issue, a special rod was machined to lift or lower the ampoules in the TAM (Figure 3.18.). This rod fits into a special rim built on top of the ampoule lid allowing the safe transport of ampoules along the chambers.

FIGURE 3.18. : Special rod used to lift and lower the new ampoules in the calorimetric chambers.

Figure 3.19. shows a scheme of the new photo-TAM, highlighting the position of the lighting columns and ampoules inside the calorimetric chambers. This design constitutes the final attempt at developing a photocalorimetric system that uses light-emitting diodes, as the light source, adapted to an isothermal heat conduction microcalorimeter, such as, the TAM 2277. To assess the performance of the instrument, several baseline repeatability tests were made and the results are discussed in the following section.
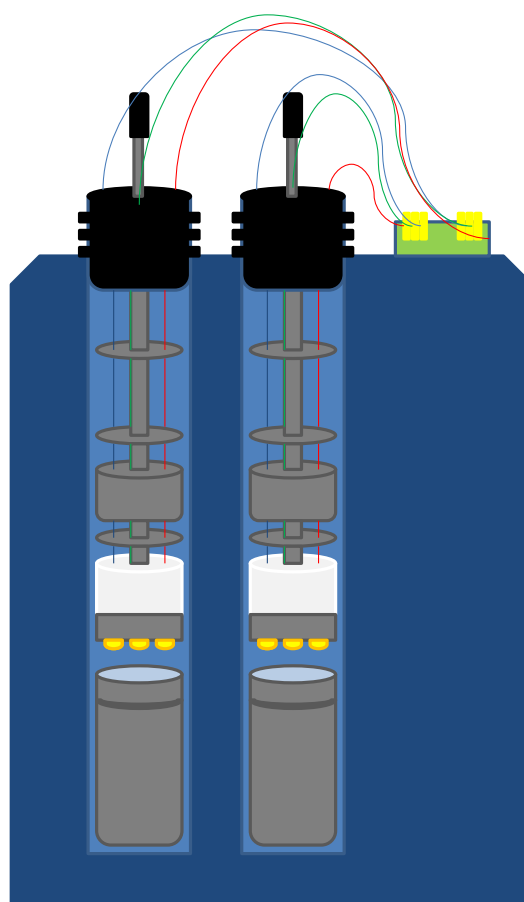
FIGURE 3.19. : Scheme of the new photo-TAM design

3.2.3. Baseline repeatability tests

Two different tests were performed on the new photo-TAM design to assess the repeatability of the calorimetric signals, before and after switching the LEDs on. One of them involved switching the LEDs on and off repeatedly without taking the ampoules and lighting columns out of the system (Test 1). The other, aimed at investigating the repeatability of the signals after simulation of the ampoule loading and unloading process (Test 2). Both experiments used an array of 5 similar 410 nm LEDs to irradiate the ampoules.

Prior to these tests, the calorimetric signal was zeroed, with and without light in the system. First, the photocalorimetric ampoules were lowered in the reference and sample chambers of the TAM 2277 and the lighting columns were placed above them. The system was left to equilibrate at the temperature of the surrounding water bath (25 ºC) and the experiment was initiated using the dedicated software in the computer. When the system reached equilibrium, the calorimetric signal stabilized to a constant value

that was forced to zero using the appropriate screw in the top panel of the TAM. Afterwards, the instrument was electrically calibrated to 1000 µW using the dedicated TAM software. These procedures allowed zeroing of the signal without light in the system.

Then, the same voltage was applied to both sets of LEDs using the autobalance power supply (7.5 V) and the switches in the circuit board were pressed down to turn the lights on. The resulting calorimetric signal was zeroed with the autobalance power supply and the final thermal power corresponds to the zero-baseline with the lights on.

3.2.3.1. *Light on/off tests*

To test the repeatability of the signals, a simple experiment where the LEDs were switched on and off, repeatedly, was performed on the photo-TAM after the signal, with and without light, was adjusted to zero. Figure 3.20. shows the calorimetric signal recorded in these light on/off experiments.
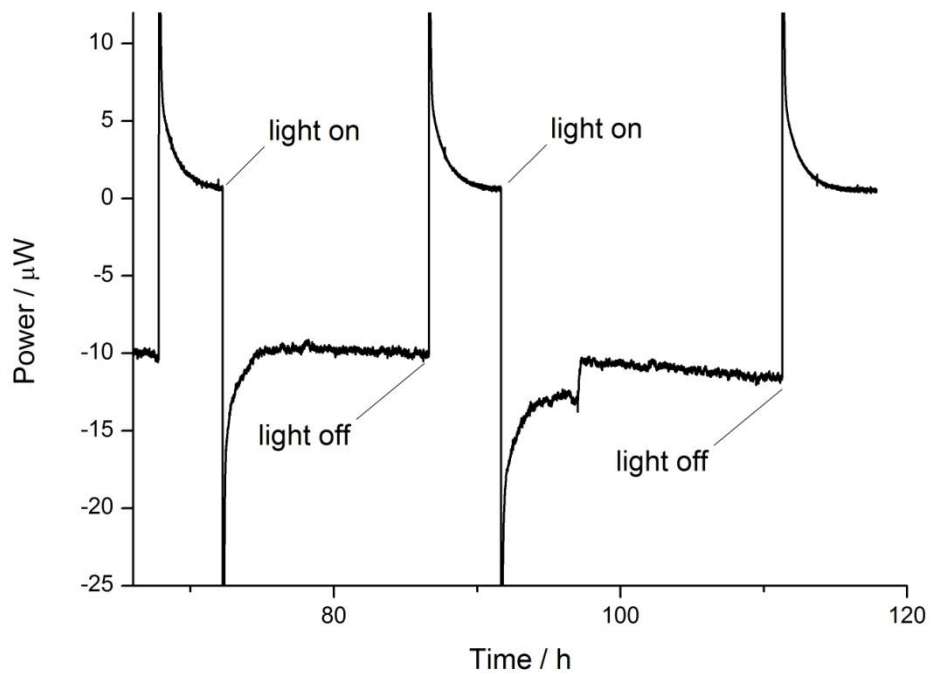
FIGURE 3.20. : Calorimetric signal recorded during the light on/off tests.

That figure shows that there is a clear difference between the signals with and without light. When no light was put into the system, the signals always returned to zero (0.7 ± 0.1 µW). On the other hand, the thermal power measured, after the LEDs were switched on, showed, repeatedly, values around -10 µW (-10.5 ± 0.7 µW). Despite both signals showing a very good repeatability, the magnitude of the average thermal powers was quite different. The inaccuracy of the autobalance process explains the magnitude of the signals measured with the lights on.

These results highlight the biggest limitation of the autobalance power supply which is the difficulty to perform adjustments of just a few microwatts. Previously, it was demonstrated that the autobalance process is a very good method to bring the calorimetric signal closer to zero without the drawbacks of doing it manually (section 3.2.2.4.). However, Figure 3.9. also shows that the last voltage steps used in that process are too large to adjust accurately the calorimetric signal to zero. These voltage adjustments (40 mV) result in a decrease of, approximately, 25 to 30 µW, in the thermal power, which is too large in case only a few microwatts are necessary for the signal to reach zero. For example, if the initial thermal power measured was 5 µW, the final value after the last adjustment would be around -25 µW. That is because the autobalance process only stops when the calorimetric signal reaches zero. Despite these voltage adjustments being too large to accurately zero the signal, other systems, with different LEDs in the array, may affect the zeroing process differently. For example, if only 3 LEDs were present in the array, the changes in the thermal power measured would be much smaller, for similar voltage adjustments, because of the smaller changes in the overall light power. Despite these limitations, the signals always showed good repeatability, proving that the same lighting conditions were created every time the LEDs were switched on.

The "light on/off" tests also showed that the amplitude of the signals was very narrow: around 200 nW for the signals without light and 500 nW for those with light in the system (Figure 3.21.). The latter is particularly important, because it proves that the great amount of energy introduced in the system is not affecting the quality and stability of the signal.
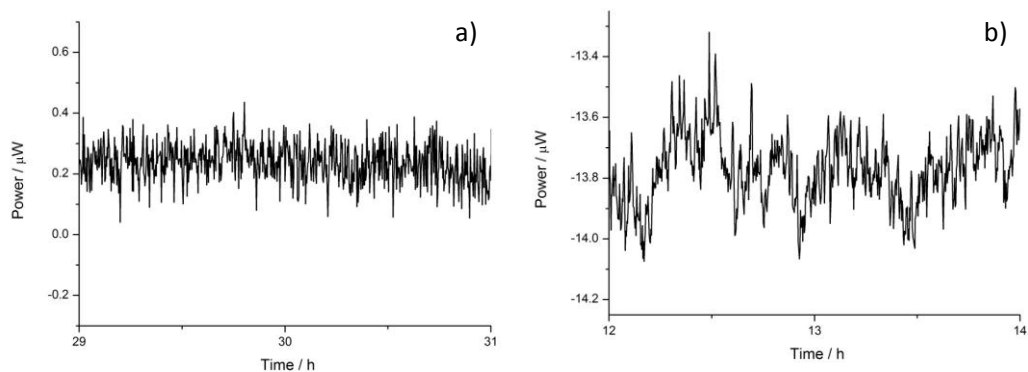
FIGURE 3.21. : Amplitude of the signals measured in the "light on/off" tests. a) signal before the LEDs were switched on. b) signal after the LEDs were switched on.

The same tests were performed by Dhuna using the photocalorimeter that had the LED-arrays outside the chambers and the baseline values with the lights off and on were 1.2 ± 0.8 µW and 2.4 ± 1.0 µW, respectively. Comparison with those obtained with the new photo-TAM design (0.7 ± 0.1 µW with no lights and -10.5 ± 0.7 µW with light) shows that the repeatability of the signals is better with the new design (smaller standard deviations). Those differences in signal repeatability may, however, be explained by the fact those tests were performed with a mixture of ethanol and water in the ampoules which may have an impact on the thermal power measured. In turn, the smaller average signal obtained with the lights on using Dhuna's photocalorimeter can be explained by the fact that, in that case, the voltage adjustments were performed, manually.

3.2.3.2. *Simulation of ampoule loading*

The baseline repeatability, after simulation of the ampoule loading process, was also assessed for the new photocalorimetric design. The method used in these tests is described below:

- The calorimetric signals were zeroed, with and without light in the system, using the method described in 3.2.3.
- After zeroing the signal with the autobalance power supply, both sets of LEDs were switched off in the circuit board.
- Then, the lighting columns and the ampoules were taken out of the calorimetric chambers and the ampoules were opened to simulate the loading process.

158

- Afterwards, the ampoules were closed and lowered in the chambers together with the lighting columns. The system was left to equilibrate at the temperature of the instrument.
- When the calorimetric signal stabilized, all LEDs were switched on and the different baseline values were compared.

Figure 3.22. shows the typical photocalorimetric signal recorded during these tests.
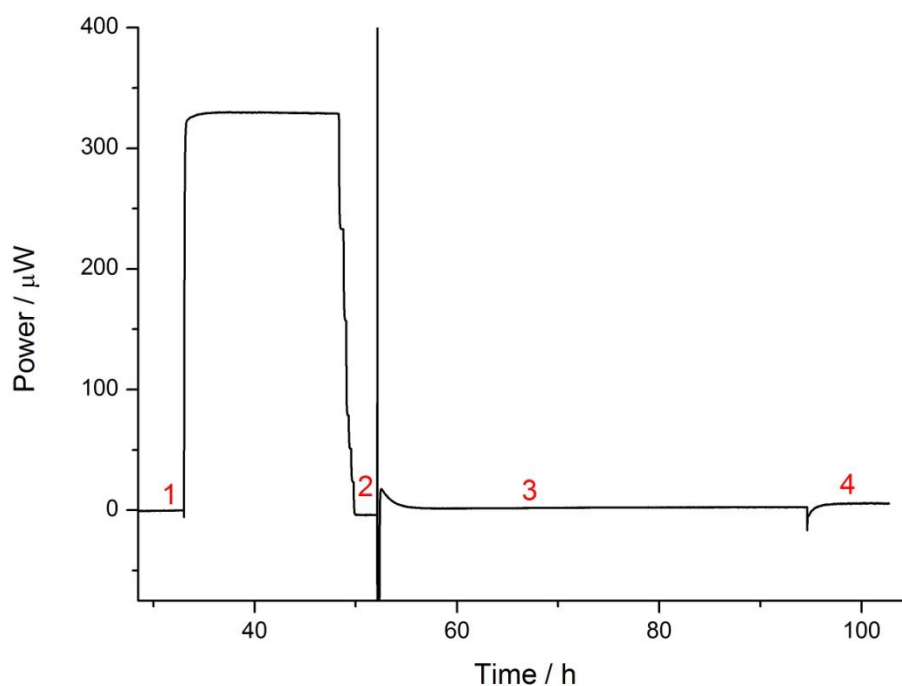
FIGURE 3.22. : Typical photocalorimetric signal recorded in the baseline repeatability tests that simulate the ampoule loading process 1. Baseline without light in the system 2. Baseline with light after the autobalance process 3. Baseline without light after simulation of ampoule loading 4. Baseline with light after simulation of ampoule loading.

All baseline signals were very close to zero, independently of the lighting conditions, demonstrating that the new design changes improved considerably the baseline repeatability in comparison to the previous design where the LEDs were incorporated in the ampoule lid. Three tests were performed on the new photo-TAM and the baseline values are listed in Table 3.1.

TABLE 3.1. : Different baseline values recorded during the signal repeatability tests. Baselines: 1-without light before ampoule loading 2-with light before ampoule loading 3-without light after ampoule loading 4-with light after ampoule loading. All values in µW.

Tests	Baseline 1 (no light)	Baseline 3 (no light)	Baseline 1-Baseline 3 (no light)	Baseline 2 (light on)	Baseline 4 (light on)	Baseline 2-Baseline 4 (light on)
1	-0.2	2.6	2.8	-3.8	5.6	9.4
2	0.3	0.1	-0.2	3.8	-1.9	-5.7
3	0.5	0.3	-0.2	9.2	9.2	0.0
Average ± Standard deviation	0.2 ± 0.3	1.0 ± 1.0	0.8 ± 1.2	3.1 ± 4.6	4.3 ± 4.0	1.2 ± 5.4

The data in Table 3.1. shows that all baseline values were smaller than ± 10 µW which is a significant improvement over the signals obtained with the previous designs (tens to hundreds of µW differences were measured with the lights on after simulation of the ampoule loading). The average values and standard deviations calculated for the signals recorded without light in the system were much smaller than those determined when the LEDs were switched on. That can be easily explained by the previously discussed issues with zeroing the signal using the autobalance power supply. A much better indicator of the repeatability of the signals is the difference between the baselines before and after simulation of the ampoule loading process because it allows investigation of the changes occurring during an experiment. Those differences were still larger for the signals recorded when light was put into the system which means that the baseline repeatability with the lights on is not as good as when the LEDs are switched off. Such results may be explained by the difficulty that is to control to perfection the amount of energy reaching the measuring sites before and after the system had been disrupted by the ampoule loading.

Unfortunately, no such tests were performed with Dhuna's photocalorimeter (with the LEDs outside the calorimeter), hence, it is not possible to compare both systems. Nevertheless, the new design has the great advantage of allowing a much greater light power into the calorimetric ampoules which is very important to study light-dependent processes that require larger activation energies.

3.3. The Photo-MCDSC

The other photocalorimetric design that was developed, during this project, consists of a Multi-Cell Differential Scanning Calorimeter (MCDSC) adapted with light-emitting diodes (LEDs) as the light source. Similarly to the photo-TAM design, this system uses LEDs to irradiate light onto the samples, allowing the investigation of causative wavelengths of degradation. In this case, however, the LEDs are adapted to a calorimetric unit that is often used to perform temperature scans, unlike the TAM that only operates in the isothermal mode. Nevertheless, isothermal conditions are also possible with the MCDSC, despite the lower sensitivity compared to the TAM's.

The photo-MCDSC comprises the calorimetric unit (MCDSC), four LEDs that irradiate, separately, four chambers in the MCDSC, four ampoules with adapted lids, an external circuit board with switches and a power supply that is used to regulate manually the voltage applied to the LEDs. Figure 3.23. shows a picture of this photocalorimeter.
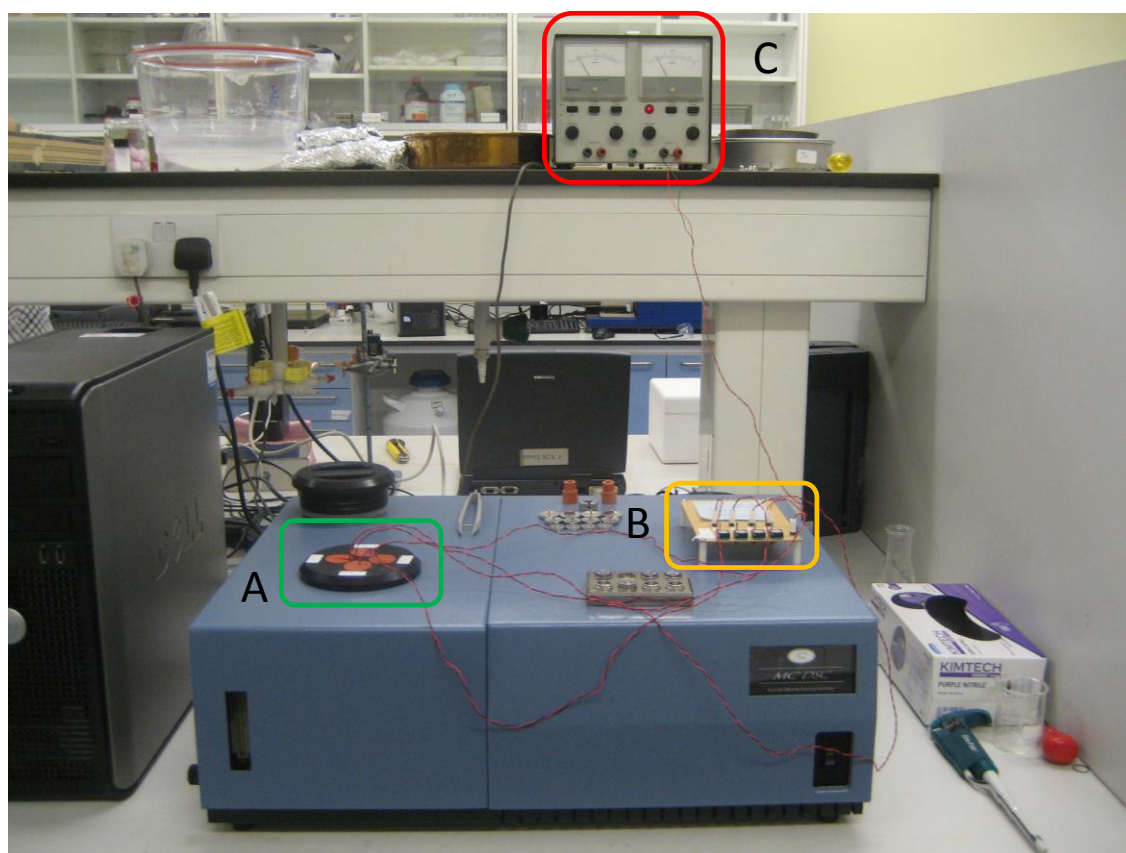
FIGURE 3.23. The photo-MCDSC A. the adapted lid where the LEDs are inserted B. circuit board C. power supply.

3.3.1. The Multi-Cell Differential Scanning Calorimeter (MCDSC)

The MCDSC is a heat conduction calorimeter, commercialized by TA Instruments, that uses semiconductor thermopiles as detectors and 1 mL sample volumes to achieve a hundred times sensitivity over classical DSC instruments (105). The large volume ampoules used in the MCDSC allow investigating a wide range of samples that would not fit traditional DSC pans, unless extensive sample preparation techniques (e.g. grinding) were used. This is particularly relevant in the case of solids where the shape, size and heterogeneous distribution of particles in the bulk affect the thermal and kinetic events occurring in a sample. Testing of liquid samples and solutions is also possible with this instrument, provided that the volume is less than 1 mL.

The MCDSC (Figure 3.24.) consists of four Thermo-Electric Devices (TED) detectors (G) mounted to a common heat sink (A). Three of those detectors measure the thermal events occurring in three different samples, simultaneously, and, under the same experimental conditions. The fourth detector is coupled to a chamber where the reference ampoule is placed. All thermal measurements are made relative to the reference chamber.
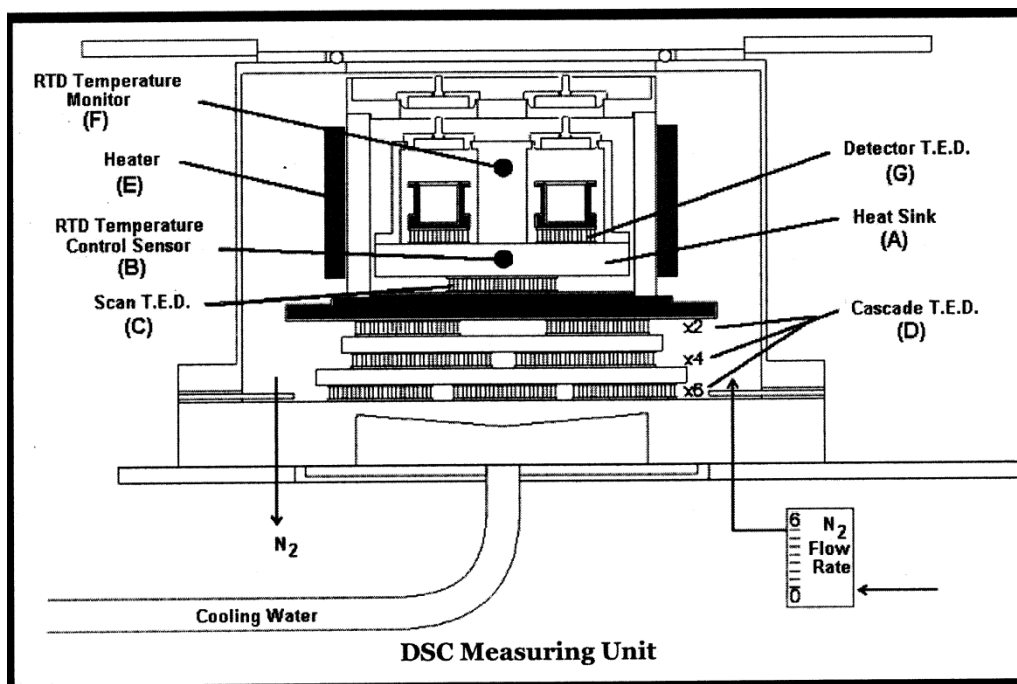
FIGURE 3.24. : Scheme of the MCDSC measuring unit (taken from (105))

The common heat sink (A) is isothermally controlled by the RTD (resistance temperature detectors) Temperature Control Sensor (B) or scanned by the Scan TED (C). A 1000-ohm platinum RTD (F) is used to monitor the DSC temperature. The adiabatic shield reduces (by an order of magnitude) the losses from the heat sink to the environment, thus reducing the high sensitivity detector's thermal noise. Dry nitrogen may be used to keep moisture from condensing on the measurement area when the DSC is operating below the ambient temperature. The heater (E) and TED cascade (D) are used to allow sufficient heating to scan to 200 ℃ and the TED cascade (D) is used to cool approximately 30 ℃ below bath temperature.

The following table contains the technical specifications for the MCDSC.

TABLE 3.2. : Multi-Cell DSC Specifications

Detectable ΔC_p	10 µCal/ ℃ (40 µJ/ ℃)
Ampoule	Hastelloy; 1 mL removable
Temperature Range	-40 to 200 ℃
Scan Rates	0 ℃ (isothermal) to 2 ℃/ minute (heating or cooling)
Short Term Noise Level	0.2 microwatts
Baseline Repeatability	2 microwatts

This calorimeter is connected to a computer that records all thermal measurements. Data capture and control of many of the calorimeter's functions are achieved by use of TA Instruments' dedicated software, "MCDSCRun".

3.3.2. The other components

Similarly to the photo-TAM, light-emitting diodes were used to irradiate the four chambers of the MCDSC. In this case, however, only one LED was allowed into each chamber. All experiments performed in the photo-MCDSC, used the 410 nm LEDs from Radioshack to emit light. However, other 5 mm diameter LEDs could have been incorporated in the instrument.

To allow entry of light in the ampoules, a new lid with a glass window was designed to fit the standard MCDSC ampoules. Ideally, that window should be made of quartz to allow ultraviolet radiation into the ampoules. However, because the type of LEDs used in this photocalorimetric design, emit in the near-UV (410 nm) range, transmission through glass is still very good. Figure 3.25. shows two pictures of the re-designed photocalorimetric ampoules.
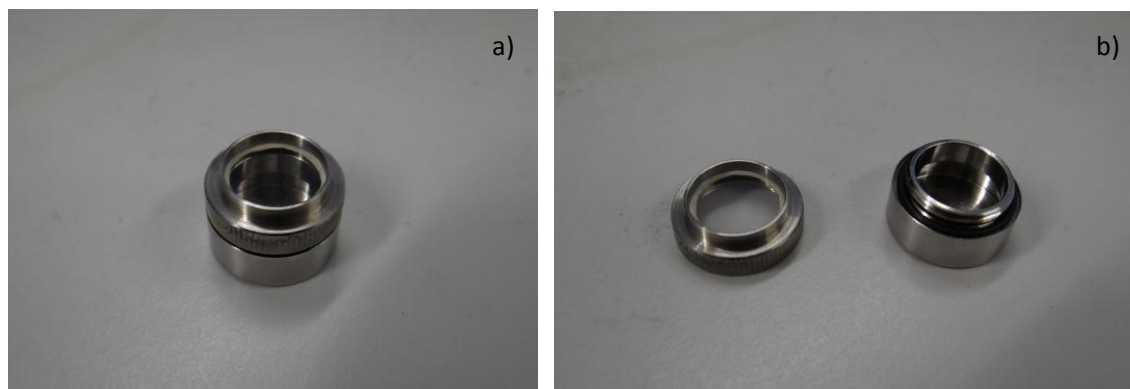
FIGURE 3.25. : The re-designed ampoules a) closed ampoule b) re-designed lid with standard MCDSC ampoule (with rubber o-ring).

In addition to the glass window, a metal rim was designed on top of the lid to lower the ampoules in the calorimetric chambers, using plastic tweezers. To suspend the LEDs above these ampoules, the light bulbs and the wires, that connect them to the circuit board, were fitted with two metal discs that seat perfectly in the platforms above the measuring sites of the chambers (Figure 3.27.). These discs also function as heat shunts that direct the heat produced by the LEDs to the calorimeter sidewalls and insulate the measuring sites. Each LED was soldered to the cathode and anode wires and embedded in the smaller metal disc, using an epoxy resin. An image of the structure that contains the LEDs is shown in Figure 3.26.
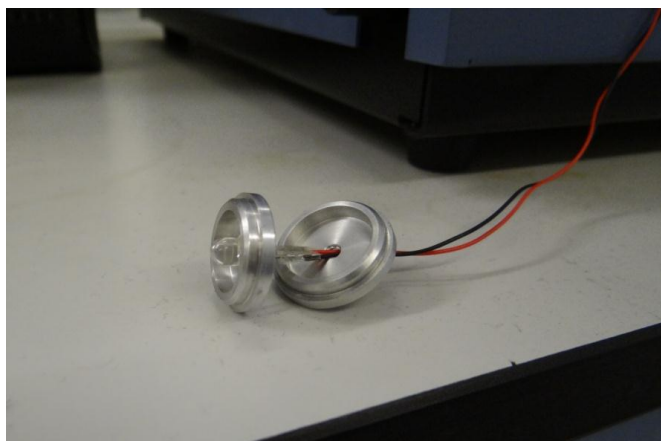
FIGURE 3.26. : A LED mounted on the two metal discs used to suspend it above the calorimetric ampoule.
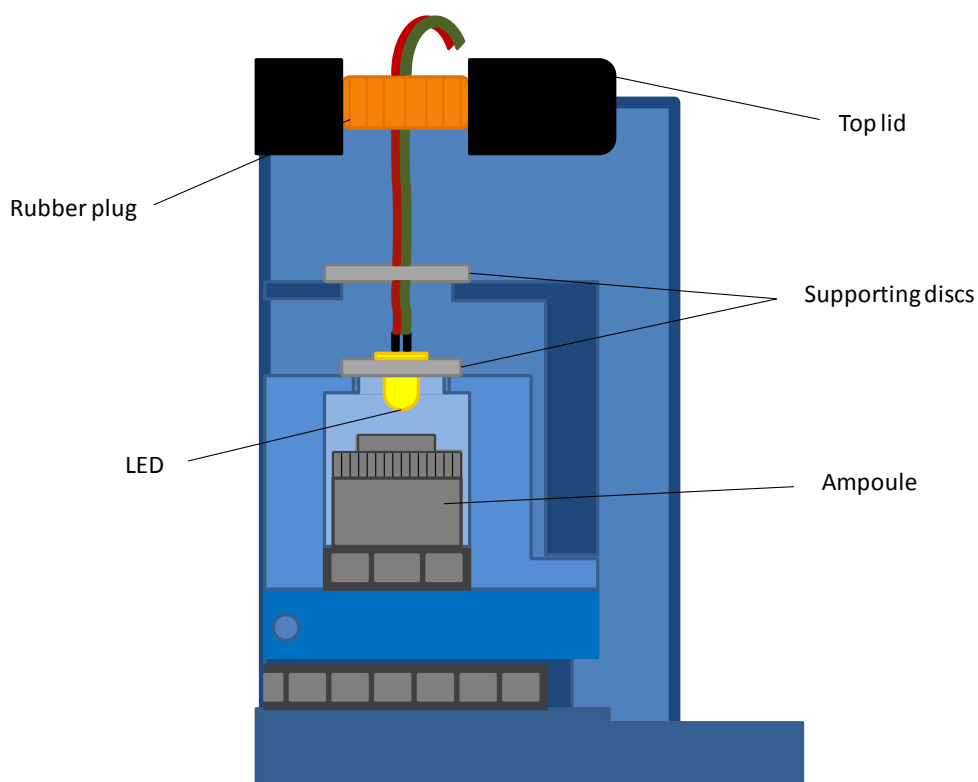
FIGURE 3.27. : Scheme of the arrangement of the LEDs inside the calorimetric chambers.

The top black cover that closes the system also had to be modified to allow passage of the wires that connect the LEDs to the external circuit board. Four holes, aligned with each calorimetric chamber, were machined in that lid and rubber plugs were fitted to them to insulate the system. These plugs had a small slit to allow passage of the wires (A in Figure 3.23).

Another important component of this photocalorimetric design is the external circuit board that is connected to both the LEDs and the power supply, via connectors A and D,

in Figure 3.28. This device has individual switches for each LED, and four knobs that regulate the current that passes through them. That current is adjusted, first, in the power supply (C in Figure 3.23.), using the voltage regulator, followed by the individual adjustments in the circuit board. A voltage of 5 V is usually set in the power supply.
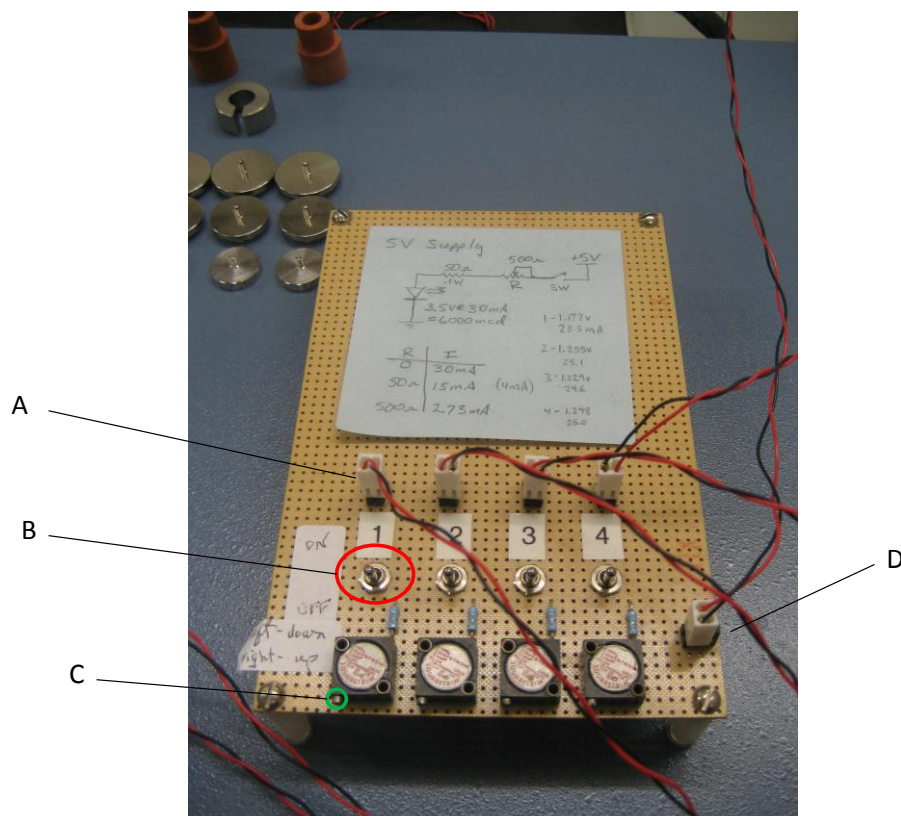
FIGURE 3.28. : The circuit board A. connectors for the LED wires B. switch C. knob that regulates the current applied to the LEDs D. connector that links the circuit board to the power supply.

3.3.3. Baseline repeatability tests

Similarly to the baseline repeatability experiments conducted on the photo-TAM, two tests were performed on the photo-MCDSC to assess the signal repeatability, with and without light in the system. One of those tests consisted of switching the LEDs on and off repeatedly to assess the repeatability of the light outputs. The other test aimed to investigate the repeatability of the calorimetric signals, with and without light, after simulation of the ampoule loading process. All experiments were done at 25 ºC (isothermally) in a single calorimetric chamber inserted with a 410 nm LED. Unlike the photo-TAM experiments, the light power going into that chamber was not balanced

with light from a reference LED because the energy from a single LED is small enough to be measured by this calorimetric unit. Furthermore, the range of thermal powers measured in the MCDSC is much broader than the ± 3000 µW maximum range in the TAM.

3.3.3.1. Light on/off tests

Only two re-designed ampoules were used in these tests: one in the reference chamber and another one in one of the test chambers. After the ampoules were positioned inside the chambers, all four LEDs were inserted in the calorimeter and the system was closed with the top cover and the rubber plugs. The system was left to equilibrate at 25 ºC for 10 minutes before data collection was initiated using the "Run" button in the MCDSC software. When the calorimetric signal stabilized to a constant value, the test LED, placed above the ampoule, was switched on and a big deflection from the initial baseline was observed. After that calorimetric signal reached a constant value, the LED was switched off and the system went back to the initial state. This procedure was repeated two more times to assess the repeatability of the light outputs. Figure 3.29. shows the signal recorded in these experiments.
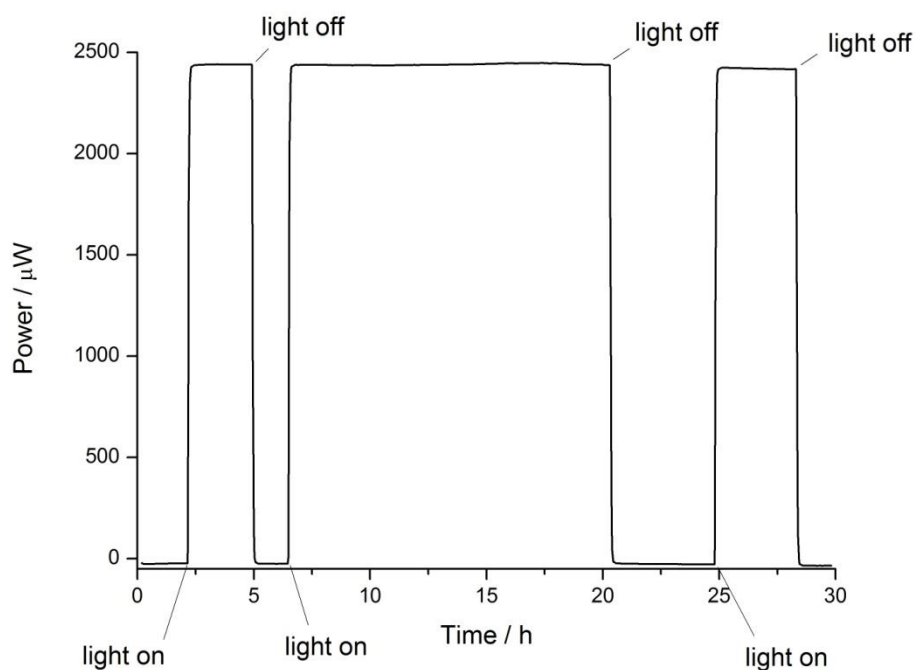
FIGURE 3.29. : Calorimetric signal recorded in the light on/off tests with the photo-MCDSC.

The average ± standard deviation for the signals recorded, before and after the LED was switched on, were -26.2 ± 2.3 µW and 2433.5 ± 9.2 µW, respectively. Comparison of the standard deviations with the stated MCDSC baseline repeatability (2 µW), allows concluding on the repeatability of the signals recorded with the photo-MCDSC. Before the LED was switched on, the baseline repeatability was within tolerance. Unsurprisingly, after the LED was switched on, there was an increase in baseline variability that can be explained by the slightly different light power emitted by the LED every time it is switched on. In addition, the signals measured, before the LED was switched on, were very different from the ideal zero baselines obtained in the photo-TAM experiments. The reason for that is that the MCDSC does not have the capacity to zero the calorimetric signal in the same way that the TAM does.

Unfortunately, comparison between these results and those obtained with the photo-TAM, is not possible, because the reference LEDs, in the photo-TAM, balance the light power emitted by the sample LEDs, therefore, masking any differences in the light outputs. Nevertheless, it is clear that the standard deviations are much smaller in the photo-TAM (0.1 µW without light and 0.7 µW with light).

3.3.3.2. Simulation of ampoule loading

The repeatability of signals after simulation of the loading of ampoules was also assessed with the photo-MCDSC. Similarly to the light on/off tests, two ampoules were place in the reference and test chambers, followed by insertion of the LEDs and closure of the system using the top cover and the rubber plugs. In this case, however, after the two baseline values were measured, the test ampoule was taken out of the calorimeter, opened, closed again and re-introduced in the calorimetric chamber to simulate the loading of ampoules. This process was followed by a re-test of the baselines, before and after irradiation with light. Figure 3.30. describes the typical calorimetric signal recorded in these tests.
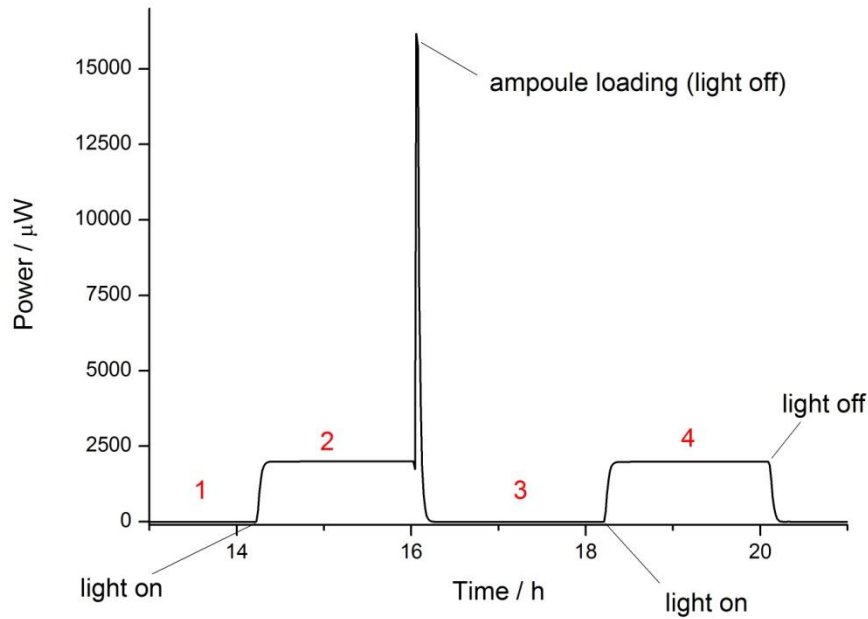
FIGURE 3.30. : Typical calorimetric signal measured during a baseline repeatability test where the loading of ampoules was simulated 1. Baseline without light in the system 2. Baseline with light in the system 3. Baseline without light after simulation of ampoule loading 4. Baseline with light after simulation of ampoule loading.

The figure above shows that the signals are not significantly different, before and after simulation of the loading process. However, the scale of the graph is not particularly helpful to discriminate between differences of only a few microwatts. Therefore, the exact baseline values were measured for three different experiments and the results are shown in Table 3.3.

TABLE 3.3. : Baseline values measured in the signal repeatability tests. Baselines: 1-without light before ampoule loading 2-with light before ampoule loading 3-without light after ampoule loading 4-with light after ampoule loading. All values in µW.

Tests	Baseline 1 (no light)	Baseline 3 (no light)	Baseline 1- Baseline 3 (no light)	Baseline 2 (light on)	Baseline 4 (light on)	Baseline 2- Baseline 4 (light on)
1	-8.4	-5.3	3.1	1995.9	1979.8	-16.1
2	-5.4	-10.5	-5.1	1977.8	1959.7	-18.1
3	-4.3	-8.5	-4.2	1953.5	1943.5	-10.0
Average ± Standard deviation	-6.0 ± 1.5	-8.1 ± 1.9	-2.1 ± 3.2	1975.7 ± 15.0	1961.0 ± 12.9	-14.7 ± 3.0

These three tests showed that the loading of ampoules does not affect the baseline repeatability with or without light in the system. Considering, for example, the baseline signals measured after the LED was switched on (Baselines 2 and 4), the standard deviations calculated before and after ampoule loading (15.0 and 12.9 µW, respectively) are very similar and so are the differences between the two baselines (14.7 ± 3.0 µW). That means that the variations in the signal are only attributed to the inevitable change in the light power irradiated by the test LED every time it is switched on. The same trend was observed for the baselines measured without light, therefore, showing that no additional variability resulted from simulating the loading of ampoules.

All average values and standard deviations calculated for these tests are consistent with what was previously discussed for the light on/off tests.

3.4. Summary

This chapter reported the development of two new photocalorimetric designs for the photostability assessment of pharmaceuticals. Both instruments use light-emitting diodes as the light source adapted to different calorimetric units.

One of the instruments, the photo-TAM, was built after re-designing Dhuna's photocalorimeter (5) and consists of a heat-conduction microcalorimeter (TAM 2277) adapted with two lighting columns that irradiate the ampoules inside the calorimetric channels. Each column has an array of 5 LEDs in the end, which can be customized to the specific requirements of the test. These arrays can fit any kind of LED as long as they fit the grooves in the end of the column. In addition to the lighting column, the ampoules had to be re-designed to allow passage of light through the lid. In order to do that, a quartz disc was inserted into each ampoule lid. Other parts of the photocalorimeter include an external circuit board with individual switches for the LEDs and an automated electronic-balancing power supply that automatically zeroes the calorimetric signal obtained after switching the LEDs on. Two signal repeatability tests were performed on this photocalorimeter using two arrays of 5 similar 410 nm LEDs to irradiate the sample and reference channels. First, the signal repeatability was assessed with a light on/off test and the average signals $\pm$ standard deviations were 0.7 ± 0.1 μW with no light and -10.5 ± 0.7 μW with light in the system. The signal repeatability was also assessed after simulating the ampoule loading process and the following values were obtained: 0.8 ± 1.2 μW without light and 1.2 ± 5.4 μW with light.

The other photocalorimeter also uses LEDs as the light source, in this case, adapted to a Multi-Cell Differential Scanning Calorimeter (photo-MCDSC). Contrary to the photo-TAM, only one LED irradiates each ampoule which limits photodegradation testing to near monochromatic irradiation. Nevertheless, this instrument has some advantages over the photo-TAM, such as its versatility, ease of operation and the possibility to test 3 samples at the same time. This design also has an external circuit board with individual switches for the LEDs and regulators to adjust the current that passes through each LED. Connected to the circuit board, there is a power supply that controls the voltage applied to the reference and sample LEDs. In this case, however, the voltage adjustments are performed manually. To assess the signals' repeatability, two different tests were performed on the photo-MCDSC, using a 410 nm LED to irradiate one of the

test calorimetric chambers. Contrary to the photo-TAM, the light power going into the sample channel was not balanced with a reference LED. The average signals ± standard deviations obtained in the light on/off tests were -26.2 ± 2.3 µW with no light and 2433.5 ± 9.2 µW with light in the system. The signals' repeatability was also assessed after simulation of the ampoule loading process and the following values were obtained: -2.1 ± 3.2 µW without light and -14.7 ± 3.0 µW with light. Comparison of the results obtained in the ampoule loading tests, using both instruments, shows that the signal repeatability is much smaller in the photo-TAM. However, that may be explained by the fact that, in the photo-MCDSC, the signals were not zeroed prior to testing.

4. Application to the photostability assessment of drugs in solution

4.1. Introduction

Chapter 3 reported the development of two new photocalorimetric designs for the investigation of photodegradation in pharmaceuticals. The two instruments were tested for signal repeatability and stability over time and the results proved very satisfactory regarding baseline reproducibility with and without light in the system. Having performed such fundamental tests, the next step consists of testing the photocalorimeters with real photosensitive systems.

Demonstration of their application to the investigation of photodegradation processes in pharmaceutical compounds is presented in two separate chapters that deal with the analysis of systems in different physical states. Since the two most common pharmaceutical physical forms are solid dosage forms and solutions of a drug molecule, only these two cases will be explored. Chapter 4 will thus deal with testing of systems in solution while Chapter 5 demonstrates the use of both photocalorimeters to analyse compounds in the solid state. This organisation is very convenient because the strategies used in the analysis of calorimetric data are significantly different in solution phase and solid state.

This chapter, therefore, aims to demonstrate the suitability of the photo-MCDSC and the photo-TAM to study photodegradation processes in solution. In order to do that, an adequate model photolabile system had to be chosen having in mind that the magnitude of the signals measured not only depends on the sensitivity of the instrument but also on the energetics and kinetics involved in the light-induced process. Since not many data are available on the thermodynamic aspects of photoreactions, the best option was to choose a compound that is known to degrade quickly upon exposure to radiation. The use of rapidly degrading systems is preferred because a greater amount of energy is exchanged per unit time thus allowing an assessment of the instruments' detection capacity.

The model photolabile reaction chosen for these tests in solution was the photodegradation of nifedipine in ethanol under near-UV radiation. Nifedipine, 2,6-dimethyl-3,5-dicarbomethoxy-4-(2'-nitrophenyl)-dihydropyridine, is one of the most used coronary vasodilators, acting as a calcium antagonist, inhibiting the excitation-contraction coupling in vascular smooth muscle. It has also been proved to be effective for the prevention of angina pectoris and in controlling the blood pressure of

hypertensive patients (106). Nifedipine is an extremely light sensitive drug that has been subject to various studies in the solution phase (3, 26, 107) and in the solid state (3, 21, 108). The degradation products and mechanism of photodegradation were studied in both forms and the most common degradants are shown in Figure 4.1.
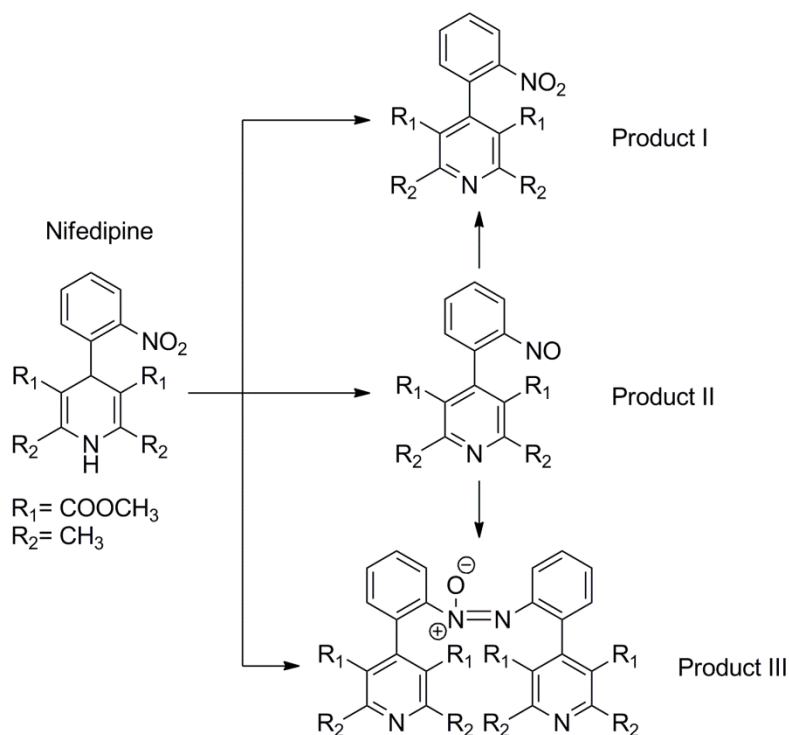
FIGURE 4.1. : The chemical structures of nifedipine and its photodegradation products; I - nitro-derivative, II - nitroso-derivative, III - azoxy-derivative (figure adapted from (108)).

The number of photoproducts present and the extent to which each product is formed is significantly different in those two physical states. In the solid state, up to four products have been reported when nifedipine is exposed to UV light (the fourth was found in trace amounts and is yet to be identified) (108). On the other hand, in solution phase, there is controversy regarding the major products resulting from exposure to different light sources. The first studies by Testa (109) and Jakobsen (110) reported the formation of the nitrosophenylpyridine product under visible light and the generation of the nitrophenylpyridine derivative when exposed to ultraviolet light. However, recent studies suggest that the primary photoprocess leads to the formation of the nitrosophenylpyridine derivative after exposure to both daylight and UV light (111-114). The mechanism of reaction involves bonding of the hydrogen in position 4 of the dihydropyridine to the nitro group and formation of an intermediate that undergoes

further loss of a water molecule with formation of nitrosophenylpyridine derivative (111, 115). The nitro-derivative and the azoxy-derivative are usually present as minor products and their formation is thought to result from additional reactions of the nitroso-derivative (111). For instance, the appearance of the nitrophenylpyridine derivative in solution results from further photo-oxidation of the nitroso-derivative in the presence of oxygen (116). However, this photo-oxidation is not significant and many authors consider nifedipine to be rather insensitive to oxygen (111, 112).

The kinetics of nifedipine photodegradation were also studied in solution and it was found that, for concentrations higher than 4×10^{-4} M, the disappearance of the reduced form and appearance of the oxidized form is best described by zero-order kinetics. At lower concentrations pseudo-first order kinetics are followed (25). Other studies suggest a change in the kinetics from zero-order to first-order after 50% to 60% of reaction has progressed (115, 117). The effects of light intensity and pH on the reaction kinetics were also assessed and the results showed an increase in the rate of reaction with increasing light power and a maximum rate for solutions of pH 2 (25). Quantum yields (ϕ) for this photoreaction were calculated under different conditions and the values obtained ranged from 0.2 to 0.3 (112, 113, 116). This parameter depends only little on solvent properties and is rather insensitive to the presence or absence of oxygen (112).

Photocalorimetry has been used before to investigate the photodegradation of nifedipine in solution (3, 76). These studies, however, focussed on the qualitative analysis of degradation signals and not much quantitative information was obtained from those experiments. For example, Dhuna's photocalorimeter was used to investigate the effect of different wavelengths on the photoreaction heat output in a very qualitative way (76).

The extreme sensitivity of nifedipine towards light and the great amount of information available on its kinetics in solution were important factors in the selection of this reaction as the test photochemical process. The photocalorimetric studies described in this chapter, therefore, aim to investigate the thermodynamic and kinetic aspects of nifedipine photodegradation in solution using the two photocalorimetric designs described in Chapter 3. Solutions of nifedipine were prepared in ethanol in different concentrations and different volumes were tested with the photo-TAM and photo-MCDSC. The effect of intensity of light on the photocalorimetric signals was also assessed. The photocalorimetric data were analysed quantitatively and the reaction parameters (reaction rate constant and enthalpy of reaction) were calculated for all experiments. The analytical strategies used were afterwards validated with a HPLC

assay to determine the rates of disappearance of nifedipine in both photocalorimetric systems. These rate values were then compared with the ones obtained with calorimetric data analysis.

4.2. Materials and methods

4.2.1. Materials

Nifedipine (>98%) was purchased from TCI Europe. Ethanol (>99.7-100%) was purchased from Hayman Ltd, UK. Methanol (HPLC grade) and Acetonitrile (HPLC grade) were purchased from Fisher Scientific. Trifluoroacetic acid (≥99%) was purchased from Sigma-Aldrich. The 410 nm LEDs (5mm high brightness Ultraviolet LEDs) were purchased from RadioShack, Fort Worth, TX, USA. The 395 nm LEDs (RLS-UV395), 380 nm LEDs (RLS-UV380), 370 nm LEDs (XSL-370-5E), 360 nm LEDs (RLT360-1.0-15) and white light LEDs (5W4HCA-P) were all purchased from Roithner LaserTechnik GmbH, Vienna, Austria.

4.2.2. Methods used in the studies performed with the photo-MCDSC

4.2.2.1. *Preparation of solutions of nifedipine*

Solutions of nifedipine were prepared in ethanol with two different concentrations, 1% *w/v* (2.9×10^{-2} M) and 1.33% *w/v* (3.8×10^{-2} M). Nifedipine was weighed (250 mg and 332.5 mg, respectively) into 25 mL volumetric flasks and ethanol was added to dissolve it. The solutions were left to stir until complete dissolution of the powder and ethanol was added until the final volume reached 25 mL. All solutions were prepared in a dark room under red light to minimise photodegradation prior to the experiments.

4.2.2.2. Photocalorimetric experiments

One of the big advantages of using a system such as the photo-MCDSC is the possibility of studying causative wavelengths of degradation by selecting the appropriate LED and plugging it to the circuit board that controls the intensity of light emitted by the LEDs. In these studies, however, only one type of LED was tested, the 410 nm LED, because the main objective was to investigate the instrument's performance and analyse quantitatively the photoreaction signals. Hence, the analysis of causative wavelengths of degradation is not going to be addressed here.

In the beginning of each photocalorimetric experiment, a specific volume of the previously prepared solutions was loaded into the photo-MCDSC ampoules. Three different volumes, 0.5 mL, 0.75 mL and 1 mL, of each preparation (1% and 1.33% *w/v* in ethanol) were used in these studies. After loading the samples and closing the ampoules with the glass-windowed lids, the ampoules were lowered into the calorimetric channels. The reference channel was always left empty. A LED was then placed on top of each ampoule allowing a very small gap between the bulb and the glass window.

After placing the LED inside the channel, rubber plugs were fitted to the holes in the top lid of the photocalorimeter and the system was left to equilibrate. In the mean time, the software that operates the instrument, MCDSCRun, was initialized and the method set up. All experiments were carried out at 25 ºC and data were recorded (*exo up*) for a period of 15 hours. Data collection started immediately after the method was set up and the calorimetric signal was displayed in the application window. Once the system reached equilibrium and the calorimetric signal stabilized, the LEDs were switched on to allow irradiation of the samples. The LEDs were kept on until the end of the experiments. All samples were analysed in triplicate and the same procedure was followed for each one of them.

The effect of increasing light intensity on the photodegradation signals was also assessed by varying the current applied to the LEDs. These studies were only performed on 1 mL samples of 1% *w/v* nifedipine in ethanol. The light power irradiated by the LEDs was measured with a spectroradiometer AvaSpec-2048 (Avantes, Apeldoorn, The Netherlands).

All calorimetric data were analysed first with the software packages Universal Analysis 2000 (TA Instruments-Waters LLC, USA) and NanoAnalyze (TA Instruments, USA). OriginPro8 (OriginLab) was afterwards used for more complex analyses and plotting of graphs.

4.2.2.3. *High-performance liquid chromatography (HPLC) analysis*

A HPLC assay was used to determine the concentration of nifedipine in solution at different time points during a photocalorimetric experiment. This analysis allows the rate of disappearance of nifedipine in solution to be calculated. The instrument used for this analysis was a Hewlett-Packard series 1050 and the separating column was a LUNA C18 (2) 150 x 4.6 mm, 5 μm. The mobile phase was composed of 50% acetonitrile in 0.1% trifluoroacetic acid in water. The experimental run time was 10 minutes, the injection volume was 10 μL, the wavelength of detection, 355nm, and an isocratic flow rate of 1 mL/min was used.

A calibration curve was first determined using standard solutions of nifedipine in 30% methanol in water. The concentrations of the standards were 10, 20, 40, 60, 80 and 100 μg/mL and the resulting straight line had a R^2 of 1.

The main experiment was conducted on samples taken from a 1 mL solution of 1% *w/v* nifedipine that was used with the photo-MCDSC. Samples were taken before exposure to light and every 60 minutes during the photocalorimetric experiment until a maximum of 6 hours. At each time point, the ampoule was removed from the instrument and a sample of 100 μL was taken from inside the ampoule. That sample was put into a 10 mL volumetric flask and a solution of 30% methanol in water was used to make the solution up to volume. This final dilution was used directly with the HPLC instrument. The results were, afterwards, collected and analysed to determine the retention times and areas under the curve.

4.2.3. Methods used in the studies performed with the photo-TAM

4.2.3.1. Preparation of solutions of nifedipine

Solutions of nifedipine were prepared in ethanol with two different concentrations, 0.5% *w/v* (1.4×10^{-2} M) and 1% *w/v* (2.9×10^{-2} M). Nifedipine was weighed (50 mg and 100 mg, respectively) into 10 mL volumetric flasks and ethanol was added to dissolve it. The solutions were left to stir until complete dissolution of the powder and ethanol was added until the final volume reached 10 mL. All solutions were prepared in a dark room under red light to minimise photodegradation prior to the experiments.

4.2.3.2. Photocalorimetric experiments

As was mentioned before in Chapter 3, one of the most useful features of the photo-TAM is the possibility to irradiate the samples with a combination of different wavelengths and test the photochemical response of samples to a customised spectrum. In the photocalorimetric studies reported here, two different arrays of LEDs were used to test the photodegradation of nifedipine. One of them consisted of 5 different LEDs with the following wavelengths: 360 nm, 370 nm, 380 nm, 395 nm and a white light LED (*Array 1*). The other array included five 410 nm wavelength LEDs (*Array 2*).

Before each photocalorimetric assay with nifedipine, a blank experiment was performed in order to balance the amount of light going into each ampoule. First, the reference and sample ampoules were filled with a volume of ethanol equal to the volume of nifedipine solution that was going to be tested. The ampoules were then closed and lowered into the photocalorimetric channels. The two lighting columns with the LED arrays were, afterwards, inserted into the photocalorimetric channels and the system was left to equilibrate at 25 ºC. Data was collected every 10 seconds using the dedicated software package Digitam 4.1 (TA Instruments LLC, USA). After reaching equilibrium, the signal was zeroed and the instrument was electrically calibrated. The amplifier's range was set to 100 µW for the experiments performed with *Array 1* and 300 µW for those with *Array 2*. After calibration, all switches in the circuit board were turned on (sample side and reference side) and the system was allowed to equilibrate with light irradiating

the ampoules. The voltage applied to the LEDs was 10 V. When the resulting calorimetric signal measured was very different from zero, the autobalance power supply was used to zero the signal by adjusting the voltage applied to the reference side. The system was then ready to be used with the solutions of nifedipine.

The two arrays used in these studies were tested with solutions of nifedipine of two different concentrations 0.5% and 1% *w/v*. The first concentration, 0.5%, was tested in two different volumes, 4 mL and 6 mL, while the second concentration was only tested in a volume of 4 mL. All these tests were performed in triplicate.

One of the photocalorimetric ampoules was filled with the test nifedipine solution while the other contained the same volume of ethanol. The two ampoules were closed tightly and lowered into the sample and reference channels, respectively. The two lighting columns with the LED arrays were, afterwards, inserted into the photocalorimetric channels and the system was left to equilibrate at 25 ºC. Data was collected every 10 seconds using the dedicated software package Digitam 4.1 (TA Instruments LLC, USA). The system eventually reached equilibrium and a stable calorimetric signal was displayed in the application screen. The LEDs in the sample and reference sides were then switched on and samples irradiated. Data was recorded until enough data was collected for analysis and the LEDs were then switched off.

The effect of increasing light power on the photodegradation of nifedipine in solution was also assessed using *Array 2* in the photo-TAM. As a result of technical problems, the LEDs used in the experiments described above had to be replaced by new bulbs which required a smaller voltage to operate in similar conditions. In these light intensity experiments, two different voltages, 5 V and 7.5 V, were applied to the LEDs and only 4 mL samples of nifedipine with a concentration of 0.5% w/v were tested. The amplifier range was set to 300 μW when 5 V were applied to the LEDs and 1000 μW when 7.5 V were used. The light power reaching the ampoules was measured calorimetrically by switching each LED individually and measuring the thermal response it caused. These measurements used 4 mL of ethanol inside the calorimetric ampoules.

4.2.3.3. *High-performance liquid chromatography (HPLC) analysis*

The rate of disappearance of nifedipine in these photo-TAM experiments was also determined using a HPLC assay similar to the one described in *4.2.2.3*. The only differences between the two methods are the use of a different instrument, an Agilent Technologies 1200 series, and a slightly different column, LUNA 5u C18 (2) 250 x 4.60 mm. These were used instead because of availability issues. A calibration curve was thus performed for these new experimental conditions followed by the main assay.

The photocalorimetric experiment carried out in the photo-TAM did not use a full array of 5 LEDs. In this case, only 2 bulbs, emitting at 395 nm wavelength, were used. This combination of LEDs was used because at the time that the HPLC studies were performed these were the only available LEDs. A voltage of 10 V was applied to both sets of LEDs (irradiating the sample and reference sides) and a typical photocalorimetric experiment (*4.2.3.2.*) was performed on a sample of 4 mL 0.5% nifedipine in ethanol. This experiment was repeated for analysis with a HPLC method similar to the one previously described (*4.2.2.3.*), the only difference being that more time points were used for sampling. Samples were taken at 0, 10, 25, 35, 45, 55, 57, 59, 61, 63, 65 hours and analysed.

4.3. Results and discussion

4.3.1. Photodegradation studies using the photo-MCDSC

4.3.1.1. The photocalorimetric signal

Figure 4.2. shows the typical photocalorimetric signal recorded for the photodegradation of nifedipine in solution under 410 nm wavelength radiation.
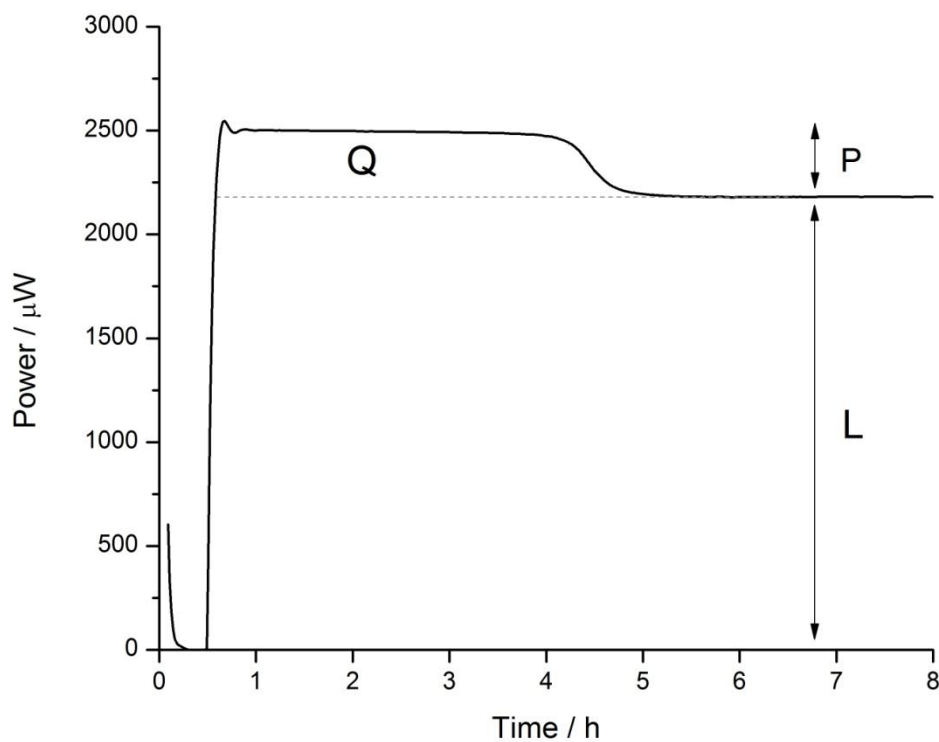
FIGURE 4.2. : Photocalorimetric signal obtained for the photodegradation of 1 mL 1% solution of nifedipine in ethanol using the photo-MCDSC (λ=410 nm)

Initially, the calorimetric signal shows a decay to zero which corresponds to the period of equilibration of the sample to the temperature of the instrument. After the signal stabilizes to zero, the LED placed above the sample is switched on and the sample is irradiated with light. That light power is immediately detected by the instrument and a

rapid increase in the calorimetric signal is observed. A few minutes after the LED was switched on, the thermal power measured by the photocalorimeter stabilizes to a value that remains constant for some hours (approximately 4 hours in the example in Figure 4.2.). At this point, the major contributor to the magnitude of the heat flow measured is the light power emitted by the LED because of its high energy output. This light energy may interact with the system in two different ways; either it is quantitatively transformed into heat by interaction with the photocalorimeter components and the sample (in case the sample is inert) or it is partially used in a photochemical reaction occurring in the sample. In this last case, the thermal power measured by the instrument will be a sum of the energy introduced into the system by the light source and the heat of the photochemical reaction. That is thought to be the case of the system tested here since nifedipine is a very photosensitive drug either in solution or in solid.

After a period of four and a half hours where the thermal power remained constant, the calorimetric signal started to drop and another baseline was reached. This decrease in the signal is thought to correspond to the later stages of the photochemical reaction with the process coming to an end once the signal stabilizes again. The difference between those two constant signals (**P** in Figure 4.2.) is the reaction heat flow and the final deflection from baseline corresponds to the light power reaching the sample (**L** in Figure 4.2.).

In order to prove that the difference between those two constant signals corresponds to the reaction power (**P**), an additional experiment was performed using a similar LED to irradiate the reference channel and balance the light power going into the sample. In this experiment, an ampoule filled with ethanol was lowered into one of the sample channels and an LED placed on top of it. A second LED was inserted in the reference channel and the system was left to equilibrate. Afterwards, both LEDs were switched on and the resulting signal was forced to zero by adjusting the light power going into the reference channel. After zeroing the signal, a photocalorimetric experiment was performed with 1 mL of 0.5% nifedipine in ethanol using the reference LED to balance the light power going into the sample ampoule. The photocalorimetric signal recorded for this experiment is shown in Figure 4.3.
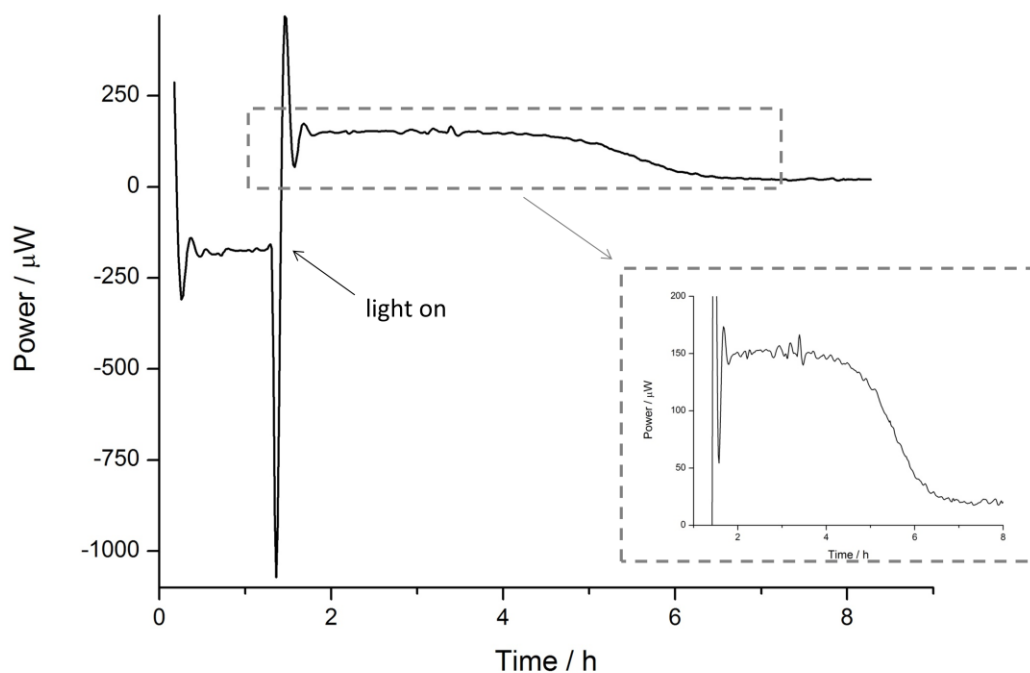
FIGURE 4.3. : Photocalorimetric signal obtained for the photodegradation of 1 mL 0.5% solution of nifedipine in ethanol (λ=410 nm) after balancing the light power going into the reference and sample channels.

Because the calorimetric signal was zeroed prior to the experiment by adjusting the light power going into both reference and sample channels, any thermal power measured under these circumstances is only due to photochemical processes occurring in the sample. Figure 4.3. clearly shows an exothermic signal after the LED was switched on which means that light induced a chemical process in the sample. That deflection from zero corresponds to the photoreaction heat flow (Φ or **P** in Figure 4.2.).

If the area under the power-time curve in Figure 4.3. is now taken (**Q** in Figure 4.2.), the total energy released in the photochemical process is determined. This parameter together with the photoreaction power (**P**), allow the calculation of other thermodynamic and kinetic reaction parameters using some of the analytical strategies explained in Chapter 1 and 2.

4.3.1.2. *Methodologies of data analysis*

Before describing the analytical strategies used in these studies, it is important to remember the kinetic aspects involved in photochemical processes in solution, in particular, the kinetics of nifedipine photodegradation. In Chapter 1, it was noted that the kinetics involved in these processes are governed by two factors: the number of absorbing species in solution and the number of photons irradiating the sample. If the number of molecules in solution is high (concentrated solutions) it is likely that the photoprocess follows zero-order kinetics as a consequence of all radiation being absorbed by these molecules. In this case, because the rate limiting factor is the intensity of light, the rate of reaction remains constant unless the light power changes. If, instead, dilute solutions are used, first-order kinetics are followed because the rate limiting factor is now the number of photodegrading molecules. With respect to the kinetics of nifedipine photodegradation in solution, both zero-order and first-order kinetics have been reported and a dependence on nifedipine concentration was also suggested (115, 117). This information is very important to understand the meaning of the data collected in the photocalorimetric studies and decide on the strategies to use in the analysis of data.

Previous analysis of the data recorded in these photocalorimetric studies (Figures 4.2. and 4.3.) showed that the photoreaction power (P) is constant for a long period of time, only decaying to baseline in the final moments of the experiment. Two reasons could explain this final decay in the signal; either the mechanism of reaction changed in that last period, or, assuming constant mechanism, a change in the kinetics was observed. Given the information presented above on the photodegradation of nifedipine, a transition from zero-order to first-order kinetics is thought to occur with the mechanism of reaction remaining constant during the experiment. The shape of the power-time curve during those two periods is also characteristic of processes following those kinetics which renders the assumptions legitimate. The thermodynamic and kinetic parameters can now be calculated for the two periods considered above using the calorimetric strategies previously described in Chapters 1 and 2.

The initial zero-order constant signal is, first, analysed using one of the strategies previously described in Chapter 2. The strategy that was chosen here is the one presented in section 2.3.1. where the enthalpy of reaction is calculated after the process progressed to completion. According to this method, knowledge of the whole thermal

history of the process allows determination of the total heat of reaction (**Q** in Figure 4.2.) and, subsequently, the molar enthalpy of reaction (ΔH) using Equation 4.1.

$$\Delta H = Q/A_0 \hspace{3cm} \text{Equation 4.1.}$$

where A_0 is the initial amount of nifedipine in solution. This method can only be used if the mechanism of reaction and the enthalpy of reaction are assumed constant throughout the whole experiment and if the reaction progresses to completion (i.e. all A_0 reacts). After ΔH is calculated, the reaction rate constant, k, is determined using Equation 4.2.

$$\mathrm{P} = \frac{\mathrm{d}q}{\mathrm{d}t} = k.\Delta H.V \hspace{3cm} \text{Equation 4.2.}$$

where P is the deflection from zero baseline in Figure 4.3. and V is the volume of solution of nifedipine tested.

After calculating those parameters, the decay period was analysed considering the previously referred change in the kinetics from zero-order to first-order. This transition, however, is not instantaneous and an initial phase is observed where the kinetics show a non-integral reaction order behaviour that is characteristic of this kind of transition in photoreactions (6). This period is followed by a first-order decay that can be analysed using the calorimetric equation that describes first-order processes (Equation 4.3.).

$$\frac{\mathrm{d}q}{\mathrm{d}t} = k_1.\Delta H.[A]_{tr}.V.e^{-k_1.t} \hspace{3cm} \text{Equation 4.3.}$$

where k_1 is the first-order rate constant, ΔH is the enthalpy of reaction, $[A]_{tr}$ is the approximate concentration of nifedipine at the beginning of the decay period (transition period), V is the volume of solution tested and t is the duration of the first-order period.

The final part of the data can thus be fitted to the equation above using a non-linear curve fit method included in the *Origin* software package. Before starting the iteration process, the known parameters need to be inserted in the software as well as an

estimation of the unknown variables. The known parameters are the volume of solution, V, and the enthalpy of reaction, ΔH, which was previously determined using the area under the power-time curve. On the other hand, k_1 and $[A]_{tr}$ constitute the unknown parameters that require determination. In order to get the correct parameters, an adjustment of the time axis needs to be done before fitting because the first-order period occurs several hours after the beginning of data collection. Ideally, time zero should correspond to the point where the first-order process begins. However, because that point is difficult to determine accurately and consistently for all experiments, an alternative strategy was used considering that the time point where the two dashed lines in Figure 4.4. intercept corresponds to time zero. That figure shows the calorimetric signal recorded for a standard photocalorimetric experiment and the first-order fit line that resulted from the iteration process. The unknown parameters were returned after the fit line was obtained.
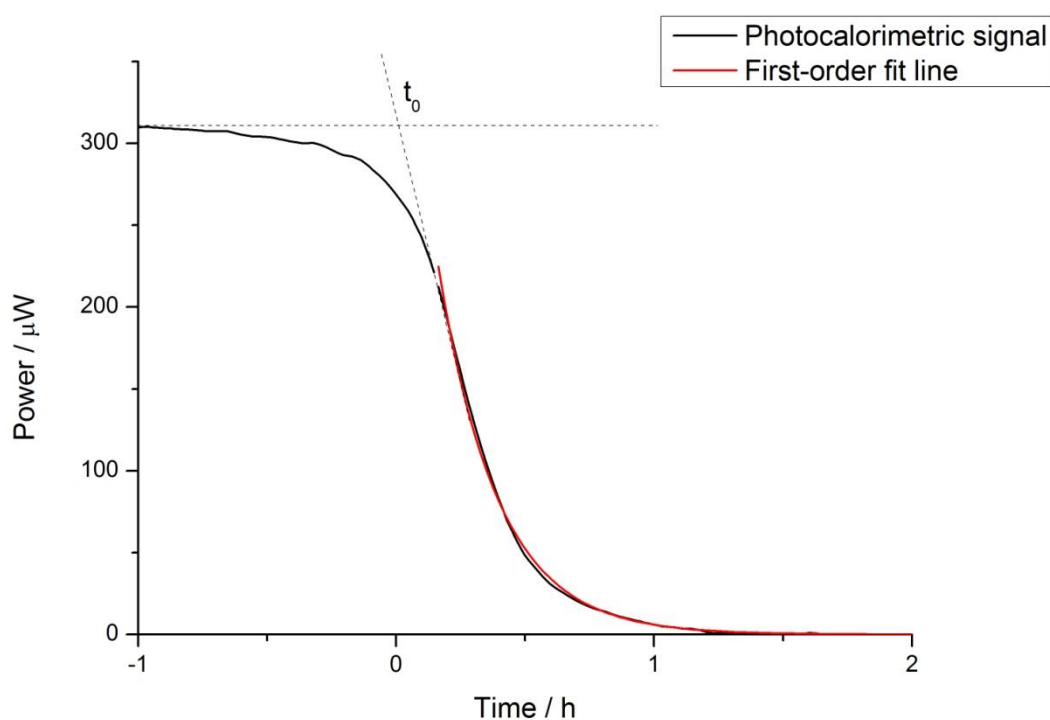
FIGURE 4.4. : Outcome of the iteration process used in the analysis of the first-order period recorded for an experiment with 1% 1mL nifedipine solution.

4.3.1.3. *Effect of sample concentration and volume on the calorimetric signals*

Figures 4.5. and 4.6. compare the photocalorimetric signals obtained when different concentrations and volumes of nifedipine are tested with the photo-MCDSC. The light power (**L** in Figure 4.2.) irradiating all samples is similar despite the few µW differences detected by the instrument. These differences are not shown in Figures 4.5. and 4.6. because the final baselines were adjusted to the same value in order to compare the magnitude of the photoreaction power (P).
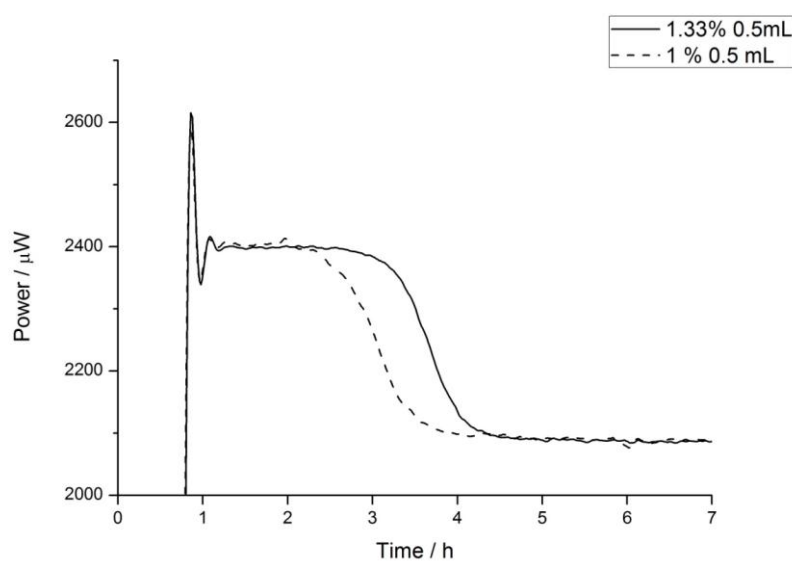
FIGURE 4.5. : Effect of different concentrations of nifedipine on the photocalorimetric signal.
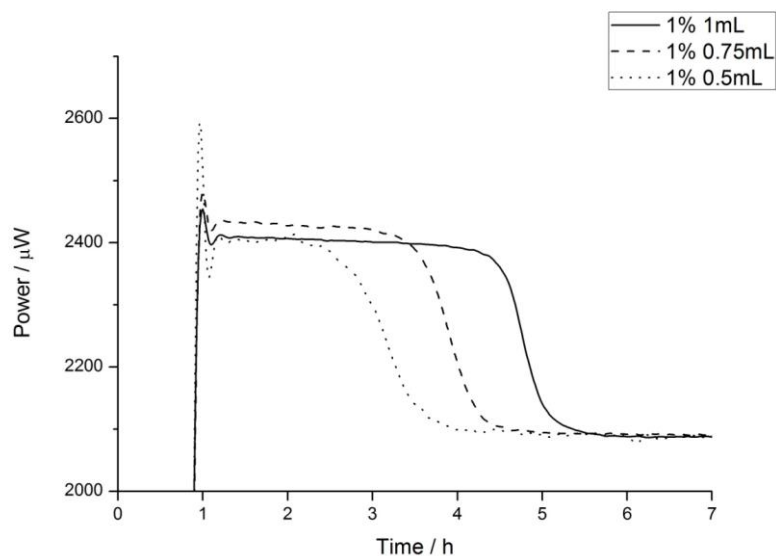
FIGURE 4.6. : Effect of different sample volume on the shape of the photocalorimetric signal.

190

All signals plotted in the figures above show a typical zero-order period that is followed by a decay to baseline in the final moments of the photodegradation process. Although the shapes of all those curves are very similar, some differences in the length of the zero-order period and in the area under the curve can be observed. These differences may, ultimately, be used to investigate the effect of the different experimental factors on the photocalorimetric signal.

For example, Figure 4.5. shows that an increase in the initial concentration of nifedipine results in a longer zero-order period and a larger area under the curve, Q. This effect was expected because the total amount of heat released in a reaction, Q, depends on the number of molecules available for photodegradation. Moreover, because the intensity of light was kept constant, the rate at which the molecules degraded was also similar, hence the longer time taken to completion. Despite these changes, the photoreaction power (P) did not significantly change with the increase in the initial concentration which is consistent with the behaviour of zero-order processes. These processes show a constant rate of reaction that is independent of the concentration of species in solution. Therefore no changes in the rate of heat production are observed during that zero-order period.

Regarding the influence of sample volume on the photocalorimetric signal, a similar effect is observed. As Figure 4.6. shows, an increase in the volume of solution tested results in a longer zero-order period and an increase in the area under the curve. This outcome can also be explained by an increase in the number of molecules available for degradation, for larger volumes, and a subsequent increase in the amount of heat released during the whole process. The only parameter that, apparently, does not agree with the theoretical expectations is the photoreaction power measured (P) that shows a constant value for all experiments. That thermal power is known to depend on the volume of solution, if zero-order processes are considered, and Equation 4.2. shows the relationship between those two parameters. In these studies, however, that dependence is not observed.

An explanation for this constant zero-order thermal power is found when considering the nature of photoreactions. It was mentioned before that photoreactions follow zero-order kinetics when all photons are absorbed by the molecules in solution (6). This means that, in those cases, no matter how many molecules exist in excess, the rate of reaction is only dependent on the light power. For similar lighting conditions, that rate of reaction is constant hence the constant rate of heat production (P). This zero-order

behaviour persists until the decrease in the number of molecules of nifedipine with time results in photons going through solution without being absorbed. The volume dependence shown in Equation 4.2. only applies if the increase in the number of molecules in solution is reflected in a proportional increase in the number of interactions.

4.3.1.4. Quantitative analysis of the zero- and first-order periods

Tables 4.1. to 4.3. show several parameters calculated for the photodegradation of nifedipine in ethanol (λ=410 nm) using the calorimetric data recorded in the photo-MCDSC studies. These parameters include the zero-order and first-order rate constants that were determined with the analytical strategies described in section *4.3.1.2.*

TABLE 4.1. : Mean and standard deviation (in parenthesis) of the reaction parameters calculated for the different samples of nifedipine.

Solution of nifedipine ([ ]$_{initial}$; volume)	Light power (µW)	Reaction Power (µW)	Total heat output (kJ)
2.9 x 10^{-2} M ; 1 mL	2080 (97)	283 (39)	4.4 (0.1) x 10^{-3}
2.9 x 10^{-2} M ; 0.75 mL	2037 (148)	259 (54)	3.6 (0.06) x 10^{-3}
2.9 x 10^{-2} M ; 0.5 mL	2006 (86)	285 (25)	2.5 (0.06) x 10^{-3}
3.8 x 10^{-2} M ; 1 mL	2011 (56)	255 (17)	5.6 (0.1) x 10^{-3}
3.8 x 10^{-2} M ; 0.75 mL	2024 (55)	267 (35)	4.7 (0.2) x 10^{-3}
3.8 x 10^{-2} M ; 0.5 mL	2093 (53)	275 (33)	2.9 (0.2) x 10^{-3}

TABLE 4.2. : Mean and standard deviation (in parenthesis) of the reaction parameters calculated for the zero-order period of the photocalorimetric signal.

Solution of nifedipine ([ ]$_{initial}$; volume)	Reaction enthalpy (kJ/mol)	Zero-order rate constant (mol/dm^3.s)	Zero-order rate constant / Volume (mol/s)
2.9×10^{-2} M ; 1 mL	-151.7 (3.6)	1.9 (0.3) x 10^{-6}	1.9 (0.3) x 10^{-9}
2.9×10^{-2} M ; 0.75 mL	-167.4 (2.6)	2.1 (0.4) x 10^{-6}	1.6 (0.3) x 10^{-9}
2.9×10^{-2} M ; 0.5 mL	-167.0 (1.1)	3.4 (0.3) x 10^{-6}	1.7 (0.1) x 10^{-9}
3.8×10^{-2} M ; 1 mL	-150.9 (4.8)	1.7 (0.1) x 10^{-6}	1.7 (0.1) x 10^{-9}
3.8×10^{-2} M ; 0.75 mL	-161.4 (7.0)	2.2 (0.4) x 10^{-6}	1.7 (0.3) x 10^{-9}
3.8×10^{-2} M ; 0.5 mL	-154.6 (11.1)	3.6 (0.3) x 10^{-6}	1.8 (0.1) x 10^{-9}

TABLE 4.3. : Mean and standard deviation (in parenthesis) of the reaction parameters calculated for the first-order period of the photocalorimetric signal.

Solution of nifedipine ([ ]$_{initial}$; volume)	First-order rate constant (s^{-1})	[A]$_{tr}$ (mol/dm^3)
2.9×10^{-2} M ; 1 mL	1.1 (0.1) x 10^{-3}	2.5 (0.08) x 10^{-3}
2.9×10^{-2} M ; 0.75 mL	0.9 (0.2) x 10^{-3}	4.1 (0.5) x 10^{-3}
2.9×10^{-2} M ; 0.5 mL	0.9 (0.1) x 10^{-3}	6.7 (0.4) x 10^{-3}
3.8×10^{-2} M ; 1 mL	1.0 (0.3) x 10^{-3}	2.7 (0.3) x 10^{-3}
3.8×10^{-2} M ; 0.75 mL	0.9 (0.05) x 10^{-3}	4.6 (0.7) x 10^{-3}
3.8×10^{-2} M ; 0.5 mL	0.8 (0.1) x 10^{-3}	7.2 (1) x 10^{-3}

The light power irradiating the samples was determined calorimetrically (**L** in Figure 4.2.) and an average value of 2044 μW was obtained. The small differences observed between experiments can be explained either by a slightly different orientation of the LED every time an experiment is set up or differences in the intensity of light each time an LED is switched on. In any case those differences proved irrelevant in terms of the overall rates of reaction.

The average photoreaction power measured in these studies was 270 μW and a standard deviation of 37 μW was calculated. The values listed in Table 4.1. show no correlation between the photoreaction power and the concentration or volume of solution which is in agreement with the explanation given on the nature of the constant signal. In fact, because the light power is similar for all experiments, and this constitutes the rate limiting factor, the rate of reaction, hence the rate of heat production (P) is similar for all experiments.

With respect to the total heat output calculated using the area under the curve (**Q** in Figure 4.2.), a clear dependence on the concentration and volume is observed (Table 4.1.). The larger values of *Q* measured for bigger volumes and concentrations of nifedipine is explained by an increase in the number of molecules available for degradation. On the other hand, the enthalpy of reaction (Table 4.2.) does not seem to depend on any of those factors, which means that, no changes in the mechanism of reaction occurred. The average and standard deviation calculated for this parameter were -158 ± 10 kJ/mol.

Considering now the tabulated values for the zero-order rate constant (Table 4.2.), an inverse proportionality is observed with respect to the volume of solution. These results are not surprising because that parameter gives information on the number of molecules reacting per unit volume and per second. Since the number of molecules reacting per unit time is assumed constant during the zero-order period, for similar lighting conditions, differences in the sample volume affect directly the calculated rate constants. These constants were multiplied by the respective volumes and the outcomes were compared (Table 4.2.). As expected, the calculated values were similar for the different experimental conditions.

On the other hand, in the light of the inverse square law ("the intensity of light is inversely proportional to the square of the distance from the source"), it would be expected that an increase in volume would bring the surface of the content closer to the light source and hence result in a higher light power reaching the surface of the solution. This higher light power would, in turn, result in an increase in the rate of nifedipine photo-conversion. However, this was not observed, probably, because the differences in distance were not significant.

Table 4.3. presents the reaction parameters calculated for the first-order period. The first-order rate constant values are all very similar showing an average and standard deviation of $9.2 \times 10^{-4} \pm 2.1 \times 10^{-4}$ s^{-1}. Regarding the concentration of nifedipine at the

time of transition between kinetics, $[A]_{tr}$, a clear decrease is observed when the volume of solution is increased. This effect is explained by the nature of the transition period that corresponds to the moment when the molecules of nifedipine stop being in excess relative to the number of photons. At that moment some of the photons go through solution without interacting with the molecules, therefore, affecting the rate of conversion. Because the number of photons irradiating the samples is kept constant, the number of absorbing molecules in solution, at the time of transition, is always the same. This constant number explains the differences in concentration observed for the different volumes (Table 4.4.).

TABLE 4.4. : Mean and standard deviation (in parenthesis) of the concentration and number of moles of nifedipine at the point of transition from zero-order to first-order kinetics.

Solution of nifedipine ($[\ ]_{initial}$; volume)	$[A]_{tr}$ (mol/dm^3)	N^o moles at the transition between kinetics
2.9×10^{-2} M ; 1 mL	$2.5\ (0.08) \times 10^{-3}$	$2.5\ (0.08) \times 10^{-6}$
2.9×10^{-2} M ; 0.75 mL	$4.0\ (0.5) \times 10^{-3}$	$3.1\ (0.4) \times 10^{-6}$
2.9×10^{-2} M ; 0.5 mL	$6.7\ (0.4) \times 10^{-3}$	$3.5\ (0.3) \times 10^{-6}$
3.8×10^{-2} M ; 1 mL	$2.7\ (0.3) \times 10^{-3}$	$2.7\ (0.3) \times 10^{-6}$
3.8×10^{-2} M ; 0.75 mL	$4.6\ (0.7) \times 10^{-3}$	$3.5\ (0.5) \times 10^{-6}$
3.8×10^{-2} M ; 0.5 mL	$7.2\ (1) \times 10^{-3}$	$3.6\ (0.5) \times 10^{-6}$

4.3.1.5. *Confirmatory studies with HPLC*

A HPLC assay was developed to analyse the change in concentration of nifedipine during the photocalorimetric experiments and compare the kinetic data obtained with the previously calculated parameters. The intention here is to validate the calorimetric strategies adopted in these studies using a well established analytical methodology such as HPLC.

After determining the calibration curve, the main assay was carried out using 1 mL of 1% solution of nifedipine and data was recorded for the different time points. The initial HPLC data showed a peak with a retention time of approximately 5.07 minutes

corresponding to nifedipine. The area under this peak progressively decreased with time while another peak, corresponding to the major photodegradation product, appeared with a retention time (RT) of 4.59 minutes. The Relative Retention Time, RRT, of this peak was 0.91 (RRT=RT$_{peak}$/RT$_{nifedipine\ peak}$). After 3 hours of exposure to light, a very small peak started to show with a retention time of 2.14 minutes (RRT=0.42). This peak area showed a very small increase with time which led to the assumption that it corresponds to a minor degradation product. For the purpose of these studies, the only peak that was analysed was nifedipine's in order to determine the change in concentration with time. The area under that peak was calculated for all time points, and the concentration values were determined using the calibration curve. Those data are plotted in Figure 4.7.
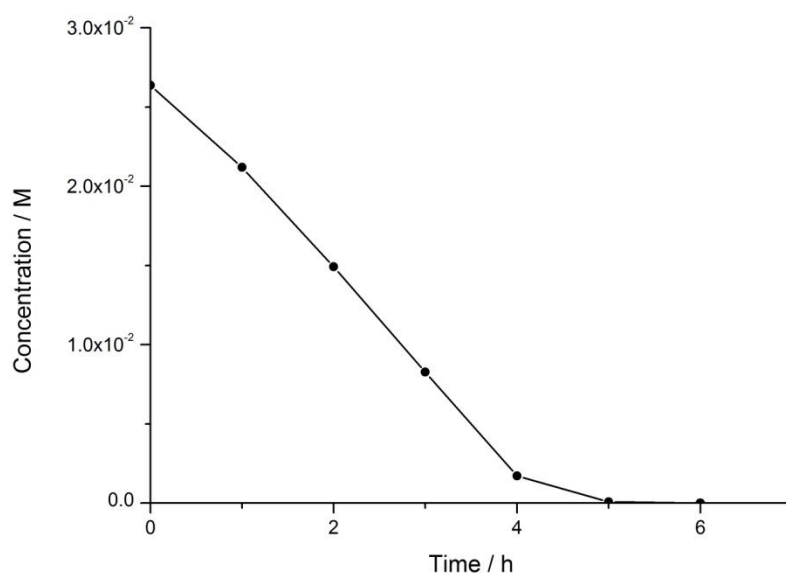
FIGURE 4.7. : Concentration of nifedipine inside the photocalorimetric ampoule at different experimental time points.

Those data show an initial linear decrease in the concentration, typical of zero-order kinetics, followed by a slower decrease in the final part of the data. The two periods were analysed separately, using the fitting functions of *Origin* software, and the rate constants were determined. The initial data, corresponding to the zero-order period, were fitted to Equation 4.4. and a rate constant of 1.7×10^{-6} mol.dm^{-3}.s^{-1} was obtained. This value is very similar to the average zero-order rate constant previously determined using 1 mL of 1% nifedipine solutions, 1.9×10^{-6} mol.dm^{-3}.s^{-1}, therefore, showing that the analytical strategy used is valid.

$$C = C_0 - k_0 . t \qquad\qquad \text{Equation 4.4.}$$

where t is the experimental time, C is the concentration at time t, C_0 is the initial concentration of nifedipine and k_0 is the zero-order rate constant. Figure 4.8. shows the initial part of data and the respective fit line.
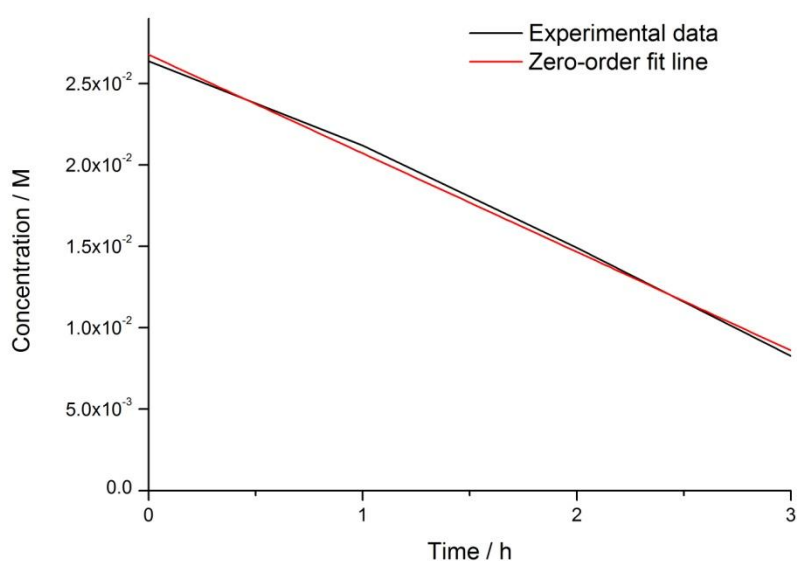
FIGURE 4.8. : Plot of the initial part of data collected in the HPLC studies and the fit line obtained with Origin.

In order to analyse the last part of data, Equation 4.5. was used to fit those data and return the kinetic parameters.

$$C = e^{\ln[A]_{tr} - k_1 . t} \qquad\qquad \text{Equation 4.5.}$$

where t is duration of the first-order decay, C is the concentration at time t, $[A]_{tr}$ is the concentration of nifedipine in the beginning of the first-order decay, and k_1 is the first-order rate constant. The first-order rate constant obtained from this analysis was 8.5×10^{-4} s^{-1} and the concentration $[A]_{tr}$ was 3.8×10^{-3} mol.dm^{-3}. These values are similar to the ones obtained previously in the analysis of calorimetric data, 1.1×10^{-3} s^{-1} for k_1 and 2.5×10^{-3} mol.dm^{-3} for $[A]_{tr}$, and the small differences observed have to do

with the fact that only 3 data points were used in this fitting process. Figure 4.9. shows the few last data points collected in these experiments and the first-order fit line obtained.
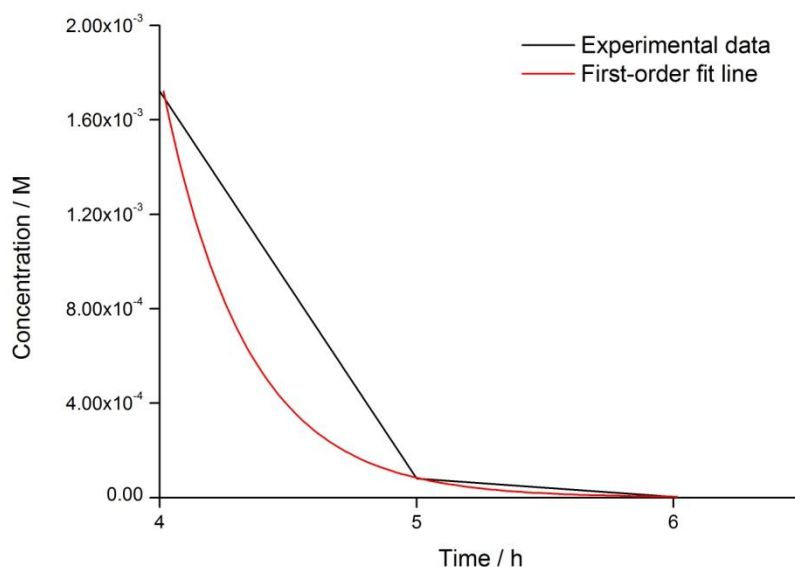
FIGURE 4.9. : Plot of the final part of data collected in the HPLC studies and the first-order fit line obtained with Origin.

All the results obtained in these studies with HPLC proved that the strategies used in the analysis of calorimetric data successfully returned the correct reaction parameters.

4.3.1.6. Determination of the photoreaction quantum yields

Another parameter that can be calculated using the data recorded in these photocalorimetric studies is the quantum yield of a reaction (ϕ). This parameter describes the efficiency of a reaction independently of the experimental conditions (intensity of light) and it can be calculated using Equation 4.6.

$$\phi = \frac{\text{number of molecules reacted/unit volume/unit time}}{\text{number of photons absorbed/unit volume/unit time}}$$

Equation 4.6.

This equation can be rearranged to give an expression that relates the zero-order rate constant with the light power absorbed, allowing the determination of ϕ using the reaction parameters previously calculated (Equation 4.7.).

$$\phi = \frac{k_0.V.N_A}{\dfrac{L.\lambda}{h.c}}$$

<div align="right">Equation 4.7.</div>

where k_0 is the zero-order rate constant (mol.dm^{-3}.s^{-1}), V is the volume of solution (dm^3), N_A is the Avogadro number (mol^{-1}), L is the light power absorbed by the sample (J.s^{-1}), λ is the wavelength of radiation (m), h is the Planck constant (J.s) and c is the speed of light (m.s^{-1}). The correct application of Equation 4.7. requires that the light power measured in the photocalorimeter (**L** in Figure 4.2.) is totally absorbed by the molecules of nifedipine and that no heat losses to other components of the system are observed. For that reason, it is not possible to use an equation that relates the first-order rate constant with the light power since the energy absorbed by the molecules decreases with time as a consequence of fewer molecules being present in solution. In that case, the light power measured by the instrument is always the same but the actual energy absorbed is continuously decreasing with time.

Equation 4.7. was applied to all data sets recorded in these studies and an average $\pm$ standard deviation was found, 0.243 ± 0.033. This average quantum yield lays within the range of values reported in literature (between 0.2 and 0.3 according to Gorner (112)), therefore, showing that Equation 4.7. can be used in the analysis of photocalorimetric data.

4.3.1.7. *Effect of light power on the photoreaction parameters*

In order to test the influence of light intensity on the kinetics of photodegradation, 1 mL samples of 1% nifedipine were irradiated with light from a LED that was electrically manipulated to generate different light powers. The photocalorimetric outputs were recorded and data were analysed using the previous analytical strategies. Figure 4.10. shows a graph with some of those photocalorimetric signals and the respective light intensities measured with a spectroradiometer.
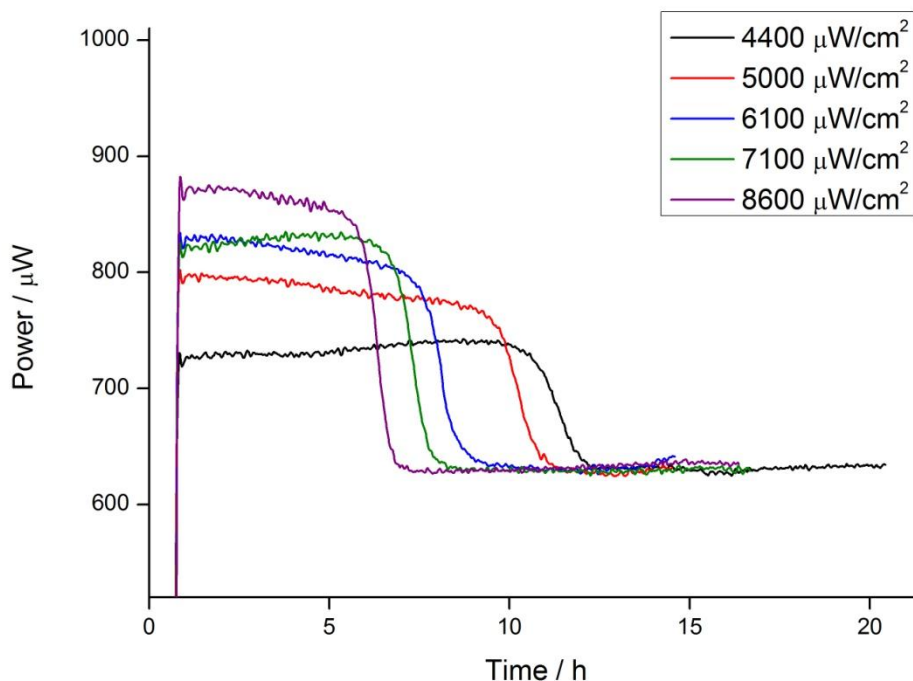
FIGURE 4.10. : Photocalorimetric signals recorded for the experiments using different light intensities. The intensities of light displayed in the legend were measured with a spectroradiometer.

As expected, the final baseline values (**L** in Figure 4.2.), corresponding to the light power introduced into the system, were different for all experiments. However, these were all adjusted to the same value in order to compare the magnitude of the photoreaction powers (P). Analysis of Figure 4.10. clearly shows that an increase in the intensity of light irradiating the sample results in a shorter time for the reaction to reach completion, as well as, an increase in the photoreaction power. These results are in agreement with an expected increase in the rate of reaction, as a consequence of more photons interacting with nifedipine molecules.

Table 4.5. and 4.6. show the different reaction parameters calculated for the zero-order and first-order periods as well as the photoreaction quantum yields.

TABLE 4.5. : Reaction parameters calculated for the photodegradation of 1mL 1% nifedipine solution using different intensities of light (λ=410 nm).

Light power (spectroradiometer) ($\mu W.cm^{-2}$)	Light power (photocalorimeter) (μW)	$\Delta_r H$ (kJ/mol)	Photoreaction Power (μW)	k_0 ($mol.dm^{-3}.s^{-1}$)	Quantum yield
4400	701	-148.9	109	0.7×10^{-6}	0.306
5000	760	-182.7	167	0.9×10^{-6}	0.350
6100	904	-172.6	188	1.1×10^{-6}	0.352
7100	1094	-161.7	202	1.3×10^{-6}	0.332
8600	1255	-162.2	242	1.5×10^{-6}	0.346

TABLE 4.6. : First-order rate constant and concentration at transition calculated for the photodegradation of 1mL 1% nifedipine solution using different intensities of light (λ=410 nm).

Light power (photocalorimeter) (μW)	k_1 (s^{-1})	$[A]_{tr}$ ($mol.dm^{-3}$)
701	6.9×10^{-4}	2.6×10^{-3}
760	6.0×10^{-4}	2.6×10^{-3}
904	7.4×10^{-4}	2.7×10^{-3}
1094	8.3×10^{-4}	2.8×10^{-3}
1255	12.1×10^{-4}	2.2×10^{-3}

The first conclusion that can be drawn from the data above is that the photo-MCDSC was able to quantitatively measure the changes in the intensity of light. Despite the similar trend observed when comparing the light power measured with the spectroradiometer and with the photo-MCDSC, it is not possible to match those results because the two units are different and conversion of the spectroradiometer data into the amount of energy reaching the sample is very difficult. Therefore, the light power measured with the photo-MCDSC is more convenient and will be used in future analyses.

Table 4.5. also shows that the enthalpy of reaction was not significantly affected by changes in the intensity of light irradiating the samples, which means that no changes in

the reaction mechanism occurred. On the other hand, the zero-order photoreaction power (P) shows a clear increase with light power which is in agreement with the nature of that period. During that phase, the rate of reaction and, hence, the rate of heat production (P), are dependent on the number of photons irradiating the sample because these are the rate-limiting factor (all photons are absorbed). Therefore, an increase in the number of photons interacting with the molecules of nifedipine results in a rise in the photoreaction power (P). For that same reason, the zero-order rate constants listed in Table 4.5. show a clear dependence on the intensity of light. With respect to the first-order rate constants, a similar effect is observed, although the rate of reaction during this decay period depends on two factors: the number of photons available for interaction and the concentration of nifedipine.

The only parameter that, apparently, does not behave as expected is the concentration at the time of transition between kinetics, $[A]_{tr}$. At that time, the number of molecules of nifedipine is no longer in excess compared to the number of photons and the rate of reaction starts decreasing as a consequence of fewer photons being absorbed. Therefore, if the number of incident photons is larger, an equally larger number of molecules at the transition time must be observed. Table 4.6. does not show this effect as similar values are found for all experiments. The small concentrations of nifedipine, at this point, and the difficulty to discriminate very small differences in concentration with those analytical methods, explain these results. To help visualize the relationships between light power and some of these parameters, all data obtained in the photocalorimetric experiments (including some data that were not shown in Figure 4.10. and Tables 4.5. and 4.6.) were plotted and fitted to a linear function using *Origin*. Figures 4.11. shows all these graphs.
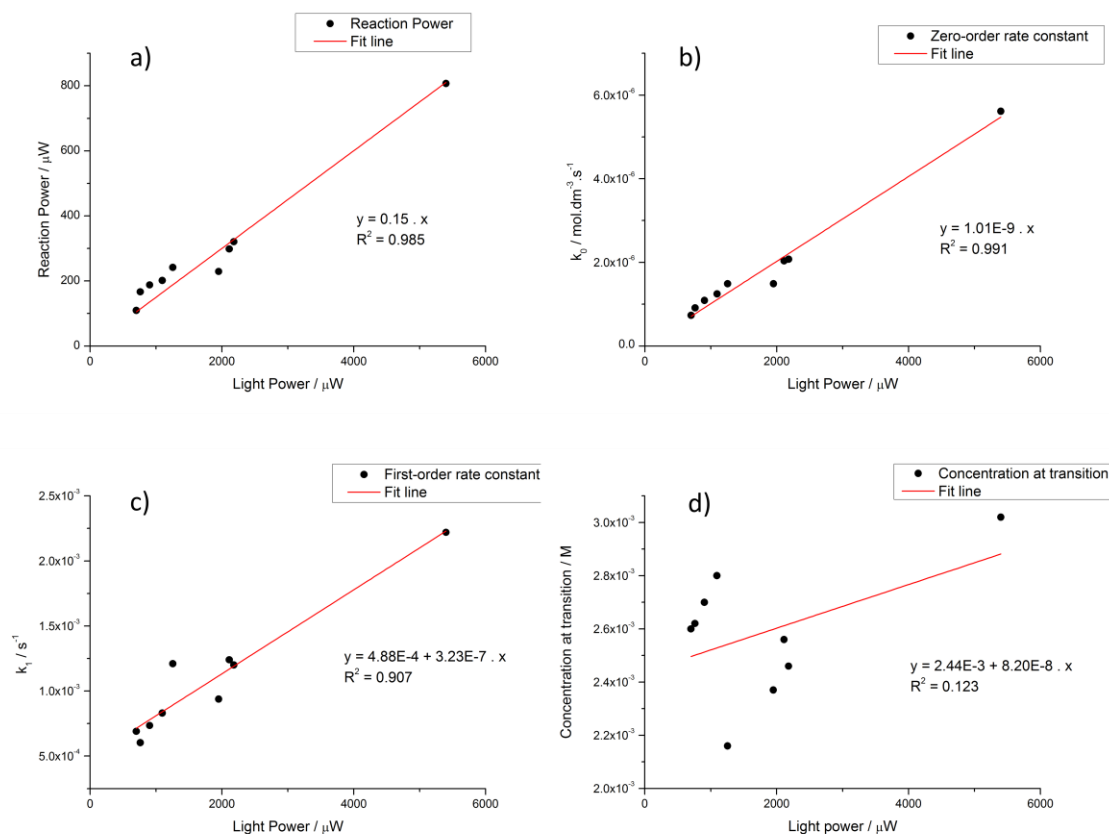
FIGURE 4.11. : Effect of light intensity on the several reaction parameters. Graphs a) to d) show the calculated values and the respective fit lines for a) the photoreaction power; b) the zero-order rate constant; c) the first-order rate constant; d) the concentration at the transition between kinetics.

The low R^2 obtained for the fit line in plot d) shows that it is not possible to correlate the increase in light power with any effect in terms of concentration at the transition time. All other previously discussed relationships were observed.

In addition to these reaction parameters, the quantum yield of the photoreaction was determined using the zero-order rate constants and the light power measured with the photo-MCDSC and an average value of 0.337 was obtained. This parameter was similar for all experiments, therefore, demonstrating its usefulness in characterising a specific photoreaction independently of the exposure conditions.

4.3.2. Photodegradation studies using the photo-TAM

The photodegradation of nifedipine in solution was also studied with the photo-TAM design using two different arrays of LEDs. One of them had 5 different wavelength LEDs with maximums at 360 nm, 370 nm, 380 nm, 395 nm and a white light LED (*Array 1*). The other array had 5 similar LEDs with maximum emission at 410 nm (*Array 2*). In general, the photocalorimetric signal recorded in the analysis of nifedipine solutions with both arrays had a similar shape to the one shown in Figure 4.12.
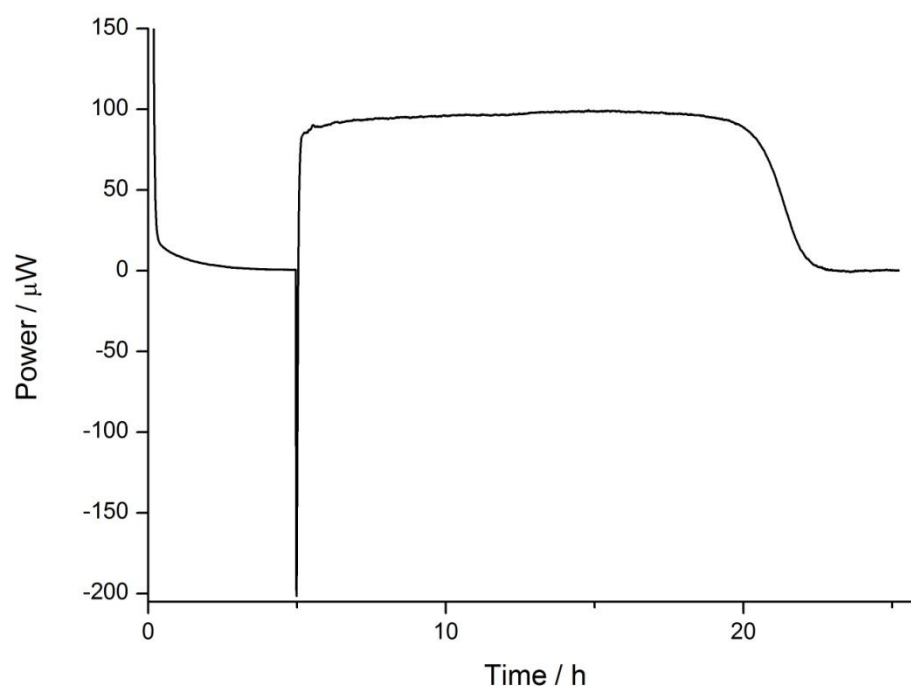
FIGURE 4.12. : Typical photocalorimetric signal recorded in the test of nifedipine solutions using the photo-TAM. In this case, the signal corresponds to the photodegradation of 4 mL of 0.5% solution of nifedipine using *Array 2*.

The figure above shows an initial decay in the signal that corresponds to the sample and reference ampoules equilibrating to the photocalorimeter's temperature. Once that signal reaches zero, the LEDs on both, sample and reference, sides are switched on and a large peak is observed corresponding to the thermal shock generated by light input. After this peak, the signal stabilizes to a constant thermal power, typical of zero-order processes, before decaying to zero towards the end of the experiment. That thermal power is always positive which means that the overall process is exothermic.

204

The typical signal measured in these experiments is very similar to those recorded with the photo-MCDSC, the only difference being that this one reaches a zero baseline, in the end of the experiment. That is because a blank experiment is performed before the main assay in order to balance the light power going into the sample and reference ampoules. This blank experiment is necessary for the photo-TAM tests because the light power emitted by 5 LEDs is likely to be larger than the 3000 µW maximum range that the TAM can measure. Therefore, the reference ampoule must be irradiated with a similar light power in order to zero the signal and allow the measurement of photoreaction powers. The principal inconvenience of this method is that it does not allow direct measurement of the light power irradiating the sample using a single experiment in the photo-TAM. However, the instrument proved sensitive enough to discriminate small photoreaction powers from the large amount of energy introduced in the system by the 5 LEDs.

All data recorded in the experiments with the photo-TAM were, afterwards, analysed with the same strategies used in the photo-MCDSC data analysis (section *4.3.1.2.*) in order to determine the photoreaction parameters. Similarly to that analysis, the signal was divided into two parts, an initial zero-order period and a first-order decay, and data were fitted to the calorimetric equations previously described. The outcomes of the fitting process were then used to study the effect of concentration and volume on the photoreaction parameters. Such experiments were performed using the two arrays of LEDs previously mentioned.

4.3.2.1. Analysis with 5 different wavelength LEDs (Array 1)

Three solutions of nifedipine were tested with *Array 1* in order to study the influence of different concentrations and volumes on the photocalorimetric signal recorded with the photo-TAM. The samples were exposed to similar lighting conditions to exclude other factors from interfering with the thermal measurements. The data collected in those experiments are plotted in Figures 4.13. and 4.14.

FIGURE 4.13. : Effect of nifedipine concentration on the photocalorimetric signal recorded in the photo-TAM experiments using *Array 1*.

FIGURE 4.14. : Effect of sample volume on the photocalorimetric signal recorded with the photo-TAM (*Array1*).

Despite all signals showing a decay to zero, towards the end of the experiment, the actual final baseline values measured were slightly different from zero and adjustments had to be done for clarity of data analysis. The non-zero final values are explained by the difficulty to match with precision the light power going into the reference and sample ampoules during the blank experiment. However, data can still be compared after the adjustments.

206

Figures 4.13. and 4.14. show that an increase in the sample volume or concentration results in longer zero-order periods and larger areas under the curve. The photoreaction power (P), however, did not show any significant changes for all experiments. These results can be explained with the kinetics involved in the beginning of the experiments where the rate of reaction shows full dependence on the number of photons irradiating the sample. Because the intensity of light was maintained constant for all experiments, a similar rate of reaction is observed, hence the similar rate of heat production (P). The longer zero-order periods observed for higher volumes and concentrations can, therefore be explained by an increase in the number of molecules in solution reacting at the same rate. The total heat of reaction, Q, given by the area under the curve, also increased with concentration and volume as a consequence of more molecules being available in solution for reaction.

Despite these results being very similar to the ones obtained with the photo-MCDSC, some of the signals measured with the photo-TAM show a rather peculiar behaviour. For example, the signal recorded for the photodegradation of 4 mL of 0.5% nifedipine, shows an initial very slow decay, instead of the constant thermal power measured in all other experiments. This behaviour was observed in all three experiments and may be explained by the fact that the initial equilibration period did not allow the zero-order period to be clearly differentiated. That effect was only observed with this sample because the zero-order period is short as a consequence of the small initial concentration of nifedipine.

Another signal that shows an unusual curve shape is the one recorded in the photodegradation of 6 mL of 0.5% nifedipine. That signal has an initial constant period that is followed by a small transition phase and a two-step decay to baseline which is very different from the usual transition period and first-order decay observed in most experiments. An explanation for this signal is found, considering that the kinetics of diffusion in a relatively large volume, 6 mL, are relevant for the overall kinetics of the system. During the zero-order period, the diffusion of molecules in solution is not so important because these are present in a large number and all photons are absorbed in the top layers of solution. However, for dilute solutions such as those in the later stages of the photodegradation process, the overall kinetics will not only depend on the rate of conversion of nifedipine but also on the rate at which new molecules are being replaced in the top layers of the solution. This extra process may be responsible for the additional

decay phase observed in the photocalorimetric signal. For smaller volumes this effect is not observed because the diffusion distance is not so significant.

Similarly to the analysis of data recorded with the photo-MCDSC, these data were also analysed with the previously described strategies and the resulting reaction parameters are listed in Tables 4.7. and 4.8. No first-order analysis was done on the 6 mL 0.5% nifedipine samples because of the atypical decay phase.

TABLE 4.7. : Mean and standard deviation (in parenthesis) of the reaction parameters calculated for the photodegradation of nifedipine in solution using *Array 1* with the photo-TAM (part I).

Solution of nifedipine ([ ]$_{initial}$; volume)	Total heat output (J)	Enthalpy of reaction (kJ/mol)	Photoreaction power (µW)	k_0 (mol.dm^{-3}.s^{-1})
2.9 x 10^{-2} M ; 4 mL	9.1 (0.9)	-79.2 (8)	49 (6)	1.8 (0.5) x 10^{-7}
1.4 x 10^{-2} M ; 4 mL	5.2 (0.02)	-90.1 (0.4)	52 (1)	1.4 (0.02) x 10^{-7}
1.4 x 10^{-2} M ; 6 mL	7.1 (0.2)	-82.3 (2.5)	50 (1)	1.0 (0.009) x 10^{-7}

TABLE 4.8. : Mean and standard deviation (in parenthesis) of the reaction parameters calculated for the photodegradation of nifedipine in solution using *Array 1* with the photo-TAM (part II).

Solution of nifedipine ([ ]$_{initial}$; volume)	k_1 (s^{-1})	[A]$_{tr}$ (mol.dm^{-3})	Nº moles at transition between kinetics
2.9 x 10^{-2} M ; 4 mL	1.4 (0.1) x 10^{-4}	2.7 (0.4) x 10^{-3}	1.1 (0.1) x 10^{-5}
1.4 x 10^{-2} M ; 4 mL	2.2 (0.3) x 10^{-4}	1.4 (0.2) x 10^{-3}	0.5 (0.09) x 10^{-5}
1.4 x 10^{-2} M ; 6 mL	-	-	-

Table 4.7. confirms some of the results previously discussed, such as, the increase in total heat output with volume and concentration and the similar photoreaction power measured for all experiments. Regarding the enthalpy of reaction, no particular trend is observed in those data and an average ± standard deviation was determined: -83.8 ± 6.7 kJ/mol. On the other hand, the zero-order rate constants show an increase for smaller volumes which is not surprising giving that, for the same number of molecules reacting per unit time, differences in the sample volume will directly affect those rate constants (expressed in mol.dm^{-3}.s^{-1}).

Regarding the parameters obtained for the first-order period (Table 4.8.), a significant increase in the first-order rate constant and a decrease in the concentration and number of moles at the time of transition between kinetics, are observed for increasing sample concentrations. These results can be explained by the fact that the signal recorded using

208

the lower sample concentration, (0.5% 4 mL in Figure 4.13.) did not show a clear zero-order period, therefore, affecting the way those parameters are calculated. The method used in that analysis requires that the time axis is modified, considering that the initial time, t_0, is the time when parallel lines to the zero-order and first order signals intercept. In that case, the parallel line was drawn half way through the initial decay, which brings some uncertainty to the outcomes.

4.3.2.2. Analysis with 5 similar 410 nm LEDs (Array 2)

The samples tested with *Array 1* were also analysed with *Array 2* and the effects of concentration and volume on the shape of the power-time curves as well as on the photoreaction parameters were assessed. The light power irradiating the samples was maintained constant for all experiments to exclude that factor from analysis. Figures 4.15. and 4.16. compare the signals obtained for the different experiments performed with *Array 2*.
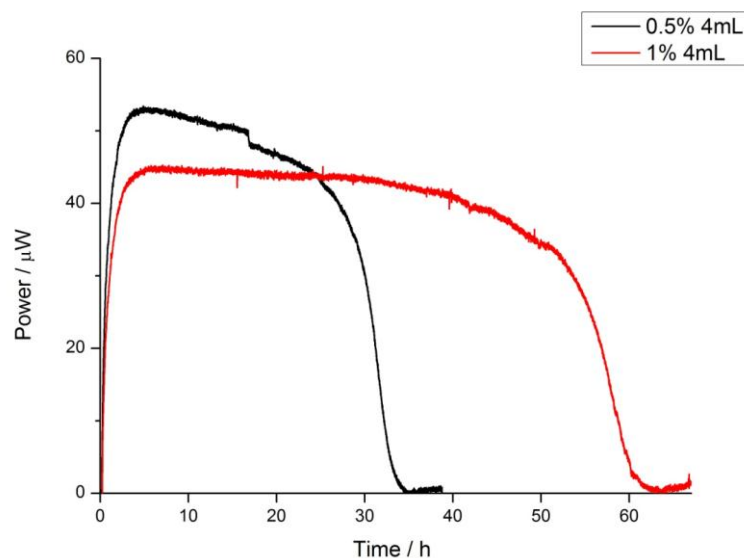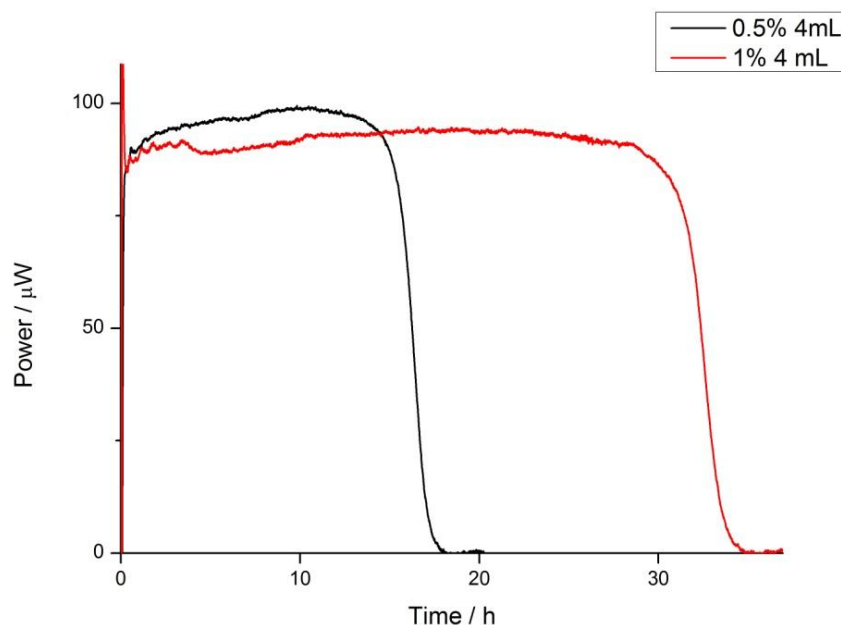

FIGURE 4.15. : Effect of nifedipine concentration on the photocalorimetric signal recorded in the photo-TAM experiments using *Array 2*.
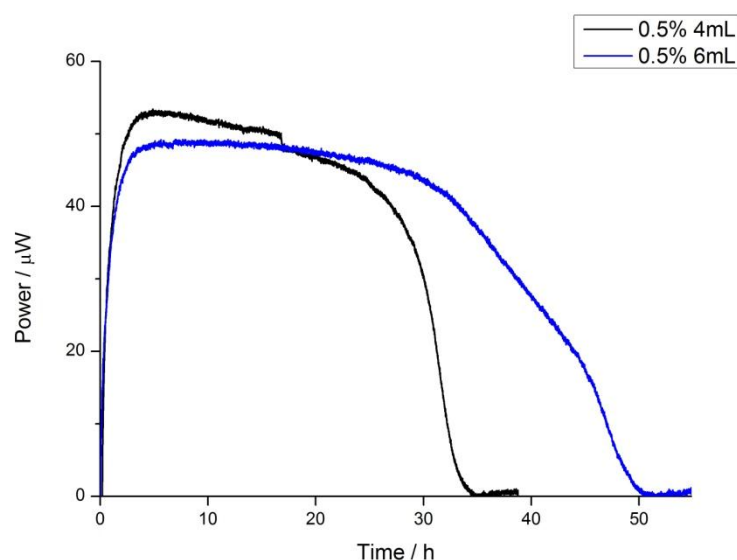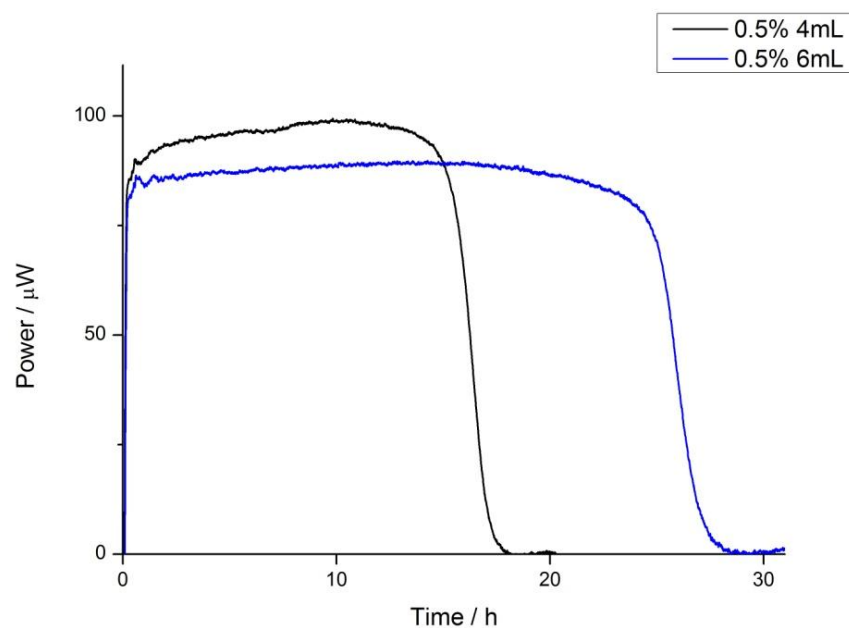
FIGURE 4.16. : Effect of sample volume on the photocalorimetric signal recorded with the photo-TAM (*Array 2*).

The signals recorded in these studies show a similar behaviour compared with those obtained with *Array 1*; an increase in concentration and volume resulted in larger areas under the curve (*Q*) and longer zero-order periods while similar photoreaction powers were measured for all experiments. Despite these similar results, no initial slow decays or two-step decay phases were observed in the signals measured with *Array 2*, contrary to those obtained with *Array 1*. These differences may be explained by different rates of reaction observed with the two arrays of LEDs although a more detailed discussion of the results obtained with the two LED-arrays is given in the following section.

Similarly to the analysis performed in the previous section, the reaction parameters of nifedipine photodegradation were calculated using the data obtained with *Array 2* (Tables 4.9. 4.10. and 4.11.).

TABLE 4.9. : Mean and standard deviation (in parenthesis) of the reaction parameters calculated for the photodegradation of nifedipine in solution using *Array 2* with the photo-TAM (part I).

Solution of nifedipine ($[\ ]_{initial}$; volume)	Total heat output (J)	Enthalpy of reaction (kJ/mol)	Photoreaction power (µW)
2.9×10^{-2} M ; 4 mL	10.8 (0.2)	-93.5 (1.8)	108 (13)
1.4×10^{-2} M ; 4 mL	5.7 (0.08)	-98.2 (1.4)	99 (1)
1.4×10^{-2} M ; 6 mL	7.9 (0.09)	-91.8 (1)	89 (1)

210

TABLE 4.10. : Mean and standard deviation (in parenthesis) of the reaction parameters calculated for the photodegradation of nifedipine in solution using *Array 2* with the photo-TAM (part II).

Solution of nifedipine ([ ]$_{initial}$; volume)	k_0 (mol.dm^{-3}.s^{-1})	k_0 x V (mol.s^{-1})
2.9 x 10^{-2} M ; 4 mL	2.9 (0.3) x 10^{-7}	1.15 (0.1) x 10^{-9}
1.4 x 10^{-2} M ; 4 mL	2.5 (0.03) x 10^{-7}	1.00 (0.01) x 10^{-9}
1.4 x 10^{-2} M ; 6 mL	1.6 (0.03) x 10^{-7}	0.97 (0.02) x 10^{-9}

TABLE 4.11. : Mean and standard deviation (in parenthesis) of the reaction parameters calculated for the photodegradation of nifedipine in solution using *Array 2* with the photo-TAM (part III).

Solution of nifedipine ([ ]$_{initial}$; volume)	k_1 (s^{-1})	[A]$_{tr}$ (mol.dm^{-3})	Nº moles at transition between kinetics
2.9 x 10^{-2} M ; 4 mL	4.3 (0.3) x 10^{-4}	1.3 (0.05) x 10^{-3}	5.3 (0.2) x 10^{-6}
1.4 x 10^{-2} M ; 4 mL	5.0 (0.3) x 10^{-4}	1.1 (0.08) x 10^{-3}	4.6 (0.3) x 10^{-6}
1.4 x 10^{-2} M ; 6 mL	3.4 (0.1) x 10^{-4}	0.7 (0.08) x 10^{-3}	4.5 (0.5) x 10^{-6}

As expected, the total heat output, calculated by integrating the area under the curve, shows an increase with concentration and volume while no significant changes are observed in terms of the photoreaction power. The enthalpies of reaction were also calculated for all experiments and an average ± standard deviation was determined: -94.5 ± 3.1 kJ/mol. The similar values obtained confirm that no changes occurred in terms of the mechanism of reaction. With respect to the values calculated for the zero-order rate constant (expressed in mol.dm^{-3}.s^{-1}), a significant increase is observed when smaller volumes are used, as a consequence of the similar number of molecules reacting per unit time during the zero-order period (Table 4.10.).

Considering now the parameters calculated for the first-order period, a slight decrease in the first-order rate constants and in the transition concentrations was observed for larger sample volumes (Table 4.11.). The smaller rate constants calculated for larger sample volumes can be explained by a decrease in the statistical chance of photons encountering molecules of nifedipine during the first-order period where the number of molecules of nifedipine in solution is small. As a consequence, the rate of photon absorption decreases with increasing volume and so does the rate of reaction. On the other hand, the decrease in concentration with volume, at the transition time, can be explained by two factors: a decrease in the probability of interactions between photons and molecules and the effect of volume on the calculation of concentration for similar

amounts of reactant (Table 4.11.). It must be noted that all comments are based on speculation because only two sample volumes were tested and the differences observed are very small and difficult to discriminate.

4.3.2.3. Comparison of data obtained with Arrays 1 and 2

Figure 4.17. compares the photocalorimetric signals measured for two 4 ml samples of 1% nifedipine tested with *Arrays 1* and *2*. The two curves show an initial constant power followed by a transition phase and a final first-order decay to zero which are characteristic of nifedipine's photodegradation using the photo-TAM. Despite the similarities, a clear difference in the length of the whole process is observed with the signals recorded with *Array 2* showing a much shorter time to completion compared to those analysed with *Array 1*. These differences were observed for all samples previously tested.
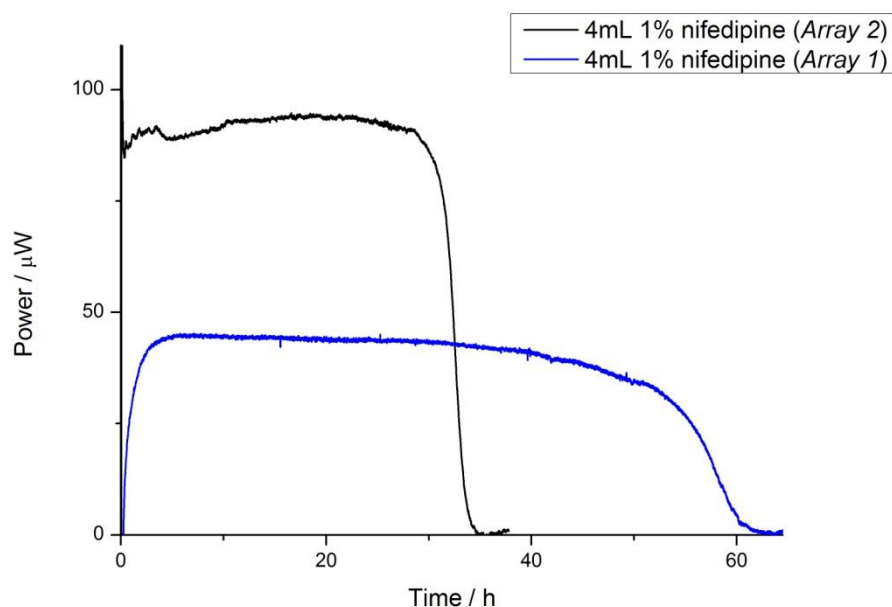
FIGURE 4.17. : Photocalorimetric signals measured for the photodegradation of 4 ml of 1% solution of nifedipine using Arrays 1 and 2.

Different rates of conversion of nifedipine explain the results obtained with both arrays of LEDs and Table 4.12. shows that by comparing the zero-order and first-order rate constant previously calculated.

TABLE 4.12. : Comparison of the mean and standard deviation values for the zero-order and first-order rate constants calculated for the photodegradation of 4mL of 1% nifedipine using *Arrays 1* and *2*.

Array	k_0 (mol.dm^{-3}.s^{-1})	k_1 (s^{-1})
1	1.8 (0.5) x 10^{-7}	1.4 (0.1) x 10^{-4}
2	2.9 (0.3) x 10^{-7}	4.3 (0.3) x 10^{-4}

These results can be explained by the fact that the two arrays have different LEDs which clearly influences the overall light power emitted, hence, the number of photons reaching the samples is different. The overall intensity of light was measured for the two arrays using the spectroradiometer and a value of 63.72 W/m^2 was obtained for *Array 1* while the intensity measured for *Array 2* was 56.00 W/m^2. Considering these values, greater rates of reaction were expected for the experiments performed with *Array 1*. However, that did not happen because most of the photons emitted by *Array 1* correspond to white light wavelengths (43.00 W/m^2) which are not absorbed by nifedipine in solution (117). Hence, it is assumed that the larger rates of reaction measured with *Array 2* result from the emission of a greater number of photons that are actually absorbed.

Such differences in the intensity of light also explain the atypical signals measured when 6 mL of 0.5% nifedipine are analysed with *Array 1*. The two-step decay observed in that signal is thought to result from the kinetics of diffusion of molecules competing with the kinetics of photodegradation. That is only observed with *Array 1* because the smaller number of photons with enough energy for interaction with nifedipine molecules, emitted by that array, may not be enough to irradiate the whole 6 mL of solution homogenously. Therefore, diffusion of molecules from the deeper layers of solution will have an impact on the kinetics.

Another parameter that is clearly dependent on the type of array used is the zero-order photoreaction power. Figure 4.17. shows that the thermal power measured for samples tested with *Array 2* is significantly larger than that measured with *Array 1*. That effect is explained by the influence of the rate constant on the zero-order thermal power, described in Equation 4.2.

The enthalpy of reaction is also slightly different for samples tested with *Array 1* and *2* (-83.8 ± 6.7 kJ/mol and -94.5 ± 3.1 kJ/mol, respectively) which means that the overall

mechanism of reaction may be different. The different wavelength spectra of the two arrays may explain those changes in the mechanism of reaction considering that different wavelengths favour the formation of different products. In that case, the final equilibrium would have a different composition in terms of the type of molecules in solution or the ratio between products. The influence of wavelength on the photodegradation of nifedipine in solution was previously investigated by Dhuna (76) and it was found that the 360 nm wavelengths had a greater effect on the photodegradation heat outputs. Such results indicated a wavelength dependence on the mechanism of photodegradation.

4.3.2.4. Confirmatory studies with HPLC

In order to validate the analytical methods used in these studies, an HPLC method was developed to quantify the degradation of nifedipine with time and compare that kinetic data with the outcomes of the calorimetric analysis. These studies were carried out in the photo-TAM using only two 395 nm LEDs on each holder to irradiate light onto the reference and sample ampoules. A standard photocalorimetric experiment was performed on 4 mL samples of 0.5% nifedipine and the calorimetric data analysed with the previously described methods. Figure 4.18. shows the signal recorded during this experiment.
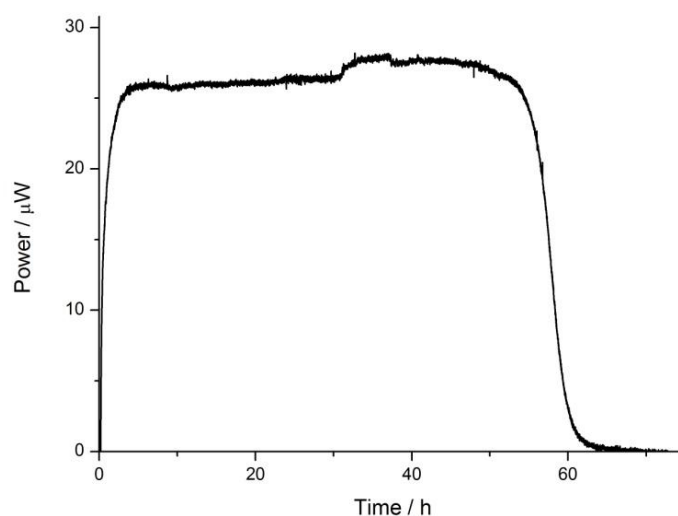
FIGURE 4.18. : Calorimetric signal recorded for the photodegradation of 4 ml of 0.5% nifedipine using two 395 nm LEDs in the photo-TAM.

The photoreaction parameters were calculated and the following values were obtained:

- Enthalpy of reaction = -94.6 kJ/mol

- Zero-order rate constant = 7.1 x 10^{-8} mol.dm^{-3}.s^{-1}

- First-order rate constant = 1.7 x 10^{-4} s^{-1}

- Number of moles of nifedipine at time of transition between kinetics = 3.3 x 10^{-6} mol

Afterwards, a similar experiment was set up in the photo-TAM to study the kinetics of photodegradation using the HPLC method previously described. Samples were taken out of the photocalorimetric ampoules at specific time points and analysed with HPLC to determine the concentration of nifedipine in solution. Initially, the HPLC data showed a single peak at around 7.40 minutes corresponding to nifedipine. The area of this peak progressively decreased with time while another peak, corresponding to the major photodegradation product, appeared with a retention time of 6.20 minutes (RRT=0.84). Despite the retention times being different from those obtained in the photo-MCDSC experiments ($RT_{nifedipine}$=5.07 minutes, $RT_{main\ product}$=4.59 minutes), the relative retention time of the main photo-product was similar using both HPLC methods (RRT= 0.91 in the photo-MCDSC experiments *vs* RRT= 0.84 in the photo-TAM experiments). This shows that that peak corresponds to the same photo-product. The different retention times can be explained by the fact that different columns were used in the two HPLC assays. Contrary to the method used in the photo-MCDSC experiments no additional peaks were observed in the later stages of this experiment ($RRT_{minor\ product}$= 0.42).

The nifedipine peak areas were, afterwards, used to determine the concentration at different times, using the calibration curve previously determined. Figure 4.19 shows the kinetic data obtained with this HPLC assay.
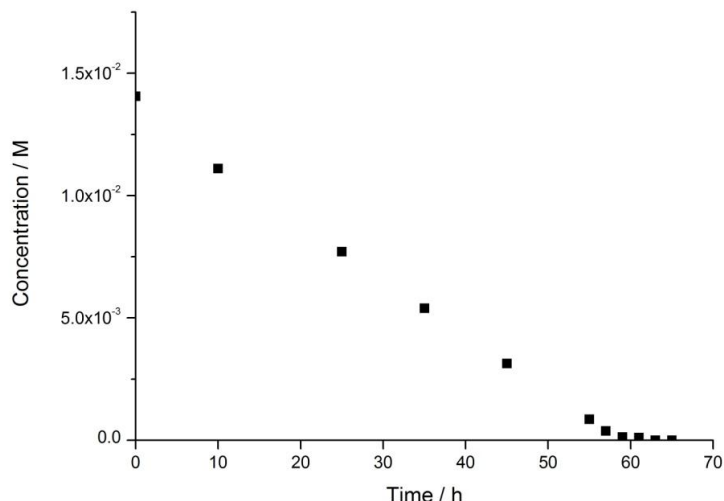
FIGURE 4.19. : Concentration of nifedipine in the photocalorimetric ampoule at different time points during the photocalorimetric experiment with the photo-TAM (λ=395 nm).

Similarly to the HPLC results obtained for the photo-MCDSC experiments, an initial linear decrease in the concentration of nifedipine was observed, followed by a slower final decay phase. Zero-order and first-order kinetics were thus assumed during these periods and data were fitted to the respective kinetic equations to calculate the reaction parameters. The fitting process used in these studies is similar to the one described in section 4.3.1.5. and the resulting fit lines are displayed in Figure 4.20.
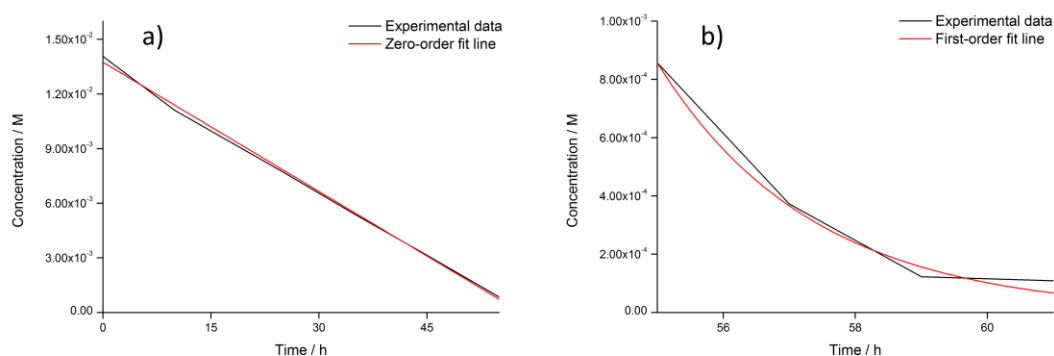
FIGURE 4.20. Fit lines obtained for the zero-order (a) and first-order (b) periods using *Origin*.

The reaction parameters obtained with these fitting techniques are listed below:

- Zero-order rate constant = 6.6 x 10^{-8} mol.dm^{-3}.s^{-1}

- First-order rate constant = 1.2 x 10^{-4} s^{-1}

- Number of moles of nifedipine at time of transition between kinetics = 3.4 x 10^{-6} mol

216

These reaction parameters are very similar to those calculated from calorimetric data analysis, therefore, proving that those methods are valid.

4.3.2.5. *Effect of light power on the photoreaction signal*

The influence of light intensity on the kinetics of photodegradation was studied with the photo-TAM using an array of five similar 410 nm LEDs (*Array 2*). The voltage applied to these LEDs was varied (5 V and 7.5 V) and two different light intensities were tested on similar samples of nifedipine (4 mL 0.5% *w/v*). Figure 4.21. shows the photocalorimetric signals recorded in these two experiments.
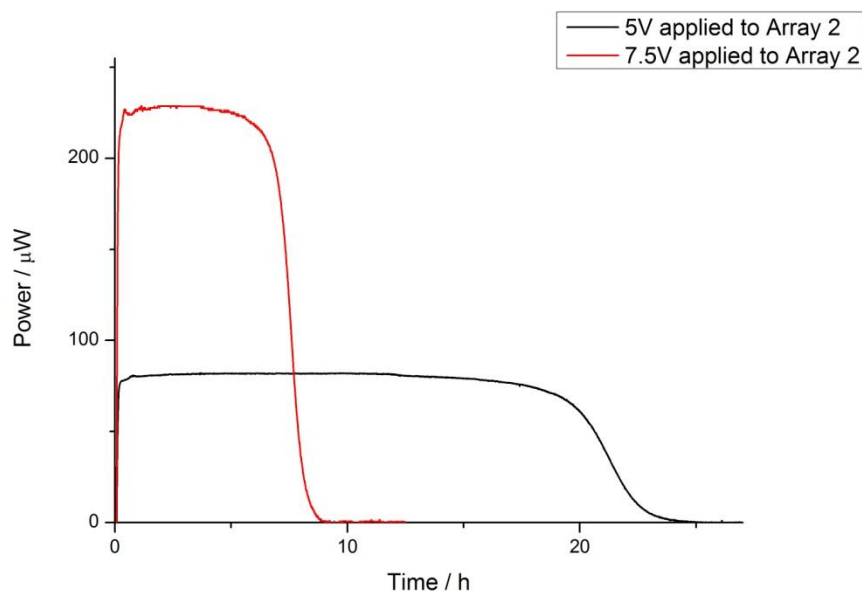
FIGURE 4.21. : Calorimetric signals obtained for the photodegradation of 4 mL 0.5% nifedipine using two different intensities of light irradiated from *Array 2*.

As demonstrated in the experiments with the photo-MCDSC (section 4.3.1.7.), the light power irradiating the samples has a great impact on the magnitude of the photoreaction signals, as well as, on the time that the processes take to progress to completion. Figure 4.21. shows that when samples are exposed to higher intensities of light, the thermal power measured is much larger and the processes are quicker. These effects are explained by an increase in the rate of reaction as a consequence of more photons interacting with molecules of nifedipine during exposure to light.

The photoreaction parameters were determined using the zero-order and first-order analytical strategies and compared to assess the influence of intensity of light on those values (Table 4.13.). The light power reaching the ampoules was also measured calorimetrically by switching each LED individually and measuring the thermal response it caused (Figure 4.22.). This experiment was performed on the two light intensities tested using ethanol on both reference and sample ampoules. The calculated light power values were then used in the determination of the quantum yields of reaction with Equation 4.7.
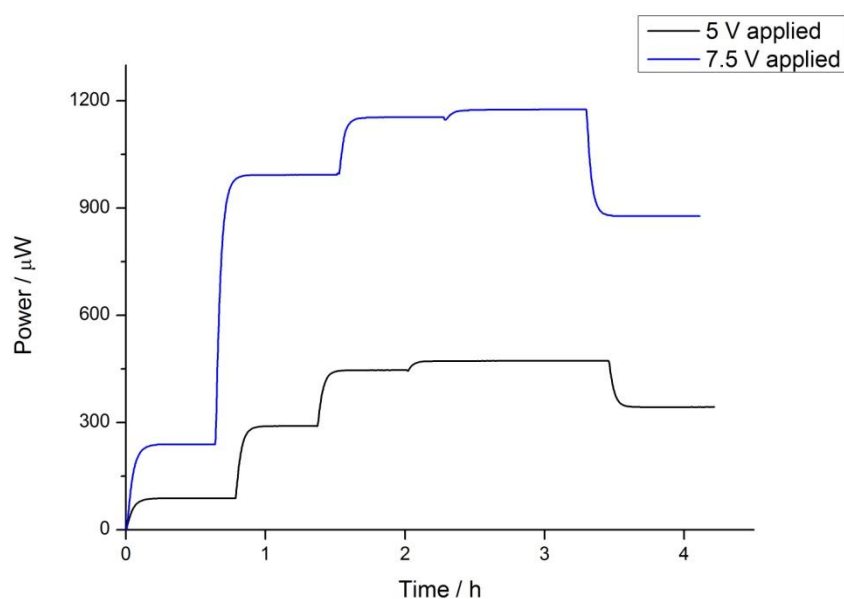
FIGURE 4.22. : Thermal contribution of each individual LED on the overall light power. Each step in the signal corresponds to a different LED irradiating the ampoule.

TABLE 4.13. : Reaction parameters calculated for the two experiments using different intensities of light (Part I).

Voltage applied	Light power measured with photo-TAM (µW)	Enthalpy of reaction (kJ/mol)	Photoreaction power (µW)	k_0 (mol.dm^{-3}.s^{-1})
5 V	1640	-104.3	82	1.9×10^{-7}
7.5 V	4440	-103.9	229	5.5×10^{-7}

TABLE 4.14. : Reaction parameters calculated for the two experiments using different intensities of light (Part II).

Voltage applied	k_1 (s^{-1})	$[A]_{tr}$ (mol.dm^{-3})	Nº moles at transition	Quantum yield
5 V	2.8×10^{-4}	1.6×10^{-3}	6.6×10^{-6}	0.139
7.5 V	6.6×10^{-4}	1.5×10^{-3}	5.9×10^{-6}	0.145

The calculated reaction parameters also show a clear dependence on the light power used. The zero-order and first-order rate constants show a 2 to 3 fold increase when 7.5 V are applied to the LEDs which is consistent with the increase in the number of photons available for reaction. The larger zero-order photoreaction powers can also be explained by that increase in the rate constants and Equation 4.2. shows that correlation. On the other hand, the enthalpy of reaction does not seem to change with increasing light power which means that no changes in the mechanism of reaction occurred. The only unexpected results obtained in these light intensity studies were those for the concentration and number of moles of nifedipine at the time of transition between kinetics. Those values should have increased with increasing number of photons irradiating the sample because the number of interactions between molecules and photons also increases, during transition between kinetics. However, similarly to the results obtained in the photo-MCDSC, no dependence on the intensity of light was found for the concentration of nifedipine at transition (Table 4.14.). The small concentrations of nifedipine, at this point, and the difficulty to discriminate very small differences in concentration with the analytical methods used, explain these results.

Regarding the photoreaction quantum yields, similar numbers were determined for the two experiments, therefore, demonstrating its value as a parameter independent of the irradiation conditions. An average quantum yield of 0.142 was found for this photoreaction which is very different from the literature values (0.2 to 0.3). Possible explanations for this difference will be given in the following section.

4.3.3. Photo-MCDSC *versus* Photo-TAM

After successfully demonstrating the application of two new photocalorimeters to analyse photochemical processes in pharmaceuticals, the results obtained with both instruments are now compared to understand the influence of the different designs on the thermal outputs. The two designs are significantly different in terms of the distance between the samples and the light source (bigger in the photo-TAM), the surface of the samples irradiated with light (larger surface areas in the photo-TAM), the number of LEDs used (5 LEDs in the photo-TAM and only one in the photo-MCDSC) and the orientation of the light bulbs in the holder (the LEDs in the photo-TAM are arranged in a circle around the perimeter of the LED-holder). All these differences will undoubtedly have a great influence on the light power absorbed by the samples and, subsequently, on the photodegradation of samples. For clarity of analysis, the only sets of data compared here are those obtained in the photo-MCDSC studies and those measured in the photo-TAM experiments with *Array 2*. Both sets of data were obtained using similar wavelength LEDs (λ=410 nm) which allows direct comparison between data.

In general, all photocalorimetric signals measured with both instruments have an initial constant phase, typical of zero-order processes, followed by a transition phase and a first-order decay to zero-baseline. These signals, however, are quite different in terms of the duration of the overall process: less than 10 hours with the photo-MCDSC and more than double that time using the photo-TAM. These differences can be explained either by different rates of conversion of nifedipine or different initial contents in nifedipine. The experiments performed in the photo-TAM used significantly larger volumes compared to those used in the photo-MCDSC which would explain the differences in length even if similar rates of conversion were observed.

The rates of conversion during the zero-order period (k_0 x V) were determined, for those experiments where the light power was maintained constant, and the values were, approximately, 1.7 x 10^{-9} mol/s using the photo-MCDSC and 1.0 x 10^{-9} mol/s using the photo-TAM. Despite the fact that the photo-TAM uses 5 LEDs to degrade the samples, while the photo-MCDSC only uses one, the rates of conversion were higher with the latter. That is because the single LED in the photo-MCDSC is placed just above the sample while the 5 LEDs in the photo-TAM are significantly further away from the sample. As a consequence, the number of photons reaching the samples is lower in the

photo-TAM experiments. The inverse-square law explains that decrease in intensity: "the intensity of light is inversely proportional to the square of the distance from the source". These differences in the intensity of light reaching the samples will thus have an impact on the number of molecules reacting per unit time (rate of conversion).

Because the rate of reaction is greatly dependent on the intensity of light, the quantum yield of reaction (ϕ) is usually preferred to characterise a specific photoreaction. These values were previously determined for the experiments performed in the two photocalorimeters and, surprisingly, different values were returned. An average value of 0.24 was found for the photo-MCDSC experiments while a quantum yield of 0.14 was determined using the photo-TAM data. Such differences can be explained by the fact that the light power measured calorimetrically is not a real measure of the number of photons absorbed by molecules of nifedipine. Instead, those values are directly related to the number of photons reaching the measuring site which, in these cases, is a combination of the number of photons absorbed by the sample and reflected out of the ampoule by the stainless steel walls. Because the headspace between the sample and the top of the ampoule is much larger in the photo-TAM ampoules, a greater number of photons are reflected out by the walls, making the light power entering solution impossible to calculate. A mitigation strategy that can be investigated, in the future, is the positioning of the LEDs closer to the photo-TAM ampoule. This should decrease the amount of photons interacting with other parts of the photocalorimeter, allowing an improvement of the accuracy of the light power measurements. However, this change must be done carefully not to remove the LEDs from the heat shunt placed above the thermopiles in the measuring site. On the other hand, the measurements with the photo-MCDSC are much closer to the real number of photons absorbed because the ampoule headspace is much smaller. That is why the quantum yields determined with the photo-MCDSC are closer to the values reported in the literature (ϕ=0.2-0.3 (112)).

Another parameter for which very different values were found is the enthalpy of reaction. This parameter is characteristic of a reaction and, unless changes in the mechanism of reaction occur, similar values are expected for the same experimental conditions. However, that is not the case and the calculated enthalpies of reaction were -158.4 ± 9.7 kJ/mol for the photo-MCDSC experiments and -94.5 ± 3.1 kJ/mol for the photo-TAM experiments. The only logical explanation for these results is that different mechanisms of reaction occurred during exposure to light which is not unreasonable

since the HPLC studies revealed the presence of an additional reaction product in the samples tested with the photo-MCDSC.

In order to explain those results, three different reaction pathways were considered for the photodegradation of nifedipine in solution and the enthalpies of reaction were estimated using Salmon and Dalmazzone prediction method (101) (Figure 4.23.). Despite that method being used in solid state predictions, the calculated enthalpies were assumed similar for the same reactions in solution, considering similar enthalpies of solvation for both reactants and products.

$$\text{Nifedipine (s)} + \frac{1}{2}\, O_2\ (g) \xrightarrow{h\nu} \text{Nifedipine nitro product (s)} + H_2O\ (l)$$

$$\Delta_r H = \text{-141.73 kJ/mol}$$

$$\text{Nifedipine (s)} \xrightarrow{h\nu} \text{Nifedipine nitro product (s)} + H_2\ (g)$$

$$\Delta_r H = \text{144.1 kJ/mol}$$

$$\text{Nifedipine (s)} \xrightarrow{h\nu} \text{Nifedipine nitroso product (s)} + H_2O\ (l)$$

$$\Delta_r H = \text{-73.63 kJ/mol}$$
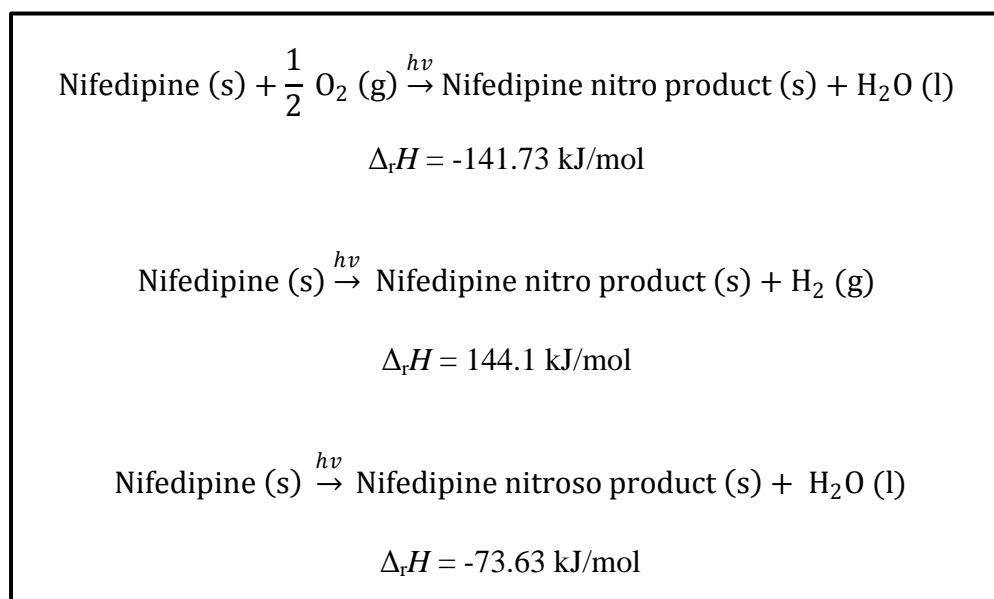
FIGURE 4.23. : Three possible reaction pathways for nifedipine photodegradation in solution.

Those estimated enthalpies were, afterwards, compared with the experimental data and it was found that the average enthalpy calculated with the photo-MCDSC data, -158.4 kJ/mol, was very similar to that determined for the reaction of nifedipine with molecular oxygen to give its nitro-derivative, -141.7 kJ/mol. Those similar values led to the assumption that a pathway involving oxygen consumption is favoured in the photodegradation experiments with the photo-MCDSC. Furthermore, the enthalpy of reaction determined with the photo-TAM, -94.5 kJ/mol, was relatively similar to that estimated for the formation of the nitroso-derivative, -73.6 kJ/mol, leading to the assumption that this is the major pathway.

Based on these predictive studies, it was reasonable to assume different mechanisms of reaction for samples analysed with the photo-TAM and photo-MCDSC. However, an

explanation for these differences was still missing because similar experimental conditions were used with both instruments. The only difference between the two experimental set-ups was the type of ampoules used in the photodegradation studies: stainless steel ampoules in the photo-TAM and Hastelloy, a nickel based metal alloy, ampoules in the case of the photo-MCDSC. The influence of different metals on the catalysis of reactions was, therefore, questioned and a possible explanation for the different mechanisms of reaction was found. Transition-metals are known to be very good catalysts of oxidations that use molecular oxygen (118). Considering that the oxygen-dependent conversion of nifedipine into its nitro-derivative (Figure 4.23.) is an example of such reactions, it is reasonable to assume that when the nickel-based photo-MCDSC ampoules are used, that reaction is favoured. The larger enthalpy values calculated for the photo-MCDSC experiments can, therefore, be explained by a predominance of that energetic photo-oxidative process catalysed by the nickel contained in the ampoule.

To prove the effect of nickel on the overall mechanism of reaction, another set of experiments was conducted with *Array 2* in the photo-TAM, this time, placing a photo-MCDSC ampoule inside each photo-TAM ampoule. These experiments would demonstrate the catalytic effect of nickel (in the MCDSC ampoules) if the calculated enthalpies of reaction were significantly larger than the average -94.5 kJ/mol previously determined. Before testing the system with solutions of nifedipine, a blank experiment was performed, using 5 mL of ethanol in each ampoule, to zero the calorimetric signal. That volume was used because it was the smallest volume capable of submersing the MCDSC ampoules completely. After zeroing the signal, the system was tested with 5 mL samples of 0.5% nifedipine (in triplicate) and the calorimetric signals were analysed to determine the enthalpies of reaction. Figure 4.24. shows the typical photocalorimetric signal recorded in these experiments.
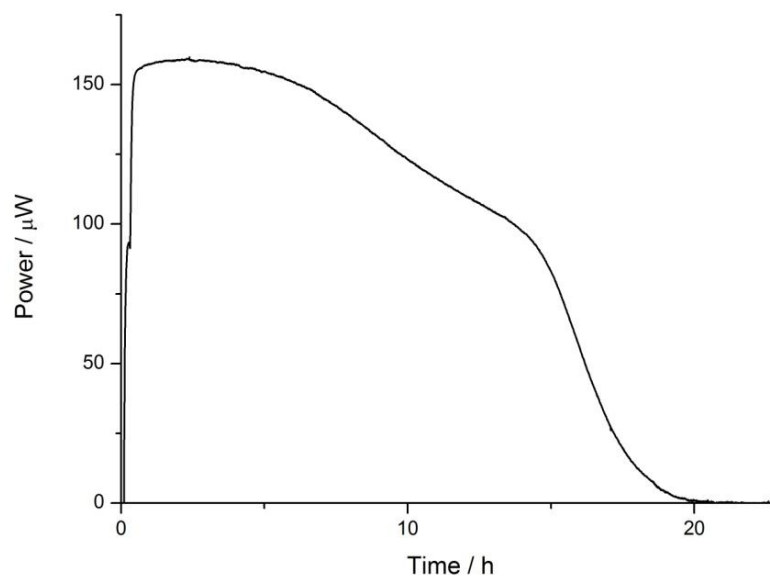
FIGURE 4.24. : Calorimetric signal recorded for the photodegradation of 5 mL 0.5% nifedipine using *Array 2* in the photo-TAM. A photo-MCDSC ampoule was placed inside each photo-TAM ampoule to test the influence of different types of ampoule on the enthalpy of reaction.

The signals measured in these studies were quite different in shape compared to all others measured with *Array 2*. An initial zero-order period is followed by a two-step decay to zero that was only observed when 6 mL samples of 0.5% nifedipine were tested with *Array 1*. The explanation found for that behaviour was that diffusion processes were interfering with the overall kinetics of the system. A similar explanation may be given, in this case, although, the diffusion processes occurring here involve movement of molecules between compartments, the inside and the outside of the photo-MCDSC ampoule. Nevertheless, the main objective of these experiments was to determine enthalpies of reaction and compare them with those calculated in the previous photo-TAM experiments. The average enthalpy of reaction ± standard deviation calculated for the experiments using a MCDSC ampoule inside the photo-TAM ampoules was -112.3 ± 4.5 kJ/mol. To compare these results with those obtained in the standard photo-TAM experiments, the enthalpies of reaction calculated for three standard experiments (4 mL of 0.5% nifedipine in ethanol), were selected and the statistical significance determined. Table 4.15. compares the values obtained in the photo-TAM experiments with and without the MCDSC ampoule inside the photo-TAM ampoules.

TABLE 4.15. : Comparison of the enthalpy values calculated in the photo-TAM experiments with and without a MCDSC ampoule inside the pho-TAM ampoules.

Photo-TAM experiments	Enthalpies of reaction (kJ/mol)		
without MCDSC ampoule inside	-96.3	-99.7	-98.7
with MCDSC ampoule inside	-106.3	-113.3	-117.3

The statistical analysis demonstrated that the two sets of results are different ($p < 0.05$) which means that there is a clear influence of the type of ampoule on the enthalpies of reaction. Although those values are still far from the average enthalpies determined in the photo-MCDSC experiments, -158.4 kJ/mol, these experiments showed that there is a clear influence of the type of ampoule on the mechanism of reaction. A more elegant and easier experiment that can be done, in the future, is to add a very small amount of nickel to the photo-TAM ampoules and test the photodegradation of nifedipine in those conditions. The diffusion issues would then be avoided with that experimental set up.

4.4. Summary

This chapter demonstrated the application of two new photocalorimetric designs (described in Chapter 3) to assess the photostability of pharmaceuticals in solution. The test reaction chosen for these studies was the photodegradation of nifedipine in solution under different irradiation conditions. To test the effect of wavelength on the photodegradation signals, two different wavelength spectra were used in the photo-TAM (5 different wavelength LEDs in *Array 1* and 5 similar 410 nm LEDs in *Array 2*) while the photo-MCDSC only used 410 nm LEDs to irradiate the samples. Several experiments were performed in the two photocalorimeters using different intensities of light, concentrations of nifedipine and volumes of solution and the resulting photocalorimetric signals were analysed.

The typical photocalorimetric signals measured in these experiments have an initial zero-order phase followed by a transition period of non-integral reaction order and a first-order decay to baseline. The zero- and first-order periods were analysed quantitatively using the calorimetric strategies described in the literature and the reaction parameters (ΔH and k) were calculated for the different experimental conditions. Furthermore, the concentration of nifedipine at the time of transition between kinetics was also calculated using the first-order calorimetric strategies. To validate these methods, an HPLC assay was developed to determine the rate of consumption of nifedipine in the two instruments and compare it with the values obtained calorimetrically. It was found that the rates of reaction were similar using both methods. In addition to the thermodynamic and kinetic parameters determined calorimetrically, the quantum yields of photodegradation were also calculated using an equation that relates this parameter with the zero-order rate constant and the light power irradiating the samples.

Comparison of the results obtained in the photo-TAM, using *Arrays 1* and *2*, showed a significant difference in terms of the zero- and first-order rate constants which can be explained by the different light powers emitted by the two arrays. Furthermore, the enthalpies of reaction were also slightly different (-83.8 ± 6.7 kJ/mol with *Array 1* and -94.5 ± 3.1 kJ/mol with *Array 2*), which shows that different mechanisms of reaction were favoured in those experiments. These results agree with the previously

226

demonstrated dependence of nifedipine photodegradation on the wavelengths tested (76).

The results obtained in the photo-MCDSC experiments were also compared with those obtained in the photo-TAM experiments with *Array 2* (410 nm LEDs). A clear difference in the rates of photodegradation was observed (1.7×10^{-9} mol/s in the photo-MCDSC and 1.0×10^{-9} mol/s in the photo-TAM) because the irradiation conditions and sample arrangement in the ampoules were very different in the two instruments. Regarding the enthalpies of reaction, the results were unexpectedly different in the two photocalorimeters: -158.4 ± 9.7 kJ/mol in the photo-MCDSC and -94.5 ± 3.1 kJ/mol in the photo-TAM. These differences were later explained by the catalytic effect of nickel (present in the MCDSC ampoules) on the photo-oxidative degradation of nifedipine. This pathway is the most exothermic, hence the larger enthalpies of reaction calculated in the photo-MCDSC. The quantum yield of photodegradation was also different for the reactions taking place in the two photocalorimeters (0.24 in the photo-MCDSC and 0.14 in the photo-TAM). These differences were explained by the inaccurate method used to calculate the light power absorbed by the samples in the two instruments.

5. Application to the photostability assessment of solid drugs

5.1. Introduction

The previous chapter demonstrated the use of photocalorimetry to investigate photodegradation processes in pharmaceuticals in the solution phase. Those studies not only showed that the two photocalorimeters described in Chapter 3 are capable of detecting photodegradation signals, but also that quantitative analysis is possible using those data.

Chapter 5, on the other hand, deals with the analysis of solid photolabile compounds, which is particularly relevant in a pharmaceutical context because the majority of medicines are commercialized as solid dosage forms. Similarly to the solution phase studies, samples of nifedipine, in the form of powder, were tested with the two photocalorimeters and the influence of different experimental conditions on the photocalorimetric signal was investigated. Furthermore, 5 different drugs that the European Pharmacopoeia recommends protection from light, were analysed in the photo-MCDSC to investigate the signals measured for a range of different photosensitive compounds. These included carbamazepine, chloramphenicol, dipyridamole, furosemide and paracetamol (119). The chemical actinometer, 2-nitrobenzaldehyde was also tested in the photo-MCDSC. In addition to these photolabile compounds, a photostable drug, acetylsalicylic acid, was tested in that photocalorimeter to compare the two types of signals. All tests were performed 3 times, at most, which may not be enough to establish clear trends in the signals. Therefore, most of the comments and assumptions made in the following sections are the result of speculation. Nifedipine was the only drug tested in the photo-TAM because the instrument took a long time to develop and not much time was left for testing.

With respect to the analysis of calorimetric data, a simple qualitative approach was followed because solid processes are usually very complex. This is particularly true in the case of light-induced processes where change occurs primarily at the surface of the sample, rendering the overall reaction scheme even more heterogeneous and complex. In addition, factors that influence light penetration, such as the particle size, crystal structure, colour or thickness of powder bed, render the process even more complex. All these factors preclude the use of the solid state calorimetric strategies described in Chapter 2 because those can only be applied to analysis of simple systems.

5.2. Materials and Methods

5.2.1. Materials

Talc GPR RECTAPUR was purchased from VWR BDH Prolabo. Nifedipine (>98%) was purchased from TCI Europe. 2-nitrobenzaldehyde (98%) was purchased from Aldrich Chemistry. Chloramphenicol (≥98%, TLC), acetaminophen (98-101%, meets USP testing specifications), acetylsalicylic acid (no purity data available), carbamazepine (no purity data available), dipyridamole (≥98%, TLC, powder) and furosemide (no purity data available) were purchased from Sigma. Activated charcoal was purchased from SGE Analytical Science as part of the refill kit for a GC (Gas Cromatography) gas purifier.

5.2.2. Methods used in the studies performed with the photo-MCDSC

5.2.2.1. Sample preparation

Amorphous nifedipine was prepared by melt-cooling. Crystalline nifedipine was melted (melting point of 173 °C) in aluminum foil on a hot plate and quench-cooled in liquid nitrogen. The sample was then ground gently using a mortar and a pestle and stored in a vial inside a desiccator using P_2O_5 to create a 0% relative humidity environment. All samples were prepared and stored under a red light in the dark room. Samples were taken immediately after preparation and after 3 days, 6 days and 9 days storage to be analysed in the photo-MCDSC and DSC.

All other drugs, including crystalline nifedipine, were passed through a 150 µm sieve prior to testing in the photo-MCDSC to break up agglomerates.

5.2.2.2. *Photocalorimetric experiments*

All photocalorimetric experiments used light from a 410 nm LED to irradiate the samples inside the photo-MCDSC ampoules. Before each measurement, the light power going into the sample and reference channels was balanced, manually, to zero the calorimetric signal. First, two ampoules were loaded with an amount of talc (a photoinert compound) equal to that of the sample that was going to be tested and closed with the re-designed lid. The ampoules were then lowered into the reference and sample chambers together with the two 410 nm LEDs. Afterwards, the rubber plugs were fitted to the holes in the top lid of the photocalorimeter and the system was left to equilibrate. In the mean time, the software that operated the instrument, MCDSCRun, was initialized and the method assigned. The temperature of the system was set to 25 ℃ before data collection started (*exo up*). The signal displayed in the software application window was allowed to stabilize and the LEDs, positioned above the reference and sample ampoules, were switched on (5 V were applied to each LED). Then, the voltage applied to the reference LED was adjusted, using the circuit board, until the calorimetric signal stabilized to a value near zero. This zeroing process was not very accurate because of the difficulty to perform small voltage adjustments in the circuit board. The following thermal power values correspond to three final baselines obtained after attempting to zero the signal: -21, 9 and -8 µW.

After zeroing the signal, the sample ampoule was emptied, cleaned and dried prior to loading with the test drugs. The sample mass weighed into the ampoule was similar to that of talc in the reference ampoule. Similarly to the blank experiment, the ampoule was closed and lowered in the sample chamber and the LED was positioned above it. The system was closed and data collection started after setting the method in the MCDSC software. The system was left to equilibrate at 25 ℃ until the signal displayed in the computer reached a stable value. Afterwards, the two LEDs were switched on and data were recorded for a maximum of 83 hours. The voltage difference between the two LEDs was as close as possible to that set in the blank experiment.

Different samples and experimental conditions were tested in the photo-MCDSC using the previous method. These experiments are described below.

Nifedipine:

- Three samples of 200 mg were tested to assess the repeatability of the signals.
- Samples of 200 mg, 100 mg, 10 mg and 5 mg were also tested to assess the effect of sample mass on the shape of the power-time curves.
- Two different intensities of light were also tested with the 200 mg samples. That intensity was regulated in the circuit board.
- Samples of amorphous nifedipine (200 mg) were taken out of the desiccators on the day it was prepared and after 3, 6 and 9 days to be tested in the photo-MCDSC.

Activated charcoal:

- 200 mg of activated charcoal (a compound that absorbs all radiation in the visible region of the spectrum) were tested to assess the effect of absorption phenomena on the calorimetric signal.

2-nitrobenzaldehyde:

- Three samples of 200 mg were tested to assess the repeatability of the signals.
- Samples of 200 mg, 10 mg and 5 mg were also tested to assess the effect of sample mass on the shape of the power-time curves. The 5 mg and 10 mg samples had a 7 mm diameter disc shape.
- Three different intensities of light were also tested with the 200 mg samples. This intensity was regulated in the circuit board.

Other compounds:

- 200 mg samples of carbamazepine, chloramphenicol, dipyridamole, furosemide, acetylsalicylic acid and acetaminophen were tested in triplicate.

All measurements were made in a differential mode ($\Phi_{\text{sample side}}$- $\Phi_{\text{reference side}}$). Because the only two chambers used were the reference and one of the sample chambers, the thermal power measured in the other two chambers corresponds to the light power going into the reference chamber. That value is assumed similar to the light power irradiating the sample because the intensities of light were balanced prior to the experiments. A calorimetric method for the determination of the light power irradiating the samples is thus given.

5.2.2.3. Differential Scanning Calorimeter (DSC)

Samples of amorphous nifedipine were taken out of the desiccators on the day it was prepared and after 3 and 6 days of storage for analysis in the DSC. Samples of crystalline nifedipine (from the bottle) were also tested. Measurements were performed in triplicate on a Q2000 DSC (TA instruments, Water, LLC). Calibration for cell constant and enthalpy was performed with indium (T_m = 156.6 °C, $\Delta_{\text{fusion}}H$ = 28.71 J/g) according to the manufacturer instructions. Nitrogen was used as purge gas with a flow rate of 50 mL/min for all the experiments. TA aluminum pans and lids (Tzero) were used and samples of about 10 mg were heated at 10 °C/min. Crystalline samples were heated from 25 ºC to 200 ºC while amorphous samples were heated between -30 ºC and 200 ºC. Data were analysed using TA Instruments Universal Analysis 2000 and Origin.

5.2.3. Photocalorimetric experiments with the photo-TAM

All photocalorimetric experiments in the photo-TAM were performed with an array of 5 similar 410 nm LEDs. Before each assay, a blank experiment was performed in order to balance the amount of light going into each ampoule. First, the sample and reference ampoules were loaded with similar amounts of talc, closed with the new lids and lowered into the calorimetric channels. Then, the lighting columns were inserted in the channels and the system was left to equilibrate at 25 ºC. Data was collected every 10 seconds using the dedicated software package Digitam 4.1. (TA Instruments LLC, USA). After equilibrium was reached, the signal was zeroed in the TAM panel and the instrument was electrically calibrated. The amplifier's range was set to 1000 µW. After calibration, all switches in the circuit board were turned on (sample side and reference side) and the system was allowed to equilibrate with light irradiating the ampoules. The voltage applied to the LEDs was 5 V. When the resulting calorimetric signal measured was very different from zero, the autobalance power supply was used to zero the signal by adjusting the voltage applied to the reference side LEDs.

After balancing the light power going into both ampoules, the LEDs were switched off and the sample ampoule was taken out of the photocalorimeter. The ampoule was emptied, cleaned with ethanol and blow-dried before loading the sample. An amount of sample, similar to that of talc on the reference ampoule, was weighed into the sample

233

ampoule. After closing it with the windowed lid, the ampoule was lowered into the sample side channel together with the lighting column. The system was left to equilibrate at 25 ℃ while the method was set in the TAM software. Then, data collection started and the calorimetric signal was displayed in the software application window. When the signal stabilized to a constant value, the sample and reference LEDs were switched on to allow irradiation of the sample. Data was recorded until enough information was obtained.

Only samples of nifedipine were tested in the photo-TAM. The effects of sample mass, light intensity and distance from the LEDs on the calorimetric signal were assessed with the following experiments:

- 3 samples of 500 mg and 100 mg nifedipine were tested to study the effect of different sample mass on the photodegradation signals.

- two 2 cm x 2.3 cm (height x diameter) stainless steel cylinders were inserted in the reference and sample ampoules, respectively, to raise the samples inside them and test the effect of distance to light source on the degradation data. All blank experiments and photodegradation assays were performed with those cylinders inside the ampoules. Three sample of 500 mg nifedipine were tested with this set-up.

- The effect of increasing light intensity on the photodegradation of solid nifedipine was also tested. The voltage applied to the LEDs was increased to 7.5 V and the method described above was used to zero the signal and degrade the samples of nifedipine. Three samples of 500 mg nifedipine were also tested, in this case. The light power going into the sample side ampoule was determined calorimetrically, for the two light intensities used, by switching on each LED and measure the deflection from zero. These measurements were made with talc on both ampoules. For the light power measurements where 7.5 V were applied to the LEDs, the amplifier range was set to 3000 µW because the light power emitted by some of the LEDs was greater than 1000 µW.

5.3. Results and discussion

5.3.1. Nifedipine

Nifedipine is a highly photolabile drug used therapeutically as a calcium channel antagonist for the treatment of cardiovascular disorders. Most studies on nifedipine photodegradation were made in solution and Chapter 4 gives a brief overview of the different aspects involved in those reactions, including the photoproducts, kinetic factors and mechanisms of reaction. Regarding its photodegradation in the solid state, it was found that four different products were formed after irradiation with light from mercury vapour or fluorescent lamps. The major products were the nitro- and nitroso-derivatives while the other minor products corresponded to the azoxy-derivative and another compound that was not identified because of the trace amounts detected (108). First-order kinetics were demonstrated for the photodegradation of solid nifedipine and a maximum degree of degradation was found for wavelengths around 380 nm, corresponding to the absorption band of the nitro group and dihydropyridine ring in the molecule (21, 108). The photostability of nifedipine in tablets was also investigated, in particular, the influence of formulation and tabletting processes on the degree of degradation (11). Whereas the particle size of the drug and the choice of lubricant had no effect, the drug content, the compression diluents and geometric alterations significantly affected the photoinstability of nifedipine.

Despite most of those photodegradation studies were made on the most stable form, nifedipine has a few polymorphs that may react differently to light. Aso et al. (120) reported that amorphous nifedipine obtained from the supercooled melt, crystallized to a metastable state (form B) at 90 ºC, which converted to the thermodynamically stable form (form A) from 110 ºC. Form B's melting point was found to be within the region of 161-163 ºC while form A had a melting point between 169-173 ºC. Furthermore, Zhou et al. (121) reported that the metastable form B produced on isothermal crystallization was enantiotropically related to another modification (form C) which formed on cooling of form B below 30 ºC. This modification converted back to form B, endothermically, on reheating at 60 ºC. In addition to these polymorphs, it is also possible that other liquid to solid as well as solid to solid transformations occur prior to

formation of form B (122). It was also found that different methods of preparation of the amorphous sample result in changes in the crystallization behaviour. For example, amorphous nifedipine prepared by fusion on a DSC alumina pan showed a slightly shifted crystallization peak compared to that measured for amorphous samples prepared after cooling on a lightweight aluminium foil. Those differences had to do with different shape and intermolecular attractions within the sample (122).

5.3.1.1. Photo-MCDSC experiments

Three samples of 200 mg nifedipine were analysed in the photo-MCDSC, using 410 nm LEDs as the light source. A change in the colour and texture of the samples was observed at the end of the experiments, with the initial yellow powder turning to a greenish wet mass in the centre of the sample. Figure 5.1. shows a picture of the samples before and after irradiation.
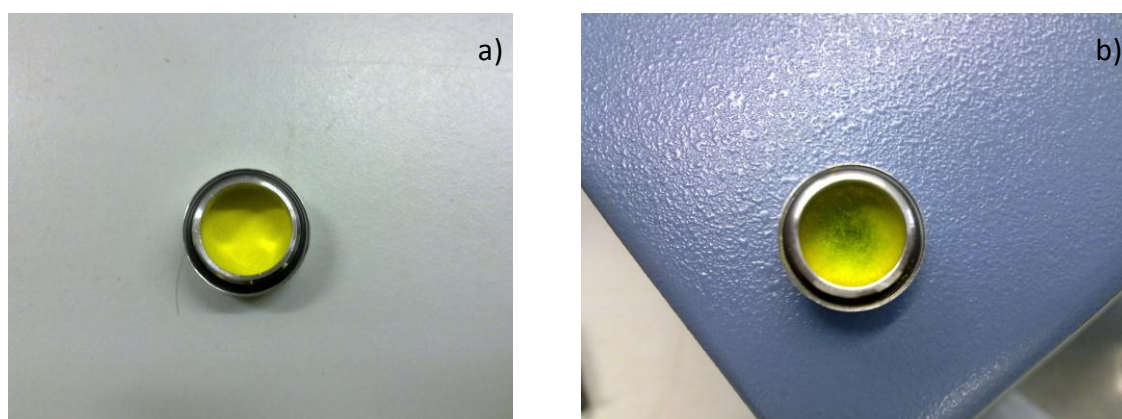
FIGURE 5.1. : Picture of the nifedipine sample a) before irradiation b) after irradiation.

The photocalorimetric signals recorded in these experiments are shown in Figure 5.2.
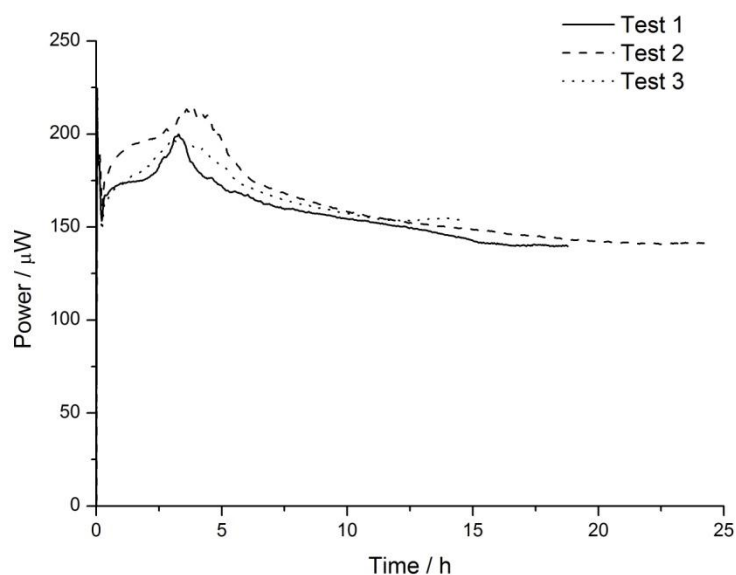
FIGURE 5.2. : Photocalorimetric signals measured during analysis of 200 mg samples of nifedipine with the photo-MCDSC (410 nm).

The shape of the power-time curves was similar for all three experiments, demonstrating the repeatability of the thermal measurements. An initial increase in the thermal power was followed by a peak, approximately 5 hours after the LEDs were switched on, and a final decay phase that lasted more than 20 hours. Two different processes can be discriminated from that overall signal; one occurring between 2 and 6 hours of exposure and another, much longer, extending from the beginning of the experiment until the end of data collection. In terms of the magnitude of the signals, a maximum thermal power of approximately 200 μW was observed corresponding to the peak maximum. This signal decreased to a stable value, around 140 μW, which was assumed to correspond to the end of the photoprocess. Curiously, this baseline value was very different from zero and much larger than the standard deviation previously determined in the baseline repeatability tests in Chapter 3 (around 15 μW). Two reasons could explain this non-zero baseline; either photodegradation was still occurring but the process started following zero-order kinetics, or the physical and thermal properties of the sample were different from talc's, resulting in that thermal imbalance. The idea that a change in the kinetics occurred in the later stages of the photoprocess was abandoned because no information on such behaviour was found in the literature. Therefore, the differences between nifedipine and talc's physical properties and their influence on the thermal measurements were investigated.

237

Differences between the sample and reference heat capacities were ruled out because the calorimetric signal returned to zero every time the samples of nifedipine and talc were equilibrated in the photo-MCDSC, with no light in the system. An alternative explanation for those final baseline values was the occurrence of different light absorption phenomena as a result of nifedipine and talc having different colours. It is well known that the colour of materials reflects the range of visible wavelengths that they absorb. For example, a white material reflects all visible wavelengths while a black one absorbs all radiation in the visible range. Such differences in the absorption of radiation would, therefore, explain the imbalance in the thermal power measured when light irradiated, simultaneously, the samples of nifedipine and talc. To prove these light absorption effects, an additional experiment was performed on the photo-MCDSC, using activated charcoal, a photo-inert black compound, instead of nifedipine. Figure 5.3. compares the calorimetric signals obtained in the nifedipine and activated charcoal tests.
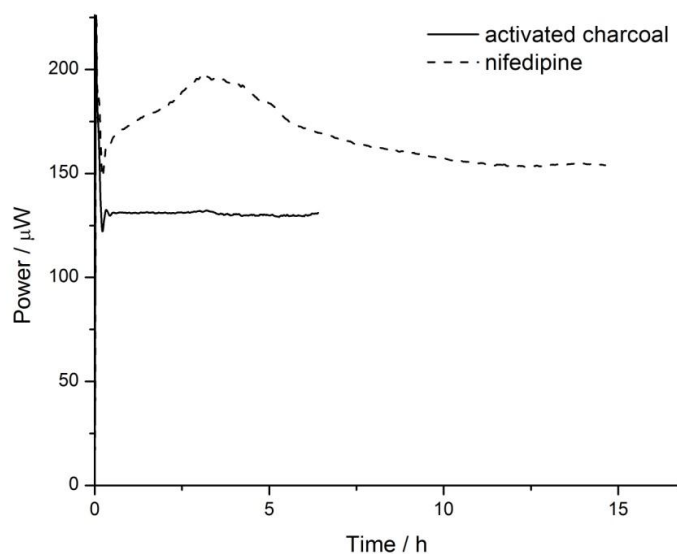
FIGURE 5.3. : Comparison of the photocalorimetric signals measured during the experiments with 200 mg nifedipine and 200 mg activated charcoal.

The calorimetric signal recorded in the experiment with activated charcoal showed a constant zero value before light was put into the system and a constant value around 130 μW after the LEDs were switched on. Because activated charcoal is photo-inert, that deflection from zero can only be attributed to different amounts of light power being absorbed by the two samples, talc and activated charcoal. In fact, activated charcoal

absorbs all visible radiation while talc, a white powder, reflects those same visible wavelengths. As a result, the energy content of the activated charcoal sample is larger than talc's, hence the positive differential signal measured by the photo-MCDSC. The similar magnitude of the signals measured with activated charcoal ($\approx$130 µW) and the final baseline measured in the experiments with nifedipine ($\approx$140 µW), also helps to demonstrate this effect.

The influence of sample mass on the shape of the power-time curves was also investigated using 4 different samples of nifedipine: 200 mg, 100 mg, 10 mg and 5 mg. Figure 5.4. shows the signals recorded in these experiments.
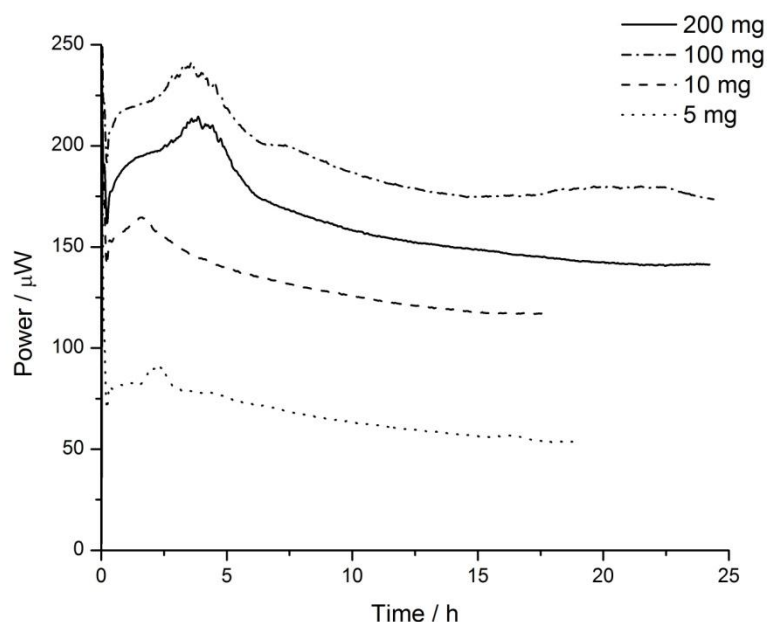
FIGURE 5.4. : Effect of sample mass on the photocalorimetric signals recorded for nifedipine photodegradation in the photo-MCDSC (410 nm).

That figure shows that sample mass has a clear influence on the magnitude of the signals, the shape of the curves and the final baseline value. Except for the large sample masses of 200 mg and 100 mg, a clear trend is observed regarding those signal properties. For example, the data show a significant increase in the size of the initial peak for larger sample sizes. This effect can be explained by an increase in the amount of sample that is available for reaction and in the rate of photodegradation. The latter can be explained, in turn, by an increase in the light power irradiating the surface of samples as the distance between that surface and the light source becomes shorter

239

(inverse square law). Furthermore, the magnitude of the signals increases with sample mass although that clearly results from a shift in the final baseline. That baseline moved up with sample mass, probably, because there was an increase in the number of particles of nifedipine absorbing in the visible range in contrast with the talc sample that reflects all visible radiation. As a consequence, the difference in energy between the sample and reference sides increased considerably, resulting in a much larger final baseline value. Such effects were not observed when the sample mass was increased from 100 mg to 200 mg, probably, because the surface area exposed to light did not change significantly for those large masses.

The effect of light power on the photocalorimetric signals was also investigated for two different intensities of light. Those light powers were determined calorimetrically using the method described in section 5.2.2.2. Figure 5.5. shows the calorimetric signals measured in those two experiments.
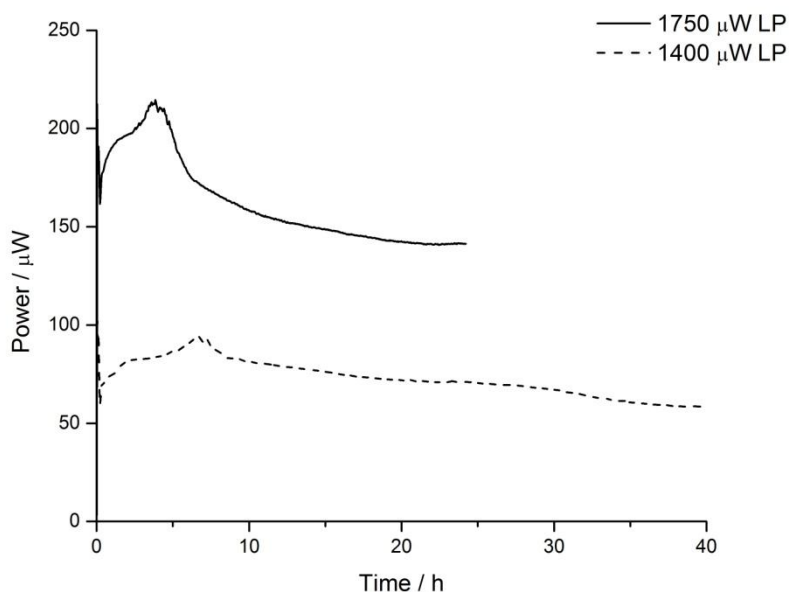
FIGURE 5.5. : Effect of different intensities of light on the photocalorimetric signals recorded in the nifedipine experiments with the photo-MCDSC.

The figure above shows that the magnitude of the photocalorimetric signal and final baseline value decreased significantly when the intensity of light was reduced. Those baseline changes may have resulted from a reduction in the number of photons absorbed by the sample which had an impact on the energy content of the sample side. In

addition, a significant reduction in the size of the peak was observed when the intensity of light was reduced. This effect can be explained by a decrease in the surface area irradiated by light which resulted from the narrowing of the light cone produced by the LED. As a consequence, a decrease in the amount of sample degraded per unit time was observed and so did the heat released in that process.

The influence of samples' molecular organization on the photodegradation of nifedipine was also investigated with the photo-MCDSC. In order to do that, crystalline samples and freshly prepared samples of amorphous nifedipine were tested and the photocalorimetric signals compared. Adding to those tests, samples of amorphous nifedipine were analysed after 3, 6 and 9 days storage in a desiccator at 0% relative humidity to investigate the occurrence of changes over time and their impact on the photoinstability of samples. Figure 5.6. shows the photocalorimetric signals recorded for the crystalline sample, freshly prepared amorphous sample (day 0) and amorphous samples taken after 3, 6 and 9 days storage.
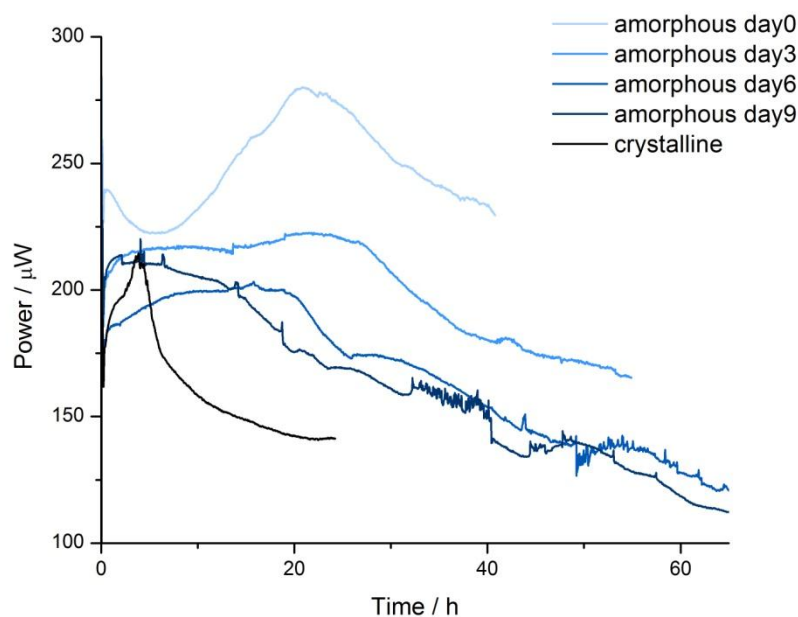
FIGURE 5.6. : Signals recorded in the photo-MCDSC experiments with crystalline and amorphous nifedipine. Amorphous samples were analysed on the day they were prepared (day 0) and 3, 6 and 9 days after that.

Figure 5.6. shows a clear difference between the signals recorded for crystalline and amorphous nifedipine which demonstrates the influence of sample molecular organization on the stability of nifedipine to light. The freshly prepared sample of amorphous nifedipine (day 0) showed a much larger and broader peak compared with the crystalline initial peak, which means that, either a more energetic process occurred during irradiation or the degree of degradation was higher for the amorphous sample. Furthermore, there seems to be a delay in the onset of the peak and in the start of the decay phase, which may indicate some sort of photoprotection effect. Based purely on these speculations, it can be assumed that, despite the degree of photodegradation being higher for amorphous samples, this molecular organization shows a photoprotective effect demonstrated by the delayed onset of photodegradation.

Regarding the effect of storage time on the photostability of amorphous samples, the photocalorimetric signals show a clear reduction in the peak size and in the onset of decay for samples taken at longer storage times, compared with the freshly prepared amorphous samples. This effect is very interesting because it shows a tendency for amorphous samples to behave like crystalline materials with increasing storage time. Therefore, it can be assumed that the samples crystallized with time in the desiccator at 0% relative humidity and ambient temperature.

To prove that crystallization occurred with time, the different samples of amorphous nifedipine (except the one taken after 9 days) were analysed in the DSC on the same day that they were taken out of the desiccators. Samples of crystalline nifedipine were also analysed and the DSC thermograms compared. The most important physical transitions investigated were the glass transition temperature (T_g) (Figure 5.7.) and crystallisation exotherms (Figure 5.8.) of the amorphous samples as well as the melting endotherms (Figure 5.9.) for all samples.
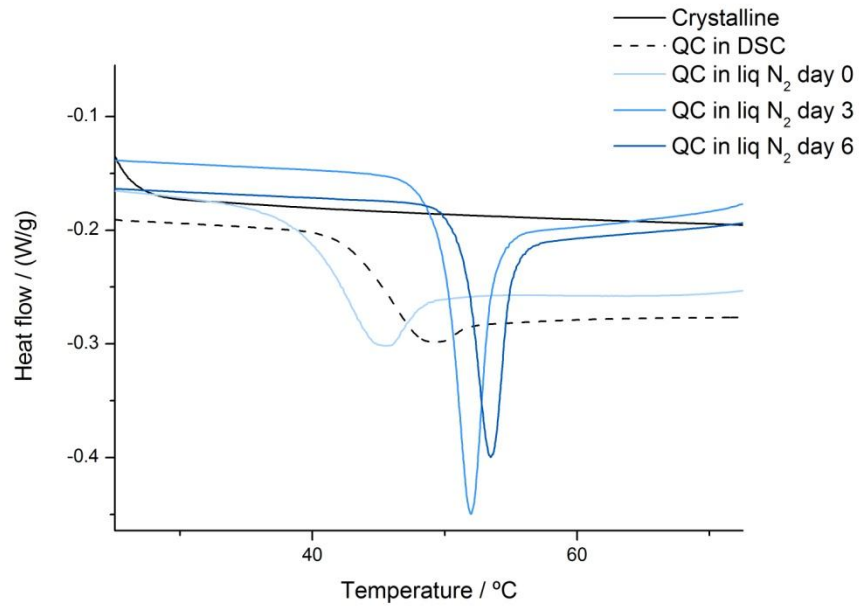
FIGURE 5.7. : DSC thermogram showing the range of temperatures that include the glass transition of amorphous nifedipine. QC- quench-cooled.
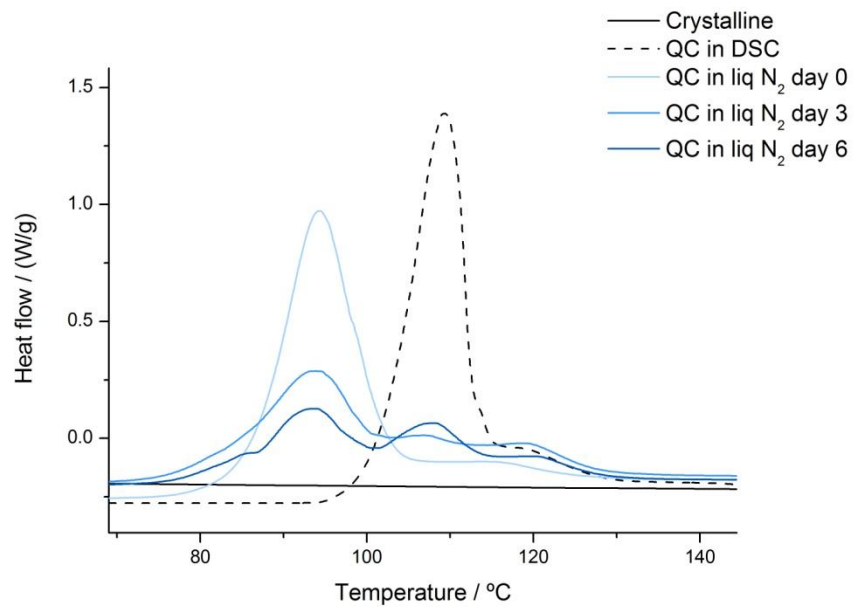
FIGURE 5.8. : DSC thermogram showing the range of temperatures that include the crystallisation exotherms for nifedipine. QC- quench-cooled.

243
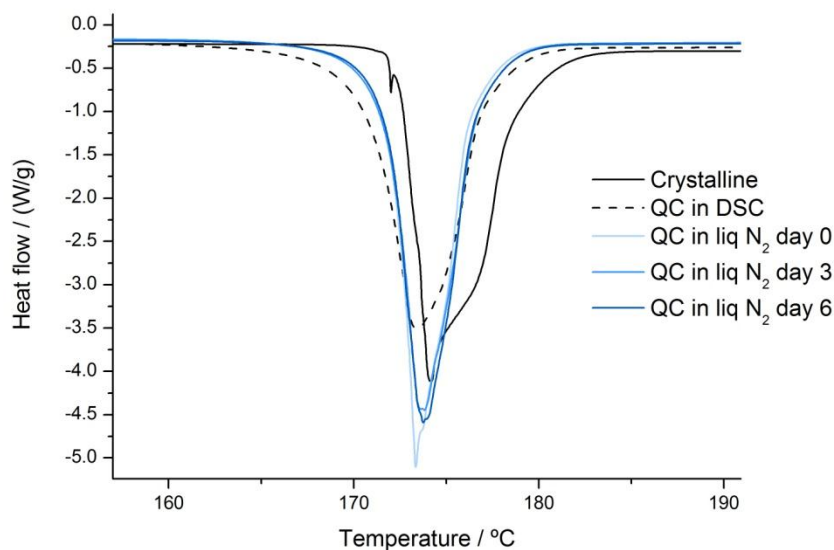
FIGURE 5.9. : DSC thermogram showing the range of temperatures that include nifedipine melting endotherms. QC- quench-cooled.

As expected, the DSC thermograms for crystalline nifedipine showed no glass transition or crystallisation exotherms. The only peak that was measured corresponds to the melting endotherm of nifedipine which seems to be a combination of two thermal events. This means that probably more than one polymorph existed in the original sample. On the other hand, the fresh amorphous samples prepared by quench-cooling in the DSC pan (QC in DSC) and in liquid nitrogen (QC in liq N_2 day 0) show similar thermograms with a glass transition step change, two crystallisation exotherms and a melting endotherm. Despite these similarities, all transition temperatures measured for the samples prepared in liquid nitrogen show a slight shift to the left compared to samples prepared in the DSC. This behaviour was previously reported by Grooff (122) and is attributed to different sample shape and intermolecular attractions as a result of distinct sample preparation methods.

Focussing only on the amorphous sample prepared in liquid nitrogen and tested on day 0, it is possible to see a glass transition combined with a relaxation phenomenon, around 40 ºC (Figure 5.7.). In addition to this transition, two crystallisation exotherms are observed around 80 º C and 100 ºC corresponding to the conversion into forms B (metastable form) and A (stable form), respectively (Figure 5.8.). The last transition, around 170 ºC, corresponds to the combination of form A and B melting endotherms (Figure 5.9.).

When those amorphous samples were analysed after 3 and 6 days storage in a desiccator, the thermograms showed significant differences in the early transition temperatures and in the crystallisation exotherms. Figure 5.7. shows that both samples went through an additional endothermic transition around 50 ºC that corresponds to the conversion of form C into form B, previously reported by Zhou (121). Because this conversion occurred around the glass transition temperature, an overlap of the two processes was observed. These results show that storage in the desiccator at ambient temperature, resulted in crystallisation of the amorphous sample into form C. Despite these changes in the initial amorphous sample, no significant increase in the amount of form C was observed from day 3 to day 6 as demonstrated by the similar peak areas.

With respect to the crystallization peaks shown in Figure 5.8., a clear decrease in the area of the first peak was observed for longer storage times, which reflects a decrease in the amount of amorphous sample converted to the metastable form B. This probably means that the amorphous content decreased with storage time. On the other hand, increasing storage times seem to favour other polymorphic conversions that were not observed with the initial samples. The appearance of an additional peak around 100 ºC demonstrates the occurrence of new polymorphic conversions. These results allow the assumption that, over time, new polymorphs were crystallised from the initial sample. Altogether, these variations in the number of transitions and peak areas show that there is a clear decrease in the amorphous content of the samples with time and the formation of new crystalline structures.

These findings confirm the assumptions made with the photocalorimetric data that the amorphous samples in the desiccators crystallised with time. Such changes in the molecular organization of samples clearly influence the photodegradation of nifedipine with amorphous samples showing a delayed onset of photodegradation and a greater degree of conversion.

5.3.1.2. Photo-TAM experiments

The photodegradation of solid nifedipine was also investigated in the photo-TAM, using an array of 5 similar 410 nm LEDs to irradiate the samples. A change in the colour and texture of the samples was also observed, in these photo-TAM experiments, as shown in Figure 5.10.
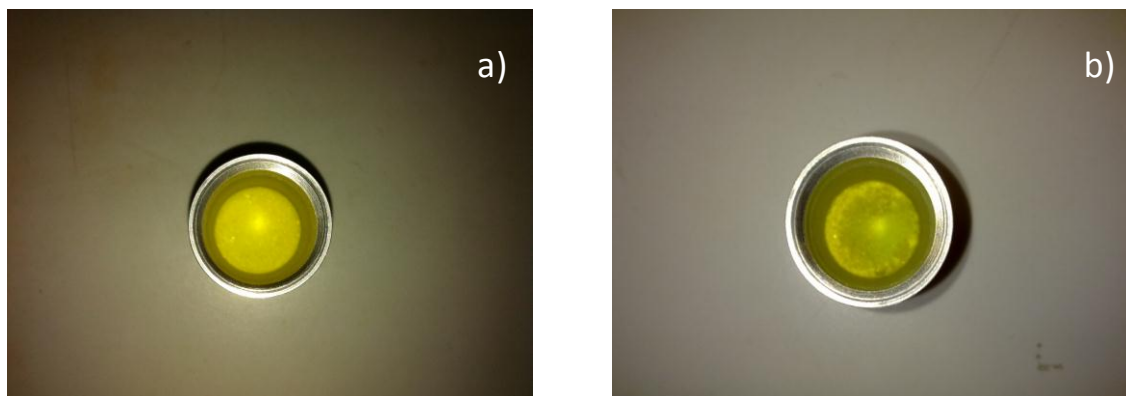
Figure 5.10. : Picture of a sample of nifedipine a) before irradiation b) after irradiation.

Three samples of 500 mg nifedipine were tested in that photocalorimeter and the resulting signals were plotted in the same graph (Figure 5.11.).
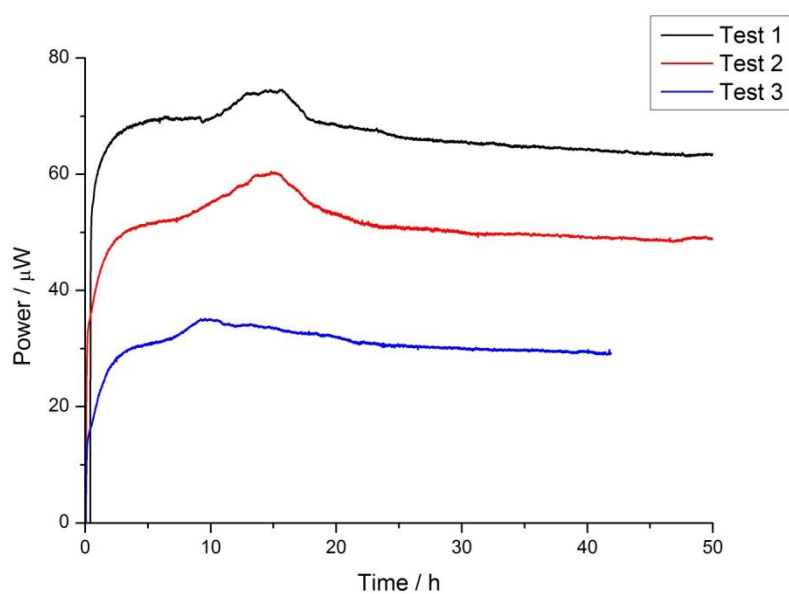
FIGURE 5.11. : Photocalorimetric signals recorded for the photodegradation of 500 mg samples of nifedipine in the photo-TAM.

Similarly to the data recorded with the photo-MCDSC, all signals measured in the photo-TAM showed an initial increase in the thermal power, followed by a peak and a decay phase that lasted more than 30 hours. Two different processes can be discriminated from that overall signal; one of them is characterised by an initial increase in the thermal power followed by a long decay until the end of data collection, while the other one shows a well defined peak that occurred between 10 and 20 hours of irradiation. The three signals plotted in Figure 5.11. show a great variability (34 μW difference between signal 1 and 3) which is mainly attributed to the fact that signal 3 is significantly different from the other two. The shape of curve number 3 suggests that that sample was slightly different or was arranged in a different way inside the ampoule.

Several differences were found when these signals were compared with those recorded with the photo-MCDSC using 200 mg of nifedipine (Figure 5.2.). The final baselines measured in the photo-TAM experiments (≈50 μW) were much smaller than those recorded with the photo-MCDSC (≈140 μW) which means that the light power absorbed by the samples of nifedipine was also smaller. Furthermore, the initial peaks measured in the photo-TAM were smaller in size (≈10 μW) and lasted much longer (≈10 hours) compared to those measured in the photo-MCDSC experiments (≈25 μW and 4 hours, respectively). Assuming that the kinetics of that process depends on the intensity of light, it is clear that the light power irradiating the photo-MCDSC samples is larger than that used in the photo-TAM. Nevertheless, all conclusions and assumptions must be made with care because the two systems are significantly different and use different amounts of sample with different surface areas.

The effect of sample mass on the photodegradation signals was also assessed in these photo-TAM studies. Three samples of 100 mg nifedipine were analysed with this system and the signals were compared with those recorded using 500 mg (Figure 5.12.).
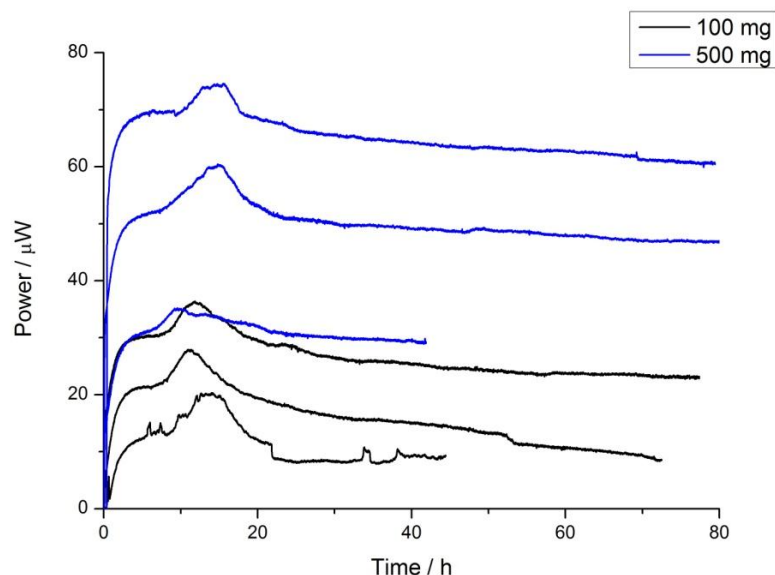
FIGURE 5.12. : Comparison of the signals measured in the photo-TAM for 100 mg and 500 mg samples of nifedipine.

Figure 5.12. shows that the magnitude of the signals and the final baseline values are much smaller for the 100 mg samples. This decrease in the baseline signal can be explained by a reduction in the light power absorbed by the samples as a result of the distance between the LEDs and the samples becoming bigger. Such decrease in absorption reduces the energy imbalance between the sample and reference sides. Alternatively, these results can be explained by a surface to volume effect. In a solid, all the light energy is absorbed by the top 2-3 mm but any heat will be distributed through the full volume and may be absorbed/insulated. Therefore, the greater the sample mass, the greater is the chance that energy will be stored in the bulk of the sample. Hence, the different baseline values measured for the two sample masses. Adding to these baseline changes, the size of the peaks is also slightly smaller for the 100 mg samples which reflects the decrease in light power reaching the samples (inverse square law).

The influence of distance between the LEDs and the samples on the photodegradation of nifedipine was also investigated with the photo-TAM. In order to do that, two stainless steel cylinders were inserted in the reference and sample ampoules, respectively, to raise the samples inside them. Three 500 mg samples were used in these tests. Figure 5.13. compares the signals obtained for the photodegradation of 500 mg nifedipine with and without those platforms.
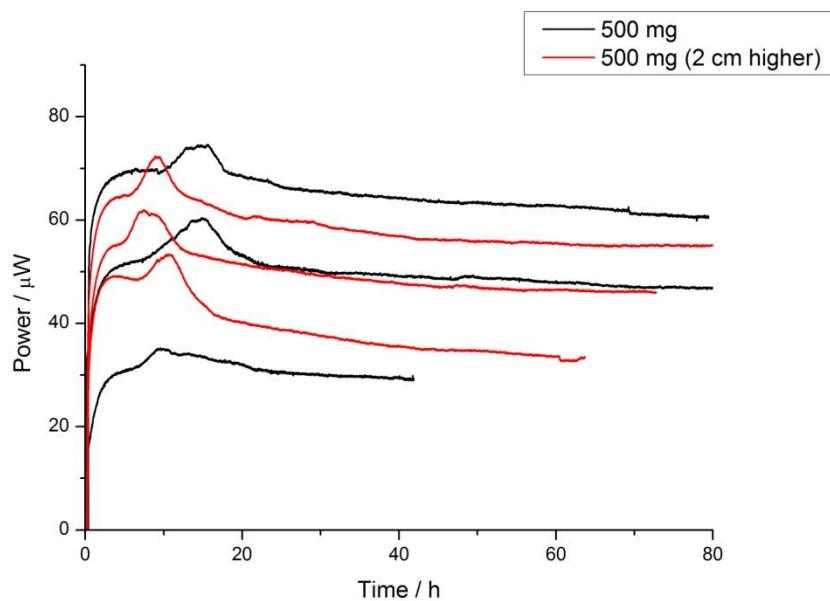
FIGURE 5.13. : Comparison of the photo-TAM signals recorded for the photodegradation of 500 mg nifedipine with and without the 2 cm platforms.

The only significant difference between the two types of signal is the appearance of the peak approximately 5 hours earlier when the samples were placed closer to the LEDs. This effect is probably due to an increase in the rate of photodegradation as a result of the intensity of light reaching the samples increasing for shorter distances to the LEDs.

Contrary to the effect observed in the sample mass studies, the magnitude of the signals and the final baselines did not change significantly for the samples positioned nearer to the light source. This unexpected result can be explained by the fact that the diameter of the stainless steel cylinders is slightly smaller than the ampoule base, resulting in a decreased surface area irradiated with light. Therefore, the increased light power reaching the sample is balanced by a decrease in the amount of sample absorbing light which is reflected in the similar baseline values.

Finally, the intensity of light emitted by the LEDs was varied in the power supply and its effect on the photodegradation of nifedipine was investigated. Figure 5.14. compares the signals obtained for the photodegradation of 500 mg using two different light powers, 1648 µW and 3275 µW.
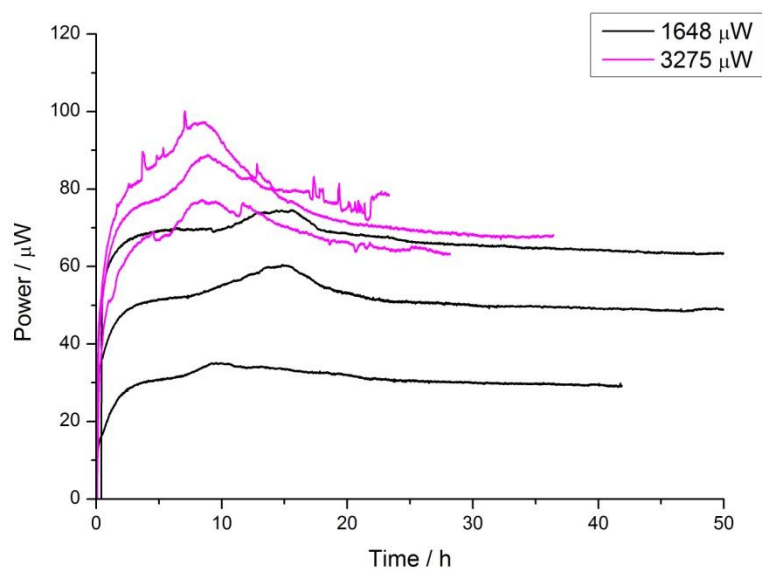
FIGURE 5.14. : Comparison of the photo-TAM signals recorded for the photodegradation of 500 mg nifedipine using two different intensities of light, 1648 μW and 3275 μW.

The graph above shows that an increase in the intensity of light resulted in the final baselines shifting to higher power values. The larger amount of energy absorbed by the samples explains these changes in the baseline. Furthermore, the initial peaks appeared much earlier in the experiment which shows that an increase in the rate of photodegradation occurred for higher intensities of light. The size of those peaks was also bigger which indicates that a greater amount of sample degraded during irradiation. An increased penetration of light in the sample is responsible for this higher degree of degradation.

5.3.2. Other compounds

A range of different photo-labile and -stable pharmaceutical compounds was also tested in the photo-MCDSC to investigate the capacity of that instrument to detect photodegradation signals for other pharmaceutical compounds. These tests were not performed in the photo-TAM because the instrument took a long time to develop and not much time was left for testing.

5.3.2.1. 2-nitrobenzaldehyde

2-nitrobenzaldehyde (2-NB) is a photolabile compound that has been used as a chemical actinometer in photostability testing of drugs (76, 103). Despite not showing any relevant therapeutic effect, this compound is very important in the synthesis of nifedipine which is a highly photolabile drug (U.S. Pat. No. 3,485,847). The photodegradation of 2-NB has been found to proceed via an intramolecular rearrangement involving transfer of an oxygen atom from a nitro group to the aldehyde functionality yielding the nitrosobenzoic acid product. A quantum yield of approximately 0.5 was determined for the photoreaction of 2-NB in solution phase and solid state (123, 124). This parameter was found to remain constant in the region of 313 nm to 436 nm (123). Most studies with 2-NB were performed in solution and it was found that this reaction follows zero-order kinetics in such conditions (76, 103). Furthermore, the effect of different experimental factors, such as the type of light source, light energy, exposure time, light path distance and concentration, on the photodegradation of 2-NB was investigated in solution (125). Different light sources and light path distances showed significant impact on the reaction rate constants and half-lives of 2-NB. The photodegradation of solid 2-NB was also investigated, in particular, the effect of wavelength and exposure time on the extent of photodegradation. However, the results were similar to those obtained in the solution phase (123, 124).

In these photocalorimetric studies, samples of 2-NB were analysed in the photo-MCDSC and the effect of sample mass and intensity of light, on the photodegradation signals, was investigated. First, 3 samples of 200 mg 2-NB were analysed in that instrument to assess the repeatability of the photocalorimetric signals (Figure 5.16.). A change in the colour of the samples was observed after irradiation, with the initial light yellow powder turning to light brown in the middle (Figure 5.15.).

FIGURE 5.15. : Sample of 2-NB after photodegradation in the photo-MCDSC

Figure 5.16. shows the three signals recorded during photodegradation of 200 mg of 2-NB in the photo-MCDSC. The light power irradiating the samples was maintained at 2250 μW for the three experiments.
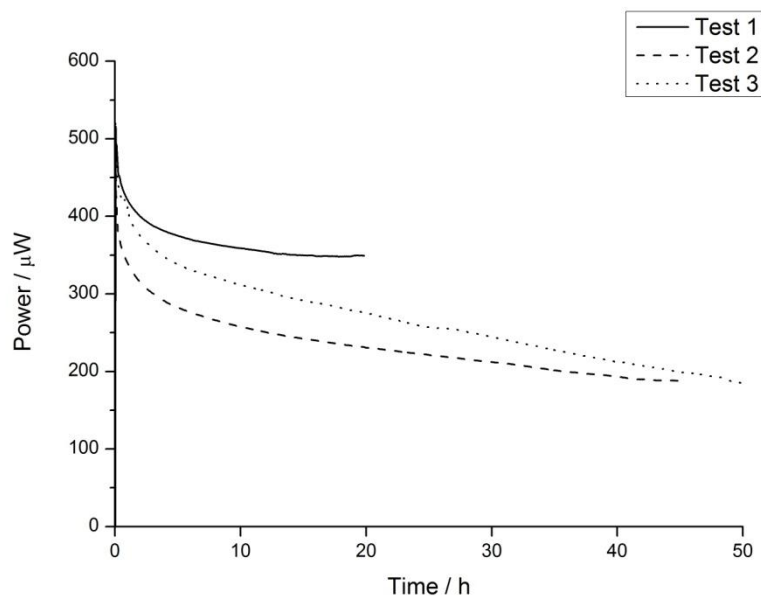
FIGURE 5.16. : Photocalorimetric signals recorded during photodegradation of 200 mg of 2-NBA in the photo-MCDSC.

All experiments showed an initial quick decrease in the signal, followed by a slower decay phase that lasted until the end of the experiment. Data collection was stopped earlier for "Test 1" because the signal seemed to have stabilized to a constant value after 20 hours. The other two signals did not stabilize within a reasonable time frame

therefore data collection was stopped before a final baseline was reached. However, a non-zero baseline would probably be measured because the powder is slightly coloured. That means that the sample absorbs more visible radiation than the talc in the reference ampoule which explains the imbalance in energy between the sample and reference materials.

The effect of sample mass on the photodegradation signals was also investigated using three different samples of 200 mg, 10 and 5 mg 2-NB (Figure 5.17.).
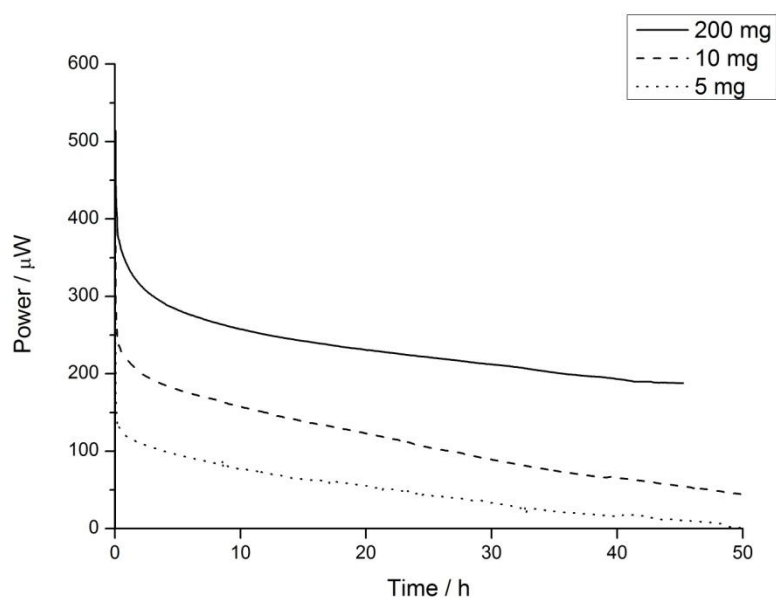
FIGURE 5.17. : Photocalorimetric signals recorded during photodegradation of 200, 10 and 5 mg of 2-NB in the photo-MCDSC.

A clear decrease in the magnitude of the signals was observed for smaller sample masses. That effect can be explained by a shift in the final baseline which resulted from a decrease in the amount of light power absorbed by the smaller samples of 2-NB. Furthermore, a slight increase in the amplitude of the initial decay signal was observed for larger samples which can be explained by an increase in the rate of photodegradation in those conditions. In fact, the shorter distances between the samples with large mass and the LED lead to an increase in the intensity of light irradiating the sample, hence, an increase in the rate of photo-conversion.

Different intensities of light were also tested, in the photo-MCDSC, to investigate the influence of light power on the photodegradation signals. Three samples of 200 mg

were analysed under 3 different intensities of light (2250, 1750 and 1300 µW) and the photocalorimetric signals were compared (Figure 5.18.).
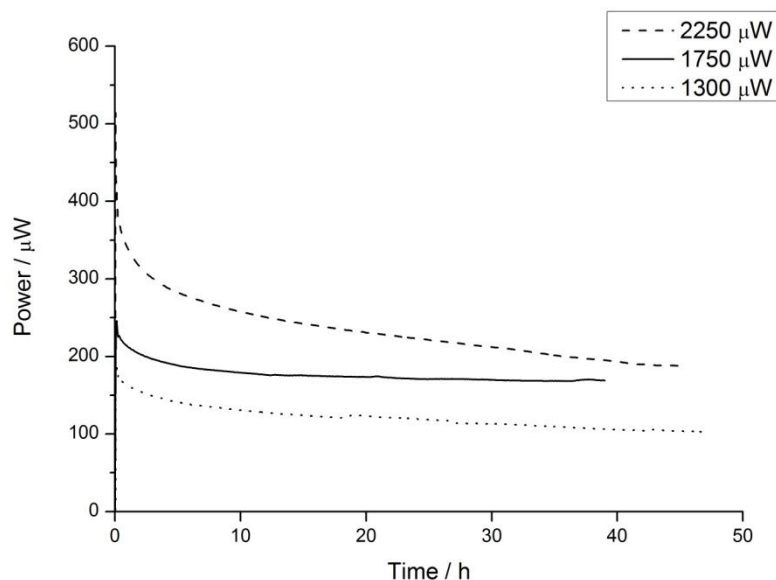
FIGURE 5.18. : Photocalorimetric signals recorded during photodegradation of 200mg of 2-NB using 3 different intensities of light.

The figure above shows a clear increase in the magnitude of the signals for higher intensities of light. This effect can be explained by, either an increase in the amount of 2-NB reacting per unit time or a shift in the final baseline, resulting from a larger amount of radiation being absorbed by the sample. Furthermore, the experiment that used the highest intensity of light (2250 µW) shows a significant increase in the magnitude of the initial decay as well as a slight increase in the slope of the longer decay phase. These changes can be explained by an increase in the rate of photodegradation, resulting from a greater number of photons interacting with molecules of 2-NB.

5.3.2.2. *Carbamazepine*

Carbamazepine is an anticonvulsant drug used to treat epilepsy and trigeminal neuralgia. The photostability of carbamazepine polymorphs in tablets was investigated using Fourier transform infrared reflection absorption spectrometry and colorimetric

assessment of all three polymorphs (I, II and III), after irradiation under near-UV fluorescent lamp. The surface of the tablets discoloured to yellow and then orange with results indicating polymorph II to be the least stable. The photodegradation followed first-order kinetics with the degradation rate constant for form II proving to be 1.5 times larger than that for forms I and III (126).

The photostability of carbamazepine (form I) was assessed in the photo-MCDSC using two 410 nm LEDs to irradiate the sample and reference sides. It was assumed that form I was the predominant polymorph because the melting point specified in the bottle, 191-192 ℃ matched that reported in the literature (189-193 ℃) (127). Three samples of carbamazepine were used in the photocalorimeter and the resulting photocalorimetric signals were compared (Figure 5.19.). The white powder initially weighed into the ampoules did not show any changes in colour or texture after irradiation.
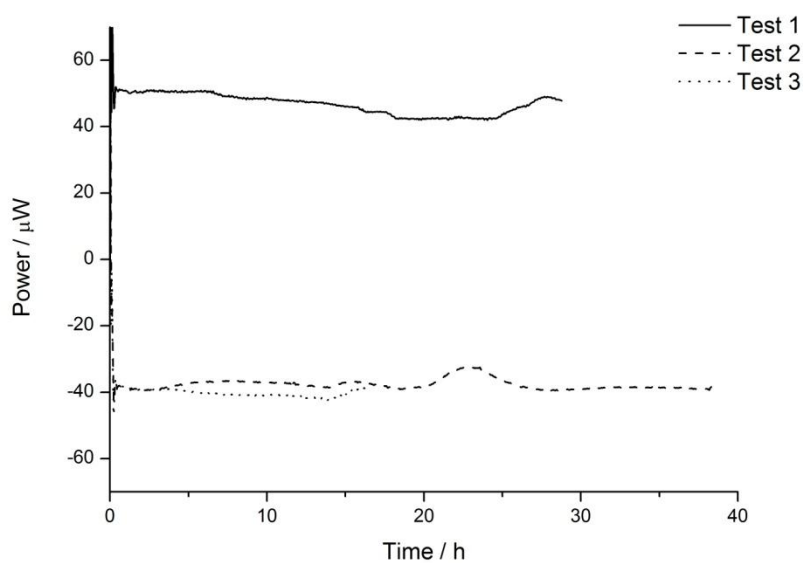
FIGURE 5.19. : Signals recorded in the photo-MCDSC experiments using 200 mg of carbamazepine.

The figure above shows that a constant thermal power was measured for all three experiments, which means that either the sample was stable across time or the photoreaction followed zero-order kinetics. Because those values are near zero, it is likely that the samples did not degrade during exposure to light. However, there is a chance that degradation was so slow that the instrument did not detect these changes in

rate. Another scenario is that the enthalpy of the process is so small that changes in the reaction power were not discriminated from the overall light power.

Two reasons can explain these small constant signals; firstly, form I is one of the least photosensitive polymorphs of carbamazepine, which may explain the slow rate of the process (126). To investigate this dependence on the polymorphism of carbamazepine it would be interesting to test, in the future, different crystal structures of the drug. Furthermore, the fact that the samples are white, means that visible radiation is not greatly absorbed by the drug, therefore, reducing photodegradation in that region of the spectrum. Although these experiments did not clearly demonstrate the predictive power of photocalorimetry, the results obtained can be explained with the literature data on the photosensitivity of carbamazepine crystal structures.

5.3.2.3. *Chloramphenicol*

Chloramphenicol is an antibiotic effective against a wide range of life-threatening bacteria. It is administered systemically, e.g. in the treatment of central nervous system infections, but also topically, e.g. against deep ocular infections, where it is a first choice drug (128). This drug is well known for its instability when exposed to UV radiation, solar light and γ-radiation (129, 130). In aqueous solution chloramphenicol undergoes decomposition into an aromatic and an aliphatic radical through photo-β-cleavage. The aromatic radical stabilizes itself to *p*-nitrobenzaldehyde while the aliphatic moiety gives glycol aldehyde and dichloroacetamide. Other photosensitized and non-photosensitized reactions may follow this conversion, depending on the environmental conditions. In the solid state, chloramphenicol is more stable to light compared with aqueous preparations. Also here, photoinduced β-cleavage takes place to a limited extent (130).

Three samples of 200 mg chloramphenicol were tested in the photo-MCDSC and the resulting signals were plotted in the same graph (Figure 5.20.). No significant changes in the light yellow powder were observed after irradiation.
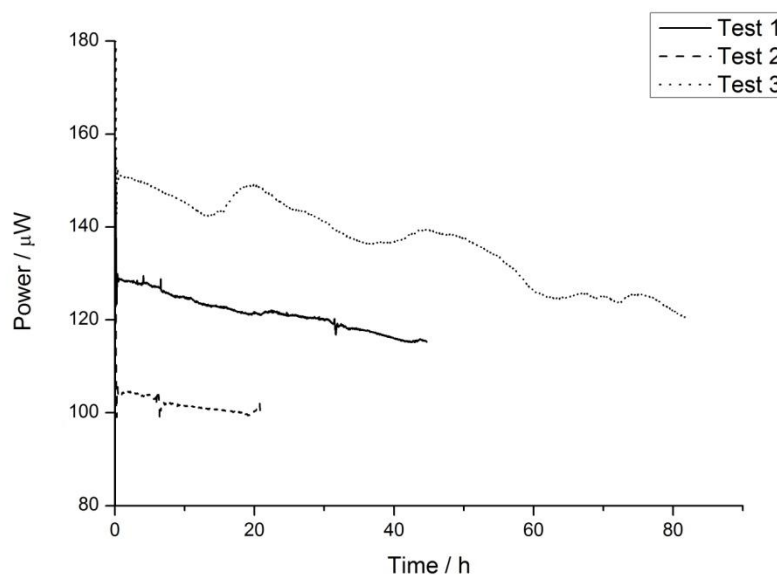
FIGURE 5.20. : Signals recorded in the photo-MCDSC experiments with 200 mg of chloramphenicol.

All three data sets showed a slow decay in the signal, indicating a decrease in the rate of photodegradation with time. Despite the similar decay, the magnitude of the signals was significantly different, for similar sample masses. Those results can be explained by differences in the intensity of light irradiating the 3 samples, as demonstrated by the light power measured in the photo-MCDSC: 1950 µW, 1900 µW and 2570 µW for Tests 1, 2 and 3, respectively. The larger signals can, therefore, be explained by an increase in the absorption of visible radiation by the light yellow sample and larger photoreaction heat outputs for samples exposed to higher intensities of light.

These experiments showed that the photo-MCDSC was capable of detecting chloramphenicol photodegradation signals which allowed following the reaction with time. Such results agree with the literature data on the photosensitivity of chloramphenicol.

5.3.2.4. Furosemide

Furosemide is widely used as a diuretic or antihypertensive drug. It exists in the solid-state as at least three polymorphs, two solvates, an amorphous form and a high-temperature form (131). According to the Pharmacopeia of Japan (JP XI, 1986),

257

furosemide undergoes gradual coloration upon exposure to light and is recommended protection from light. The photostability of furosemide's crystal forms was previously investigated by exposing tablet surfaces to UV-light from a 400 W mercury-vapour lamp (131). Changes of colour of the tablets' surface and of a powder sample of form II (difficult to compress into a tablet), were monitored with time by colorimetry. Striking differences in the degree of colouration were observed among polymorphs I, II and III. Although forms II and III showed a significant increase in colouration, even after short-term irradiation, form I showed only a "noticeable" change in colour regardless of the condition of the sample after prolonged irradiation. Therefore, form I was demonstrated to be reasonably stable against light. Despite these results, it remained unclear as to whether the changes in colour correlated with the extent of chemical stability of furosemide.

De Villiers also studied the photodegradation of furosemide polymorphs using an HPLC assay to determine the kinetics of the process (132). Powder samples of forms I and II were exposed to prolonged UV irradiation and direct sunlight, in a normal and nitrogen atmosphere. The solid state photolytic degradation of furosemide followed apparent first-order kinetics as described by a model consisting of nucleation and growth periods with eventual deceleration as it reached a maximum fraction degraded. Form I was photochemically more stable than form II, especially under nitrogen atmosphere, and the major photodegradation product, detected in both samples, was 4-chloro-5-sulphamoylanthranilic acid.

In these photocalorimetric studies, 3 samples of 200 mg of furosemide were tested in the photo-MCDSC and the signals analysed afterwards. No significant changes in the colour of the samples (white powder) were observed which may indicate the presence of the most stable form I. Figure 5.21. shows the signals measured for the three furosemide samples.
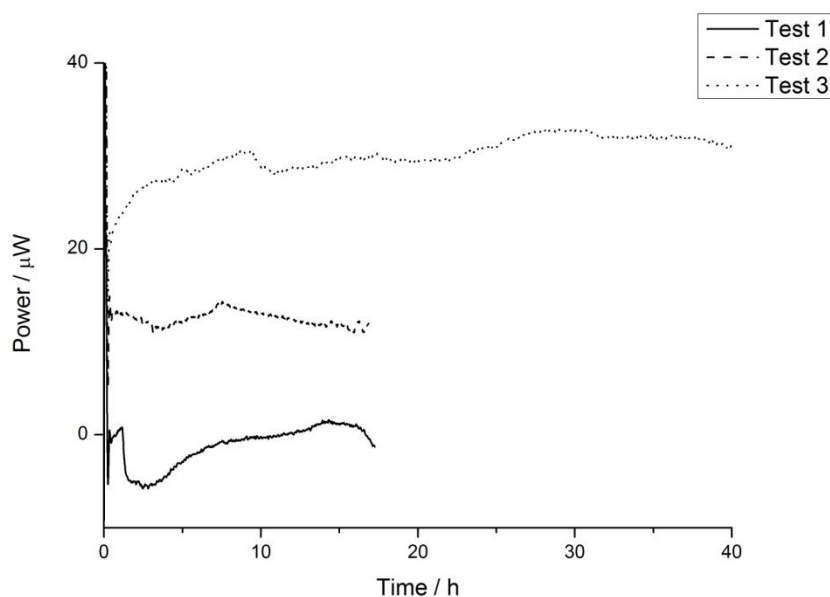
FIGURE 5.21. : Signals recorded in the photo-MCDSC experiments with 200 mg of furosemide.

All curves showed a stable thermal power in the region of 0 to 30 µW which is not significant considering that it is very difficult to bring the signal exactly to zero when the blank experiment is performed, and that signal repeatability with the lights on is around 15 µW. Therefore, it was assumed that no significant photodegradation occurred in the samples of furosemide when exposed to 410 nm radiation. Two explanations were found for this apparent photostability of furosemide; either the rate of reaction was too slow and the system did not detect any changes in the heat of reaction, or the enthalpy of the process was too small. These results also suggest that form I of furosemide was present in the initial sample because that is the most photostable form.

5.3.2.5. Dipyridamole

Dipyridamole is a well known coronary vasodilator and antiplatelet agent widely used in medicine. Its crystalline form shows a bright yellow colour while the solution phase preparations have a yellowish-blue fluorescence. In solution, dipyridamole undergoes oxidation of one of the piperidine side chains upon irradiation with UV light (133). However, under inert atmosphere (argon), this drug was shown to be photostable. The photodegradation of dipyridamole, in solution, occurs probably via a type II mechanism involving irreversible trapping of self-photogenerated reactive oxygen species which

259

can be indicative of its antioxidant activity (134). Although a few studies were performed in the solution phase, no relevant photodegradation data were found for its crystal form. Nevertheless, the photostability of solid dipyridamole was assessed in these photo-MCDSC studies.

Three samples of 200 mg dipyridamole were tested in the photo-MCDSC and the resulting photocalorimetric signals plotted in Figure 5.22. Those samples showed no change in their yellow colour after irradiation with the 410 nm radiation.
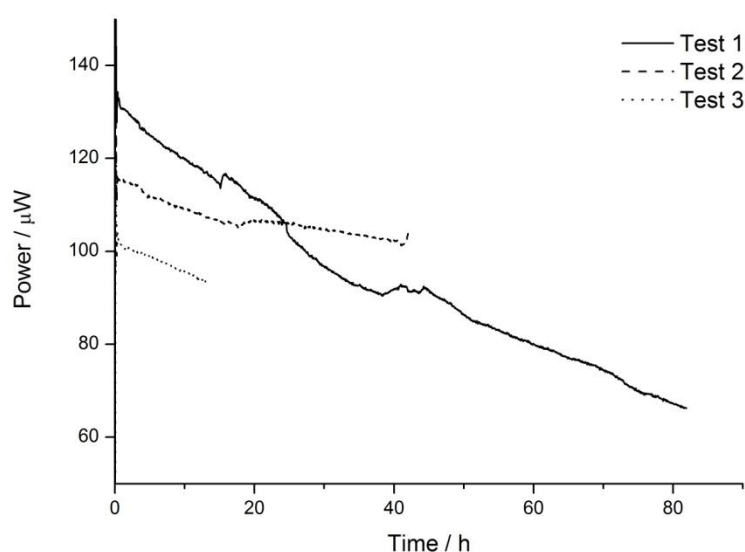
FIGURE 5.22. : Signals recorded in the photo-MCDSC experiments with 200 mg of dipyridamole.

Initially, the magnitude of the signals ranged between 100 and 130 µW, demonstrating that the signals were fairly repeatable. With time, those signals decreased linearly, which means that the rate of heat production/photodegradation decreased with continuous exposure to light. To conclude, the results obtained in these experiments show that dipyridamole degrades under 410 nm radiation and that the rate of photodegradation decreases linearly with time.

5.3.2.6. Paracetamol

Paracetamol is an antipyretic and analgesic drug that acts by selectively inhibiting the cyclooxygenase-2 pathway. Although the European Pharmacopoeia recommends light protection for paracetamol (119), it was demonstrated that photodegradation in solution (135, 136) and solid (137) is, in most cases, negligible. In solution, photodegradation only occurred in the presence of dissolved oxygen and catalyst (TiO_2) (135, 136). Several reaction intermediates such as hydroquinone and benzoquinone were detected in solution, degrading to CO_2 afterwards. Similarly to the solution phase studies, solid paracetamol showed negligible photodegradation under UV light (138). The photostability of paracetamol in tablets containing tramadol was also investigated and it was found that only 0.65% of the drug degraded after 12 hours of irradiation (137).

Samples of solid paracetamol were also analysed in the photo-MCDSC to assess their photostability. Three samples of 200 mg paracetamol were tested and the results are shown in Figure 5.23. No changes in the colour of the white powder were observed after irradiation.
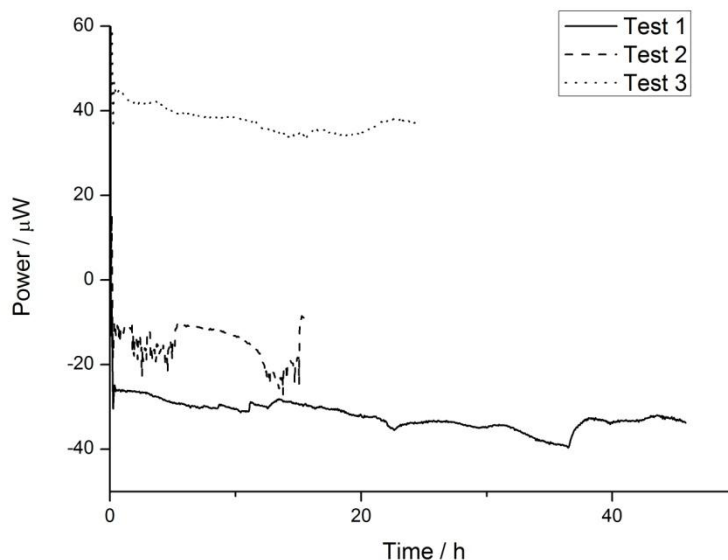
FIGURE 5.23. : Signals recorded during irradiation of 200 mg paracetamol in the photo-MCDSC.

Figure 5.23. shows that the thermal power measured for all three experiments remained constant during irradiation. Furthermore, the magnitude of the signals was very small (except for Test 3 because of variability issues) which shows that no significant

degradation was detected by the instrument. These results are in agreement with the negligible photodegradation of solid paracetamol previously observed (137, 138). Despite the power values being close to zero, the variability of the signals was not very good because there were some difficulties in the zeroing process. Nevertheless, it was shown that no significant photodegradation occurred during irradiation with the 410 nm wavelength.

5.3.2.7. *Acetylsalicylic acid*

Acetylsalicylic acid (or aspirin) is an analgesic, antipyretic and anti-inflammatory drug that can also be used in the prevention of heart attacks when administered in low doses. Contrary to all previous drugs, acetylsalicylic acid does not degrade with light, hence the absence of light protection recommendations in the European Pharmacopoeia 6. To test the photostability of aspirin, three samples of 200 mg were analysed in the photo-MCDSC. Figure 2.24. shows the signals recorded during irradiation of samples.
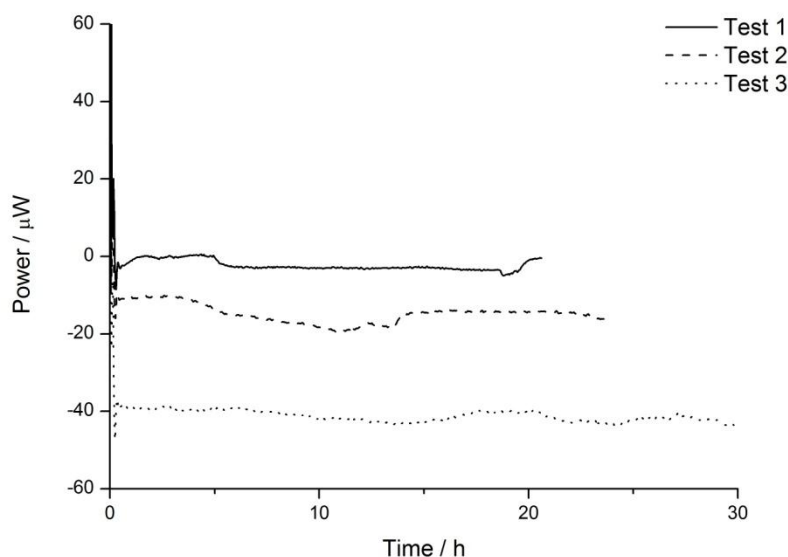
FIGURE 5.24. : Signals recorded during irradiation of 200 mg acetylsalicylic acid in the photo-MCDSC.

As expected, all photocalorimetric signals remained constant with time and near zero microwatts. These results show that acetylsalicylic acid is stable to 410 nm radiation,

262

therefore, confirming that light protection is not required for this drug. Regarding the repeatability of the signals, the relatively large differences in magnitude can be explained by the difficulty to zero accurately the signals and the variability inherent in switching the LEDs on and off repeatedly. One of the designs changes that can be made to improve the signal repeatability consists of developing of an automated electronic-balancing power supply similar to the one used in the photo-TAM. That would minimise errors inherent to manual adjustments by an operator.

5.4. Summary

The studies reported in this chapter demonstrated the potential of photocalorimetry to assess the photostability of solid pharmaceuticals. The model photolabile drug, nifedipine, was tested in the two photocalorimeters described in Chapter 2 and the effect of different experimental conditions on the photodegradation signals was investigated. Because the experiments were only repeated three times, at most, and the signals were quite variable, all comparisons and assumptions are tentative. Nevertheless, the calorimetric signals seemed to depend on the amount of sample used in the ampoules, their physical properties and the intensity of light they were exposed to. Although all studies were performed with the 410 nm LEDs, the two photocalorimetric systems can be used to study the effect of many other wavelengths, provided that the appropriate LEDs are available.

Furthermore, a range of different photo-labile and -stable drugs were tested in the photo-MCDSC to investigate the instrument's ability to detect and measure different degrees of photodegradation. From all the compounds, the only ones that showed clear photodegradation heat outputs were 2-nitrobenzaldehyde, chloramphenicol and dipyridamole. In these three cases, the signals showed, initially, a large deflection from zero (over 100 µW) and a decay phase that extended until data collection was stopped. Regarding the photolabile drugs that did not show a clear photodegradation signal (carbamazepine, furosemide and paracetamol), the thermal behaviour may be explained by one or more of the following reasons:

- the amount of light absorbed by the samples was not enough to cause photodegradation of the samples.
- the rate of reaction was too slow for changes in heat of reaction to be detected during the experimental time.
- the overall enthalpy of the systems was too small to be detected by the photo-MCDSC.
- the drugs had several polymorphs and the crystal form used in the tests was the most photostable.

On the other hand, acetylsalicylic acid behaved as expected, showing no significant heats of reaction upon irradiation.

An important issue that must be addressed here is the type of reference material used in the photocalorimetric experiments. Based on the results obtained with coloured samples, it seems that differences in the absorption of visible radiation by the reference and sample materials have an impact on the baseline signals. These differences are critical for the correct analysis of signals because it is difficult to separate photodegradation from light absorption phenomena, when the sample and reference have different spectra of absorption. Therefore, this aspect must be taken in consideration when choosing the reference material.

6. Summary and future work

Photocalorimetry is, undoubtedly, a very useful and versatile technique for the photostability assessment of pharmaceuticals. Not only does it offer significant potential for the routine screening of compounds (especially in solution), but also proves to be an invaluable tool for the quantitative analysis of photodegradation. The work presented in this thesis demonstrates this with the development and testing of two new photocalorimetric designs for the qualitative and quantitative assessment of photostability of drugs. Both instruments used light-emitting diodes as the light source adapted to two different calorimetric units: a Multi-Cell Differential Calorimeter (MCDSC), in one case, and an isothermal heat conduction microcalorimeter, TAM 2277, in the other. The two photocalorimeters were tested with photosensitive pharmaceutical compounds and the resulting data showed that the instruments were sensitive enough to discriminate small heats of photodegradation from the large light powers irradiating the calorimetric chambers. Such heat flow measurements were very important because they allowed collecting proof-of-concept data. Quantitative analysis of those data was also performed using the appropriate calorimetric equations and strategies to determine the kinetic and thermodynamic reaction parameters. This quantitative assessment of photodegradation was not addressed in the previous studies by Lehto, Morris and Dhuna that focused on the development and application of photocalorimetry to the qualitative analysis of processes. The present studies aimed for a more comprehensive analysis of photocalorimetric data, both qualitatively and quantitatively.

Some of these analytical considerations were addressed in Chapter 2 which described the development and application of new strategies for the analysis of isothermal calorimetric data. Those strategies were specific for the analysis of two types of processes that are particularly relevant in a context of photostability testing of pharmaceuticals and for which no adequate analytical strategies were available: solid state reactions and zero-order kinetic processes in solution. The main issue with solid state analysis is that the existing calorimetric equation that describes these processes does not fit data in the form of power versus time. Determination of the reaction parameters using the standard calorimetric equation is possible only if the total heat released during the process had to be calculated prior to analysis. This could be difficult in cases where only partial data was collected (e.g. very slow or fast processes). To overcome this problem, several mathematical methods were developed for the direct calculation of all solid state parameters by selection of just a few data points when only

partial data is available. In addition to these strategies, two graphical methods for the generation of power-time data for solid state processes were also developed. The validity of the calculation methods was, afterwards, demonstrated using simulated calorimetric data obtained with those methods. Application of those methodologies to the analysis of real calorimetric data was successfully demonstrated using isothermal calorimetric data for the crystallization of indomethacin from an amorphous glass. Although great progress was made in the analysis of solid state calorimetric data, it was not possible to develop a calorimetric equation that fits solid state isothermal data in the form of power versus time. That equation would be very important to complete the set of fundamental calorimetric equations and extend analysis to more complex solid state kinetic schemes.

Regarding the analysis of processes that follow zero-order kinetics in solution, the major issue was that, similarly to the solid state equation, the zero-order calorimetric equation (Equation 2.67.) does not fit data in the form of power versus time. To address this issue, three methods were developed for the analysis of zero-order processes without the need for ancillary methods. While the three methods have been successfully tested with real data (the method described in section 2.3.1. was later tested with the data obtained in the nifedipine photodegradation studies), their application to calorimetric data is not universal nor free from assumptions. For example, the method described in section 2.3.1. can only be applied to data for processes that progress to completion. On the other hand, the method presented in section 2.3.2. can only be used if the zero-order reaction generates protons that can be exchanged with the buffer components. Although the concept behind this method is valid for other types of reactions, the combination of the zero-order process with a secondary pathway is still a requirement. Furthermore, the secondary reaction needs to be quicker than the zero-order process so that the rate of reaction is governed by the latter. Regarding the method described in section 2.3.3., the fact that it is based on predictions and estimations, renders the approach potentially inaccurate. However, it constitutes a very good method to support other analytical approaches, such as empirical fitting techniques. In conclusion, despite the validity of the three methods, a universal method for the analysis of calorimetric data for zero-order reactions in solution is still missing.

The following chapter (Chapter 3) reported the development of two new photocalorimetric designs for the photostability assessment of pharmaceuticals and showed a detailed description of the different photocalorimetric components. Both

instruments used LEDs as the light source adapted to different calorimetric units: a MC-DSC (photo-MCDSC), in one case, and a TAM 2277 (photo-TAM), in the other. In the photo-TAM, two lighting columns, with 5 LEDs in the end, were placed inside the reference and sample channels of the calorimeter to irradiate the two re-designed photocalorimetric ampoules. These new ampoules had a quartz window in the lid to allow passage of light. Other photocalorimetric parts included an external circuit board with individual switches for the LEDs and an automated electronic-balancing power supply that automatically zeroes the calorimetric signal obtained after switching the LEDs on. On the other hand, the photo-MCDSC only has one LED irradiating each photocalorimetric ampoule which limits the range of wavelengths that can be tested simultaneously. This photocalorimeter has 4 calorimetric chambers which allows testing of 3 samples at the same time and under the same conditions (the fourth chamber contains the reference ampoule). Furthermore, the instrument has an external circuit board with individual switches and voltage regulators for each LED and a power supply that only allows manual adjustments to the LEDs' voltage. In theory, these voltage adjustments can also be made with the automated electronic balancing power supply developed for the photo-TAM. However, this application still needs to be tested.

Despite both instruments using LEDs as the light source, they are very different in many other aspects of their design. Not only were they built from different calorimetric units with different sensitivities (the TAM is a more sensitive instrument), but also, they differ in terms of the number of LEDs irradiating each ampoule, the maximum volume allowed inside the ampoules and the surface area exposed to light. Furthermore, the photo-TAM allows testing of drugs under customized wavelength spectra which is very useful for the examination of the wavelength dependence of photochemical processes (causative wavelengths). The major issue with these instruments is the limited number of different LEDs that are commercially available and that have the right size to fit the holders. To date, the minimum wavelength LEDs (5 mm diameter) that are manufactured by the company that supplied the LEDs (Roithner LaserTechnik, Vienna, Austria) are the 351 nm wavelength LEDs. Ideally wavelengths down to 320 nm, allowing the exploration of the entire solar spectrum at sea level, would be available.

The chapters that followed demonstrated the application of the two photocalorimeters to the photostability assessment of drugs. Chapter 4 presented some photocalorimetric studies using drugs in the solution phase while Chapter 5 described the experiments performed with solid pharmaceutical compounds.

The solution phase studies presented in Chapter 4 demonstrated the application of the two photocalorimeters to the photostability testing of nifedipine in ethanol. This reaction was studied in the photo-MCDSC using a 410 nm LED and in the photo-TAM using two different arrays of LEDs to irradiate the samples. The effect of sample volume, concentration and intensity of light on the photodegradation signals was also investigated and data were analysed using the calorimetric strategies described in Chapter 1 and 2. Typically, the photocalorimetric signals recorded in these experiments had an initial zero-order phase followed by a transition period of non-integral reaction order and a first-order decay to baseline. The zero- and first-order periods were analysed quantitatively using the strategies described in the literature and Chapter 2 and the reaction parameters, k_0, k_1, ΔH and $[A]_{tr}$ (concentration at the transition between kinetics) were determined. The quantum yields of photodegradation were also calculated using the kinetic data obtained in the analysis of the zero-order period. To validate the methods used in this quantitative analysis, an HPLC assay was performed in order to determine the rate of photodegradation of nifedipine.

These studies demonstrated, for the first time, that it is possible to quantitatively analyse photocalorimetric data and determine the kinetic and thermodynamic parameters for photodegradation processes directly without the need for an orthogonal analytical method. The main reason why Lehto (3), Morris (4) and Dhuna (5) were not able to do that was that the instruments developed then were only capable of measuring constant heat outputs which were impossible to analyse with the zero-order calorimetric strategies available at that time. In this case, however, the signals measured with the two instruments showed a zero-order period followed by a first-order phase that allowed quantitative analysis of data using the zero-order strategies described in Chapter 2. That was only possible because the rates of photodegradation were high enough to allow the processes to progress to completion in an acceptable period of time.

As future work, it is of interest to test the two photocalorimeters with other photosensitive drugs in solution to understand the possibilities and limitations of the technique when other less sensitive compounds are tested. It would also be interesting to test the effect of different wavelengths on the photodegradation of nifedipine to determine the causative wavelength of degradation. These studies were previously performed by Dhuna, although data was only analysed qualitatively (76). The number of samples per test should also be increased, at least to five, to better discriminate differences between the parameters calculated for the different experimental conditions.

For example, an increase in the number of samples could help understanding if the apparent similarity between all values obtained for the concentration of nifedipine during the transition period is not a result of sensitivity issues or variability. For the same reasons, the range of volumes and concentrations tested in the photocalorimeters should also be wider.

The following chapter (Chapter 5) demonstrated the application of photocalorimetry to the photostability assessment of solid pharmaceutical compounds. Similarly to the solution phase studies, the model photolabile drug, nifedipine, was tested in the two instruments and the effect of different experimental factors on the photodegradation of nifedipine was investigated. In this case, however, data were only analysed qualitatively because the complexity of the signals did not allow the solid state calorimetric strategies presented in Chapter 2 to be used.

In addition to nifedipine, a range of different photo-sensitive drugs was tested in the photo-MCDSC to investigate the instrument's ability to measure different degrees of photodegradation. The compounds 2-nitrobenzaldehyde, chloramphenicol and dipyridamole showed a clear photodegradation signal while carbamazepine, furosemide and paracetamol did not show significant changes in the baseline. The thermal behaviour of the 3 last drugs can be explained by either an insufficient absorption of light power, very slow rates of degradation, small enthalpies of reaction or the presence of stable polymorphs. However, it is likely that the light absorption issues were the main reason behind this behaviour because there is a clear difference in colour between the two groups of drugs. The fact that 2-nitrobenzaldehyde, chloramphenicol and dipyridamole are coloured means that they absorb in the visible range while the white drugs carbamazepine, furosemide and paracetamol only absorb in the UV region. That explains the small absorption of 410 nm wavelength radiation by these drugs. When the photo-stable drug, acetylsalicylic acid, was tested no significant heats of reaction were measured.

As previously mentioned, one of the major issues with these photocalorimetric experiments is the selection of an appropriate reference material for these tests. As demonstrated earlier, differences in the absorption of visible radiation by the reference and sample materials have an impact on the baseline signals. To prevent these effects from interfering with the analysis of data, there must be a standardization of the testing procedures including the type of reference used. As future work, it would be interesting to use the photo-TAM to test the same drugs that were analysed in the photo-MCDSC.

That would allow comparison between the two sets of data and investigate the possibilities and limitations of both instruments. The effects of humidity and other wavelengths on the photodegradation of solid drugs could also be studied. Finally, it must be stressed that the number of samples per experiment was too small and that it is recommended to test at least 5 samples per experiment.

In addition to all future work previously suggested it is of great importance to establish a reference photoreaction for the photostability assessment of pharmaceuticals using photocalorimetry. Nifedipine proved to be a very good candidate for the analysis of drugs in solution. However, its multiple pathways of degradation constitute a problem in establishing this photoreaction as a reference. The task of finding a solid state reference is even more complicated because this material should have specific characteristics in terms of the thickness of the powder bed, particle size and distribution, weight of the sample and colour. All these factors interfere with the photodegradation of solids, hence, the difficulty of establishing an adequate reference. The preparation of uniform polymeric films containing nifedipine was considered but there was no time to develop a good method of preparation for these films.

Many other experiments can now be done with the two photocalorimeters described in Chapter 3. Two examples of very interesting experiments are the testing of coated tablets prepared with a photosensitive drug or the analysis of the photocalorimetric signals measured during irradiation of UV-sunscreens. Having developed the instruments and demonstrated their use in the assessment of the photostability of drugs, the only major obstacle to their application is imagination.

REFERENCES

1. ICH. (2003) Q1A(R2): Stability Testing of New Drug Substances and Products (Second Revision).

2. ICH. (1996) Q1B: Photostability Testing of New Drug Substances and Products.

3. Lehto, V.P., Salonen, J. and Laine, E. (1999) Real time detection of photoreactivity in pharmaceutical solids and solutions with isothermal microcalorimetry. *Pharm. Res.*, **16**, 368-373.

4. Morris, A.C. (2004), Ph.D Thesis. University of Greenwich, Kent, UK.

5. Dhuna, M. (2008), Ph.D Thesis. The School of Pharmacy, University of London, London, UK.

6. Tønnesen, H.H. (2004) *Photostability of drugs and drug formulations*. CRC Press. ISBN 0-415-30323-0.

7. De Vries, H., Beijersbergen Van Henegouwen, G.M.J. and Huf, F.A. (1984) Photochemical decomposition of chloramphenicol in a 0.25 percent eyedrop and in a therapeutic intraocular concentration. *Int. J. Pharm. (Kidlington)*, **20**, 265-272.

8. De Mol, N.J., Van Henegouwen, G.M.J.B. and Van Beele, B. (1981) Singlet oxygen formation by sensitization of furocoumarins complexed with, or bound covalently to DNA. *Photochem. Photobiol.*, **34**, 661-666.

9. Albini, A. and Fasani, E. (1998), *Drugs Photochemistry and Photostability*. The Royal Society of Chemistry, pp. 1-73. ISBN 9780854047437.

10. Tønnesen, H.H. (2001) Formulation and stability testing of photolabile drugs. *Int. J. Pharm.*, **225**, 1-14.

11. Aman, W. and Thoma, K. (2002) The influence of formulation and manufacturing process on the photostability of tablets. *Int. J. Pharm.*, **243**, 33-41.

12. Thoma, K. and Klimek, R. (1991) Photostabilization of drugs in dosage forms without protection from packaging materials. *Int. J. Pharm.*, **67**, 169-175.

13. Daisuke, T., Kenji, O., Shun, H., Fumitoshi, H., Kaneto, U. and Toshinobu, A. (1989) Effects of cyclodextrins on degradations of emetine and cephaeline in aqueous solution. *Chem. Pharm. Bull.*, **37**, 1591-1594.

14. Diette, K.M., Momtaz-T, K., Stern, R.S., Arndt, K.A. and Parrish, J.A. (1984) Role of ultraviolet A in phototherapy for psoriasis. *J. Am. Acad. Dermatol.*, **11**, 441-447.

15. Awan, M.A. and Tarin, S.A. (2006) Review of photodynamic therapy. *Surg. J. R. Coll. Surg. Edinb. Irel.*, **4**, 231-236.

16. Derycke, A.S.L. and de Witte, P.A.M. (2004) Liposomes for photodynamic therapy. *Adv. Drug Deliver. Rev.*, **56**, 17-30.

17. Griffin, D.R., Patterson, J.T. and Kasko, A.M. (2010) Photodegradation as a mechanism for controlled drug delivery. *Biotechnol. Bioeng.*, **107**, 1012-1019.

18. Chang, R. (2005) *Physical chemistry for the biosciences*. University Science. ISBN 9781891389337.

19. Rohatgi-Mukherjee, K.K. (1978) *Fundamentals of photochemistry*. Wiley Eastern. ISBN 9781891389337.

20. Carstensen, J.T. (1974) Stability of solids and solid dosage forms. *J. Pharm. Sci.*, **63**, 1-14.

21. Marciniec, B. and Rychcik, W. (1994) Kinetic-analysis of nifedipine photodegradation in the solid-state. *Pharmazie*, **49**, 894-897.

22. Baertschi, S.W., Alsante, K.M. and Tønnesen, H.H. (2010) A critical assessment of the ICH guideline on photostability testing of new drug substances and products (Q1B): Recommendation for revision. *J. Pharm. Sci.*, **99,** 2934-2940.

23. Sunada, H., Iba, K., Ogawa, S., Arakawa, E., Masuyama, T., Hara, K. and Otsuka, A. (1985) Hydrolysis of acetylsalicylsalicylic acid and salicylsalicylic acid in aqueous-solution. *Chem. Pharm. Bull.*, **33**, 2158-2161.

24. Ahmad, I., Fasihullah, Q., Noor, A., Ansari, I.A. and Ali, Q.N.M. (2004) Photolysis of riboflavin in aqueous solution: a kinetic study. *Int. J. Pharm.*, **280**, 199-208.

25. Majeed, I.A., Murray, W.J., Newton, D.W., Othman, S. and Alturk, W.A. (1987) Spectrophotometric study of the photodecomposition kinetics of nifedipine. *J. Pharm. Pharmacol.*, **39**, 1044-1046.

26. Sadana, G.S. and Ghogare, A.B. (1991) Mechanistic studies on photolytic degradation of nifedipine by use of 1H-NMR and 13C-NMR spectroscopy. *Int. J. Pharm.*, **70**, 195-199.

27. Skaria, C.V., Gaisford, S., O'Neill, M.A.A., Buckton, G. and Beezer, A.E. (2005) Stability assessment of pharmaceuticals by isothermal calorimetry: two component systems. *Int. J. Pharm.*, **292**, 127-135.

28. Gaisford, S. and O'Neill, M.A.A. (2006) *Pharmaceutical Isothermal Calorimetry*. Informa Healthcare. ISBN 9780849331558.

29. Atkins, P.W. and Paula, J.D. (2006) *Physical Chemistry*. W.H. Freeman. ISBN 9780716787594.

30. Khawam, A. and Flanagan, D.R. (2006) Basics and applications of solid-state kinetics: A pharmaceutical perspective. *J. Pharm. Sci.*, **95**, 472-498.

31. Sesták, J. and Berggren, G. (1971) Study of the kinetics of the mechanism of solid-state reactions at increasing temperatures. *Thermochim. Acta*, **3**, 1-12.

32. Ng, W.L. (1975) Thermal-decomposition in solid-state. *Aust. J. Chem.*, **28**, 1169-1178.

33. Perez-Maqueda, L.A., Criado, J.M. and Sanchez-Jimenez, P.E. (2006) Combined kinetic analysis of solid-state reactions: A powerful tool for the simultaneous determination of kinetic parameters and the kinetic model without previous assumptions on the reaction mechanism. *J. Phys. Chem. A*, **110**, 12456-12462.

34. Cai, J.M. and Liu, R.H. (2009) Kinetic Analysis of Solid-State Reactions: A General Empirical Kinetic Model. *Ind. Eng. Chem. Res.*, **48**, 3249-3253.

35. Willson, R.J. (1995), Ph.D Thesis. University of Kent, Kent, UK.

36. Hills, A.K. (2001), Ph.D Thesis. University of Kent, Kent, UK.

37. Gaisford, S. (1997), Ph.D Thesis. University of Kent, Kent, UK.

38. Gaisford, S., Hills, A.K., Beezer, A.E. and Mitchell, J.C. (1999) Thermodynamic and kinetic analysis of isothermal microcalorimetric data: applications to consecutive reaction schemes. *Thermochim. Acta*, **328**, 39-45.

39. Beezer, A.E., Morris, A.C., O'Neill, M.A.A., Willson, R.J., Hills, A.K., Mitchell, J.C. and Connor, J.A. (2001) Direct determination of equilibrium thermodynamic and kinetic parameters from isothermal heat conduction microcalorimetry. *J. Phys. Chem. B*, **105**, 1212-1215.

40. Beezer, A.E. (2001) An outline of new calculation methods for the determination of both thermodynamic and kinetic parameters from isothermal heat conduction microcalorimetry. *Thermochim. Acta*, **380**, 205-208.

41. Willson, R.J. and Beezer, A.E. (2003) A mathematical approach for the calculation of reaction order for common solution phase reactions. *Thermochim. Acta*, **402**, 75-80.

42. Willson, R.J., Beezer, A.E. and Mitchell, J.C. (1996) Solid state reactions studied by isothermal microcalorimetry; The solid state oxidation of ascorbic acid. *Int. J. Pharm.*, **132**, 45-51.

43. O'Neill, M.A.A., Beezer, A.E., Morris, A.C., Urakami, K., Willson, R.J. and Connor, J.A. (2003) Solid-state reactions from isothermal heat conduction microcalorimetry - Theoretical approach and evaluation via simulated data. *J. Therm. Anal. Calorim.*, **73**, 709-714.

44. Teixeira, C. (1999), *Energetics of stable molecules and reactive intermediates*. Kluwer Academic Publishers, Vol. 535, pp. 105-136. ISBN 9780792357407.

45. Magee, J.L., DeWitt, T.W., Smith, E.C. and Daniels, F. (1939) A Photocalorimeter. The quantum efficiency of photosynthesis in algae. *J. Am. Chem. Soc.*, **61**, 3529-3533.

46. Magee, J.L. and Daniels, F. (1940) The heat of photobromination of the phenyl methanes and cinnamic acid, and the influence of oxygen. *J. Am. Chem. Soc.*, **62**, 2825-2833.

47. Seybold, P.G., Gouterman, M. and Callis, J. (1969) Calorimetric, photometric and lifetime determinations of fluorescence yields of fluorescein dyes. *Photochem. Photobiol.*, **9**, 229-242.

48. Mardelli, M. and Olmsted, J. (1977) Calorimetric determination of the 9,10-diphenyl-anthracene fluorescence quantum yield. *J. Photochem.*, **7**, 277-285.

49. Magde, D., Brannon, J.H., Cremers, T.L. and Olmsted, J. (1979) Absolute luminescence yield of cresyl violet. A standard for the red. *J. Phys. Chem.*, **83**, 696-699.

50. Olmsted, J. (1980) Photocalorimetric studies of singlet oxygen reactions. *J. Am. Chem. Soc.*, **102**, 66-71.

51. Adamson, A.W., Vogler, A., Kunkely, H. and Wachter, R. (1978) Photocalorimetry. Enthalpies of photolysis of trans-azobenzene, ferrioxalate and cobaltioxalate ions, chromium hexacarbonyl, and dirhenium decarbonyl. *J. Am. Chem. Soc.*, **100**, 1298-1300.

52. Nakashima, M. and Adamson, A.W. (1982) Photocalorimetry. 2. Enthalpies of ligand substitution reactions of some group 6 metal carbonyl complexes in solution. *J. Phys. Chem.*, **86**, 2905-2909.

53. Nakashima, M. and Adamson, A.W. (1982) Photocalorimetry. 3. Enthalpies of substitution reactions of some chromium(III) ammines and chromium(III) and cobalt(III) cyano complexes in aqueous solution. *J. Phys. Chem.*, **86**, 2910-2912.

54. Harel, Y., Adamson, A.W., Kutal, C., Grutsch, P.A. and Yasufuku, K. (1987) Photocalorimetry. 6. Enthalpies of isomerization of norbornadiene and of substituted norbornadienes to corresponding quadricyclenes. *J. Phys. Chem.*, **91**, 901-904.

55. Harel, Y. and Adamson, A.W. (1986) Photocalorimetry. 4. Enthalpies of substitution reactions of rhodium(III) and iridium(III) pentaammine halides and of ruthenium(II) hexaammine. *J. Phys. Chem.*, **90**, 6690-6693.

56. Harel, Y. and Adamson, A.W. (1986) Photocalorimetry. 5. Enthalpies of reaction of $M_2(CO)_{10}$ (M = Mn, Re) compounds with iodine in cyclohexane solution at 25 ºC. *J. Phys. Chem.*, **90**, 6693-6696.

57. Cooper, A. and Converse, C.A. (1976) Energetics of primary processes in visual excitation - photocalorimetry of rhodopsin in rod outer segment membranes. *Biochemistry*, **15**, 2970-2978.

58. Cooper, A. (1979) Energy uptake in the first step of visual excitation. *Nature*, **282**, 531-533.

59. Cooper, A. and Lester, P. (1982), *Methods in Enzymology*. Academic Press, Vol. Volume 88, pp. 667-673. ISBN 0076-6879.

60. Cooper, A., Dixon, S.F. and Tsuda, M. (1986) Photoenergetics of octopus rhodopsin. *Eur. Biophys. J.*, **13**, 195-201.

61. Johansson, P. and Wadsö, I. (1999) An isothermal microcalorimetric titration/perfusion vessel equipped with electrodes and spectrophotometer. *Thermochim. Acta*, **342**, 19-29.

62. Schaarschmidt, B., Lamprecht, I., Plesser, T. and Müller, S.C. (1986) Simultaneous measurements of heat production and optical density in oscillating reactions. *Thermochim. Acta*, **105**, 205-213.

63. Wendlandt, W.W. and Stranahan, J. (1976) A combined titration calorimeter and fixed wavelength colorimeter. *Thermochim. Acta*, **17**, 295-300.

64. Neal, L. and Marlene, A.D. (1978), *Methods in Enzymology*. Academic Press, Vol. Volume 57, pp. 540-549. ISBN 0076-6879.

65. McIlvaine, P. and Langerman, N. (1977) A calorimetric investigation of the growth of the luminescent bacteria *Beneckea harveyi* and *Photobacterium leiognathi*. *Biophys. J.*, **17**, 17-25.

66. Appelt, B.K. and Abadie, M.J.M. (1985) Thermal analysis of photocurable materials. *Polym. Eng. Sci.*, **25**, 931-933.

67. Appelt, B.K. and Abadie, M.J.M. (1988) Calorimetric characterization of photosensitive materials. *Polym. Eng. Sci.*, **28**, 367-371.

68. Abadie, M.J.M. and Appelt, B.K. (1989) Photocalorimetry of light-cured dental composites. *Dent. Mater.*, **5**, 6-9.

69. Tasaki, I. and Nakaye, T. (1985) Heat generated by the dark-adapted squid retina in response to light pulses. *Science*, **227**, 654-655.

70. Klassen, J.K., Selke, M., Sorensen, A.A. and Yang, G.K. (1990) Metal-ligand bond dissociation energies in CpMn(CO)2L complexes. *J. Am. Chem. Soc.*, **112**, 1267-1268.

71. Atkinson, R. (1985) Development of a wavelength scanning laser calorimeter. *Appl. Opt.*, **24**, 464-471.

72. Suurkuusk, J. and Wadsö, I. (1982) A multichannel microcalorimetry system. *Chem. Scr.*, **20**, 155–163.

73. Johansson, P. and Wadsö, I. (1997) A photo microcalorimetric system for studies of plant tissue. *J. Biochem. Bioph. Meth.*, **35**, 103-114.

74. Mukhanov, V. and Kemp, R. (2009) Design and experience of using light-emitting diodes (LEDs) as the inbuilt light source for a customised differential photomicrocalorimeter. *J. Therm. Anal. Calorim.*, **95**, 731-736.

75. Lehto, V.P., Salonen, J. and Laine, E. (1999) A microcalorimetric study on the role of moisture in photolysis of nifedipine powder. *J. Therm. Anal. Calorim.*, **56**, 1305-1310.

76. Dhuna, M., Beezer, A.E., Connor, J.A., Clapham, D., Courtice, C., Frost, J. and Gaisford, S. (2008) LED-array photocalorimetry: Instrument design and application to photostability of nifedipine. *J. Pharm. Biomed. Anal.*, **48**, 1316-1320.

77. Douglas, M. (2004), *Photostability of Drugs and Drug Formulations, Second Edition*. CRC Press, pp. 41-65. ISBN 9780415303231.

78. Sousa, L.A.E, Alem, N., Beezer, A.E., O'Neill, M.A.A., Gaisford S. (2010) Quantitative analysis of solid-state processes studied with isothermal microcalorimetry. *J. Phys. Chem. B*, **114**, 13173-13178.

79. Almeida e Sousa, L., Beezer, A.E., Hansen, L.D., Clapham, D., Connor, J.A., Gaisford, S. (2012) Calorimetric determination of rate constants and enthalpy changes for zero-order reactions. *J. Phys. Chem. B*, **116**, 6356-6360.

80. Gaisford, S., Verma, A., Saunders, M. and Royall, P.G. (2009) Monitoring crystallisation of drugs from fast-dissolving oral films with isothermal calorimetry. *Int. J. Pharm.*, **380**, 105-111.

81. O'Neill, Beezer, A.E., Tetteh, J., Gaisford, S. and Dhuna, M. (2007) Application of chemometric analysis to complexity in isothermal calorimetric data. *J. Phys. Chem. B*, **111**, 8145-8149.

82. Willson, R.J., Beezer, A.E., Mitchell, J.C. and Loh, W. (1995) Determination of thermodynamic and kinetic parameters from isothermal heat conduction microcalorimetry: Applications to long-term-reaction studies. *J. Phys. Chem.*, **99**, 7108-7113.

83. Tobin, M.C. (1974) Theory of phase transition kinetics with growth site impingement. I. Homogeneous nucleation. *J. Polym. Sci. Pol. Phys.*, **12**, 399-406.

84. Hansen, L.D., Eatough, D.J., Lewis, E.A., Bergstrom, R.G., Degraft-Johnson, D. and Cassidy-Thompson, K. (1990) Shelf-life prediction from induction period

calorimetric measurements on materials undergoing autocatalytic decomposition. *Can. J. Chem.*, **68**, 2111-2114.

85. Lundgren, R., Sanden, R. and Albertsson, A.C. (1989) A facile method for the study of slow physical and chemical processes in polymeric systems. *J. Appl. Polym. Sci.*, **37**, 1221-1231.

86. Raemy, A., Froelicher, I. and Loeliger, J. (1987) Oxidation of lipids studied by isothermal heat-flux calorimetry. *Thermochim. Acta*, **114**, 159-164.

87. O'Neill, M.A.A., Beezer, A.E., Mitchell, J.C., Orchard, J. and Connor, J.A. (2004) Determination of Michaelis-Menten parameters obtained from isothermal flow calorimetric data. *Thermochim. Acta*, **417**, 187-192.

88. Logan, S.R. (1997) Does a photochemical reaction have a reaction order? *J. Chem. Educ.*, **74**, 1303.

89. Li, X., Chow, D.-C. and Tu, S.-C. (2006) Thermodynamic analysis of the binding of oxidized and reduced FMN cofactor to *Vibrio harveyi* NADPH-FMN oxidoreductase FRP apoenzyme. *Biochemistry.*, **45**, 14781-14787.

90. Ortiz-Salmerón, E., Yassin, Z., Clemente-Jimenez, M.J., Las Heras-Vazquez, F.J., Rodriguez-Vico, F., Barón, C. and García-Fuentes, L. (2001) A calorimetric study of the binding of S-alkylglutathiones to glutathione S-transferase. *BBA-Protein Struct. M.*, **1548**, 106-113.

91. Laidler, K.J. and Hoare, J.P. (1949) The molecular kinetics of the urea-urease system. I. The kinetic laws. *J. Am. Chem. Soc.*, **71**, 2699-2702.

92. Huang, T.-C. and Chen, D.-H. (1991) Kinetic study of urease-catalysed urea hydrolysis. *J. Chem. Technol. Biot.*, **52**, 433-444.

93. Goldberg, R.N., Kishore, N. and Lennen, R.M. (2002) Thermodynamic quantities for the ionization reactions of buffers. *J. Phys. Chem. Ref. Data*, **31**, 231-370.

94. Hüttl, R., Bohmhammel, K., Wolf, G. and Oehmgen, R. (1995) Calorimetric investigations into enzymatic urea hydrolysis. *Thermochim. Acta*, **250**, 1-12.

95. Peeters, H. (1973) *Protides of the biological fluids: proceedings of the twentieth colloquium, Brugge, 1972*. Pergamon Press. ISBN 9780080171319.

96. Atkins, P., De Paula, J. (2006) *Physical chemistry for the life sciences*. Oxford University Press. ISBN 0199280959.

97. Benson, S.W. and Buss, J.H. (1958) Additivity rules for the estimation of molecular properties. Thermodynamic properties. *J. Chem. Phys.*, **29**, 546-572.

98. Pedley, J.B. (1994) *Thermochemical data and structures of organic compounds, Volume 1*. Taylor & Francis. ISBN 1883400015.

99. Cohen, N. (1996) Revised group additivity values for enthalpies of formation (at 298 K) of carbon-hydrogen and carbon-hydrogen-oxygen compounds. *J. Phys. Chem. Ref. Data*, **25**, 1411-1481.

100. Salmon, A. and Dalmazzone, D. (2006) Prediction of enthalpy of formation in the solid state (at 298.15 k) using second-order group contributions. Part 1. Carbon-hydrogen and carbon-hydrogen-oxygen compounds. *J. Phys. Chem. Ref. Data*, **35**, 1443-1457.

101. Salmon, A. and Dalmazzone, D. (2007) Prediction of enthalpy of formation in the solid state (at 298.15 K) using second-order group contributions - Part 2: Carbon-hydrogen, carbon-hydrogen-oxygen, and carbon-hydrogen-nitrogen-oxygen compounds. *J. Phys. Chem. Ref. Data*, **36**, 19-58.

102. Skaria, C.V. (2007), Ph.D Thesis. The School of Pharmacy, University of London, London, UK.

103. Allen, J.M., Allen, S.K. and Baertschi, S.W. (2000) 2-Nitrobenzaldehyde: a convenient UV-A and UV-B chemical actinometer for drug photostability testing. *J. Pharm. Biomed. Anal.*, **24**, 167-178.

104. Thermometric AB (2002) *2277 Thermal Activity Monitor Instruction Manual*

105. TA Instruments. (2008) *Multi-Cell Differential Scanning Calorimeter - Getting Started Guide, Revision C*.

106. Olivari, M.T., Bartorelli, C., Polese, A., Fiorentini, C., Moruzzi, P. and Guazzi, M.D. (1979) Treatment of hypertension with nifedipine, a calcium antagonistic agent. *Circulation*, **59**, 1056-1062.

107. Matsuura, I., Imaizumi, M. and Sugiyama, M. (1990) Method of kinetic analysis of photodegradation: nifedipine in solutions. *Chem. Pharm. Bull.*, **38**, 1692-1696.

108. Matsuda, Y., Teraoka, R. and Sugimoto, I. (1989) Comparative evaluation of photostability of solid-state nifedipine under ordinary and intensive light irradiation conditions. *Int. J. Pharm.*, **54**, 211-221.

109. Testa, R., Dolfini, E., Reschiotto, C., Secchi, C. and Biondi, P.A. (1979) GLC determination of nifedipine, a light sensitive drug, in plasma. *Farmaco Prat.*, **34**, 463-473.

110. Jakobsen, P., Pedersen, O.L. and Mikkelsen, E. (1979) Gas chromatographic determination of nifedipine and one of its metabolites using electron capture detection. *J. Chromatogr. B*, **162**, 81-87.

111. Fasani, E., Dondi, D., Ricci, A. and Albini, A. (2006) Photochemistry of 4-(2-nitrophenyl)-1,4-dihydropyridines. Evidence for electron transfer and formation of an intermediate. *Photochem. Photobiol.*, **82**, 225-230.

112. Görner, H. Nitro group photoreduction of 4-(2-nitrophenyl)- and 4-(3-nitrophenyl)-1,4-dihydropyridines. *Chem. Phys.*, **373**, 153-158.

113. Fasani, E., Albini, A. and Mella, M. (2008) Photochemistry of Hantzsch 1,4-dihydropyridines and pyridines. *Tetrahedron*, **64**, 3190-3196.

114. Memarian, H.R., Abdoli-Senejani, M. and Dopp, D. (2007) Photoinduced aromatization of unsymmetrically substituted 1,4-dihydropyridines. *J. Chin. Chem. Soc.*, **54**, 131-139.

115. Berson, J.A. and Brown, E. (1955) Studies on dihydropyridines. II. The photochemical disproportionation of 4-(2-nitrophenyl)-1,4-dihydropyridines. *J. Am. Chem. Soc.*, **77**, 447-450.

116. Sang, C.S., Ae, N.P. and Yong, J.L. (1988) Mechanistic studies on the photochemical degradation of nifedipine. *Bull. Korean Chem. Soc.*, **9**, 271-274.

117. Shamsipur, M., Hemmateenejad, B., Akhond, M., Javidnia, K. and Miri, R. (2003) A study of the photo-degradation kinetics of nifedipine by multivariate curve resolution analysis. *J. Pharm. Biomed. Anal.*, **31**, 1013-1019.

118. Whitten, J.L., Yang, H. (1996) Theory of chemisorption and reactions on metal surfaces. *Surf. Sci. Rep.*, **24**, 55-124.

119. Council of Europe. European Directorate for the Quality of Medicines and HealthCare. (2007) *European Pharmacopoeia: Published in Accordance with the Convention on the Elaboration of a European Pharmacopoeia (European Treaty Series No. 50)*. Council of Europe. ISBN 9789287160546.

120. Aso, Y., Yoshioka, S., Otsuka, T. and Kojima, S. (1995) The physical stability of amorphous nifedipine determined by isothermal microcalorimetry. *Chem. Pharm. Bull.*, **43**, 300-303.

121. Zhou, D., Schmitt, E.A., Zhang, G.G., Law, D., Vyazovkin, S., Wight, C.A. and Grant, D.J.W. (2003) Crystallization kinetics of amorphous nifedipine studied by model-fitting and model-free approaches. *J. Pharm. Sci.*, **92**, 1779-1792.

122. Grooff, D., De Villiers, M.M. and Liebenberg, W. (2007) Thermal methods for evaluating polymorphic transitions in nifedipine. *Thermochim. Acta*, **454**, 33-42.

123. Philip, A.L. and Frank Allen, L. (1934) The photoisomerization of the o-nitrobenzaldehydes I. Photochemical results. *J. Chem. Phys.*, **2**, 756-759.

124. Bowen, E.J., Hartley, H., Scott, W.D. and Watts, H.G. (1924) CXLVIII.-Rate of photochemical change in solids. *J. Chem. Soc., Trans.*, **125**, 1218-1221.

125. Lin, Y.-J., Lee, A., Teng, L.-S. and Lin, H.-T. (2002) Effect of experimental factors on nitrobenzaldehyde photoisomerization. *Chemosphere*, **48**, 1-8.

126. Matsuda, Y., Akazawa, R., Teraoka, R. and Otsuka, M. (1994) Pharmaceutical evaluation of carbamazepine modifications: Comparative study for photostability of carbamazepine polymorphs by using Fourier-transformed reflection-absorption infrared spectroscopy and colorimetric measurement. *J. Pharm. Pharmacol.*, **46**, 162-167.

127. Grzesiak, A.L., Lang, M., Kim, K. and Matzger, A.J. (2003) Comparison of the four anhydrous polymorphs of carbamazepine and the crystal structure of form I. *J. Pharm. Sci.*, **92**, 2260-2271.

128. Beijersbergen van Henegouwen, G.M.J. (1991) New trends in photobiology: (Systemic) phototoxicity of drugs and other xenobiotics. *J. Photoch. Photobio. B*, **10**, 183-210.

129. Zeegers, F., Gibella, M. and Tilquin, B. (1997) Analysis of some products from the irradiation of solid chloramphenicol. *Radiat. Phys. Chem.*, **50**, 149-153.

130. Reisch, J. and Weidmann, K.G. (1971) Photo- und radiolyse des chloramphenicols. *Arch. Pharm.*, **304**, 911-919.

131. Matsuda, Y. and Tatsumi, E. (1990) Physicochemical characterization of furosemide modifications. *Int. J. Pharm.*, **60**, 11-26.

132. De Villiers, M.M., van der Watt, J.G. and Lötter, A.P. (1992) Kinetic study of the solid-state photolytic degradation of two polymorphic forms of furosemide. *Int. J. Pharm.*, **88**, 275-283.

133. Kigasawa, K., Shimizu, H., Hayashida, S. and Ohkubo, K. (1984) Decomposition and stabilization of drugs. 20. Photodecomposition and stabilization of dipyridamol. *Yakugaku Zasshi,* **104**, 1191-1197.

134. Vargas, F., Rivas, C., Fuentes, A., Cheng, A.T. and Velutini, G. (2002) The photochemistry of dipyridamole. *J. Photoch. Photobio. A*, **153**, 237-243.

135. Xiong, P. and Hu, J. (2012) Degradation of acetaminophen by UVA/LED/TiO$_2$ process. *Sep. Purif. Technol.*, **91**, 89-95.

136. Aguilar, C.A., Montalvo, C., Ceron, J.G. and Moctezuma, E. (2011) Photocatalytic degradation of acetaminophen. *Int. J. Environ. Res.*, **5**, 1071-1078.

137. Kamble, R.M. and Singh, S.G. (2012) Stability-indicating RP-HPLC method for analysis of paracetamol and tramadol in a pharmaceutical dosage form. *E-J. Chem.*, **9**, 1347-1356.

138. Menard, K., Brostow, W. and Menard, N. (2011) Photodegradation of pharmaceuticals studied with UV irradiation and Differential Scanning Calorimetry. *Chem. & Chem. Technol.*, **5**, 385-388.

PRESENTATIONS, AWARDS AND PUBLICATIONS

Oral presentations:

- at the UK PharmSci conference in Nottingham, UK, London, September 2010, on the application of photocalorimetry to assess the photostability of solutions of nifedipine.

- at Glaxo Smith Kline (GSK) organized by the R&D department in Ware, UK, April 2011. "The use of photocalorimetry in photostability testing of pharmaceuticals".

- at the "PhD Research Day" in the School of Pharmacy, University of London, London, UK, April 2011. "The use of photocalorimetry in photostability testing of pharmaceuticals".

- at ULLA Summer School 2011 in Parma, Italy, July, 2011. "Photostability studies using photocalorimetry".

- at the Analytical Research Forum organized by the Royal Society of Chemistry in Manchester, UK, July 2011. "The use of photocalorimetry to assess photostability of drugs".

- at the Thermal Analysis Conference 2012 (TAC 12) organized by the Thermal Methods Group (TMG) in Nottingham, UK, April 2012. "New strategies for the analysis of solid state calorimetric data".

- at the International Conference on Chemical Thermodynamics (ICCT) 2012 and 67th Calorimetry Conference organized by the International Association for Chemical Thermodynamics (IACT) in Búzios, Brazil, August 2012. "New strategies for the analysis of solid state calorimetric data".

Awards:

- Geoffrey Phillips Analytical Science Award for 2010 by the Joint Pharmaceutical Analysis Group (JPAG).

- FCT – Fundação para a Ciência e a Tecnologia Doctoral Grant - SFRH / BD / 71024 / 2010.

Publications:

- Sousa, L.A.E., Alem, N., Beezer, A.E., O'Neill, M.A.A. and Gaisford, S. Quantitative analysis of solid-state processes studied with isothermal microcalorimetry. *J. Phys. Chem. B*, **114**, 13173-13178, 2010.

- Almeida E Sousa, L., Beezer, A.E., Hansen, L.D., Clapham, D., Connor, J.A. and Gaisford, S. Calorimetric determination of rate constants and enthalpy changes for zero-order reactions. *J. Phys. Chem.. B*, **116**, 6356-6360, 2012.